

UNCLASSIFIED

AD NUMBER

AD921329

LIMITATION CHANGES

TO:

Approved for public release; distribution is unlimited.

FROM:

Distribution authorized to U.S. Gov't. agencies only; Test and Evaluation; JUL 1974. Other requests shall be referred to Air Force Armament Development Test Center, Eglin AFB, FL 32543.

AUTHORITY

ADTC ltr 1 Oct 1980

THIS PAGE IS UNCLASSIFIED

AEDC-TR-74-68
AFATL-TR-74-110

2 Cy 2

AUG 15 1974
OCT 9 1974

NOV 11 1978
OCT 10 1978

JAN 24 1986
SEP 18 1990



**STATIC STABILITY AND CONTROL EFFECTIVENESS OF
THE SUPER HOBOS/MK-84 (EOGB-II) MUNITION AT
MACH NUMBERS FROM 0.4 TO 1.6**

D. K. Smith
ARO, Inc.

PROPULSION WIND TUNNEL FACILITY
ARNOLD ENGINEERING DEVELOPMENT CENTER
AIR FORCE SYSTEMS COMMAND
ARNOLD AIR FORCE STATION, TENNESSEE 37389

**TECHNICAL REPORTS
FILE COPY**

July 1974

RECEIVED
AUG 12 1974
per TAB 80-26

Final Report for Period January 7 to 19, 1974

~~Distribution limited to U.S. Government agencies only; this report contains information on test and evaluation of military hardware; July 1974; other requests for this document must be referred to Air Force Armament Development Test Center (SDTT), Eglin AFB, FL 32542.~~

PROPERTY OF U. S. AIR FORCE
AEDC LIBRARY
#40600-74-C-0001

Prepared for

AIR FORCE ARMAMENT LABORATORY (DLMA)
AND
AIR FORCE ARMAMENT DEVELOPMENT TEST CENTER (SDTT)
EGLIN AFB, FLORIDA 32543

NOTICES

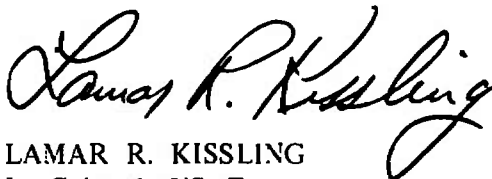
When U. S. Government drawings specifications, or other data are used for any purpose other than a definitely related Government procurement operation, the Government thereby incurs no responsibility nor any obligation whatsoever, and the fact that the Government may have formulated, furnished, or in any way supplied the said drawings, specifications, or other data, is not to be regarded by implication or otherwise, or in any manner licensing the holder or any other person or corporation, or conveying any rights or permission to manufacture, use, or sell any patented invention that may in any way be related thereto.

Qualified users may obtain copies of this report from the Defense Documentation Center.

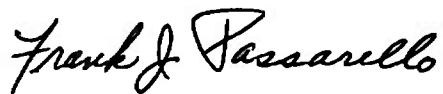
References to named commercial products in this report are not to be considered in any sense as an endorsement of the product by the United States Air Force or the Government.

APPROVAL STATEMENT

This technical report has been reviewed and is approved.



LAMAR R. KISSLING
Lt Colonel, USAF
Chief Air Force Test Director, PWT
Directorate of Test



FRANK J. PASSARELLO
Colonel, USAF
Director of Test

UNCLASSIFIED

SECURITY CLASSIFICATION OF THIS PAGE (When Data Entered)

REPORT DOCUMENTATION PAGE		READ INSTRUCTIONS BEFORE COMPLETING FORM
1. REPORT NUMBER AEDC-TR-74-68 AFATL-TR-74-110	2. GOVT ACCESSION NO.	3. RECIPIENT'S CATALOG NUMBER
4. TITLE (and Subtitle) STATIC STABILITY AND CONTROL EFFECTIVENESS OF THE SUPER HOBOS/MK-84 (EOGB-II) MUNITION AT MACH NUMBERS FROM 0.4 TO 1.6		5. TYPE OF REPORT & PERIOD COVERED Final Report, January 7 to 19, 1974
		6. PERFORMING ORG REPORT NUMBER
7. AUTHOR(s) D. K. Smith, ARO, Inc.		8. CONTRACT OR GRANT NUMBER(s)
9. PERFORMING ORGANIZATION NAME AND ADDRESS Arnold Engineering Development Center Arnold Air Force Station, Tennessee 37389		10. PROGRAM ELEMENT, PROJECT, TASK AREA & WORK UNIT NUMBERS Program Element 64733F
11. CONTROLLING OFFICE NAME AND ADDRESS Air Force Armament Development Test Center (SDTT), Eglin AFB, FL 32542		12. REPORT DATE July 1974
		13. NUMBER OF PAGES 170
14. MONITORING AGENCY NAME & ADDRESS (if different from Controlling Office)		15. SECURITY CLASS. (of this report) UNCLASSIFIED
		15a. DECLASSIFICATION/DOWNGRADING SCHEDULE N/A
16. DISTRIBUTION STATEMENT (of this Report) Distribution limited to U. S. Government agencies only; this report contains in- formation on test and evaluation of military hardware; July 1974; other requests for this document must be referred to Air Force Armament Development Test Center (SDTT), Eglin AFB, FL 32542.		
17. DISTRIBUTION STATEMENT (of the abstract entered in Block 20, if different from Report)		
18. SUPPLEMENTARY NOTES Available in DDC		
19. KEY WORDS (Continue on reverse side if necessary and identify by block number) Super HOBOS/Mk-84 transonic flow deflection guided bombs munition performance static stability wind tunnel tests control flaps (control surfaces)		
20. ABSTRACT (Continue on reverse side if necessary and identify by block number) Wind tunnel tests were conducted on a 0.25-scale model to determine the static stability and control characteristics of the Super HOBOS/MK-84 (EOGB-II) munition. The tests were performed in the Aerodynamic Wind Tunnel (4T) over a Mach number range from 0.4 to 1.6 at angles of attack from -4 to 26 deg. Aerodynamic coefficients and control effectiveness data are presented. Two techniques, one using multiple flap deflections and the other single flap deflections, were employed during the test. A comparison		

UNCLASSIFIED

SECURITY CLASSIFICATION OF THIS PAGE(When Data Entered)

20. ABSTRACT (Continued)

of the two methods is presented and the results are discussed.

AFSC
Arnold AFS Tenn

UNCLASSIFIED

SECURITY CLASSIFICATION OF THIS PAGE(When Data Entered)

PREFACE

The work reported herein was conducted by the Arnold Engineering Development Center (AEDC) and sponsored by the Air Force Armament Laboratory (AFATL/DLMA/Richard Batchelder) and the Air Force Armament Development Test Center (ADTC/SDTT/Capt F. H. Wheeler), Air Force Systems Command (AFSC) under Program Element 64733.

The test results presented were obtained by ARO, Inc. (a subsidiary of Sverdrup & Parcel and Associates, Inc.), contract operator of AEDC, AFSC, Arnold Air Force Station, Tennessee. The test was conducted from January 7 to 19, 1974, under ARO Projects No. PA461 and PA466. The manuscript (ARO Control No. ARO-PWT-TR-74-43) was submitted for publication on May 22, 1974.

CONTENTS

	<u>Page</u>
1.0 INTRODUCTION	7
2.0 APPARATUS	
2.1 Test Facility	7
2.2 Test Article	7
2.3 Instrumentation	8
3.0 TEST DESCRIPTION	
3.1 General Test Procedures	8
3.2 Multiple and Single Flap Test Procedures	9
3.3 Corrections	12
3.4 Precision of Measurements	12
4.0 RESULTS AND DISCUSSION	
4.1 Configuration Buildup	12
4.2 Control Effectiveness for Pure Control Deflections (Multiple Flap Technique)	13
4.3 Control Effectiveness for Combined Control Deflections (Multiple Flap Technique)	14
4.4 Comparison of Control Effectiveness Data Obtained by Single Flap and Multiple Flap Techniques	16
4.5 Axial-Force Data	16
4.6 Control Flap Hinge-Moment Coefficients	17
4.7 Calibration Data for Vane Angle-of-Attack Indicator	17
5.0 SUMMARY OF RESULTS	17
REFERENCES	18

ILLUSTRATIONS

Figure

1. Details and Dimensions of the Super HOBOS/MK-84 Model	19
2. Details and Dimensions of the Vane-Type Angle-of-Attack Indicator	24
3. Photographs of the Test Model	25
4. Orientation of Model Forces and Moments and Control Flap Deflections	27
5. Model Roll Angles Required to Obtain Negative Deflections of Flap Number 2 and Positive Deflections of Flap Numbers 3 and 4 Using Negative Deflections of Flap Number 1	29
6. Model Roll Angles Required to Obtain Mirror Images of Positive Deflections of Flap Numbers 1 and 2 Using Negative Deflections of Flap Number 1	30

<u>Figure</u>	<u>Page</u>
7. Comparison of Normal-Force and Pitching-Moment Coefficients for Configurations B2, B2S13, B2S13W4F7, B2W4T3F7, and B2S13W4T3F7	31
8. Comparison of Rolling-Moment and Axial-Force Coefficients for Configurations B2, B2S13, B2S13W4F7, B2W4T3F7, and B2S13W4T3F7	35
9. Comparison of Side-Force and Yawing-Moment Coefficients for Configurations B2, B2S13, B2S1W4F7, B2W4T3F7, and B2S13W4T3F7	39
10. Effect of Pitch Control Deflections on the Normal-Force and Pitching-Moment Coefficients of the Super HOBOS/MK-84	43
11. Effect of Pitch Control Deflections on the Rolling-Moment and Axial-Force Coefficients of the Super HOBOS/MK-84	48
12. Normal-Force Increment and Pitch Control Effectiveness for Several Pitch Control Deflections	53
13. Axial-Force Increment for Several Pitch Control Deflections	58
14. Effect of Roll Control Deflections on the Rolling-Moment and Axial-Force Coefficients of the Super HOBOS/MK-84	60
15. Roll Control Effectiveness for Several Roll Control Deflections	65
16. Effect of Yaw Control Deflections on the Side-Force and Yawing-Moment Coefficients of the Super HOBOS/MK-84	67
17. Side-Force Increment and Yaw Control Effectiveness for Several Yaw Control Deflections	72
18. Effect of Roll Control, $\delta p = -5$ deg, and Pitch Control, $\delta q = -10$ deg, Deflections on the Normal-Force and Pitching-Moment Coefficients of the Super HOBOS/MK-84	77
19. Effect of Roll Control, $\delta p = -5$ deg, and Pitch Control, $\delta q = -10$ deg, Deflections on the Rolling-Moment and Axial-Force Coefficients of the Super HOBOS/MK-84	82
20. Effect of Roll Control, $\delta p = -5$ deg, and Pitch Control, $\delta q = -15$ deg, Deflections on the Normal-Force and Pitching-Moment Coefficients of the Super HOBOS/MK-84	87
21. Effect of Roll Control, $\delta p = -5$ deg, and Pitch Control, $\delta q = -15$ deg, Deflections on the Normal-Force and Pitching-Moment Coefficients of the Super HOBOS/MK-84	92
22. Effect of Roll Control, $\delta p = -5$ deg, Pitch Control, $\delta q = -10$ deg, and Yaw Control, $\delta r = 5$ deg, Deflections on the Normal-Force and Pitching-Moment Coefficients of the Super HOBOS/MK-84	97

<u>Figure</u>	<u>Page</u>
23. Effect of Roll Control, $\delta p = -5$ deg, Pitch Control, $\delta q = -10$ deg, and Yaw Control, $\delta r = 5$ deg, Deflections on the Rolling-Moment and Axial-Force Coefficients of the Super HOBOS/MK-84	102
24. Effect of Roll Control, $\delta p = -5$ deg, Pitch Control, $\delta q = -10$ deg, and Yaw Control, $\delta r = 5$ deg, Deflections on the Side-Force and Yawing-Moment Coefficients of the Super HOBOS/MK-84	107
25. Effect of Pitch Control, $\delta q = -10$ deg, and Yaw Control, $\delta r = 5$ deg, Deflections on the Normal-Force and Pitching-Moment Coefficients of the Super HOBOS/MK-84	112
26. Effect of Combined Pitch Control, $\delta q = -10$ deg, and Yaw Control, $\delta r = 5$ deg, Deflections on the Side-Force and Yawing-Moment Coefficients of the Super HOBOS/MK-84	117
27. Effect of Pitch Control, $\delta q = -15$ deg, and Yaw Control, $\delta r = 5$ deg, Deflections on the Normal-Force and Pitching-Moment Coefficients of the Super HOBOS/MK-84	122
28. Effect of Pitch Control, $\delta q = -15$ deg, and Yaw Control, $\delta r = 5$ deg, Deflections on the Side-Force and Yawing-Moment Coefficients of the Super HOBOS/MK-84	127
29. Normal-Force Increment and Pitch Control Effectiveness for a Pitch Control Deflection of $\delta q = -10$ deg, Combined with Roll and Yaw Control Deflections	132
30. Normal-Force Increment and Pitch Control Effectiveness for a Pitch Control Deflection of $\delta q = -15$ deg, Combined with Roll and Yaw Control Deflections	137
31. Roll Control Effectiveness for a Roll Control Deflection of $\delta p = -5$ deg, Combined with Pitch and Yaw Control Deflections	142
32. Side-Force Increment and Yaw Control Effectiveness for a Yaw Control Deflection of $\delta r = 5$ deg, Combined with Roll and Pitch Control Deflections	144
33. Comparison of Normal-Force Increment Calculated from Single Flap and Multiple Flap Techniques	149
34. Comparison of Pitch Control Effectiveness Calculated from Single Flap and Multiple Flap Techniques	151
35. Comparison of Roll Control Effectiveness Calculated from Single Flap and Multiple Flap Techniques	153

<u>Figure</u>	<u>Page</u>
36. Comparison of Side-Force Increment Calculated from Single Flap and Multiple Flap Techniques	155
37. Comparison of Yaw Control Effectiveness Calculated from Single Flap and Multiple Flap Technique	157
38. Axial-Force Coefficients versus Mach Number	159
39. Control Surface Hinge-Moment Coefficients for Several Pitch Control Deflections	160
40. Vane Calibration Data, a_a versus a_v	165

TABLES

1. Summary of Model Configurations and Flap Deflections Tested	166
2. Summary of Nominal Test Conditions	167
3. Summary of Model Roll Angles Required for Single Flap Imaging	167
4. Summary of Data Precision	167

NOMENCLATURE	168
------------------------	-----

1.0 INTRODUCTION

Wind tunnel tests were conducted to determine the static stability, control effectiveness, and performance of a 0.25-scale model of the Super-HOBOS/MK-84 munition. The Super-HOBOS, also called the Electrical-Optical Guided Bomb-II (EOGB-II), is a high-speed air-launched glide weapon system that has evolved from the MK-84 HOBOS configuration. The Super-HOBOS has forward strakes, wings, and wing tips. The wing tips are deployed after aircraft carriage release. Control surfaces or flaps on the wings are used to provide aerodynamic pitch, yaw, and roll control of the vehicle.

The tests were conducted in the Aerodynamic Wind Tunnel (4T), Propulsion Wind Tunnel Facility (PWT) at Mach numbers from 0.4 to 1.6 and angles of attack from -4 to 26 deg. The effect of control flap deflections on static stability and control effectiveness of the Super-HOBOS configuration were determined. The control effectiveness characteristics were obtained by two techniques: one employing the conventional method of multiple flap deflections, and the other employing the technique of single flap deflections described in this report and Ref. 1. Also the hinge moments on the control surfaces were determined, and the calibration of a vane-type angle-of-attack indicator located on the model was accomplished during the test.

2.0 APPARATUS

2.1 TEST FACILITY

The Aerodynamic Wind Tunnel (4T) is a closed-loop, continuous flow, variable-density tunnel in which the Mach number can be varied from 0.1 to 1.3. Nozzle block inserts are used to obtain Mach numbers at 1.6 and 2.0. At all Mach numbers, the stagnation pressure can be varied from 300 to 3700 psfa. The test section is 4 ft square and 12.5 ft long with perforated, variable porosity (0.5- to 10-percent open) walls. It is completely enclosed in a plenum chamber from which the air can be evacuated, allowing part of the tunnel airflow to be removed through the perforated walls of the test section. A more thorough description of the tunnel may be found in Ref. 2.

2.2 TEST ARTICLE

The test article was a 0.25-scale model of the Super-HOBOS/MK-84 (EOGB-II) munition. Dimensions of the Super-HOBOS model configuration and its components are shown in Fig. 1. The Super-HOBOS configuration consists of three basic components which include a fuselage, strakes, and wing assemblies with four flap control surfaces. The basic fuselage configuration shown in Figs. 1a and c is a standard MK-84 bomb with the KMU-353X control and guidance kit and a boattail. The strakes and wing assembly are

shown in Figs. 1d and e, respectively. The flap geometry is shown in Fig. 1f, and deflection angles could be set at nominal values of 0, ± 5 , ± 10 , ± 15 , and ± 20 deg by a remote control system. Strain-gage balances were attached to the control flaps for measuring the hinge moments. A vane-type angle-of-attack indicator was calibrated on the Super-HOBOS model and is shown in Fig. 2. Photographs of the model installed in the wind tunnel are shown in Fig. 3.

2.3 INSTRUMENTATION

A six-component, internal strain-gage balance was used to obtain the aerodynamic forces and moments acting on the model. Four one-component strain-gage balances were used to determine the hinge moments on the control flaps. Four potentiometers were used to measure the angular position of the flap surfaces. The outputs from the potentiometers were used in a closed-loop control system to maintain a specified flap angle setting regardless of the load on the flap. The vane-type angle-of-attack indicator used a potentiometer to measure the angle of rotation of the vane shaft with respect to fuselage centerline. Four model base pressure measurements and one model cavity pressure measurement were made using differential pressure transducers. Electrical signals from the balances, potentiometers, pressure transducers, and standard tunnel instrumentation were processed by the PWT data acquisition system and digital computer for on-line data reduction.

3.0 TEST DESCRIPTION

3.1 GENERAL TEST PROCEDURES

Force and moment data were obtained by two procedures as follows:

1. The model angle of attack was varied at a constant Mach number, roll angle, and flap deflection.
2. The model roll angle was varied from -180 to 180 deg in 22.5-deg increments at a constant Mach number, angle of attack, and flap deflection.

Force and moment data were obtained with multiple flap deflections (four flaps) at Mach numbers from 0.4 to 1.6 for angles of attack from -4 to 26 deg using Procedure 1. Data were also obtained with a single flap deflection where flap number 1 was deflected to negative flap angles at Mach numbers from 0.65 to 1.05 for angles of attack of 0, 6, 12, 16, and 20 deg using Procedure 2.

The data are presented in the aeroballistic axis system. The orientation of the axis system, control flap numbering, and flap deflection sign convention is shown in Fig. 4.

A summary of the model configurations and flap deflections is shown in Table 1, and the test conditions are shown in Table 2.

3.2 MULTIPLE AND SINGLE FLAP TEST PROCEDURES

3.2.1 Multiple Flap Deflection Method

The cruciform flap configuration of the Super-HOBOS (KMU-353X control system) is governed by three control deflection equations and one control actuator equation as follows:

$$\delta p = (-\delta 1 - \delta 2 + \delta 3 + \delta 4)/4 \quad (1)$$

$$\delta q = (\delta 1 + \delta 2 + \delta 3 + \delta 4)/4 \quad (2)$$

$$\delta r = (-\delta 1 + \delta 2 - \delta 3 + \delta 4)/4 \quad (3)$$

$$\delta 1 + \delta 4 = \delta 2 - \delta 3 \quad (4)$$

These equations can be written in terms of the individual flap deflections required for a desired control deflection as follows:

$$\delta 1 = -\delta p + \delta q - \delta r \quad (5)$$

$$\delta 2 = -\delta p + \delta q + \delta r \quad (6)$$

$$\delta 3 = \delta p + \delta q - \delta r \quad (7)$$

$$\delta 4 = \delta p + \delta q + \delta r \quad (8)$$

The multiple flap deflection testing method is the conventional method in which all four flaps are positioned to produce a specified δp , δq , and δr as shown in Eqs. (5) through (8). The number of combinations of δp , δq , and δr utilized during the test for a particular configuration is normally dictated by the predicted maneuverability, load factors, trim conditions, and test time available.

The data obtained by the multiple flap deflection method during these tests were used to calculate the control effectiveness of the Super-HOBOS. The control effectiveness, in the context of this report, is defined as the incremental change in any aerodynamic coefficient per degree of control deflection attributable to a change in a particular control deflection from its previously undeflected position. The change in the aerodynamic coefficients between the deflected and undeflected control settings is calculated at corresponding Mach numbers, angles of attack, and roll angles. The change in the

coefficients is divided by the control deflection change to obtain the incremental change in the coefficients per degree of control deflection.

For example, the change in the pitching-moment coefficient per degree (pitch control effectiveness) attributable to a pitch control deflection, $C_{m\delta q}$, for a pitch control deflection of 5 deg would be calculated as follows:

$$C_{m\delta q} = \frac{\left[(C_{m,a})_{\delta q = 5} - (C_{m,a})_{\delta q = 0} \right]}{\delta q = 5} \bigg|_{\delta p, \delta r = 0} \quad (9)$$

The control effectiveness coefficients to be presented in Section 4.2 have been calculated in the preceding manner.

For combined control deflections involving pitch, yaw, and roll, the control effectiveness was evaluated between its value for a combined pitch, yaw, or roll control and its value when pitch, yaw, and roll control were zero. For example, when $\delta r = 5$ deg and $\delta q = -10$ deg, $C_{m\delta q}$ would be calculated as follows:

$$C_{m\delta q} = \frac{\left[(C_{m,a})_{\substack{\delta r = 5 \\ \delta q = -10}} - (C_{m,a})_{\substack{\delta r = 0 \\ \delta q = 0}} \right]}{\delta q = -10} \bigg|_{\delta p = 0} \quad (10)$$

All control effective coefficients for combined control deflections to be presented in Section 4.3 are calculated in this manner.

3.2.2 Single Flap Deflection Technique

The single flap deflection testing technique is a method wherein only one flap is deflected and control effectiveness data are obtained at various roll angles for a given Mach number and angle of attack. Using an imaging technique, only one flap need be deflected in only one direction to obtain all of the desired combinations of δp , δq , and δr . This method is particularly applicable to symmetric bodies with a cruciform tail arrangement. The method becomes questionable if there are protuberances on the body that would affect the control effectiveness of one or more flaps, but not all four flaps. Furthermore, if flap-to-flap interference occurs the imaging technique would be suspect. However, one of the objectives of the test was to determine if these adverse effects would preclude the use of the single flap technique on a configuration such as the Super-HOBOS. The results of these studies are presented in Section 4.4.

The method for calculating the control effectiveness using the single flap imaging technique for a negative deflection of flap number 1 is presented in the remainder of this section.

The incremental coefficient data for a single flap deflection is calculated by subtracting the coefficient data of the undeflected configuration from the corresponding coefficients of the configuration with a single flap deflected. For flap number 1, this is described by the following equation:

$$\text{DEI, } C_N = [(C_N)_{\delta 1=-x} - (C_N)_{\delta 1=0}] \text{ where } M_\infty, \dot{\phi}_a, \alpha_a = \text{constant} \quad (11)$$

This is the change in the aerodynamic coefficients (six equations to describe six components) for a given negative deflection of flap number 1 at a given Mach number, roll angle, and angle of attack.

It is assumed that the configuration has aerodynamic symmetry in the pitch and yaw planes at zero roll angle. This assumption permits the data that would be obtained by a negative deflection of flap number 2 to be idealized as the data obtained with a negative deflection of flap number 1 at a model roll angle of 90, since flap number 2 is located at a roll angle of 90 deg with respect to flap number 1. This can be written in equation form as

$$[\text{DEI, } C_N]_{\substack{\delta 2 = -x \\ \phi_a = 0}} = [\text{DEI, } C_N]_{\substack{\delta 1 = -x \\ \phi_a = 90}} \quad (12)$$

Likewise the data that would be obtained by a positive deflection of flap numbers 3 and 4 are idealized as the data obtained by a negative deflection of flap number 1 at model roll angles of 180 deg and -90 deg, respectively. The model roll angles required to obtain data for negative deflections of flap number 2 and positive deflections of flap numbers 3 and 4 using negative deflections of flap number 1 are shown in Fig. 5.

Thus far no imaging has been employed. The control effectiveness data for positive deflections of flap numbers 1 and 2 and negative deflections of flap numbers 3 and 4 are idealized by the control effectiveness data obtained using negative deflections of flap number 1 oriented in a roll position which is the mirror image of the desired deflection. A positive deflection of flap number 1 can be idealized as the mirror image of a negative deflection of flap number 1 at a model roll angle of -90 deg (see Fig. 6). The magnitudes of the incremental data are the same; however, the signs on the incremental aeroballistic side-force, yawing-moment, and rolling-moment coefficients must be changed. A positive deflection of flap number 2 can be idealized as the mirror image of a negative deflection of flap number 1 at a model roll angle of 180 deg. Likewise, a negative deflection of flap numbers 3 and 4 can be idealized as the mirror image of a negative deflection of flap number 1 at model roll angles of 90 and 0 deg, respectively. The model roll angles and signs on the incremental data required to image data using a negative deflection of flap number 1 are summarized in Table 3.

Once the incremental data have been obtained for all four flaps, the control effectiveness is obtained by adding the incremental contribution of each flap and dividing by the control deflection angle. This can be written in equation form as follows:

$$C_{m\delta q} = \left\{ [\text{DEL } C_{m,a}]_{\delta 1 = -x} + [\text{DEL } C_{m,a}]_{\delta 2 = -x} + [\text{DEL } C_{m,a}]_{\delta 3 = -x} + [\text{DEL } C_{m,a}]_{\delta 4 = -x} \right\} / \delta q = -x \text{ where } \alpha_a, M_\infty, \text{ and } \phi_a = \text{constant} \quad (13)$$

The total incremental data for combined flap deflections are obtained by adding the incremental data for each flap at the appropriate deflection angle. A description of the single flap and multiple flap techniques of data acquisition can be found in Ref. 1.

3.3 CORRECTIONS

The model angle of attack was corrected for tunnel flow angularity. The maximum correction applied to the data was 0.50 deg and is a function of Mach number. Balance and sting deflections caused by aerodynamic loads on the model were also accounted for in the data reduction to determine model angle of attack. Model tare corrections were also made to calculate the net aerodynamic forces on the model.

3.4 PRECISION OF MEASUREMENTS

The precision of the data presented which can be attributed to errors in the balance measurements and tunnel conditions were determined for a confidence level of 95 percent, and the values are presented in Table 4. The precision in setting Mach number was ± 0.005 . The Mach number variation in the test section occupied by the model was no greater than ± 0.002 for Mach numbers up to 0.95 and ± 0.01 for Mach numbers greater than 1.0. The uncertainty in the model angle of attack and angle of roll was ± 0.1 deg. The precision of the flap control surface deflections and vane angle-of-attack indicator was ± 0.2 deg.

4.0 RESULTS AND DISCUSSION

4.1 CONFIGURATION BUILDUP

The aerodynamic coefficients for various buildup stages of the Super HOBOS/MK-84 configuration are shown in Figs. 7 through 9. The normal-force and pitching-moment coefficients varied greatly for the different buildup stages as would be expected (Fig. 7). The addition of the strakes to the body alone (B2S13) produced a much larger increase in $C_{N,a}$ than the addition of the strake to the body with wings (B2S13W4T3F7) for all Mach numbers. In fact, adding the strakes when the wings were present produced little,

if any, contribution to the total normal-force coefficient. Thus, a loss of wing lift was indicated when the strakes were added to the vehicle. The strakes destabilized the vehicle as shown in $C_{m,a}$ versus $C_{N,a}$. The rolling-moment coefficient (Fig. 8) had a non-zero value for configurations with wing tips at $M_\infty = 0.65$ and 0.95 at the lower angles of attack. The model with wing tips (B2S13W4T3F7 or B2W4T3F7) should have been symmetrical and not produced any rolling-moment coefficients at the lower angles of attack. The non-zero value for C_q was felt to be a result of some asymmetries in the tips attributable to fabrication. Also, as shown in Fig. 8, the $C_{A,F}$ increased significantly when the wings, wing tips, and strakes were added, especially at the higher Mach numbers. The side-force and yawing-moment coefficients were approximately zero for the various buildup configurations at the lower angles of attack (Fig. 9); yaw control, δr deflection, would be required to trim the vehicle at angles of attack greater than 16 or 17 deg.

All the data presented in the following sections are for configuration B2S13W4T3F7 which is the Super HOBOS/MK-84.

4.2 CONTROL EFFECTIVENESS FOR PURE CONTROL DEFLECTIONS (MULTIPLE FLAP TECHNIQUE)

The aerodynamic coefficients for several values of flap deflections in pitch, δq , are shown in Figs. 10 and 11. The data show (Fig. 10) that the Super HOBOS/MK-84 was neutrally or slightly stable for all δq flap deflections in the 0 - to 10 -deg angle-of-attack range at the lower Mach numbers. The longitudinal stability increased with Mach number, attaining a static margin of approximately $-0.45d$ at $M_\infty = 1.6$. The rolling-moment coefficients showed only a slight variation for different δq at the lower angles of attack, but changed significantly at the higher angles of attack (Fig. 11). The forebody axial-force coefficient increased with increasing δq (Fig. 11) as would be expected.

The normal-force increments and pitch control effectiveness are shown in Fig. 12 for several values of δq . In general, $C_{N_{\delta q}}$ and $C_{m_{\delta q}}$ increased for a $\delta q = -5$ to -10 deg and decreased for a $\delta q = -15$ to -20 deg at $M_\infty = 0.4$ and 0.65 . For $M_\infty = 0.95$, there was a large decrease in longitudinal control parameters for $\delta q = -5$ as compared with $\delta q = -5$ for other Mach numbers and as compared with other δq 's at $M_\infty = 0.95$. At the higher Mach numbers, $C_{N_{\delta q}}$ and $C_{m_{\delta q}}$ showed less change with δq especially at $M_\infty = 1.6$.

The axial-force increments are shown in Fig. 13 for several pitch control deflections. The axial-force increments increased with increasing δq 's as would be expected.

The rolling-moment and forebody axial-force coefficients for several values of δp are shown in Fig. 14. Both coefficients increased in absolute values with increasing δp 's as would be expected.

The roll control effectiveness coefficients are shown in Fig. 15. For $M_\infty = 0.4$ and 0.65 , $C_{l_{\delta p}}$ decreased with increasing δp , starting from a δp of -5 deg. Whereas for $M_\infty = 0.95$, $C_{l_{\delta p}}$ increased for a δp of -5 to -15 deg, then decreased for a δp of -20 deg. The changes in roll control effectiveness with changes in δp were small for $M_\infty = 1.2$ and 1.6 .

The side-force and yawing-moment coefficients for several values of δr are shown in Fig. 16. The coefficients increased in absolute value with increasing δr as would be expected.

The side-force increments and yaw control effectiveness are shown in Fig. 17. For $M_\infty = 0.4$ and 0.65 , $C_{Y_{\delta r}}$ and $C_{n_{\delta r}}$ generally tended to decrease with increasing δr , starting with a δr of 5 deg. For $M_\infty = 0.95$, however, the directional control parameters increased for a δr of 5 to 15 deg, then decreased for a $\delta r = 20$ deg. For $M_\infty = 1.2$ and 1.6 the changes in $C_{Y_{\delta r}}$ and $C_{m_{\delta r}}$ were small with changes in δr .

4.3 CONTROL EFFECTIVENESS FOR COMBINED CONTROL DEFLECTIONS (MULTIPLE FLAP TECHNIQUE)

The effect of combined pitch and roll control deflections on the aerodynamic coefficients of the Super HOBOS is shown in Figs. 18 through 21. The effect of superimposing roll control on pitch control with regard to the normal-force and pitching-moment coefficients was small when compared with pure pitch control as shown in Figs. 18 and 20. If anything, some small decrease occurred in $C_{m,a}$ when δp was added to δq . The rolling-moment coefficient for $M_\infty = 0.4$ and 0.65 showed a marked decrease in absolute value at the lower angles of attack for combined pitch and roll deflections as compared with just roll deflections (Figs. 19 and 21). For $M_\infty \geq 0.95$, the absolute value of the rolling-moment coefficient increased significantly for combined pitch and roll control deflections at positive angles of attack. At negative angles of attack the opposite is true.

The effect of combined pitch, roll, and yaw control deflections on the aerodynamic coefficients of the Super HOBOS is shown in Figs. 22 through 24. As shown in Fig. 22, the effect of combined pitch, roll and yaw control on the normal-force and pitching-moment coefficients was small. However, the effect on the rolling-moment coefficient was the same as mentioned above and tended to decrease the absolute values for $M_\infty = 0.4$ and 0.65 and increase the values for $M_\infty \geq 0.95$ for positive angles of attack (Fig. 23). The side-force and yawing-moment coefficients showed an increase in absolute values attributable to the effect of combining pitch, roll, and yaw control as compared with pure yaw control, particularly at the higher Mach numbers, $M_\infty \geq 0.95$ (Fig. 24).

The effect of combined pitch and yaw control deflections on the aerodynamic coefficients is shown in Figs. 25 through 28. Again, the effect of superimposing yaw control on pitch control with regard to the normal-force and pitching-moment coefficients was small when compared with pure pitch control (Figs. 25 and 27). The effect of combined pitch and yaw control on the side-force and yawing-moment coefficients at $M_\infty = 0.4$ and 0.65 was to decrease the absolute values when compared to pure yaw control (Figs. 26 and 28), especially for a combined δq of 15 deg and δr of 5 deg (Fig. 28). For $M_\infty \geq 0.95$, the effect of combined pitch and yaw control on the side-force and yawing-moment coefficient was the same as mentioned earlier and tended to increase their absolute values as compared to pure yaw control.

The control effectiveness coefficients for combined control deflections are shown in Figs. 29 through 32. Figure 29 shows the influence of roll and/or yaw control added to a pitch control of $\delta q = -10$ deg on the normal-force increment and pitch control effectiveness. As shown in the figure, the combined control deflections caused a 20- to 30-percent decrease in both $C_{N_{\delta q}}$ and $C_{m_{\delta q}}$ at the lower Mach numbers as compared with a pure pitch control of $\delta q = -10$ deg. Figure 30 shows the effect of roll or yaw control added to a pitch control of $\delta q = -15$ deg on $C_{N_{\delta q}}$ and $C_{m_{\delta q}}$. Again, the combined control deflections showed a decrease of approximately 10 percent in the longitudinal control parameters at the lower Mach numbers.

The effect of pitch and/or yaw control added to a roll control of $\delta p = -5$ deg on the roll control effectiveness is shown in Fig. 31. As shown in the figure, the influence of both pitch and/or yaw control deflections added to a roll control deflection of $\delta p = -5$ deg was to significantly decrease the value of the roll control effectiveness at $M_\infty = 0.4$ and 0.65 when compared with a pure roll control of $\delta p = -5$ deg. The reduction of $C_{l_{\delta p}}$ was particularly severe for $\delta q = -15$ deg at negative angles of attack at the lower Mach numbers. At the higher Mach numbers, $M_\infty \geq 0.95$, the effect of combined control deflections was to increase $C_{l_{\delta p}}$ at the positive angles of attack when compared with a pure roll control of $\delta p = -5$ deg. The opposite was true for the negative angles of attack at $M_\infty \geq 0.95$.

The effect of pitch and/or roll control added to a yaw control of $\delta r = 5$ deg on the side-force increments and yaw control effectiveness is shown in Fig. 32. In general, the effect of combining pitch and/or roll control with yaw control was to significantly decrease $C_{Y_{\delta r}}$ and $C_{n_{\delta r}}$ at $M_\infty = 0.4$ and 0.65, particularly at the lower angles of attack, when compared with a pure yaw control of $\delta r = 5$ deg. At the higher Mach numbers, $M_\infty \geq 0.95$, the effect of adding pitch and/or roll control with yaw control was to increase the absolute values of $C_{Y_{\delta r}}$ and $C_{n_{\delta r}}$ when compared with a pure yaw control of $\delta r = 5$ deg, except for a $\delta q = -15$ deg at negative angles of attack.

4.4 COMPARISON OF CONTROL EFFECTIVENESS DATA OBTAINED BY SINGLE FLAP AND MULTIPLE FLAP TECHNIQUES

The control effectiveness coefficients presented in this section were obtained using negative deflections on flap number 1 (single flap technique) and negative or positive deflections of all four flaps (multiple flap technique). The procedure and data reduction technique have been presented earlier in Section 3.2.

The comparisons of the control effectiveness coefficients obtained by single flap and multiple flap techniques are shown in Figs. 33 through 37. As shown in the figures, the comparisons do not agree. The control effectiveness coefficients obtained by the single flap technique were significantly less than those obtained by the multiple flap technique. The best agreement between data obtained by single flap and multiple flap techniques was the roll control effectiveness at $M_\infty = 0.65$ (Fig. 35). Also, all the control effectiveness data agreed better at $M_\infty = 0.65$ than 0.95.

The large differences between data obtained using the single flap and multiple flap techniques may have been the result of a combination of several effects including balance inaccuracies, flap-setting errors, flap-to-body interference, and flap-to-flap interference. It should be noted that the uncertainties in the coefficient data were larger when only one flap was deflected (single flap technique). One reason for this was that the data were obtained by adding the four incremental contributions at each fin location as shown in Eq. (16), and this adding of the incremental data could have increased the uncertainties by a factor of four. Also the incremental force attributable to the fin deflection only is normally very small when compared with the gross balance force and is one-fourth or less of the increment obtained by deflecting all four fins. However, the moment data should not be affected to the same degree as the force data since the moment arms caused by fin deflection are large enough to give good balance resolution for relatively small forces.

Previous tests using this technique (Ref. 1) did not produce results that exhibited such a large discrepancy. However, the previous data were obtained using smaller flaps with the same size body diameter. The problem herein appears to have been a result of flap-to-flap interference and was worse when using δq controls where flap numbers 1 and 4 ($-\delta q$) were positioned toward each other. The same was true for δr control where flap numbers 3 and 4 were positioned together. The best agreement occurred when all flaps were positioned away from each other as was the case for δp control.

4.5 AXIAL-FORCE DATA

The axial-force and forebody axial-force coefficients versus Mach number for $\alpha = 0$ arc presented in Fig. 38 for Super HOBOS/MK-84 configuration B3S13W4T3F7. As

shown in the figure, the drag rise began at approximately $M_\infty = 0.90$, reached a maximum C_A of 1.02 at $M_\infty = 1.05$, and remained fairly constant up to $M_\infty = 1.60$.

4.6 CONTROL FLAP HINGE-MOMENT COEFFICIENTS

The control surface hinge-moment coefficients for flap numbers 1 and 2 are presented in Fig. 39 for several pitch control deflections. The hinge-moment coefficients generally remained constant or increased with angle of attack for $M_\infty = 0.4$ and 0.65, except for $\delta q = -20$ deg where the coefficient first decreased, then increased with α_a . Also, the center of pressure was forward of the hinge line, producing aiding moments for $M_\infty = 0.4$ and 0.65, except for zero control deflections and the higher angles of attack for $\delta q = -5$ deg. For $M_\infty = 0.95$, the hinge-moment coefficients increased significantly with angle of attack except for $\delta q = -20$ deg where the coefficients decreased slightly with α_a . The center of pressure was forward of the hinge line at the lower angles of attack for $M_\infty = 0.95$ and aft of the hinge line at the higher angles of attack. For the higher Mach numbers, $M_\infty \geq 1.2$, the hinge-moment coefficients generally decreased with angle of attack and the center of pressure was always aft of the hinge line except for no control deflections ($\delta q = 0$). These hinge-moment coefficients are typical of those obtained with flap numbers 3 and 4 and of those obtained for various other flap control deflections. The maximum hinge-moment coefficient was approximately 0.031 and occurred at $M_\infty = 1.6$. For full-scale conditions where the reference area equals 1.76 ft², the reference diameter equals 1.5 ft, and the dynamic pressure equals approximately 500 psf, the maximum hinge moment would be 500 in.-lb. For subsonic flow the maximum hinge-moment coefficient was approximately 0.020 which would give a hinge-moment torque of 300 in.-lb at full-scale conditions.

4.7 CALIBRATION DATA OF VANE ANGLE-OF-ATTACK INDICATOR

The calibration data for the vane angle-of-attack indicator are presented in Fig. 40. The slope of the calibration curve, α_a versus α_v , was fairly linear at the lower angles of attack for all Mach numbers. The slope remained approximately constant with Mach number for $M_\infty \leq 0.85$ and increased for $M_\infty = 0.95$ to 1.2. The α_a intercept for the calibration curve varied somewhat with Mach number, but the intercept was negative for $M_\infty \leq 0.85$ and 1.6 and was positive for $M_\infty = 0.95$ to 1.2.

5.0 SUMMARY OF RESULTS

The results of this wind tunnel test of a 0.25-scale model of the Super HOBOS/MK-84 (EOGB-II) munition are summarized as follows:

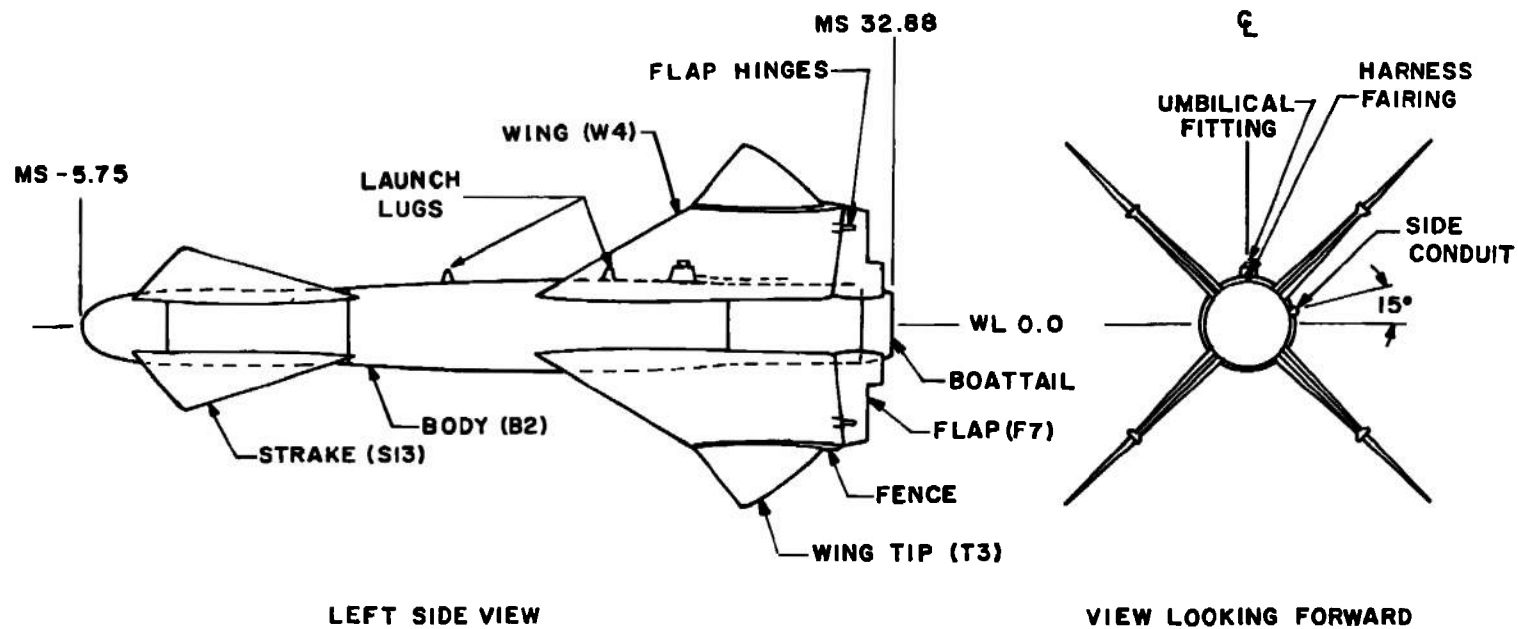
1. The control effectiveness obtained for pitch, yaw, or roll control deflections showed no anomalies except at a Mach number of 0.95 and a control

deflection of -5 deg where the control effectiveness in either pitch, roll, or yaw showed a large loss compared with results at other Mach numbers and control settings.

2. The effect of adding roll and/or yaw control deflections to a pitch control deflection was to decrease the normal-force increments and pitch control effectiveness coefficients.
3. The effect of adding pitch and/or yaw control deflections to a roll control deflection was to significantly decrease the roll control effectiveness for Mach numbers 0.4 and 0.65 and to increase the roll control effectiveness for Mach number ≥ 0.95 at positive angles of attack.
4. The effect of adding pitch and/or roll control deflections to a yaw control deflection was to significantly decrease the side-force increment and yaw control effectiveness coefficients for Mach numbers 0.4 and 0.65 and to increase these coefficients for Mach numbers ≥ 0.95 at positive angles of attack.
5. The agreement between the control effectiveness coefficients obtained by single flap and multiple flap techniques was not satisfactory and is believed to be a consequence of flap-to-flap interference.
6. The hinge-moment coefficients show some variation with angle of attack, especially at Mach number 0.95 and, in general, the center of pressure on the flaps was forward of the hinge line for the lower Mach numbers, ≤ 0.95 , and aft of the hinge line for the higher Mach numbers.
7. The angle-of-attack vane calibration data were linear with angle of attack up to 10 deg and indicated a small negative angle offset for Mach numbers ≤ 0.85 and 1.6 and a small positive angle offset for Mach numbers 0.95 to 1.2.

REFERENCES

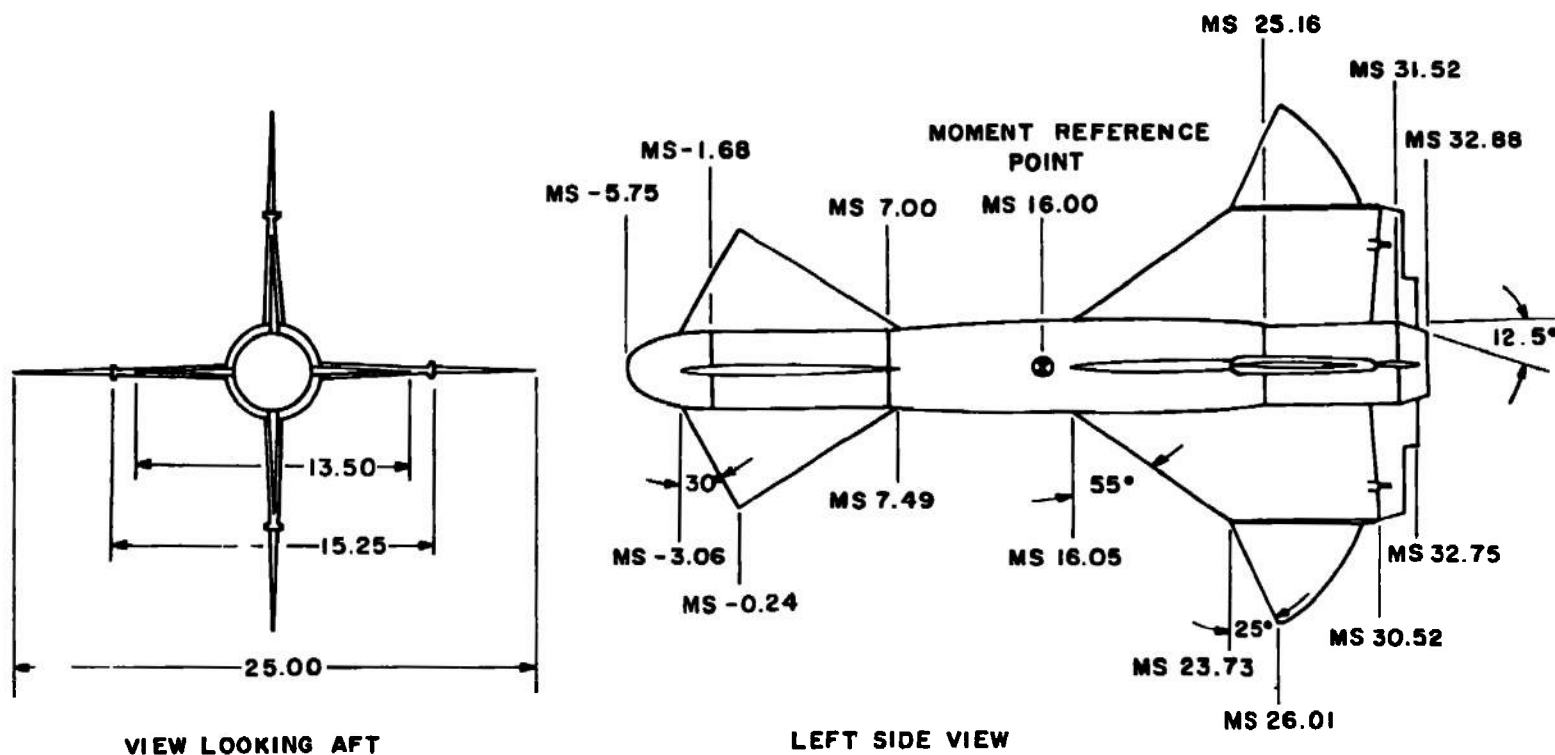
1. Webb, J. A., Whoric, J. M., and Rittenhouse, L. E. "Aerodynamic Coefficients for the Pavestorm II Weapon Configuration Using Multiple and Single Fin Deflection Techniques." AEDC-TR-74-00, to be published.
2. Test Facilities Handbook (Tenth Edition). "Propulsion Wind Tunnel Facility, Vol. 4." Arnold Engineering Development Center, May 1974.



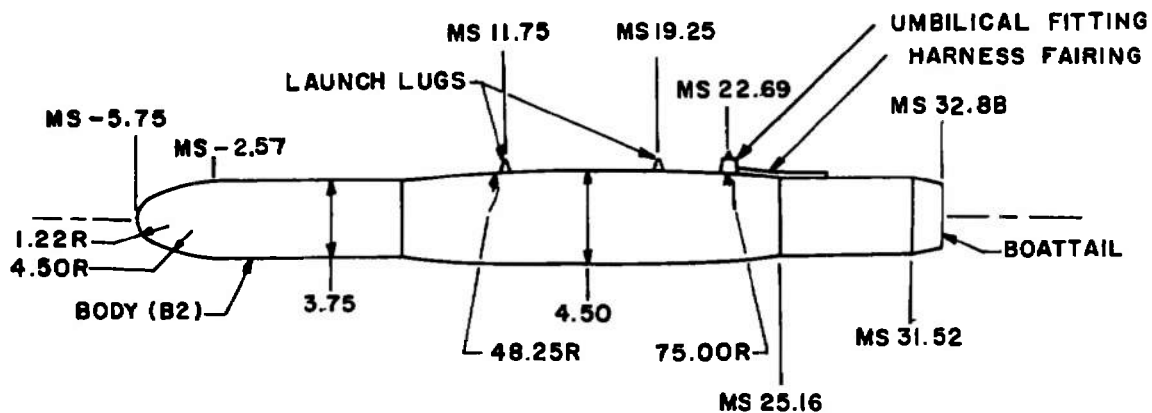
ALL DIMENSIONS IN INCHES

a. Basic model geometry, $\phi = 0$

Figure 1. Details and dimensions of the Super HOBOS/MK-84 model.

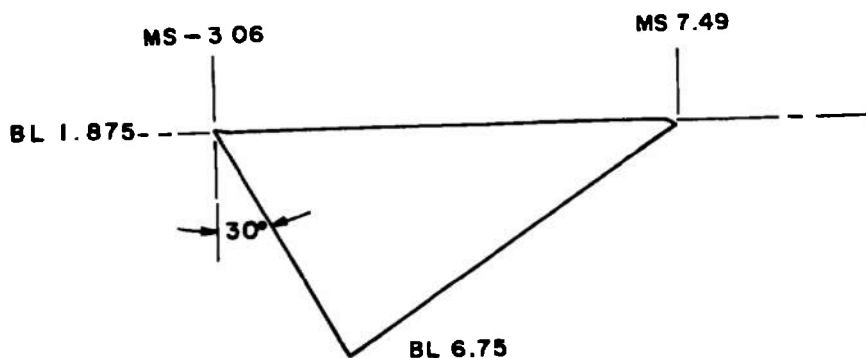


b. Basic model geometry, $\phi = 45$ deg
Figure 1. Continued.



ALL DIMENSIONS IN INCHES

c. Fuselage geometry (B2)

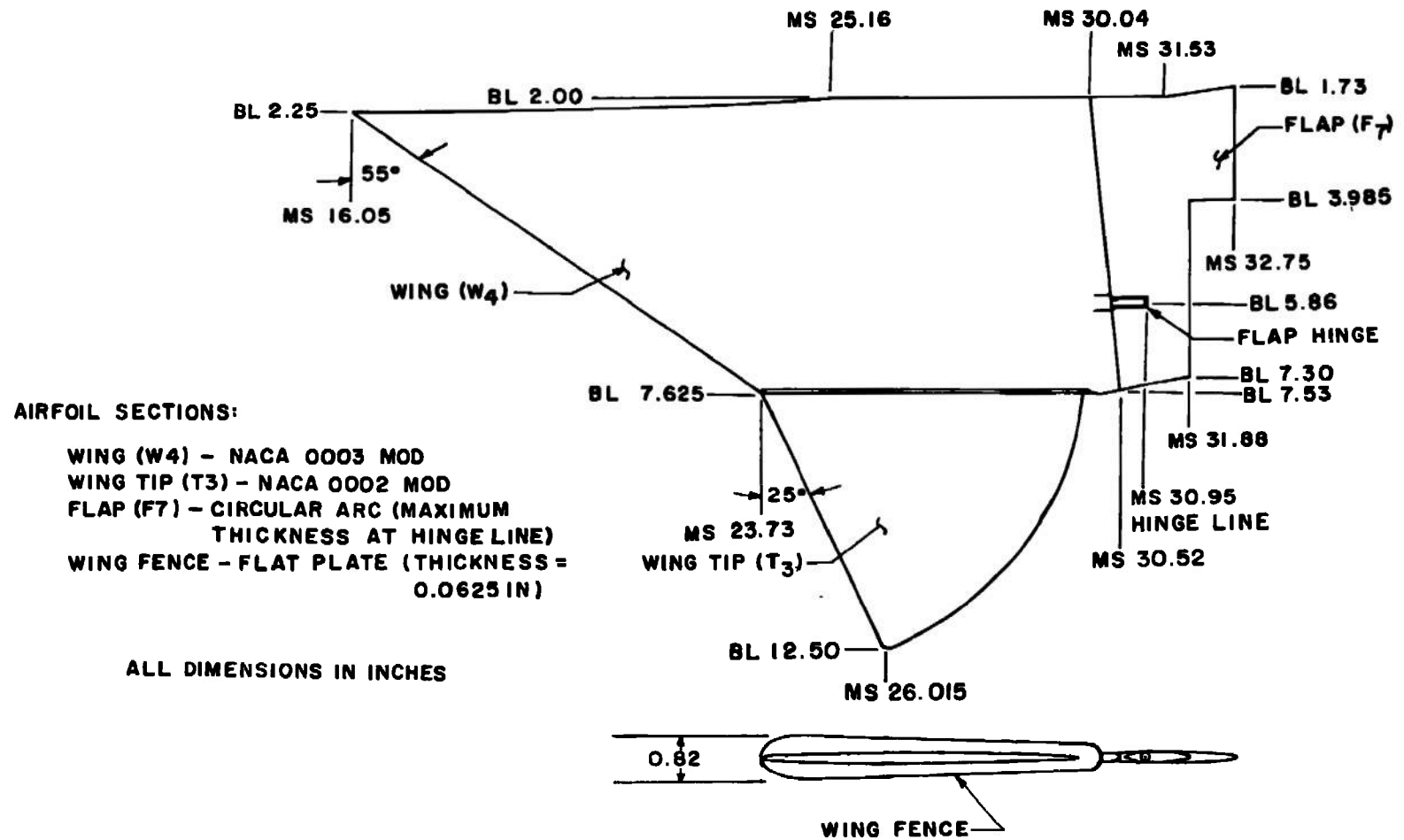


AIRFOIL SECTION - NACA 0003 MOD

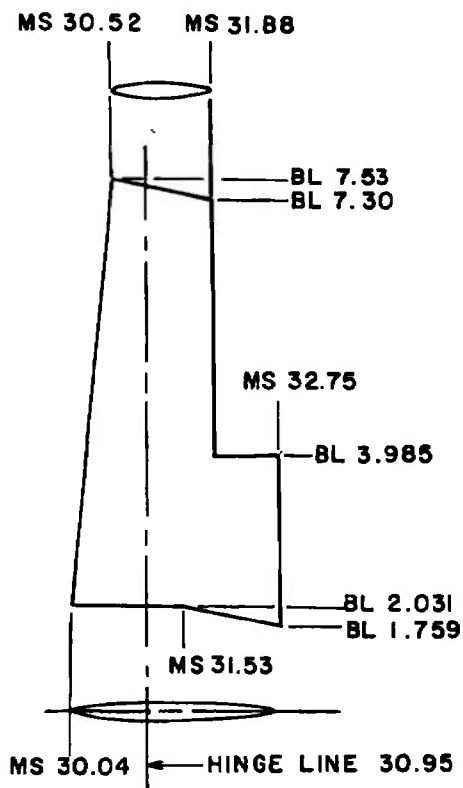
STRAKE (S13)

ALL DIMENSIONS IN INCHES

d. Strake (S13)
Figure 1. Continued.



e. Wing assembly geometry
Figure 1. Continued.



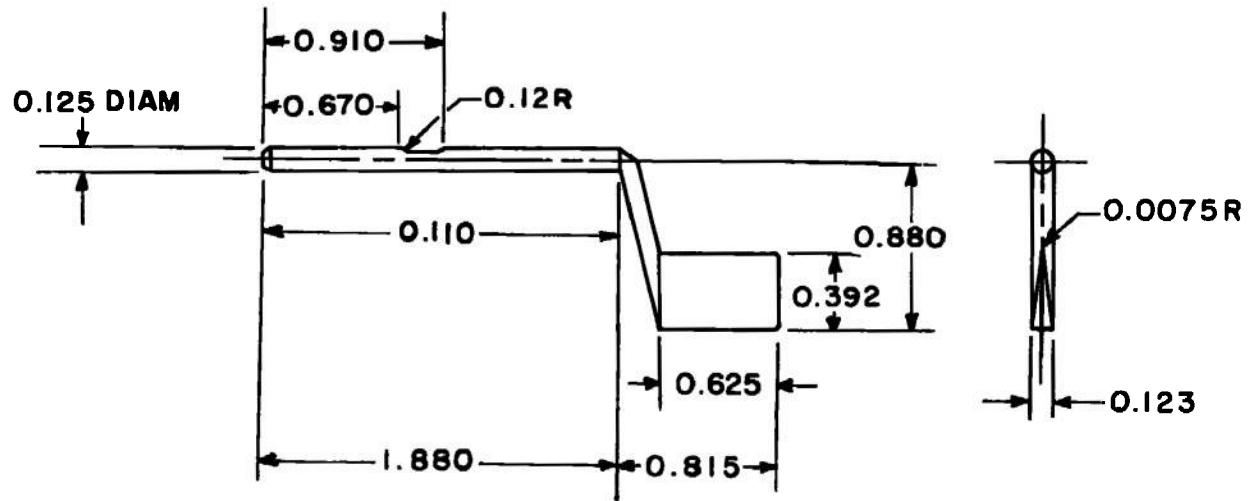
AIRFOIL SECTION - CIRCULAR ARC (MAXIMUM THICKNESS OVER CHORD
LENGTH = 0.10 IN AT HINGE LINE FOR
BOTH ROOT CHORD AND TIP CHORD)

FLAP (F7)

ALL DIMENSIONS IN INCHES

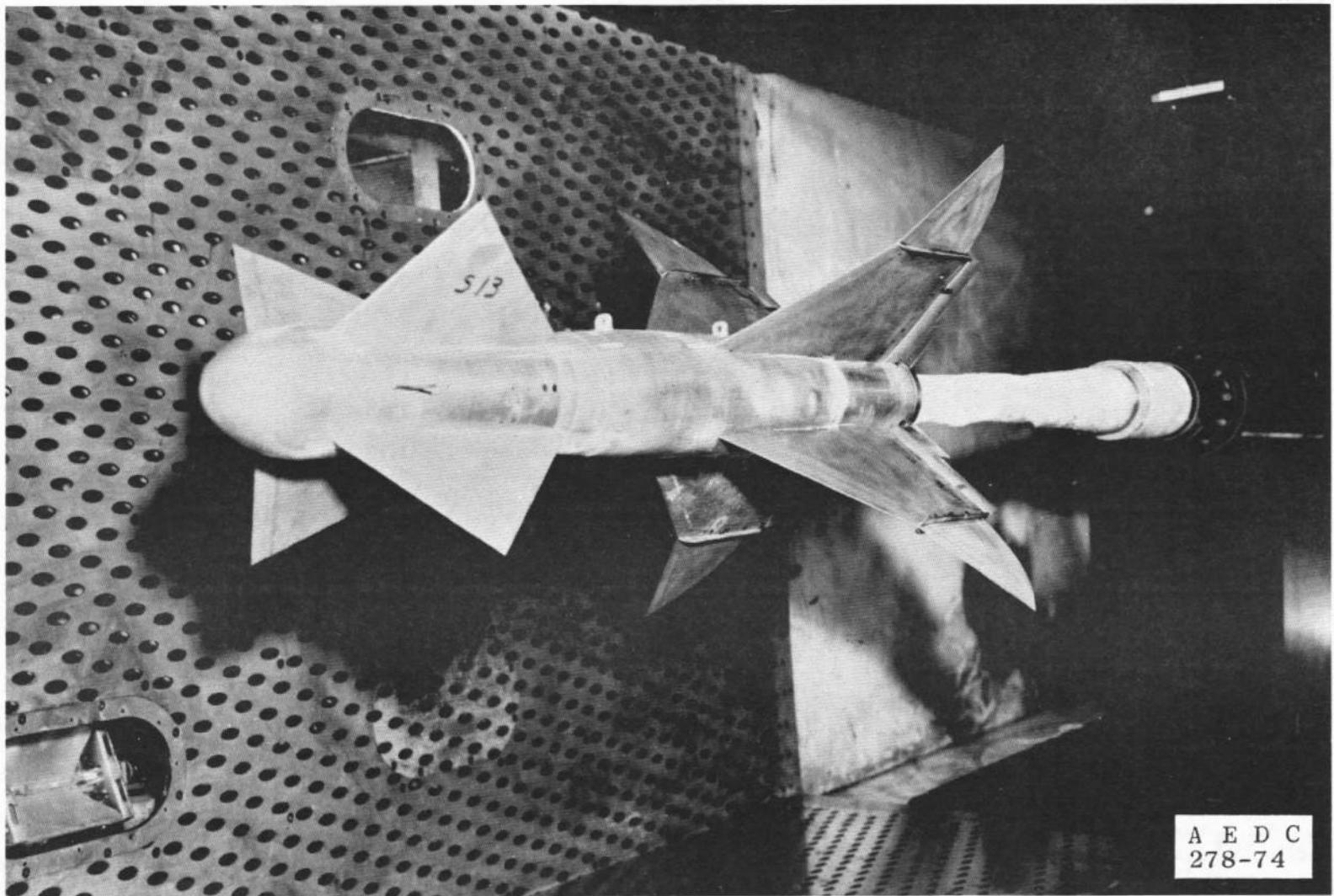
f. Flap (F7)

Figure 1. Concluded.



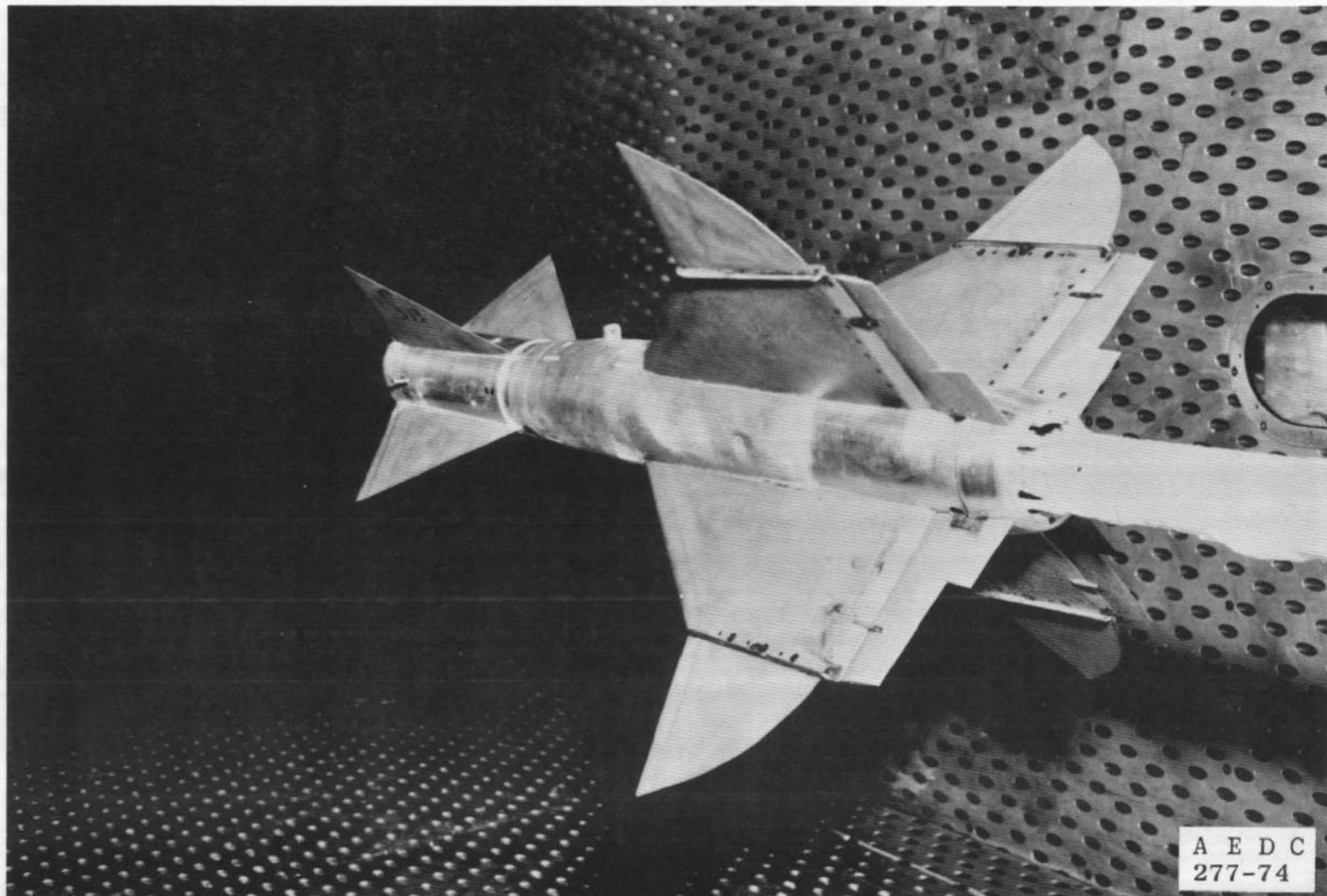
ALL DIMENSIONS IN INCHES

Figure 2. Details and dimensions of the vane-type angle-of-attack indicator.

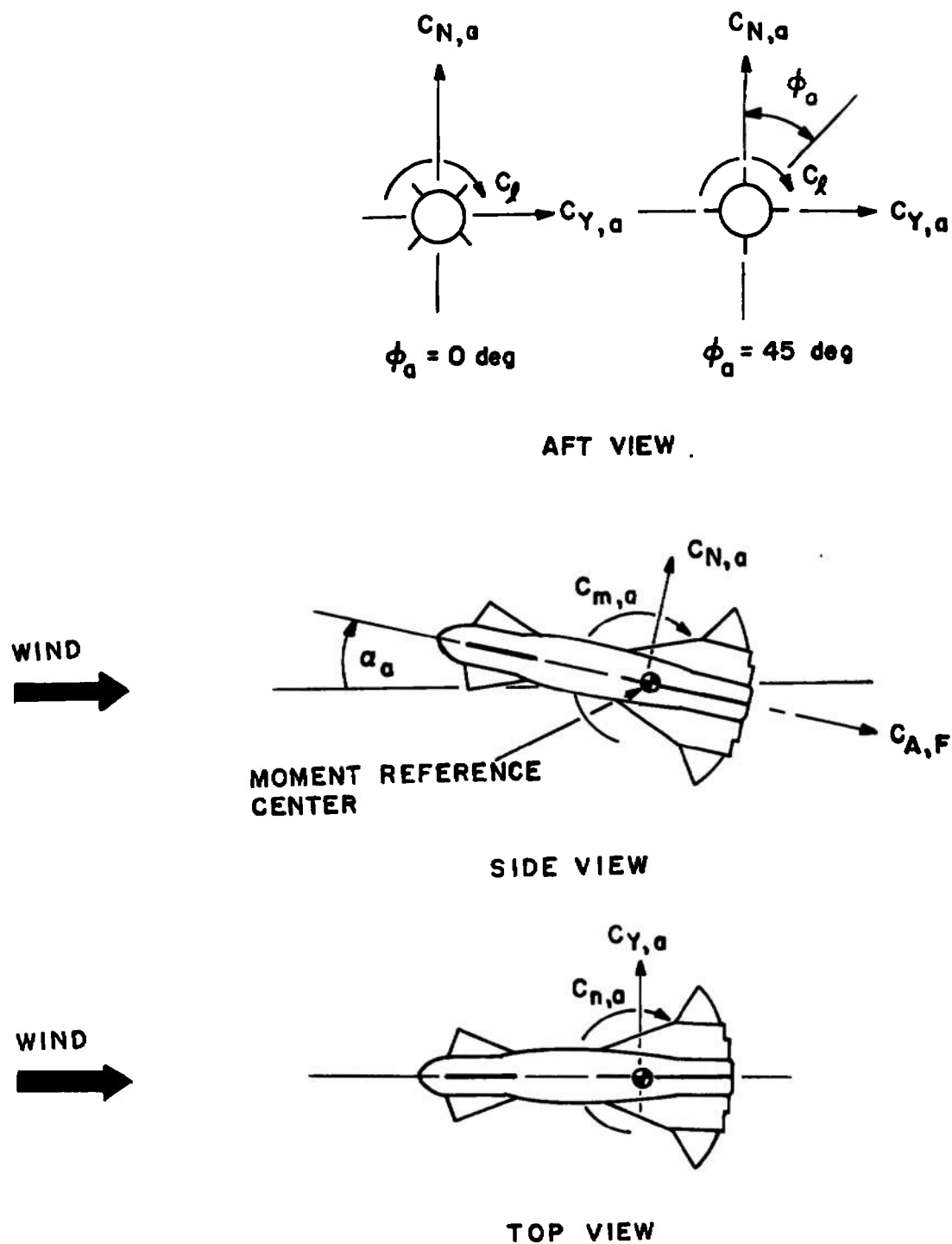


a. Front view

Figure 3. Photographs of the test model.

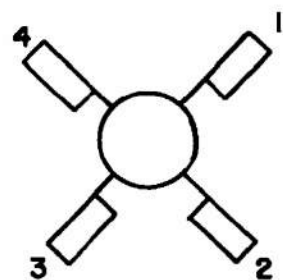


b. Aft view
Figure 3. Concluded.

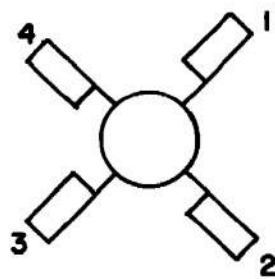


a. Orientation of model forces and moments

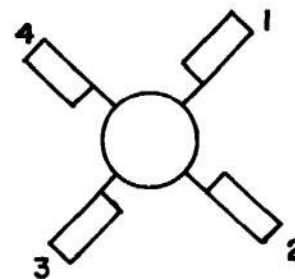
Figure 4. Orientation of model forces and moments and control flap deflections.

 δq

PITCH CONTROL

 δr

YAW CONTROL

 δp

ROLL CONTROL

AFT VIEW
ZERO ROLL ANGLE

b. Control flap deflections
Figure 4. Concluded.

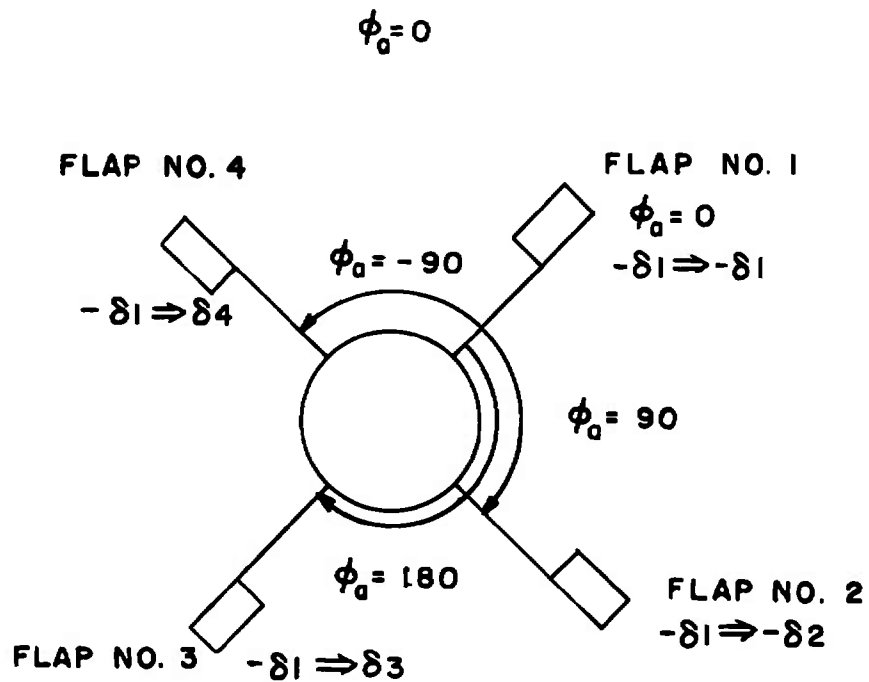


Figure 5. Model roll angles required to obtain negative deflections of flap number 2 and positive deflections of flap numbers 3 and 4 using negative deflections of flap number 1.

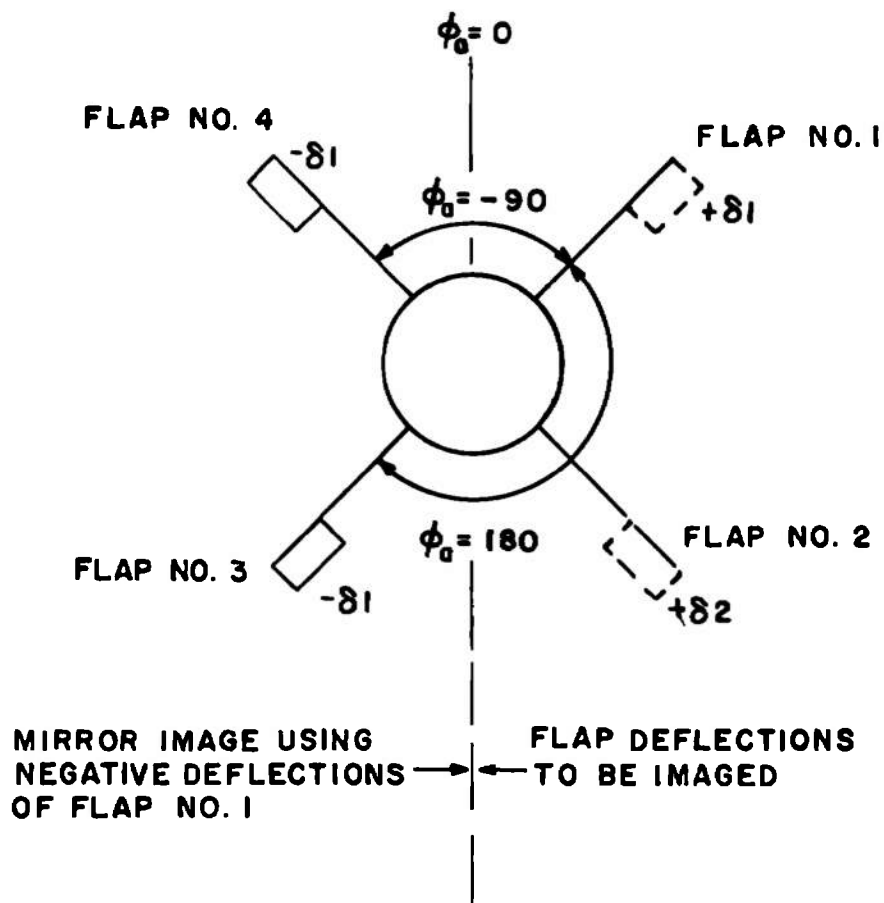


Figure 6. Model roll angles required to obtain mirror images of positive deflections of flap numbers 1 and 2 using negative deflections of flap number 1.

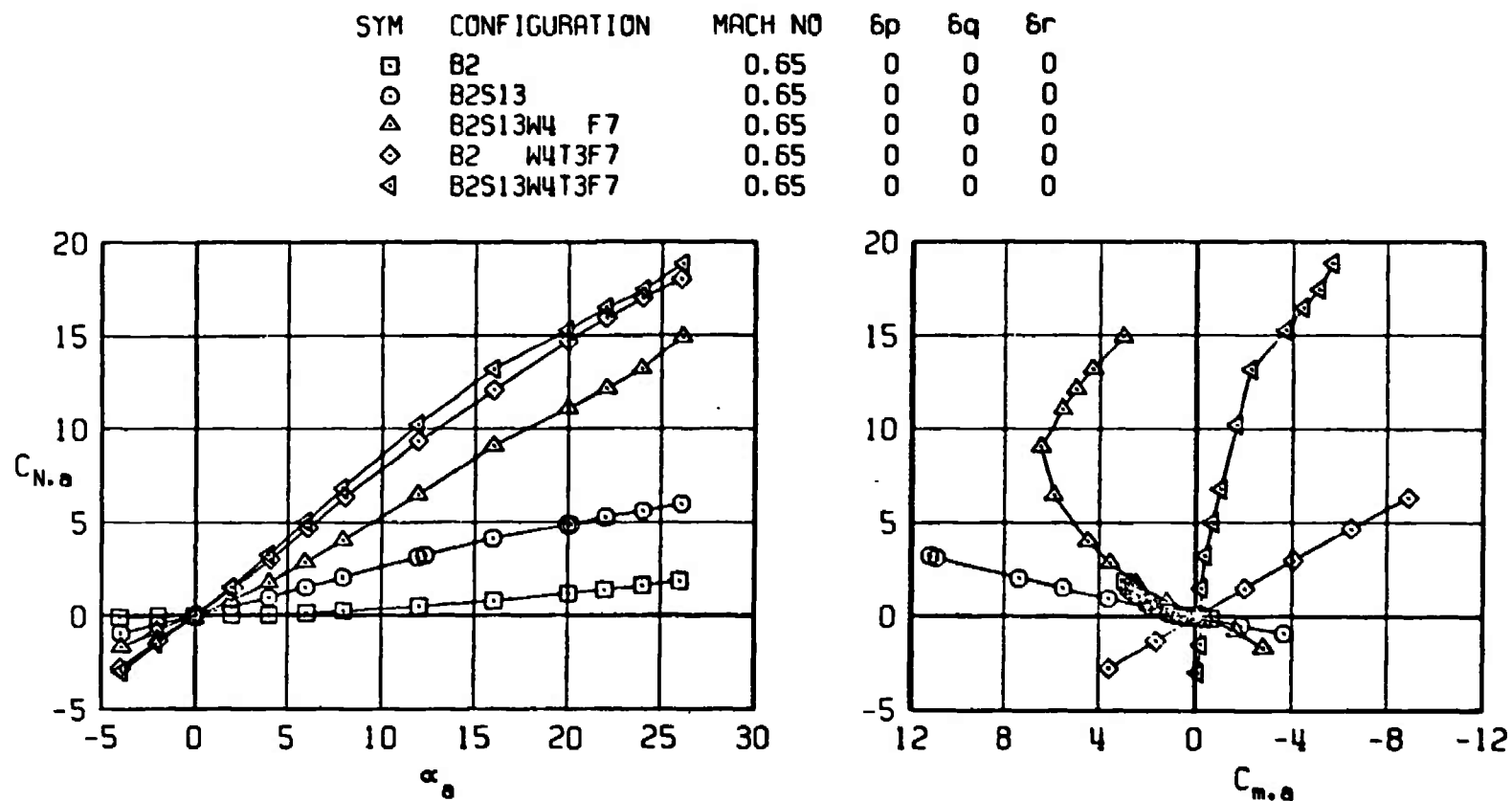


Figure 7. Comparison of normal-force and pitching-moment coefficients for configurations B2, B2S13, B2S13W4F7, B2W4T3F7, and B2S13W4T3F7.

SYM	CONFIGURATION	MACH NO	δp	δq	δr
□	B2	0.95	0	0	0
○	B2S13	0.95	0	0	0
△	B2S13W4 F7	0.95	0	0	0
◇	B2 W4T3F7	0.95	0	0	0
◁	B2S13W4T3F7	0.95	0	0	0

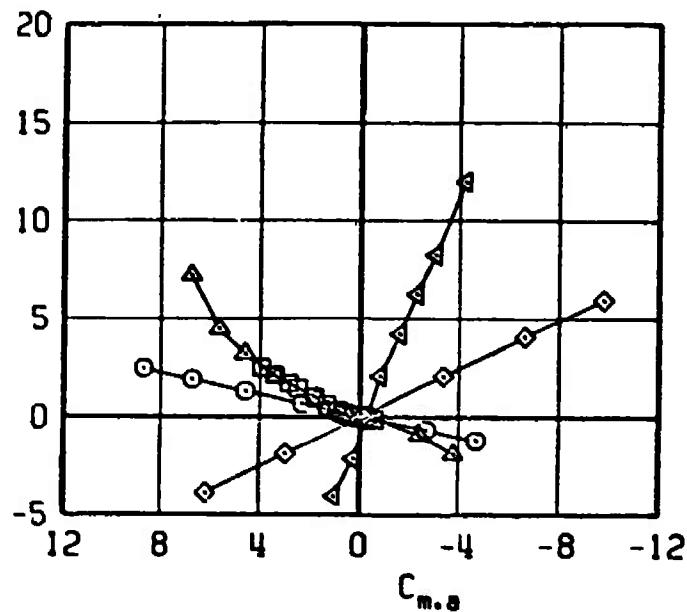
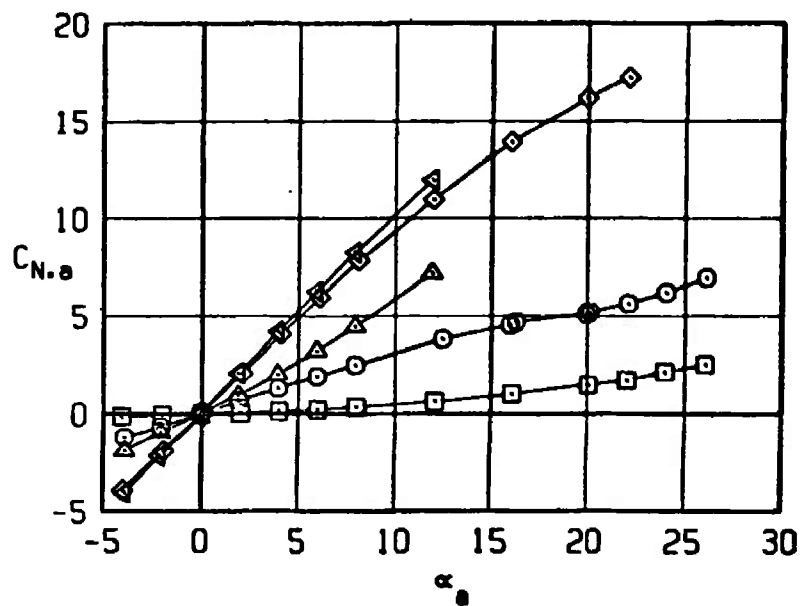


Figure 7. Continued.

SYM	CONFIGURATION	MACH NO	δp	δq	δr
□	B2	1.20	0	0	0
○	B2S13	1.20	0	0	0
△	B2S13W4 F7	1.20	0	0	0
◇	B2 W4T3F7	1.20	0	0	0
◁	B2S13W4T3F7	1.20	0	0	0

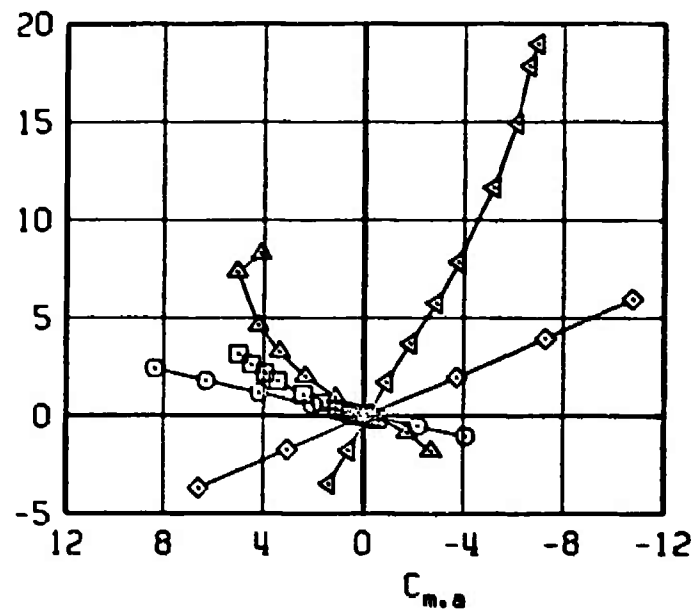
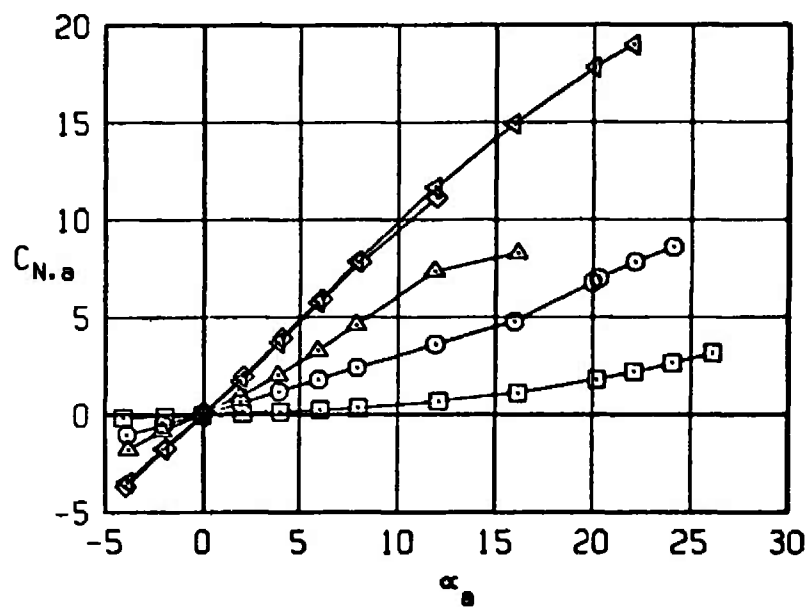


Figure 7. Continued.

SYM	CONFIGURATION	MACH NO	δp	δq	δr
□	B2	1.60	0	0	0
○	B2S13	1.60	0	0	0
△	B2S13W4 F7	1.60	0	0	0
◇	B2S13W4T3F7	1.60	0	0	0

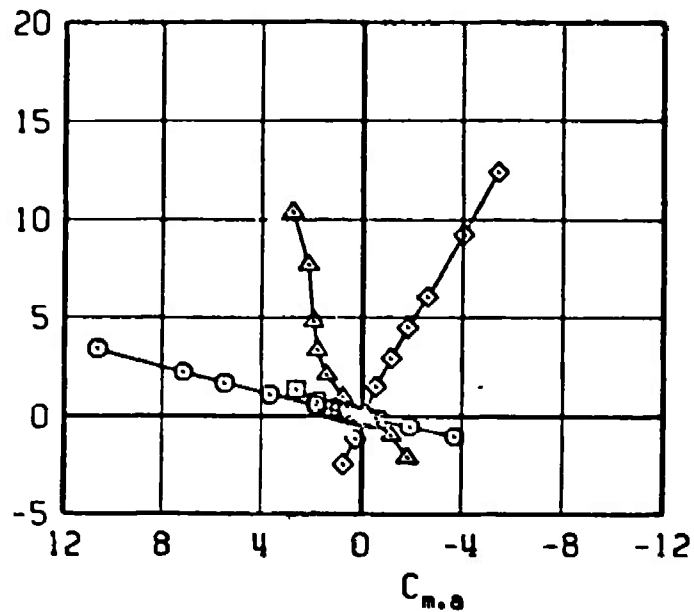
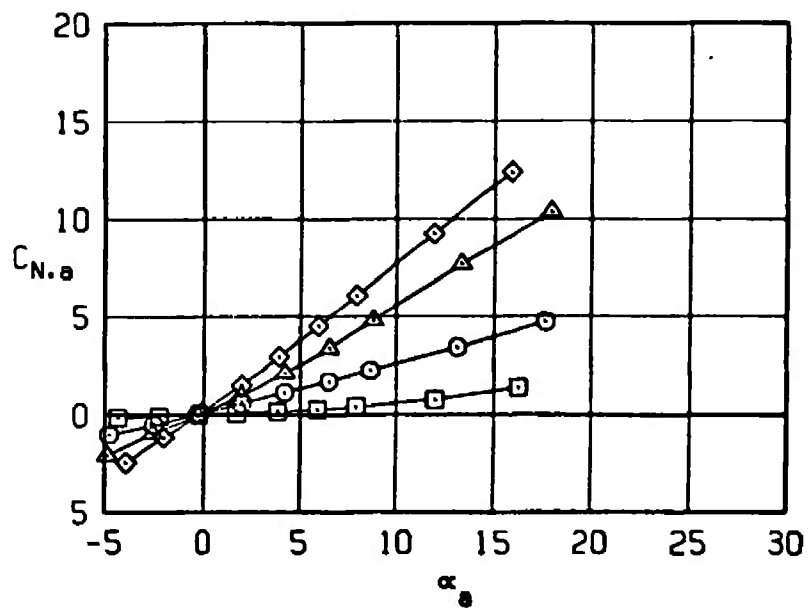


Figure 7. Concluded.

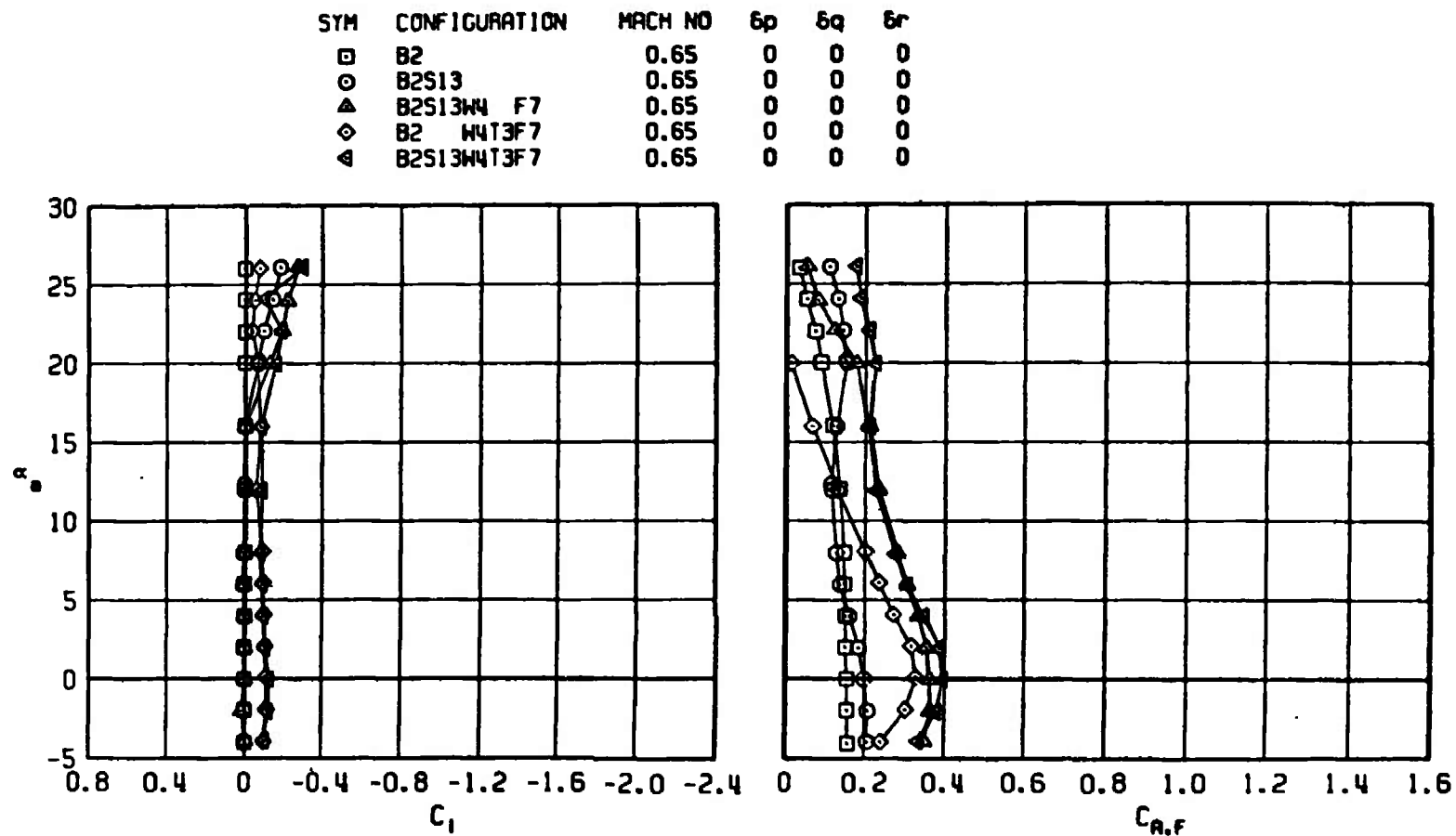


Figure 8. Comparison of rolling-moment and axial-force coefficients for configurations B2, B2S13, B2S13W4F7, B2W4T3F7, and B2S13W4T3F7.

SYM	CONFIGURATION	MACH NO	δp	δq	δr
□	B2	0.95	0	0	0
○	B2S13	0.95	0	0	0
△	B2S13W4 F7	0.95	0	0	0
◇	B2 W4T3F7	0.95	0	0	0
◀	B2S13W4T3F7	0.95	0	0	0

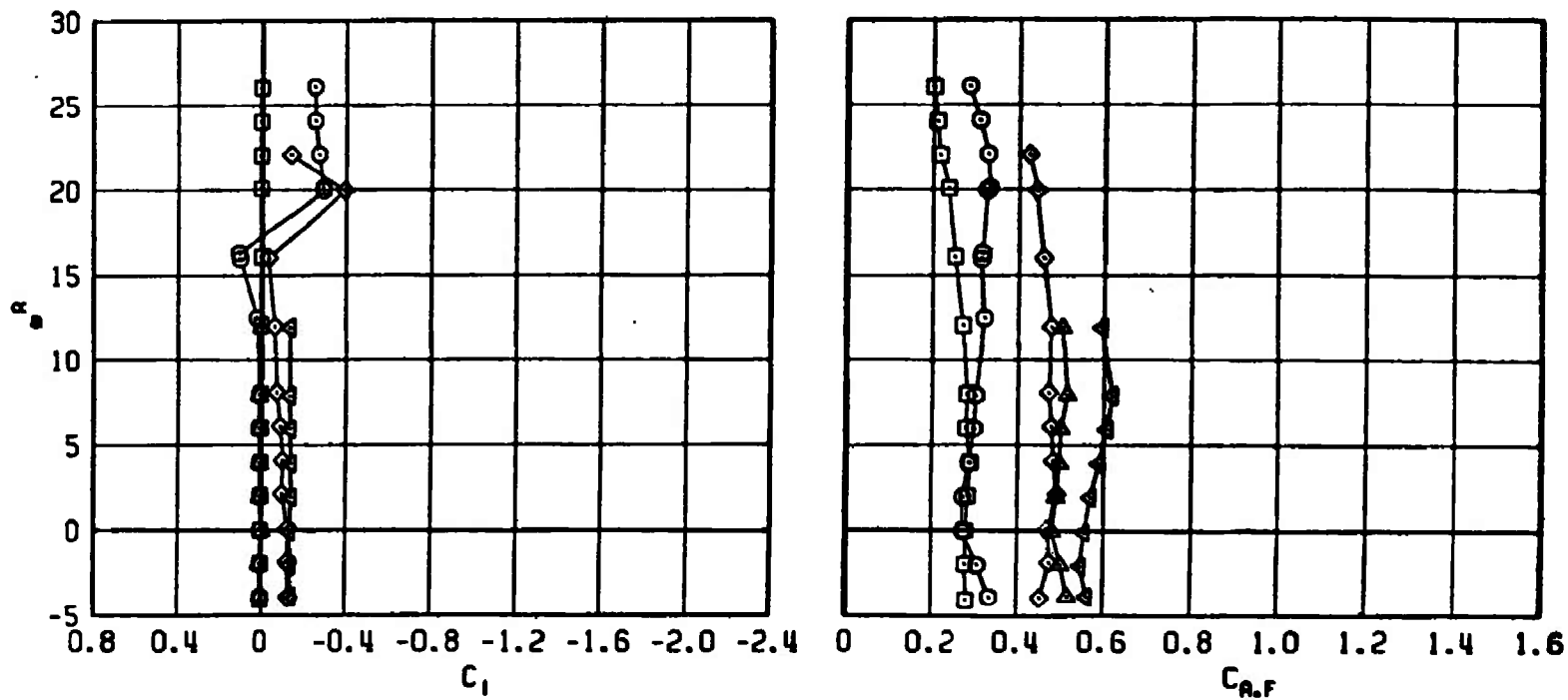


Figure 8. Continued.

SYM	CONFIGURATION	MACH NO	δp	δq	δr
□	B2	1.20	0	0	0
○	B2S13	1.20	0	0	0
△	B2S13W4 F7	1.20	0	0	0
◇	B2 W4T3F7	1.20	0	0	0
◀	B2S13W4T3F7	1.20	0	0	0

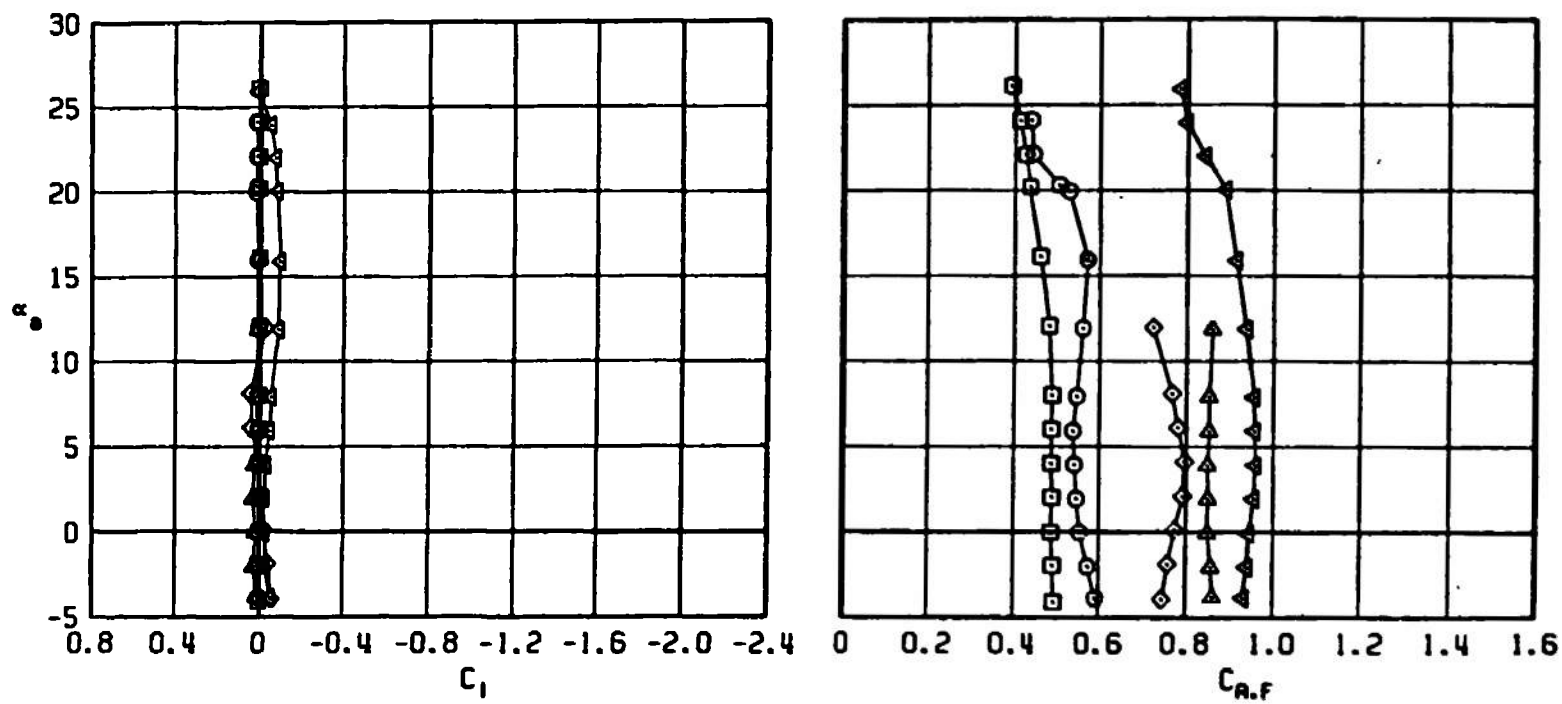


Figure 8. Continued.

SYM	CONFIGURATION	MACH NO	δp	δq	δr
□	B2	1.60	0	0	0
○	B2S13	1.60	0	0	0
△	B2S13W4 F7	1.60	0	0	0
◇	B2S13W4T3F7	1.60	0	0	0

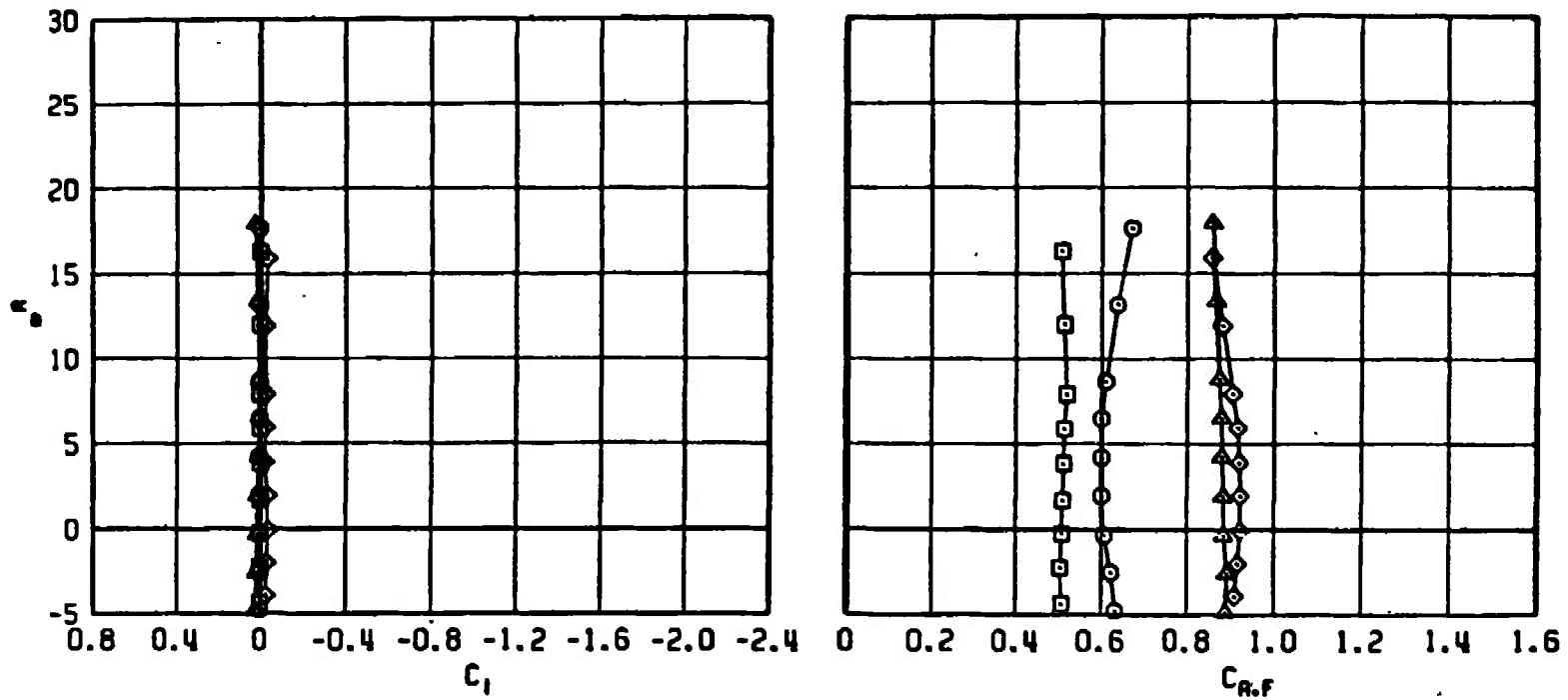


Figure 8. Concluded.

SYM	CONFIGURATION	MACH NO	δp	δq	δr
□	B2	0.65	0	0	0
○	B2S13	0.65	0	0	0
△	B2S13W4 F7	0.65	0	0	0
◇	B2 W4T3F7	0.65	0	0	0
◁	B2S13W4T3F7	0.65	0	0	0

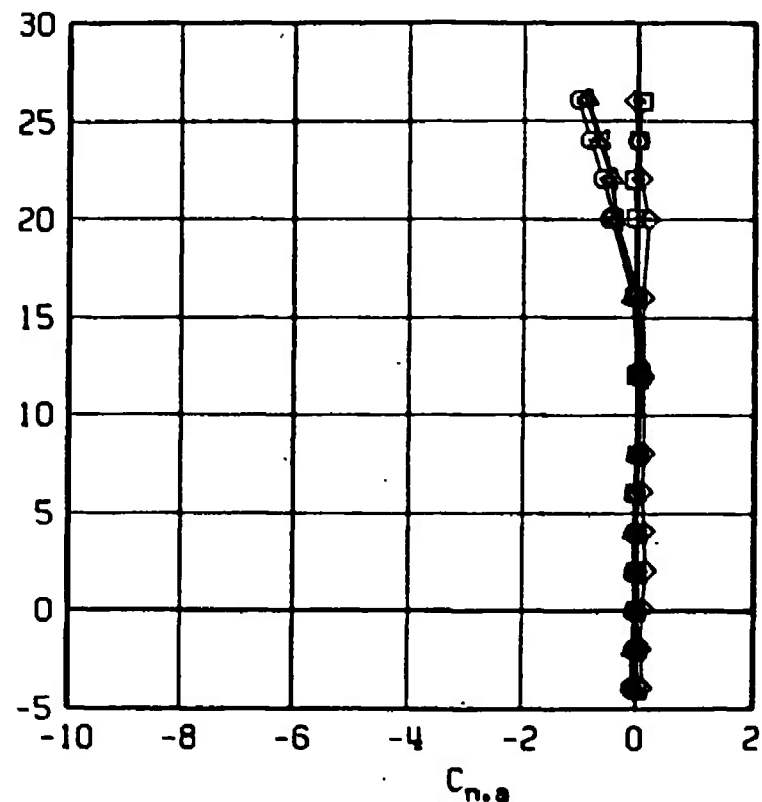
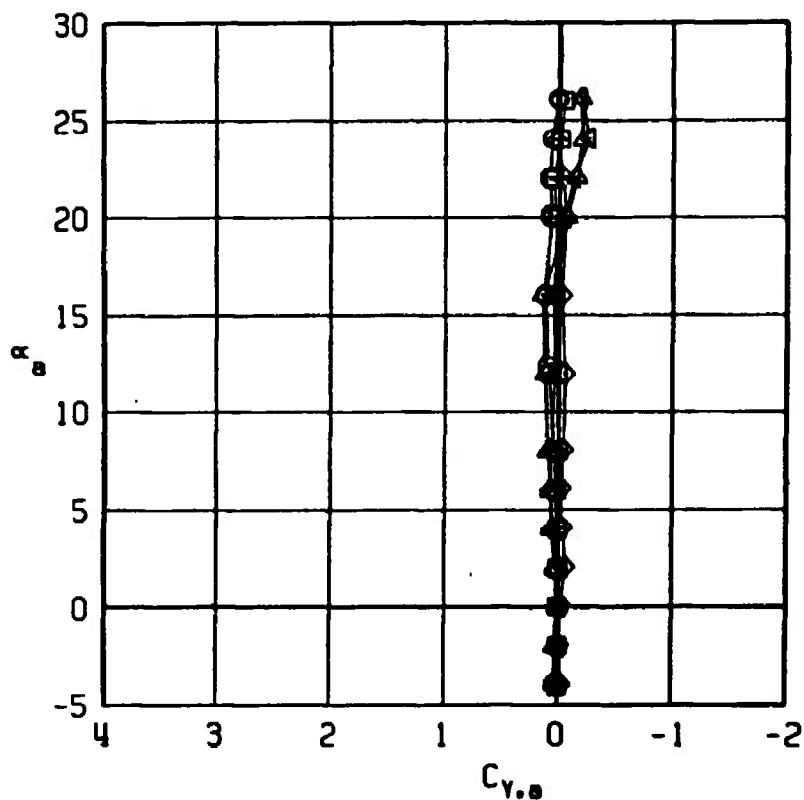


Figure 9. Comparison of side-force and yawing-moment coefficients for configurations B2, B2S13, B2S1W4F7, B2W4T3F7, and B2S13W4T3F7.

SYM	CONFIGURATION	MACH NO	δp	δq	δr
□	B2	0.95	0	0	0
○	B2S13	0.95	0	0	0
△	B2S13W4 F7	0.95	0	0	0
◇	B2 W4T3F7	0.95	0	0	0
◁	B2S13W4T3F7	0.95	0	0	0

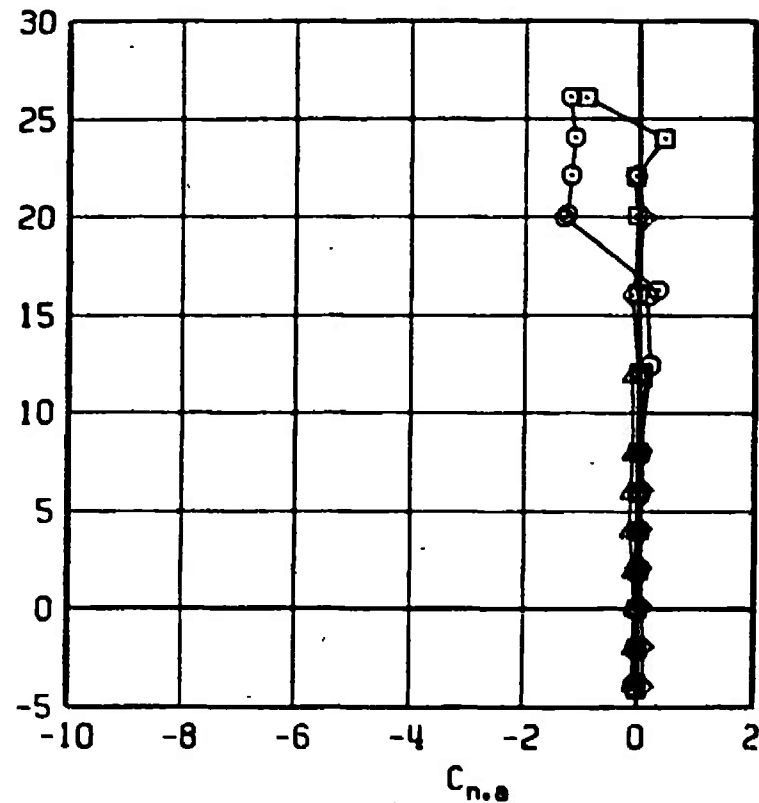
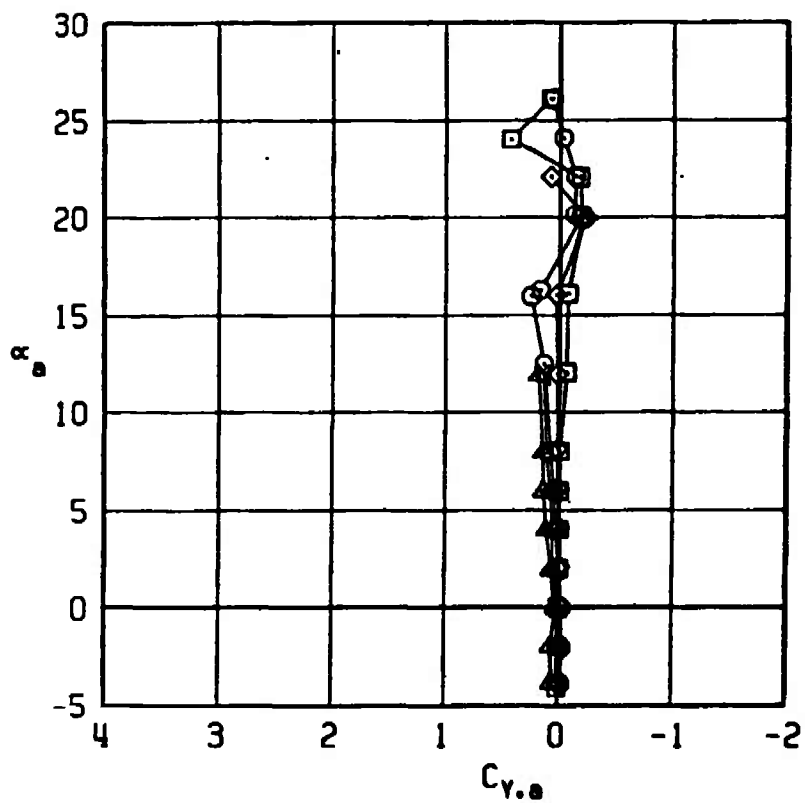


Figure 9. Continued.

SYM	CONFIGURATION	MACH NO	δp	δq	δr
□	B2	1.20	0	0	0
○	B2S13	1.20	0	0	0
△	B2S13W4 F7	1.20	0	0	0
◇	B2 W4T3F7	1.20	0	0	0
◄	B2S13W4T3F7	1.20	0	0	0

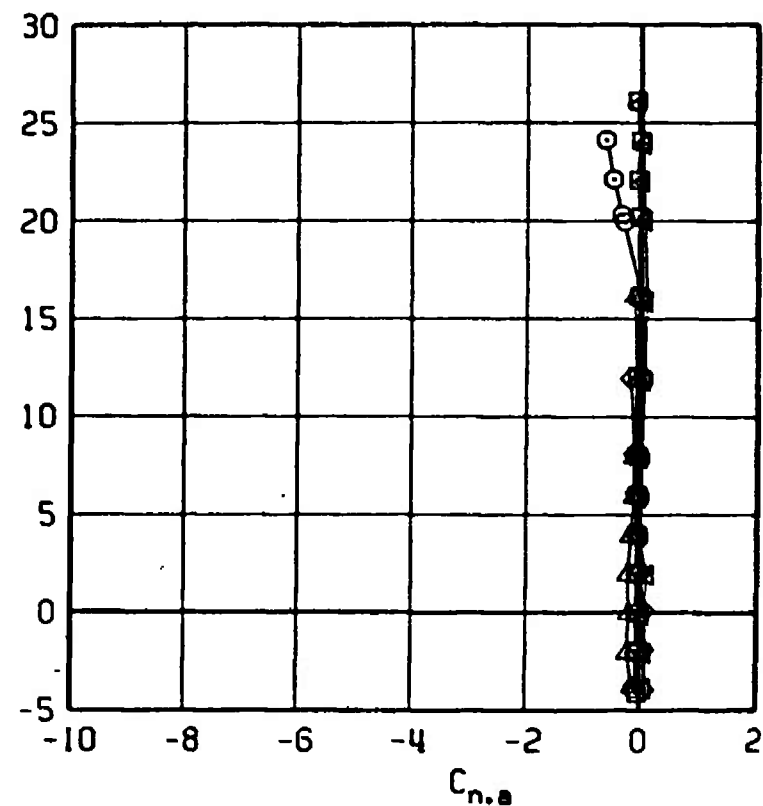
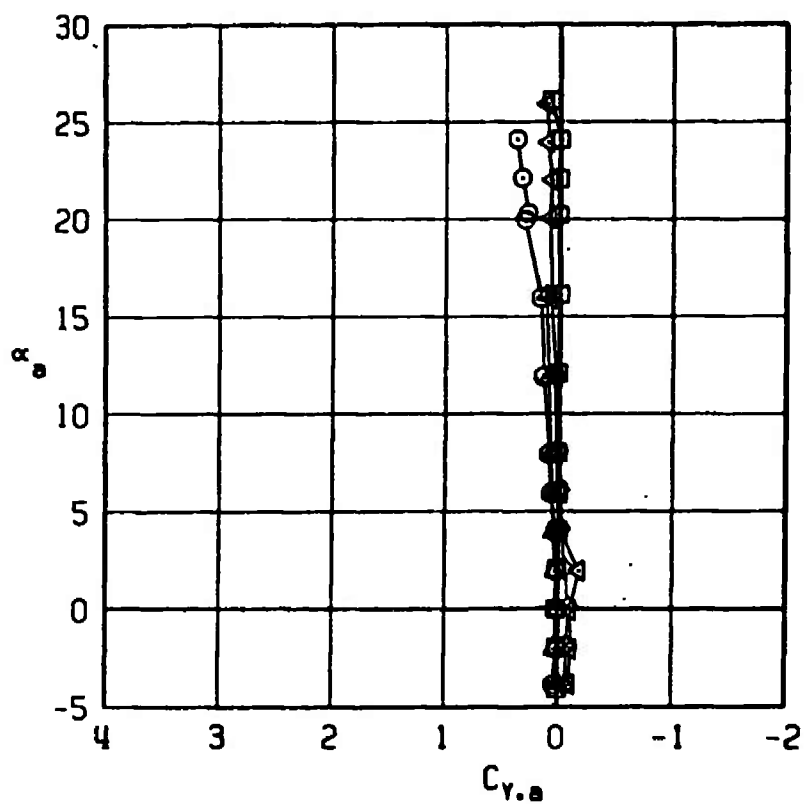


Figure 9. Continued.

SYM	CONFIGURATION	MACH NO	δp	δq	δr
□	B2	1.60	0	0	0
○	B2S13	1.60	0	0	0
△	B2S13W4 F7	1.60	0	0	0
◇	B2S13W4T3F7	1.60	0	0	0

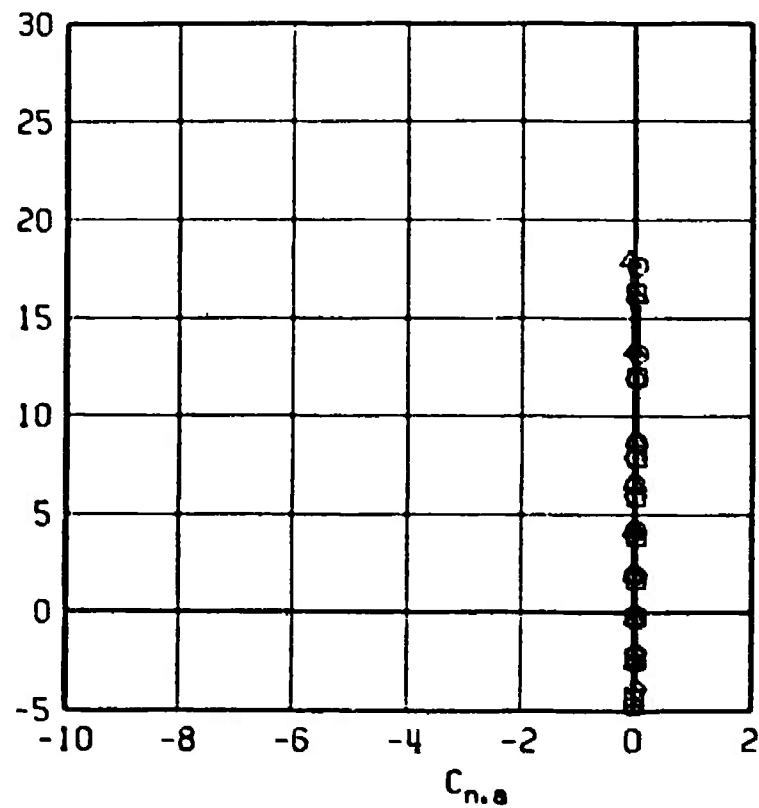
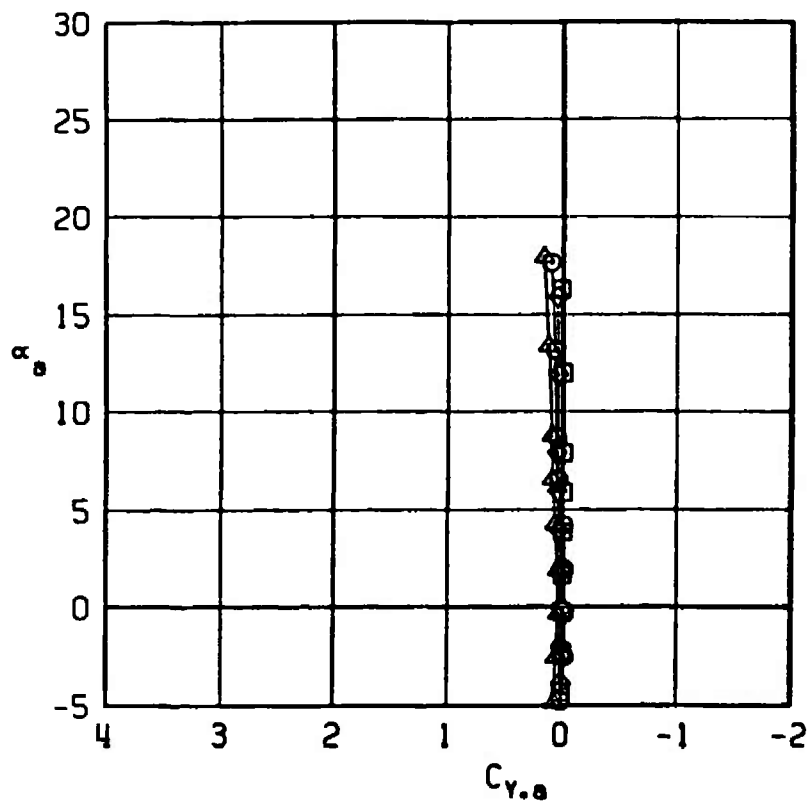


Figure 9. Concluded.

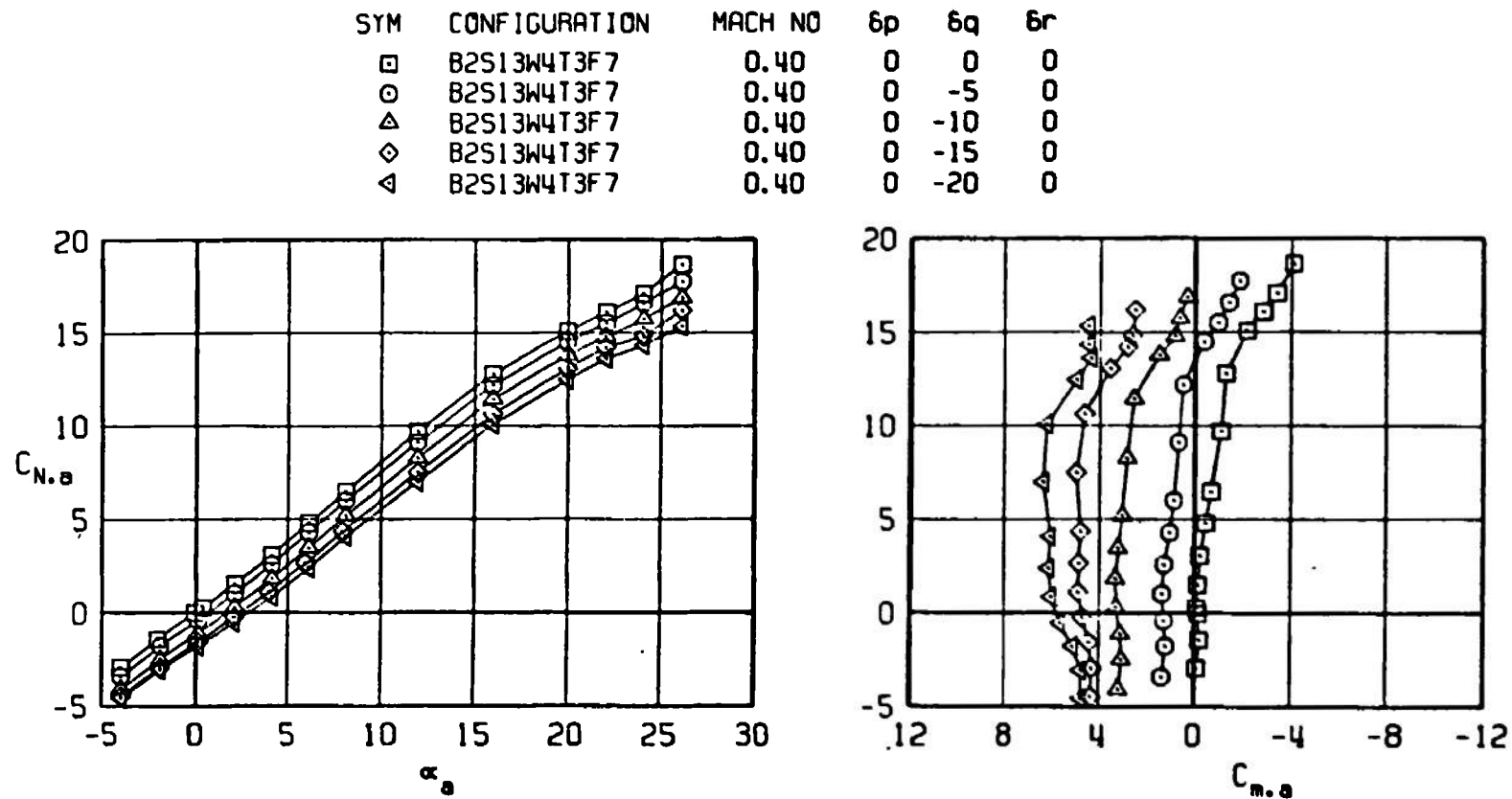


Figure 10. Effect of pitch control deflections on the normal-force and pitching-moment coefficients of the Super HOBOS/MK-84.

SYM	CONFIGURATION	MACH NO	δp	δq	δr
□	B2S13W4T3F7	0.65	0	0	0
○	B2S13W4T3F7	0.65	0	-5	0
△	B2S13W4T3F7	0.65	0	-10	0
◇	B2S13W4T3F7	0.65	0	-15	0
▽	B2S13W4T3F7	0.65	0	-20	0

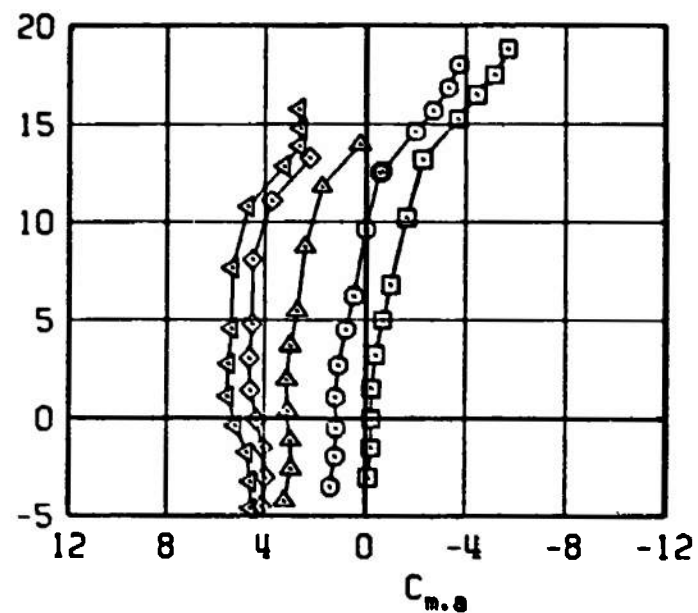
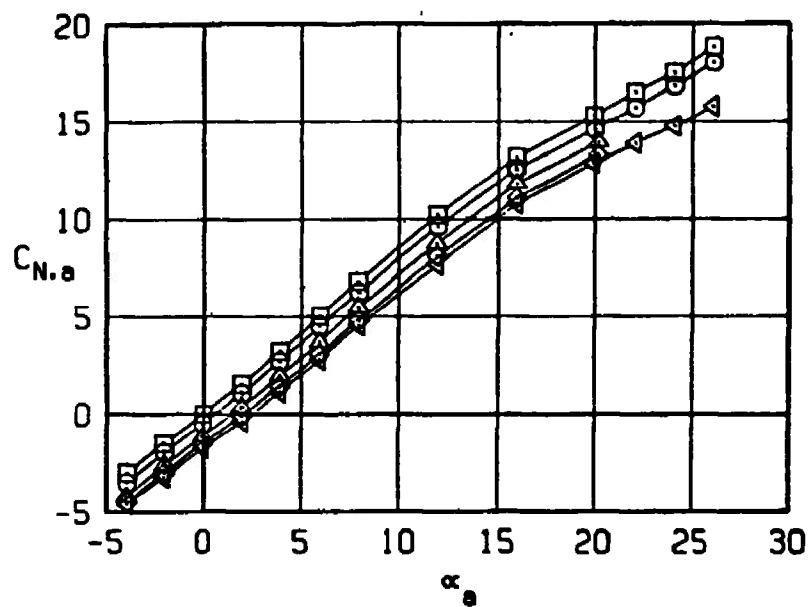


Figure 10. Continued.

SYM	CONFIGURATION	MACH NO	δp	δq	δr
□	B2S13W4T3F7	0.95	0	0	0
○	B2S13W4T3F7	0.95	0	-5	0
△	B2S13W4T3F7	0.95	0	-10	0
◇	B2S13W4T3F7	0.95	0	-15	0
◁	B2S13W4T3F7	0.95	0	-20	0

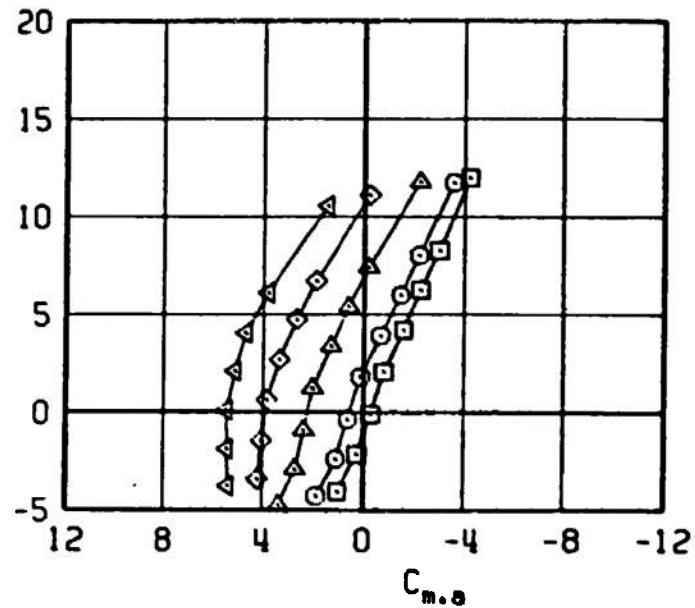
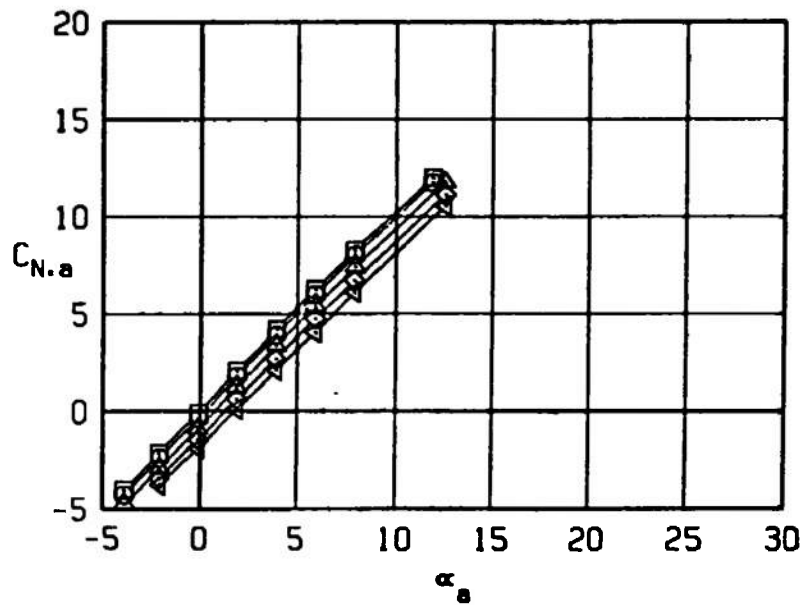


Figure 10. Continued.

SYM	CONFIGURATION	MACH NO	δp	δq	δr
□	B2S13W4T3F7	1.20	0	0	0
○	B2S13W4T3F7	1.20	0	-5	0
△	B2S13W4T3F7	1.20	0	-10	0
◇	B2S13W4T3F7	1.20	0	-15	0
◁	B2S13W4T3F7	1.20	0	-20	0

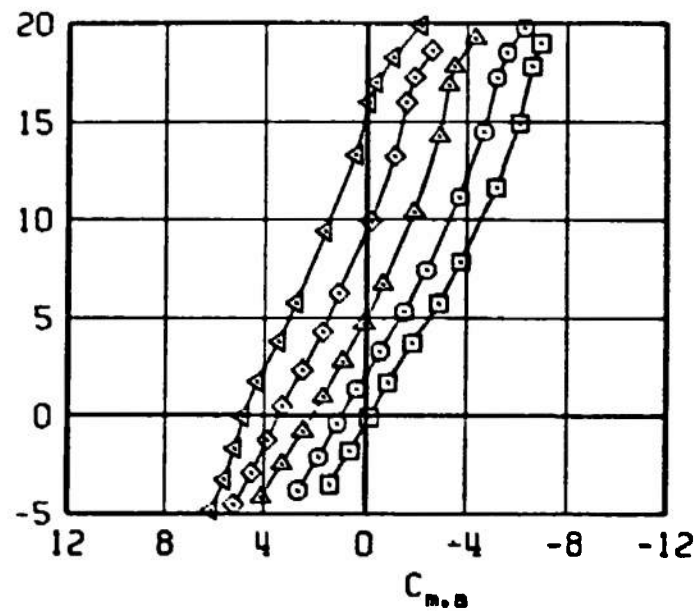
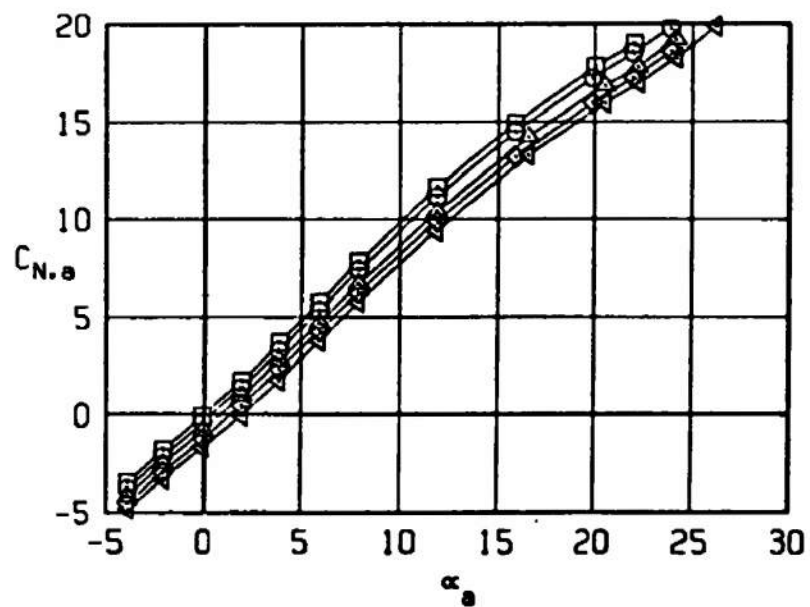


Figure 10. Continued.

SYM	CONFIGURATION	MACH NO	δp	δq	δr
□	B2S13W4T3F7	1.60	0	0	0
○	B2S13W4T3F7	1.60	0	-5	0
△	B2S13W4T3F7	1.60	0	-10	0
◇	B2S13W4T3F7	1.60	0	-15	0
◁	B2S13W4T3F7	1.60	0	-20	0

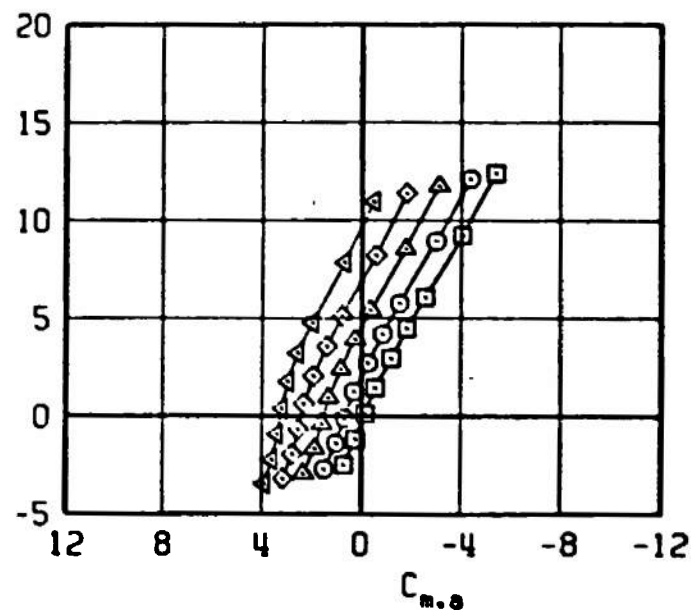
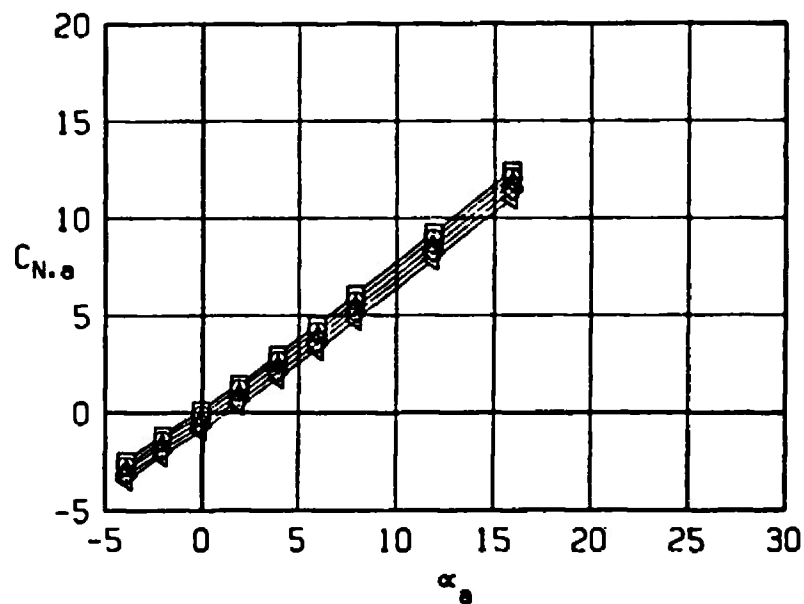


Figure 10. Concluded.

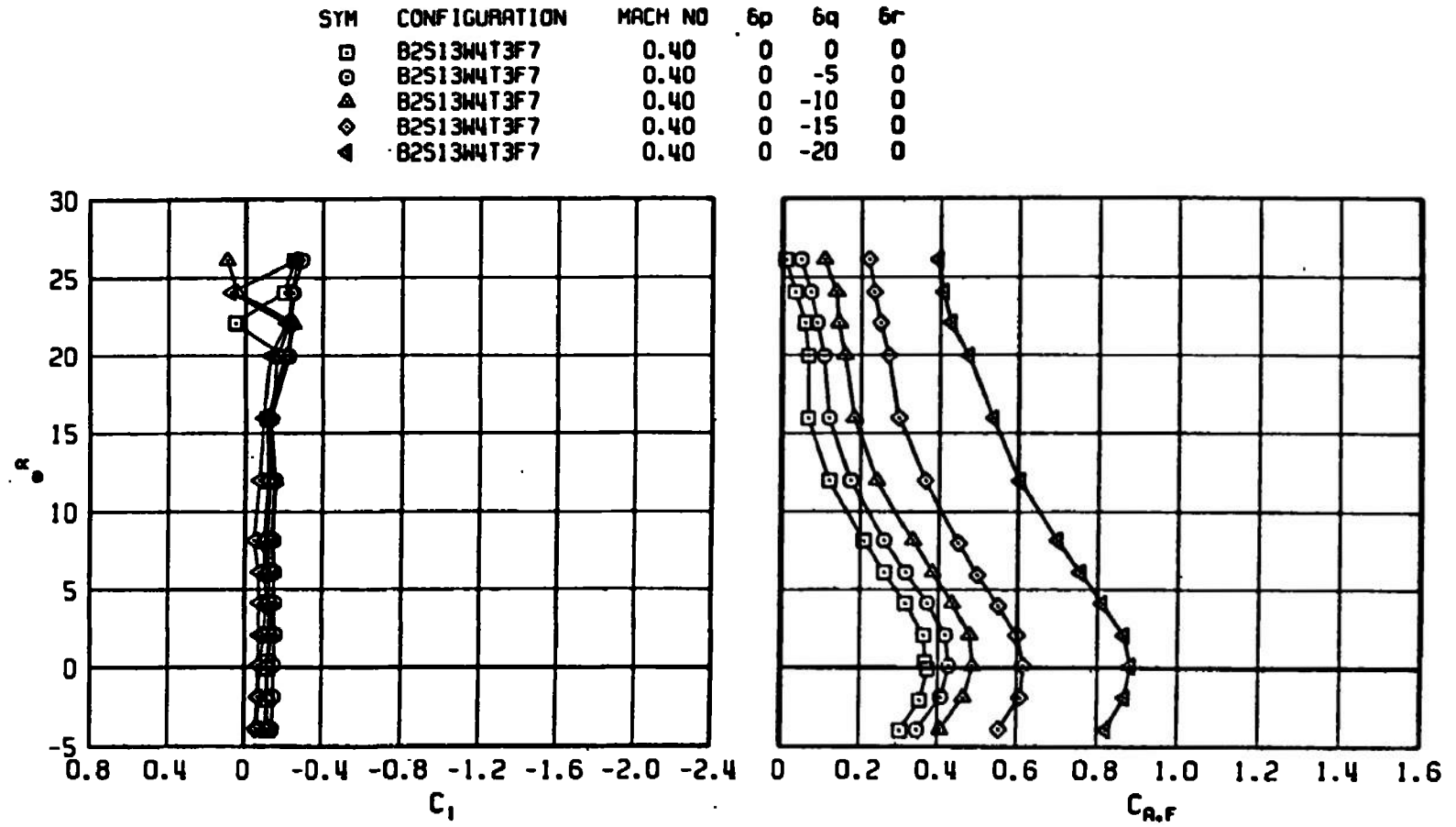


Figure 11. Effect of pitch control deflections on the rolling-moment and axial-force coefficients of the Super HOBOS/MK-84.

SYM	CONFIGURATION	MACH NO	δp	δq	δr
□	B2S13W4T3F7	0.65	0	0	0
○	B2S13W4T3F7	0.65	0	-5	0
△	B2S13W4T3F7	0.65	0	-10	0
◇	B2S13W4T3F7	0.65	0	-15	0
◄	B2S13W4T3F7	0.65	0	-20	0

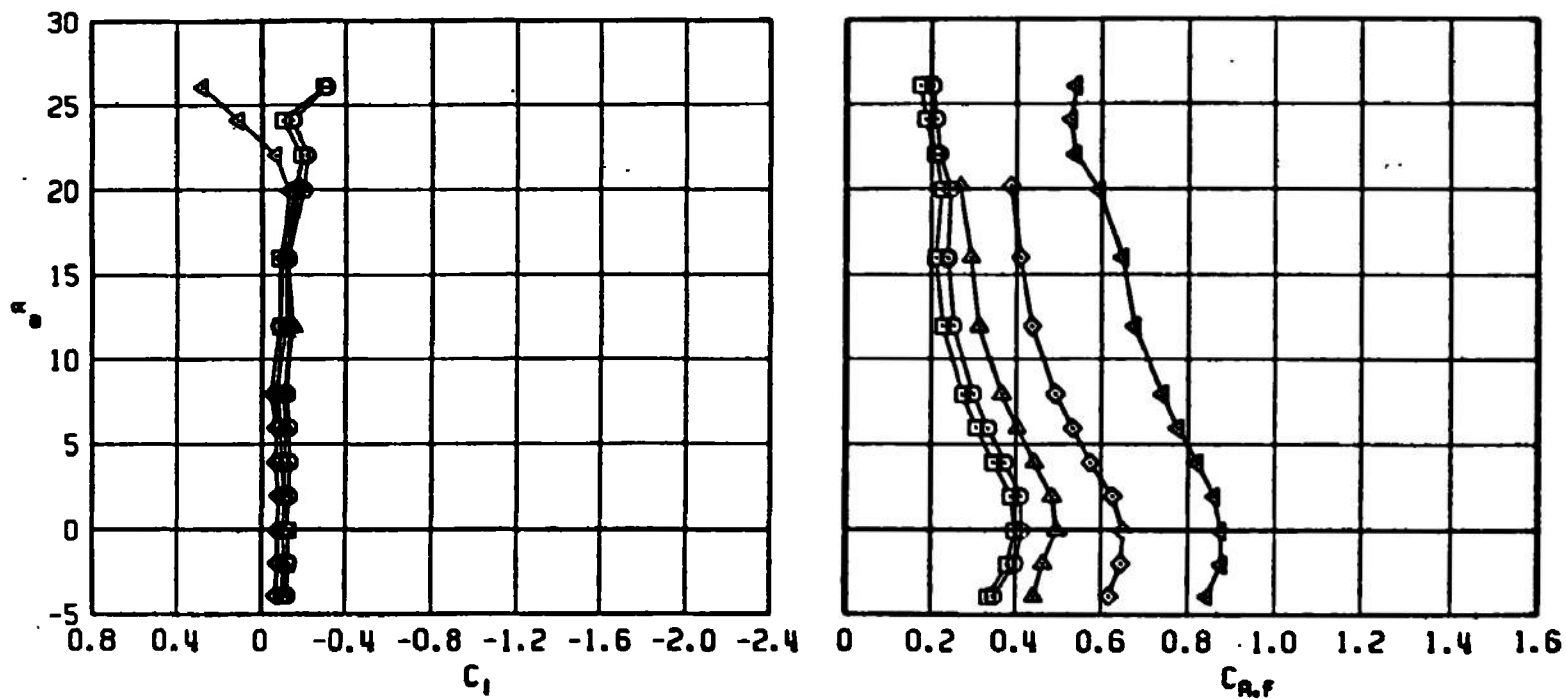


Figure 11. Continued.

SYM	CONFIGURATION	MACH NO	δp	δq	δr
□	B2S13W4T3F7	0.95	0	0	0
○	B2S13W4T3F7	0.95	0	-5	0
△	B2S13W4T3F7	0.95	0	-10	0
◇	B2S13W4T3F7	0.95	0	-15	0
◄	B2S13W4T3F7	0.95	0	-20	0

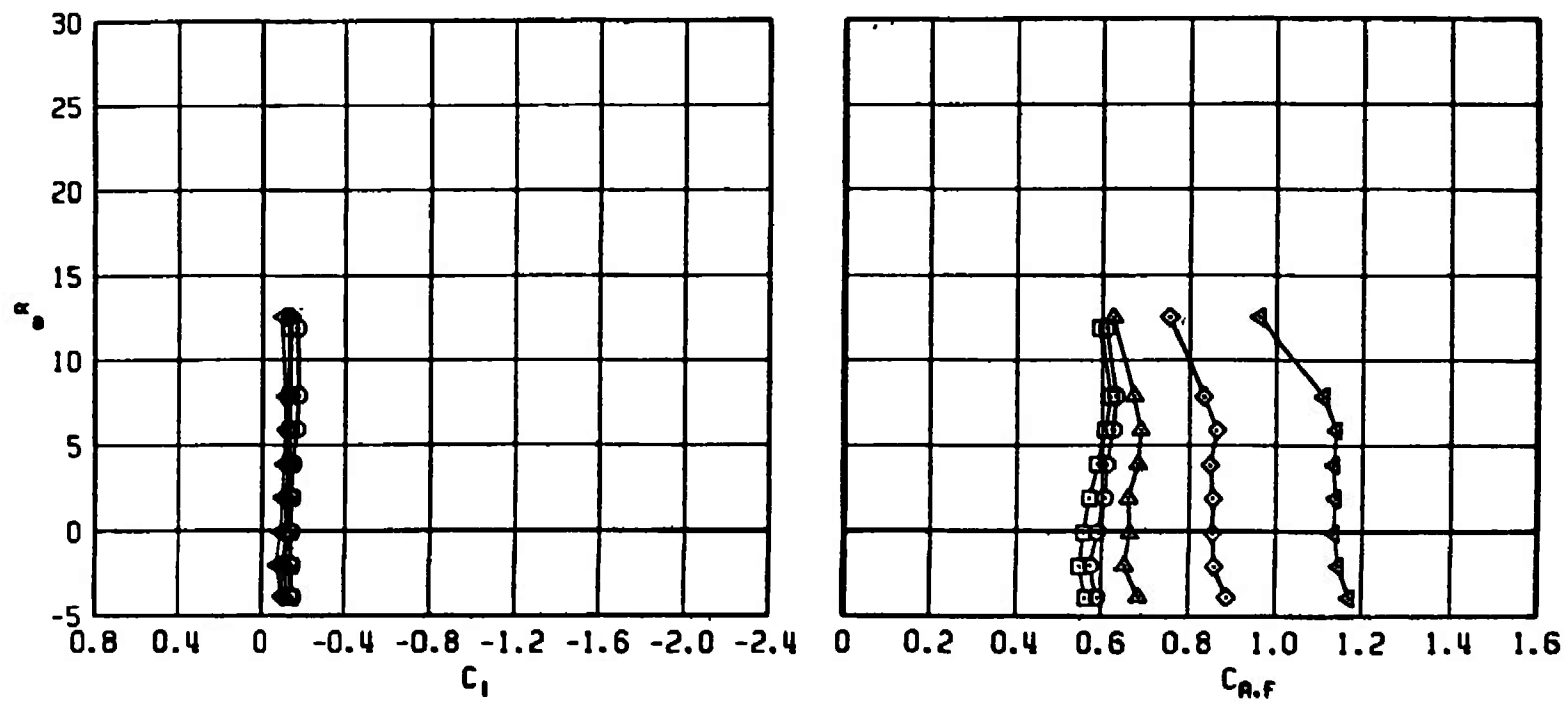


Figure 11. Continued.

SYM	CONFIGURATION	MACH NO	δp	δq	δr
□	B2S13W4T3F7	1.20	0	0	0
○	B2S13W4T3F7	1.20	0	-5	0
△	B2S13W4T3F7	1.20	0	-10	0
◇	B2S13W4T3F7	1.20	0	-15	0
◀	B2S13W4T3F7	1.20	0	-20	0

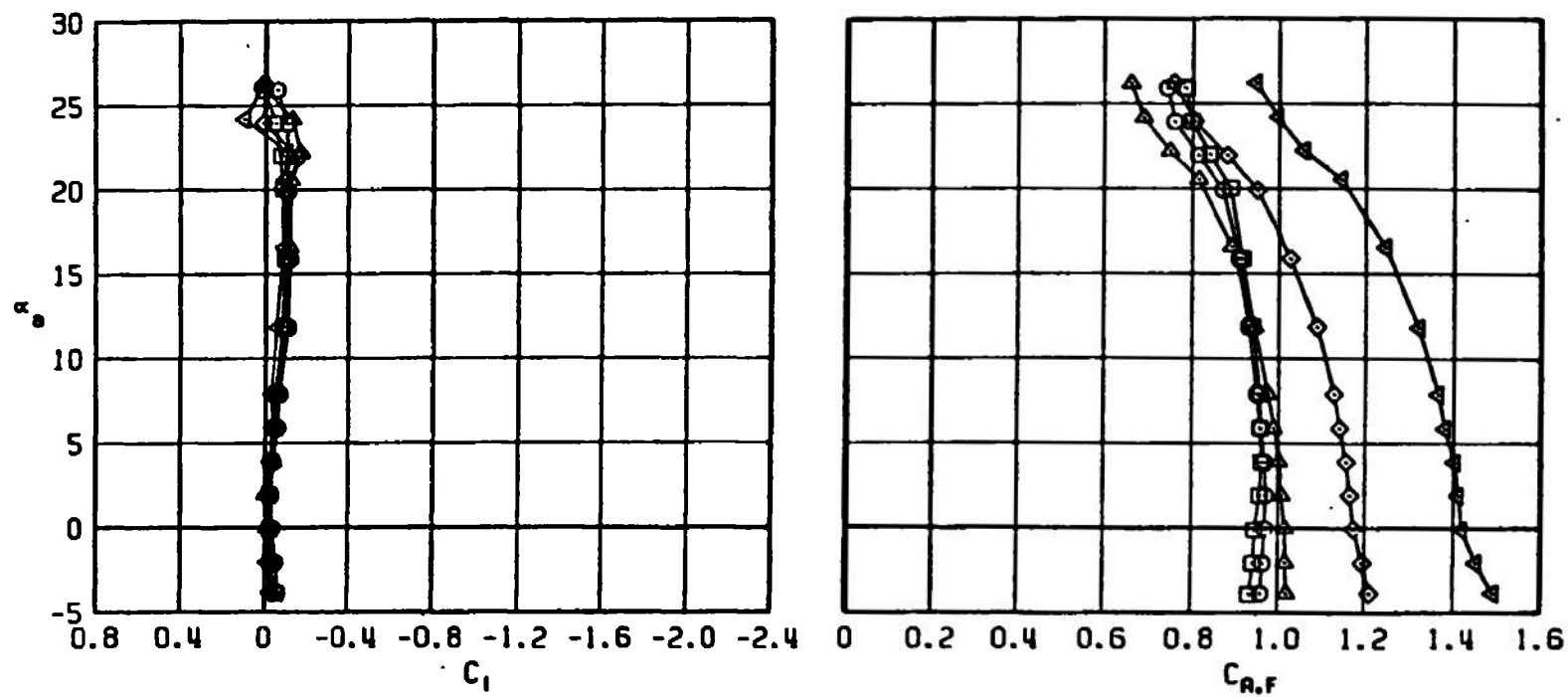


Figure 11. Continued.

SYM	CONFIGURATION	MACH NO	δp	δq	δr
□	B2S13W4T3F7	1.60	0	0	0
○	B2S13W4T3F7	1.60	0	-5	0
△	B2S13W4T3F7	1.60	0	-10	0
◇	B2S13W4T3F7	1.60	0	-15	0
◀	B2S13W4T3F7	1.60	0	-20	0

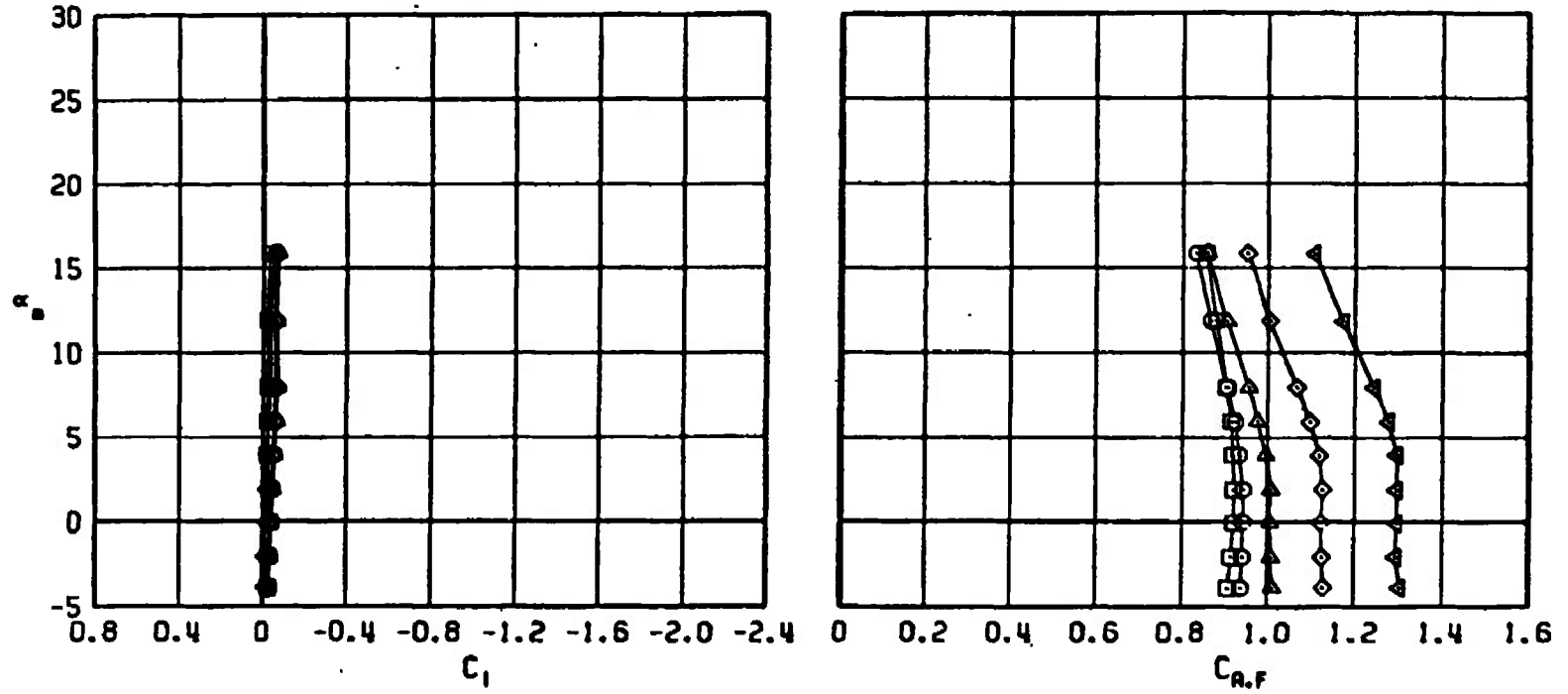


Figure 11. Concluded.

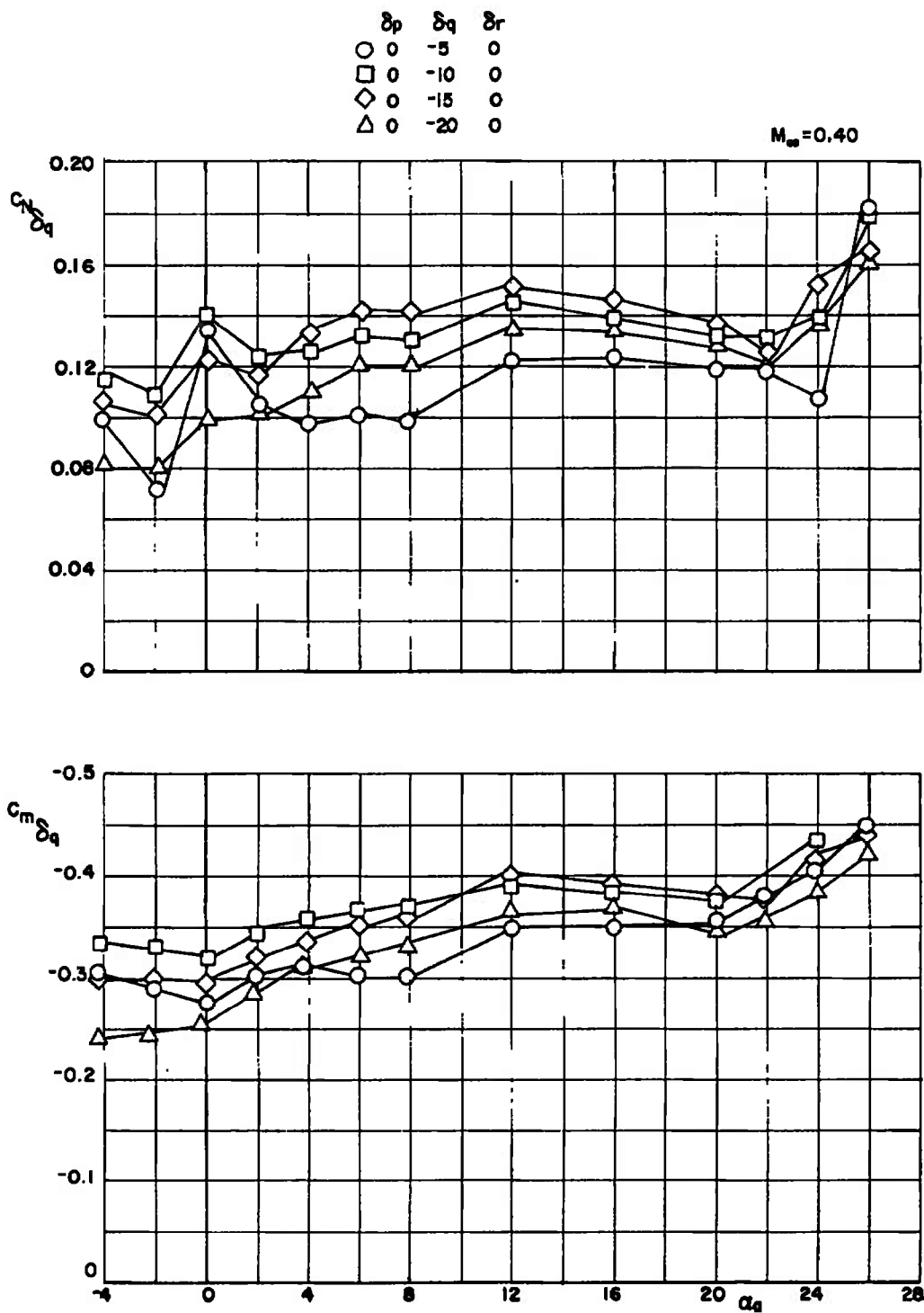


Figure 12. Normal-force increment and pitch control effectiveness for several pitch control deflections.

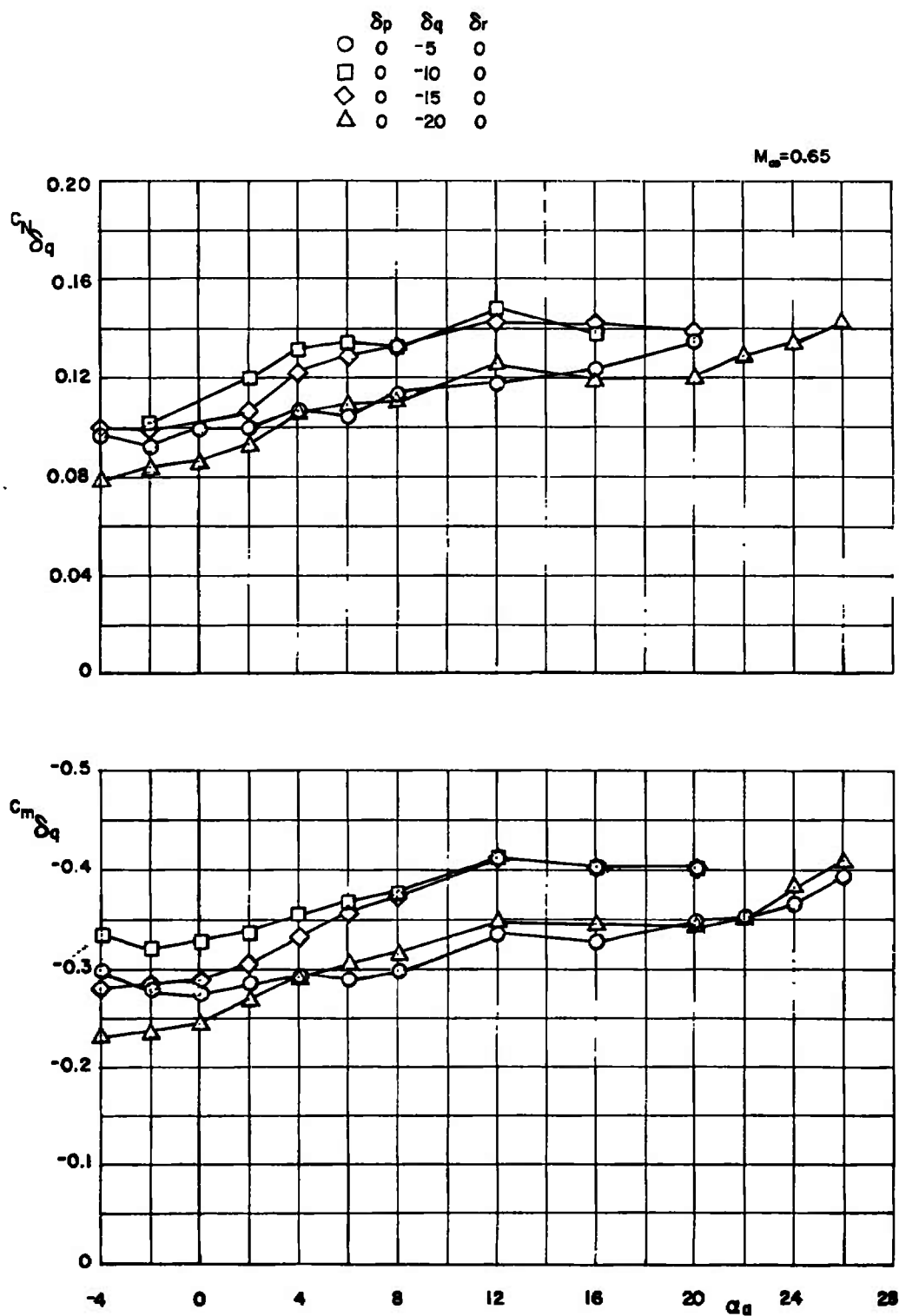


Figure 12. Continued.

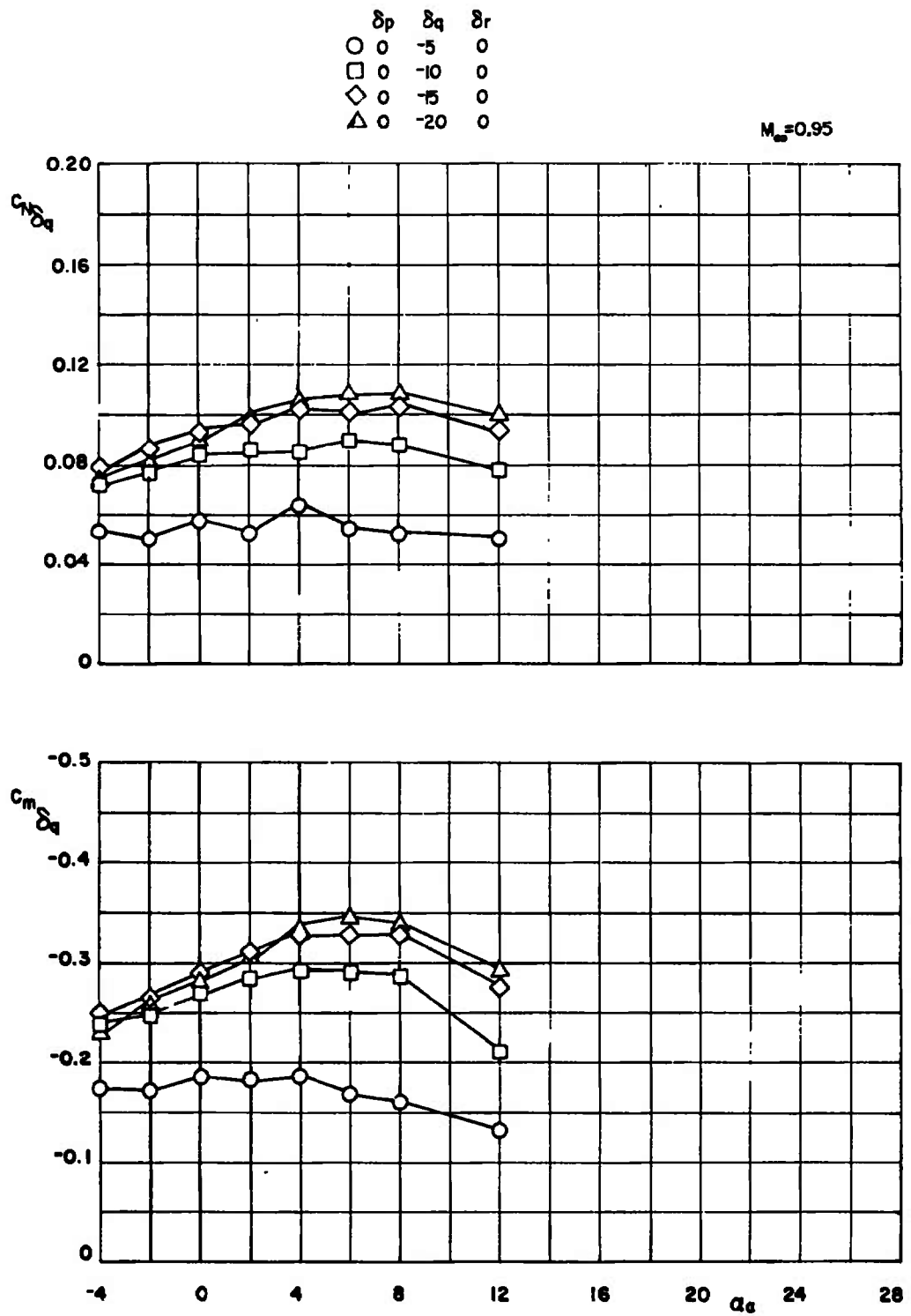


Figure 12. Continued.

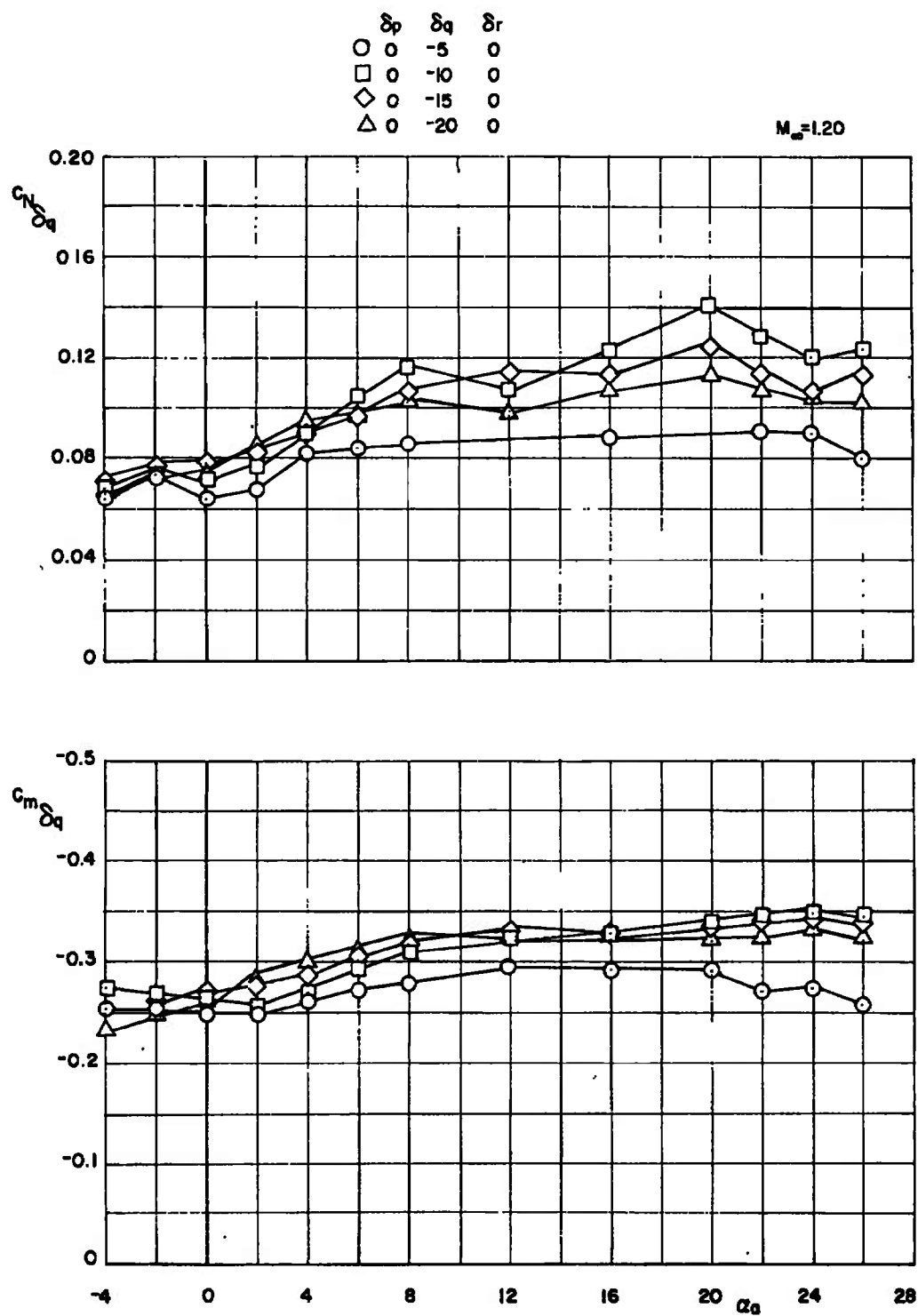


Figure 12. Continued.

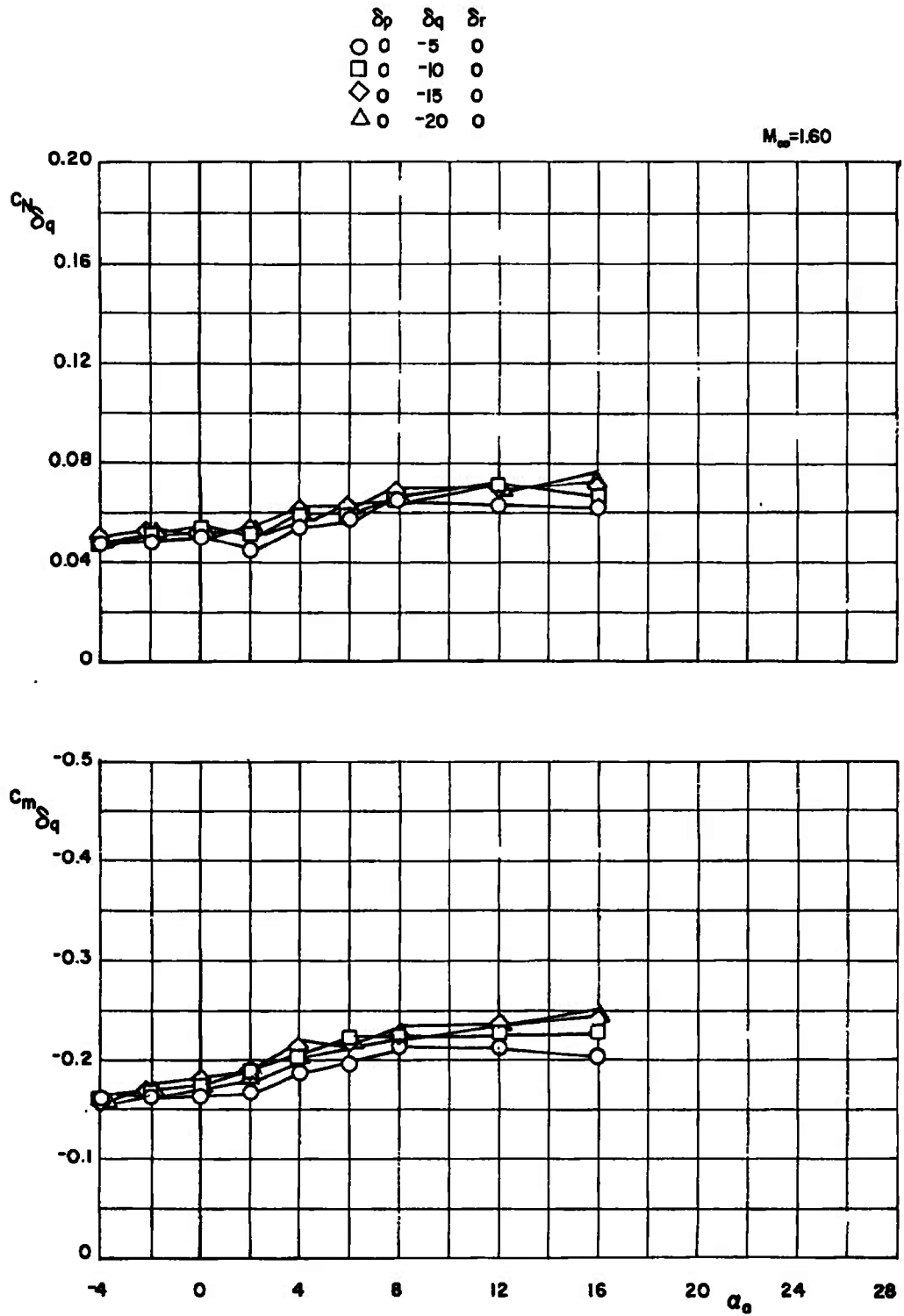


Figure 12. Concluded.

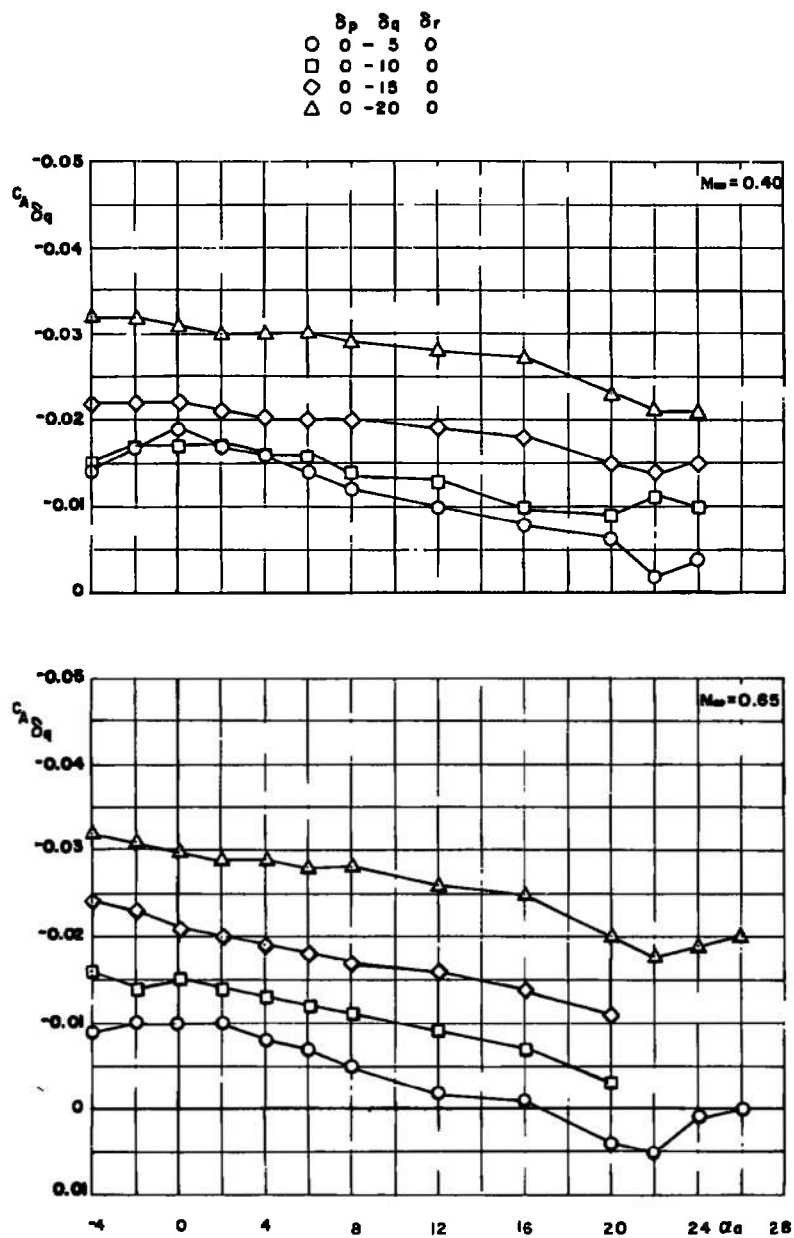


Figure 13. Axial-force increment for several pitch control deflections.

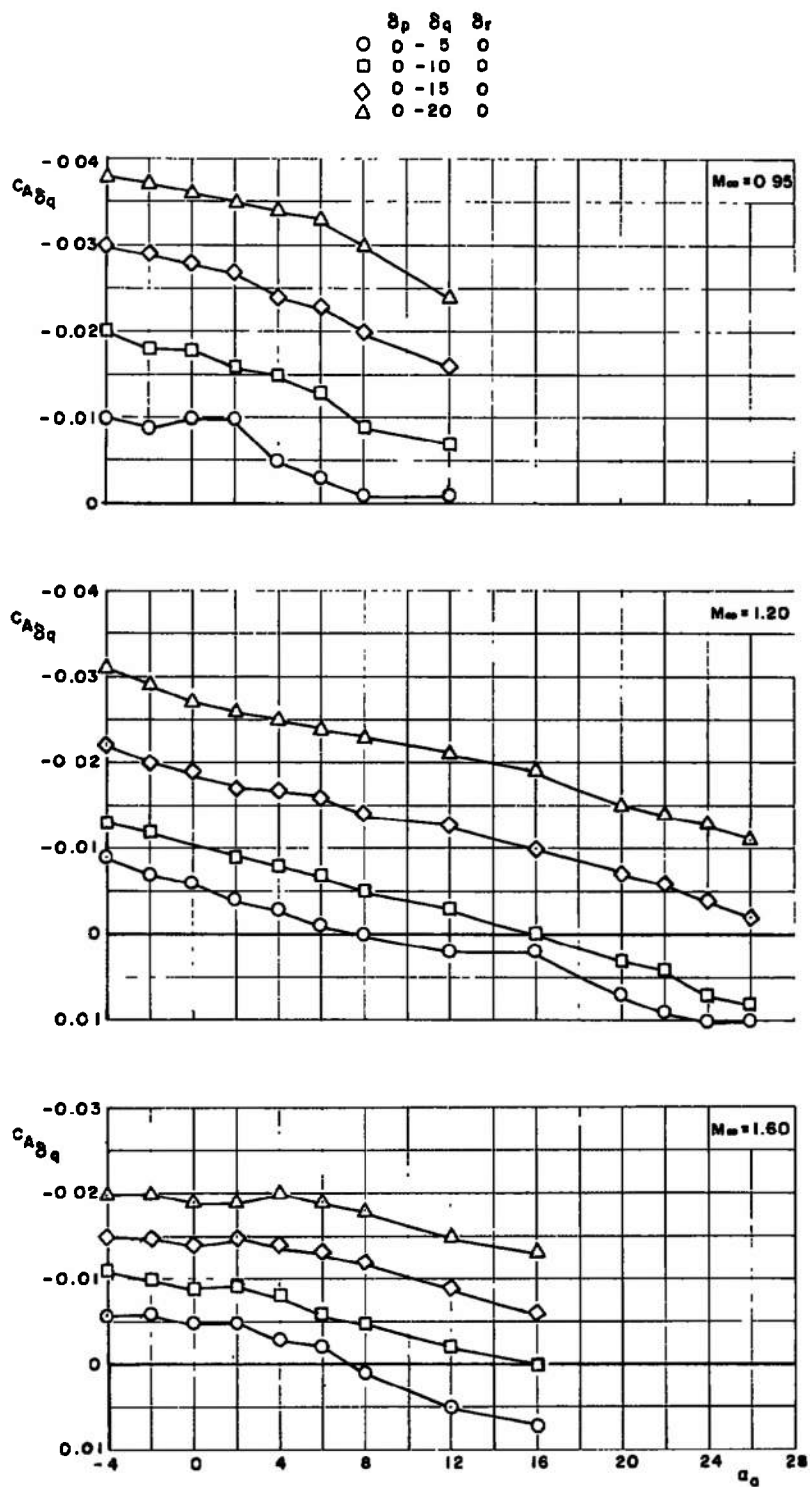


Figure 13. Concluded.

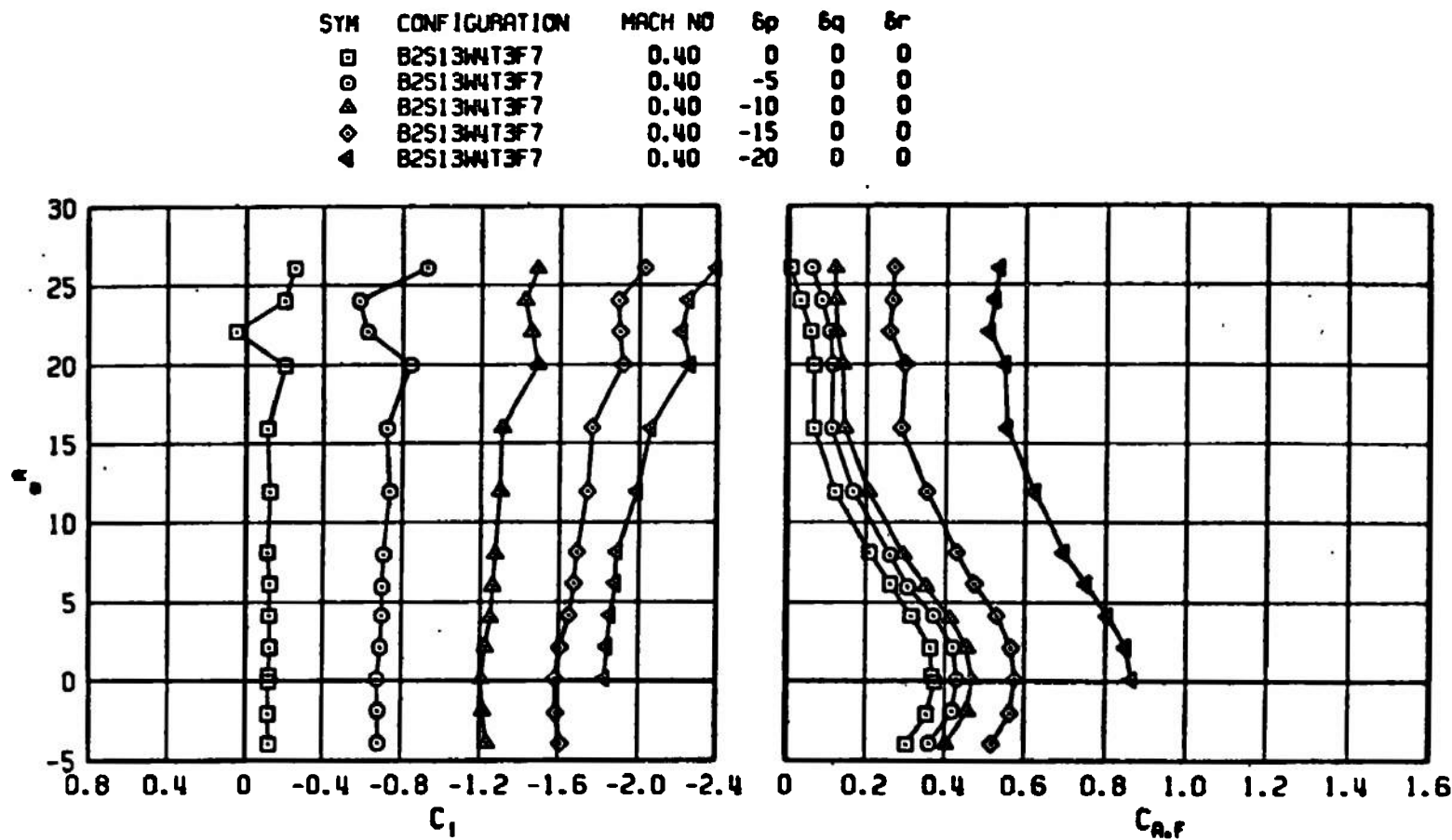


Figure 14. Effect of roll control deflections on the rolling-moment and axial-force coefficients of the Super HOBOS/MK-84.

SYM	CONFIGURATION	MACH NO	δp	δq	δr
□	B2S13W4T3F7	0.65	0	0	0
○	B2S13W4T3F7	0.65	-5	0	0
△	B2S13W4T3F7	0.65	-10	0	0
◇	B2S13W4T3F7	0.65	-15	0	0
◀	B2S13W4T3F7	0.65	-20	0	0

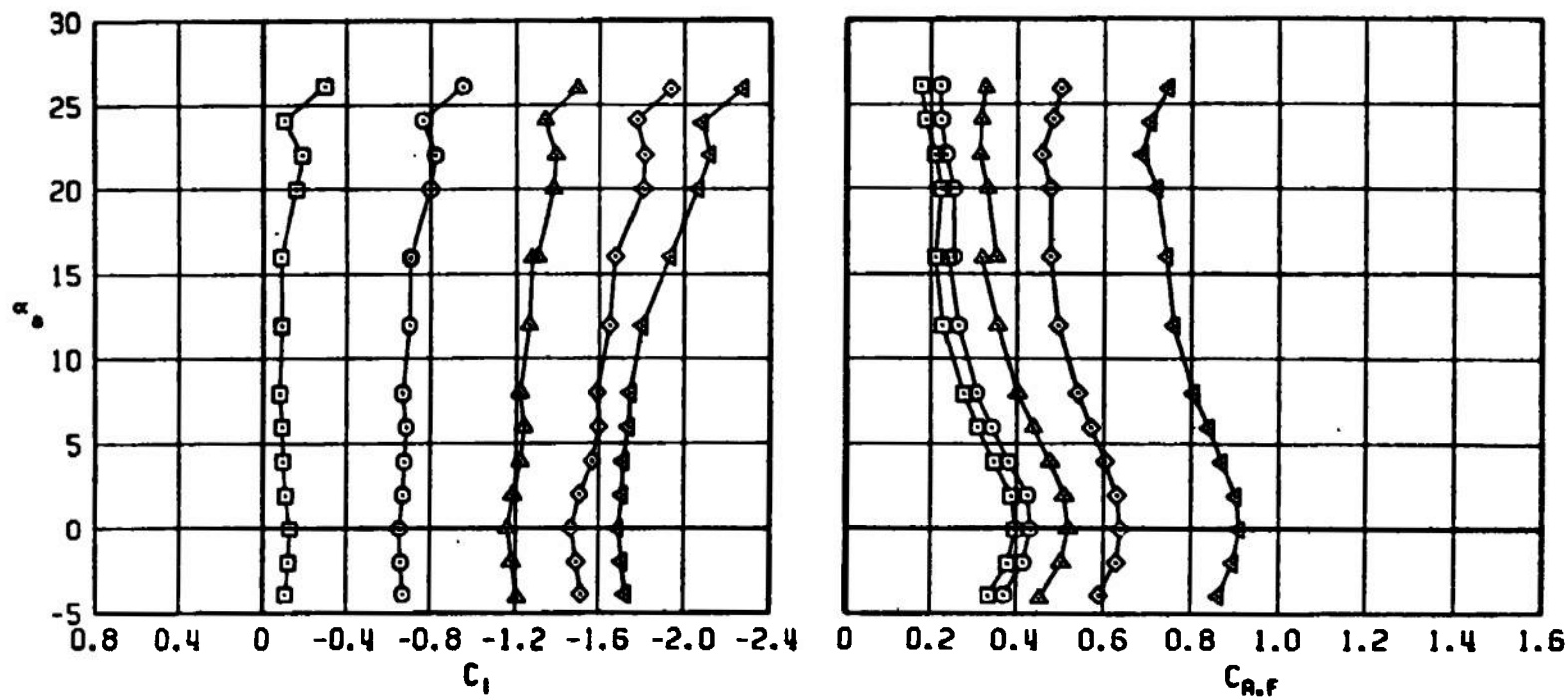


Figure 14. Continued.

SYM	CONFIGURATION	MACH NO	δp	δq	δr
□	B2S13W4T3F7	0.95	0	0	0
○	B2S13W4T3F7	0.95	-5	0	0
△	B2S13W4T3F7	0.95	-10	0	0
◇	B2S13W4T3F7	0.95	-15	0	0
◀	B2S13W4T3F7	0.95	-20	0	0

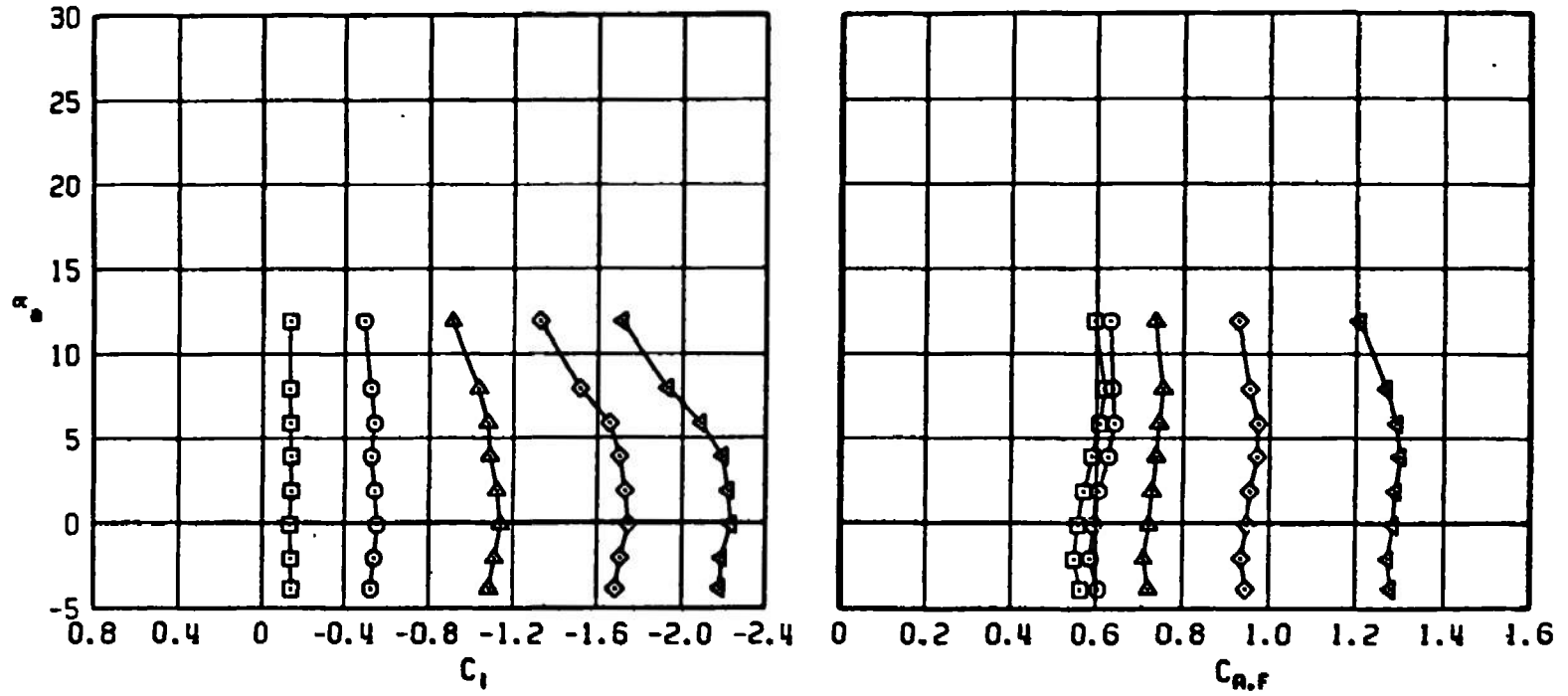


Figure 14. Continued.

SYM	CONFIGURATION	MACH NO	δp	δq	δr
□	B2S13WNT3F7	1.20	0	0	0
○	B2S13WNT3F7	1.20	-5	0	0
▲	B2S13WNT3F7	1.20	-10	0	0
◇	B2S13WNT3F7	1.20	-15	0	0
◄	B2S13WNT3F7	1.20	-20	0	0

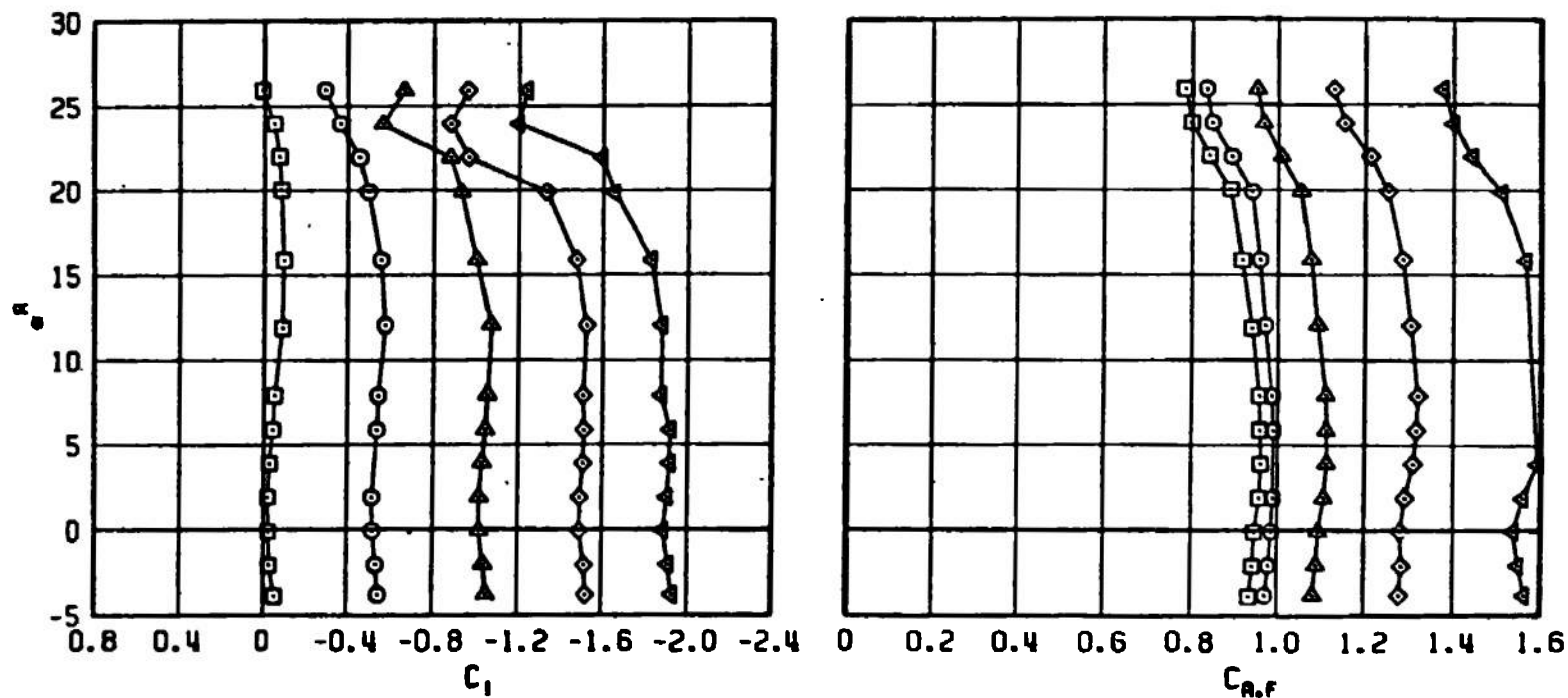


Figure 14. Continued.

SYM	CONFIGURATION	MACH NO	δp	δq	δr
□	B2S13W4T3F7	1.60	0	0	0
○	B2S13W4T3F7	1.60	-5	0	0
△	B2S13W4T3F7	1.60	-10	0	0
◇	B2S13W4T3F7	1.60	-15	0	0
◀	B2S13W4T3F7	1.60	-20	0	0

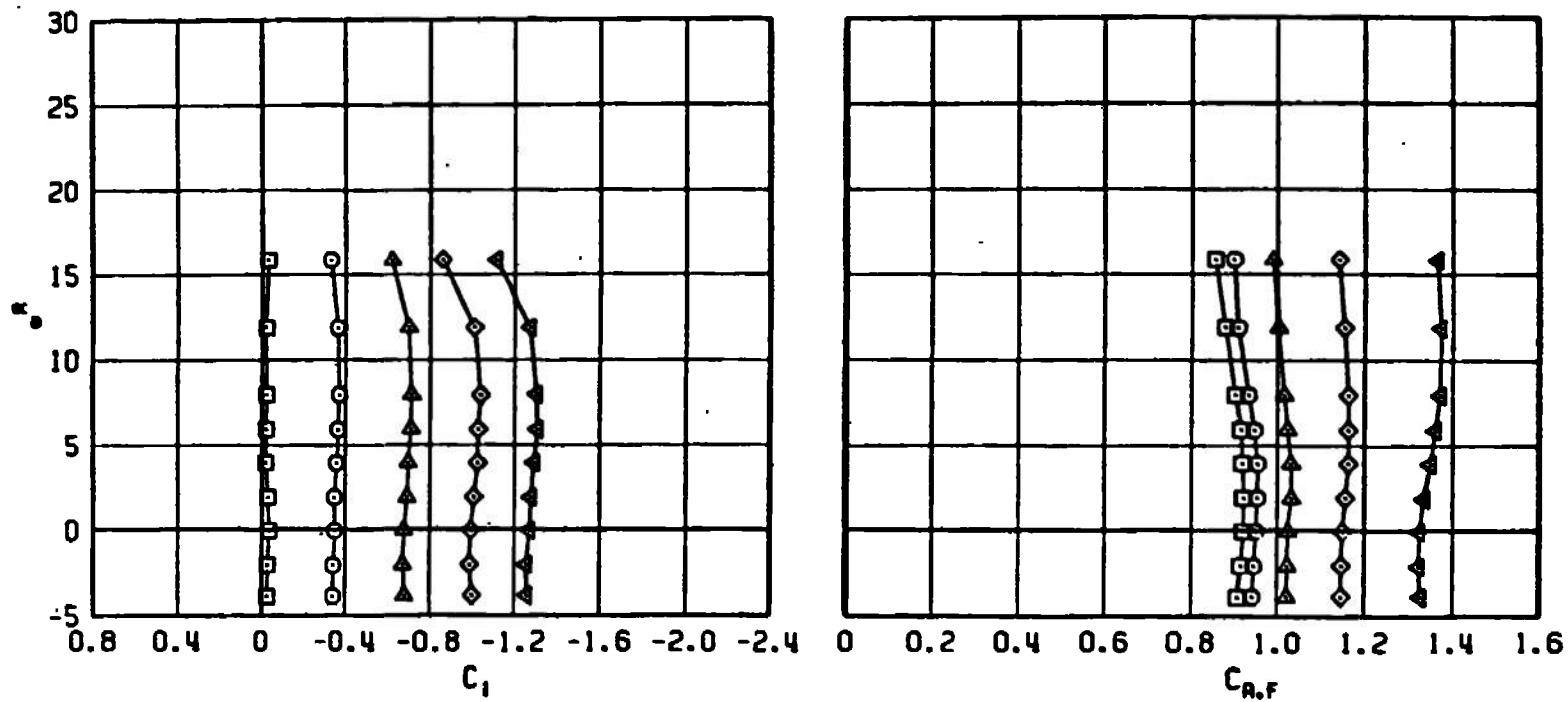


Figure 14. Concluded.

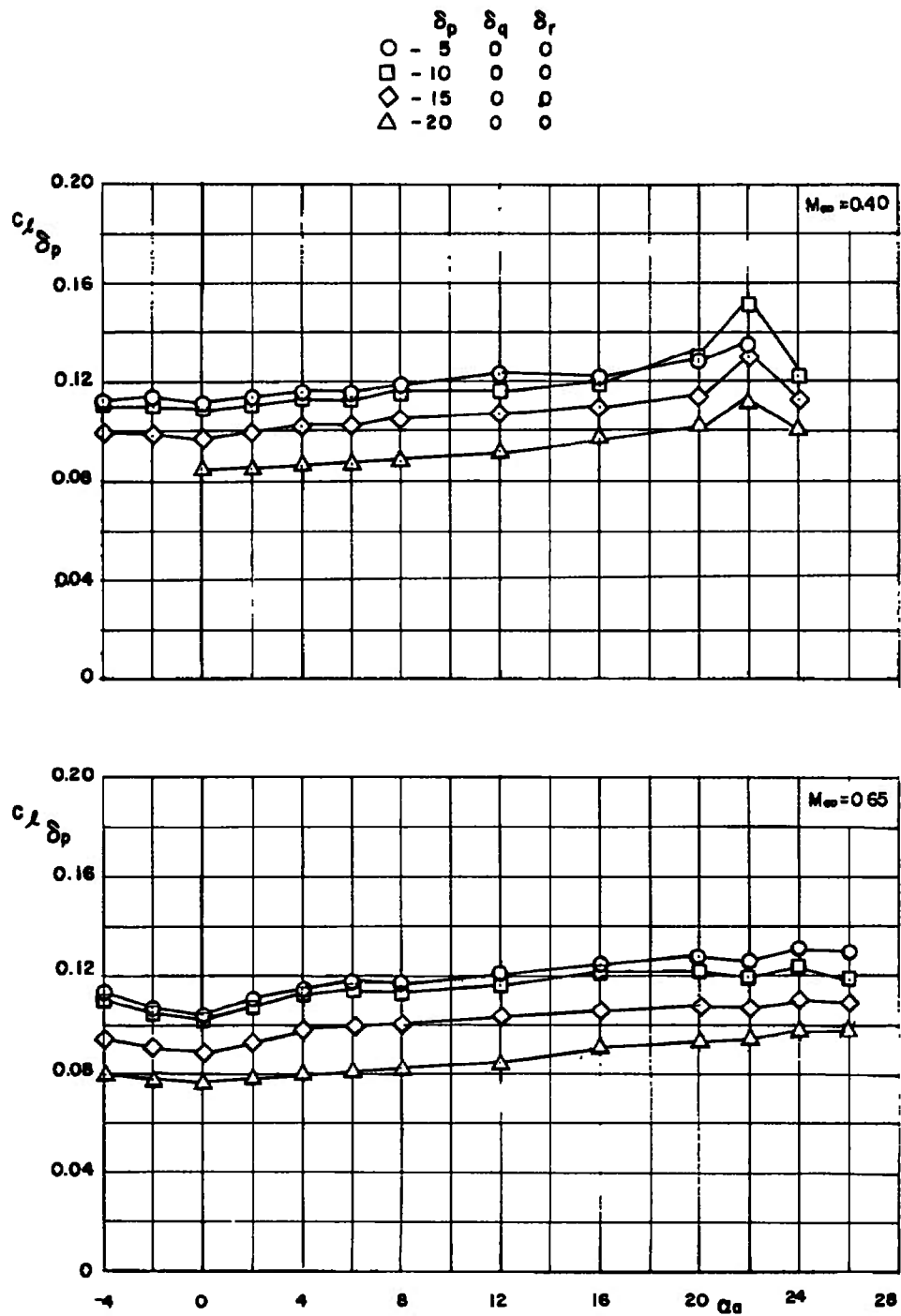


Figure 15. Roll control effectiveness for several roll control deflections.

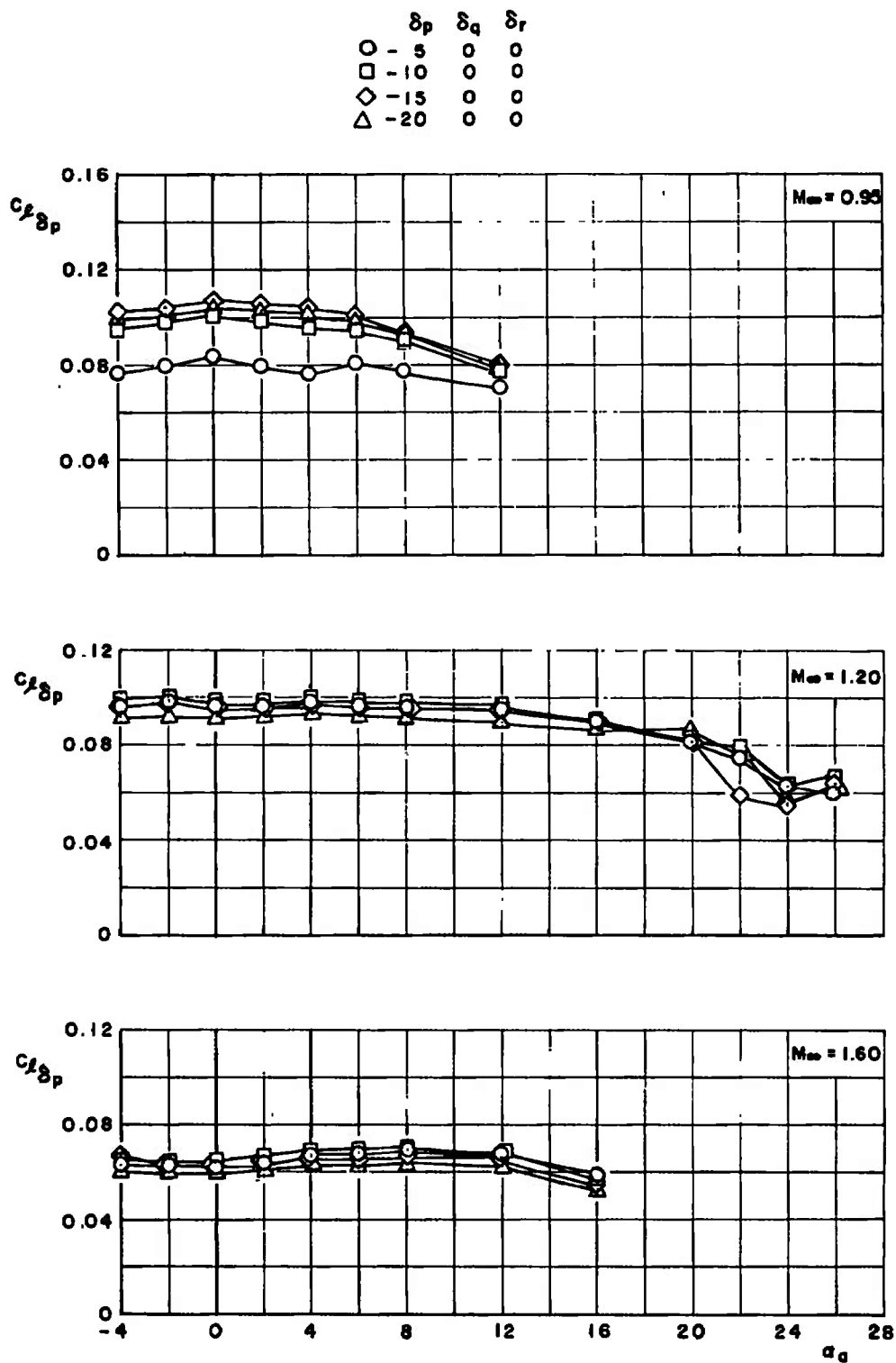


Figure 15. Concluded.

SYM	CONFIGURATION	MACH NO	δp	δq	δr
□	B2S13W4T3F7	0.40	0	0	0
○	B2S13W4T3F7	0.40	0	0	5
△	B2S13W4T3F7	0.40	0	0	10
◇	B2S13W4T3F7	0.40	0	0	15
◀	B2S13W4T3F7	0.40	0	0	20

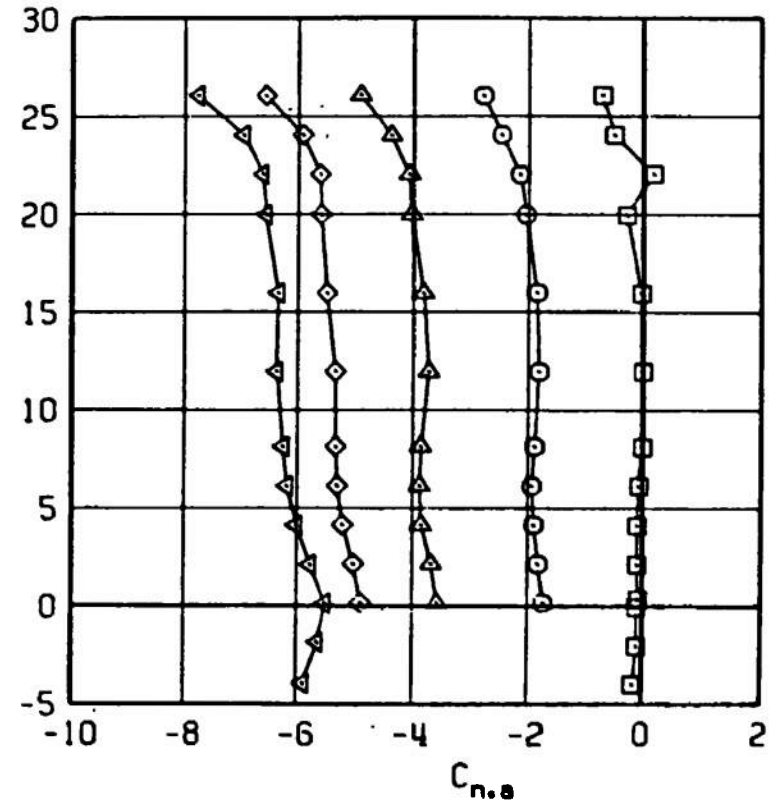
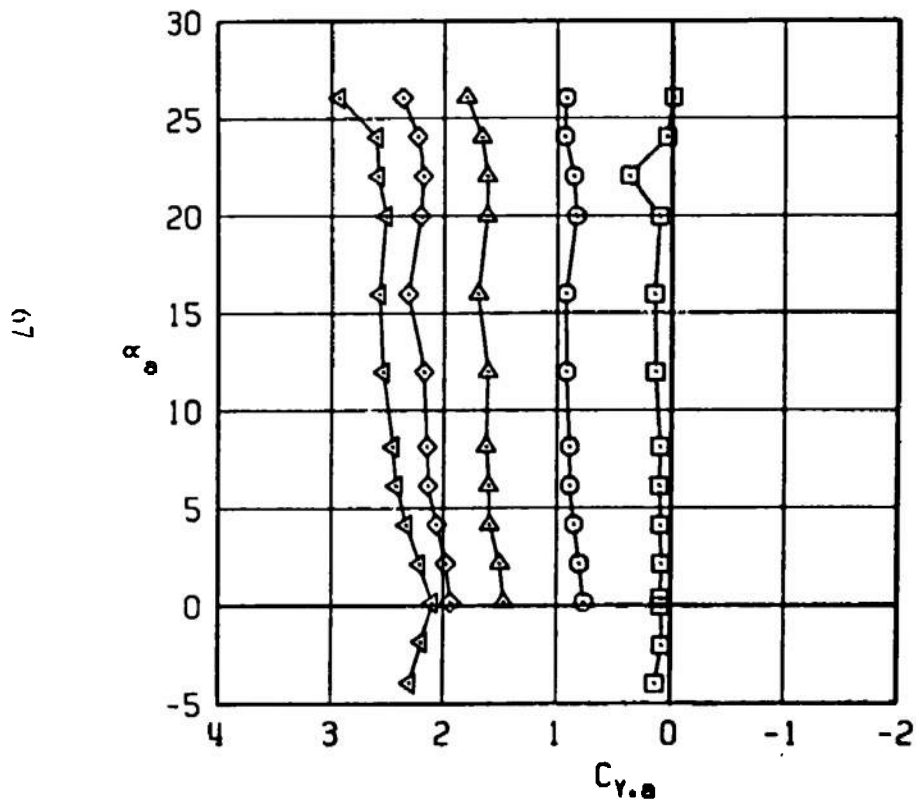


Figure 16. Effect of yaw control deflections on the side-force and yawing-moment coefficients of the Super HOBOS/MK-84.

SYM	CONFIGURATION	MACH NO	δp	δq	δr
□	B2S13W4T3F7	0.65	0	0	0
○	B2S13W4T3F7	0.65	0	0	5
△	B2S13W4T3F7	0.65	0	0	10
◇	B2S13W4T3F7	0.65	0	0	15
◄	B2S13W4T3F7	0.65	0	0	20

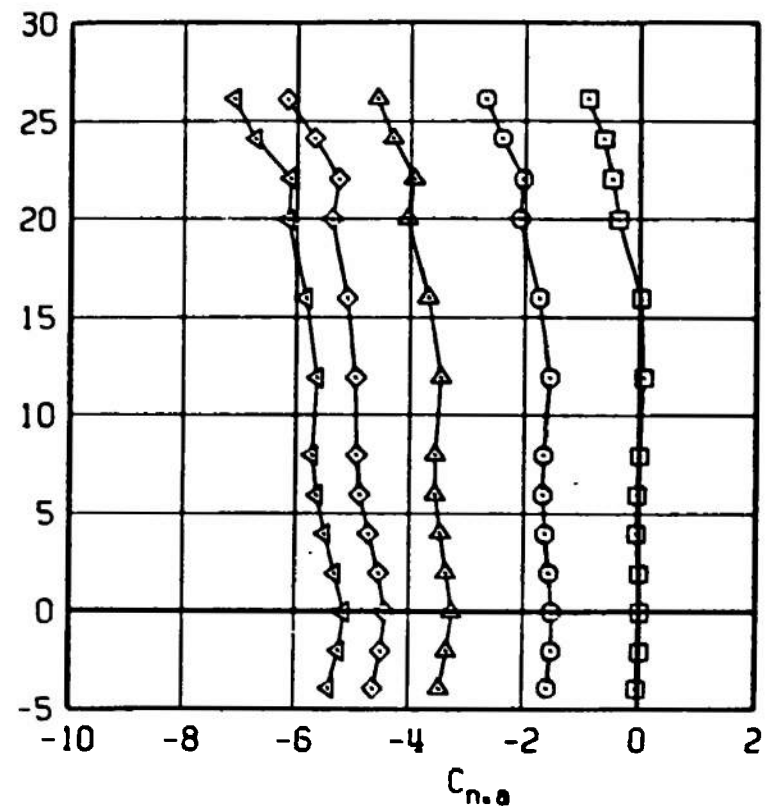
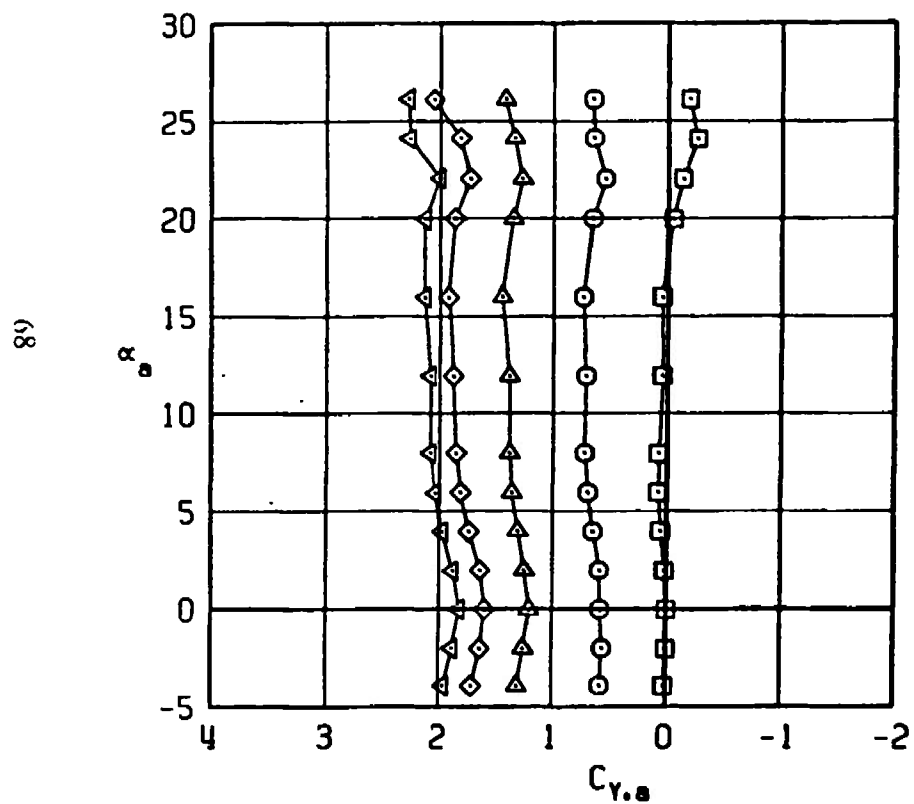


Figure 16. Continued.

SYM	CONFIGURATION	MACH NO	δp	δq	δr
□	B2S13W4T3F7	0.95	0	0	0
○	B2S13W4T3F7	0.95	0	0	5
△	B2S13W4T3F7	0.95	0	0	10
◇	B2S13W4T3F7	0.95	0	0	15
◁	B2S13W4T3F7	0.95	0	0	20

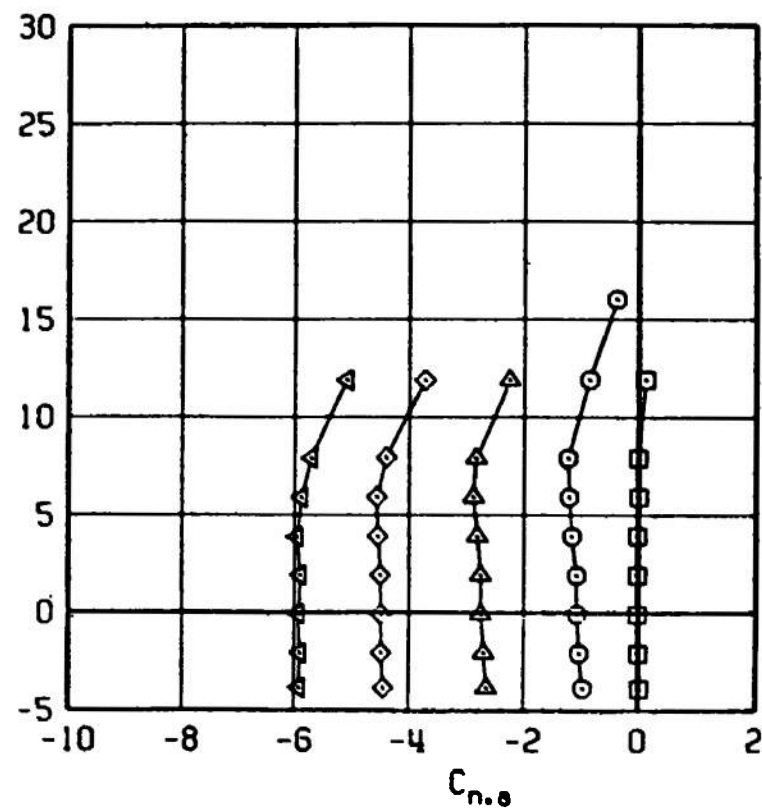
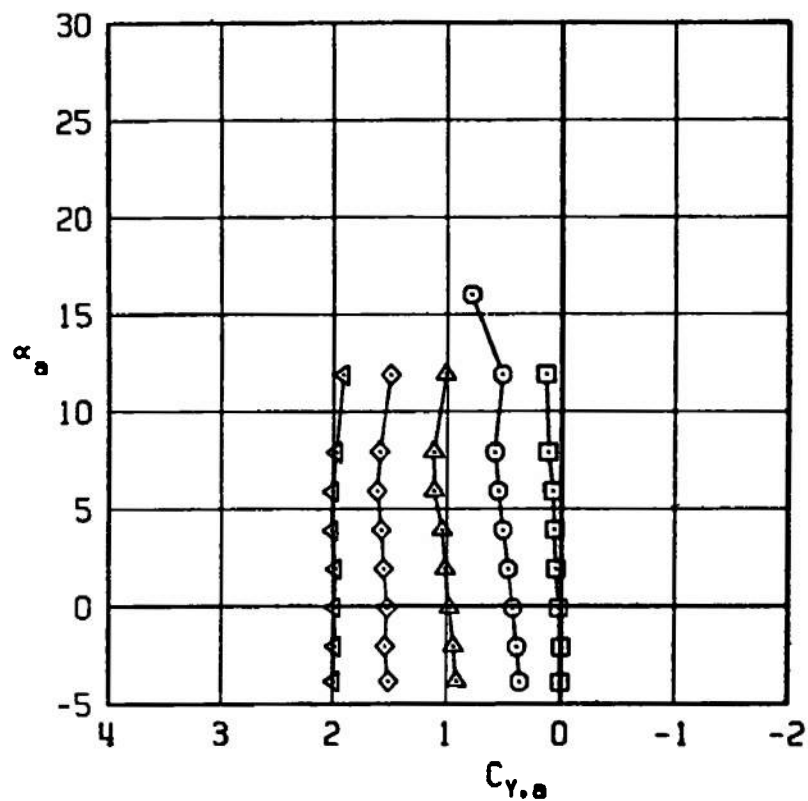


Figure 16. Continued.

SYM	CONFIGURATION	MACH NO	δp	δq	δr
□	B2S13W4T3F7	1.20	0	0	0
○	B2S13W4T3F7	1.20	0	0	5
△	B2S13W4T3F7	1.20	0	0	10
◇	B2S13W4T3F7	1.20	0	0	15
◁	B2S13W4T3F7	1.20	0	0	20

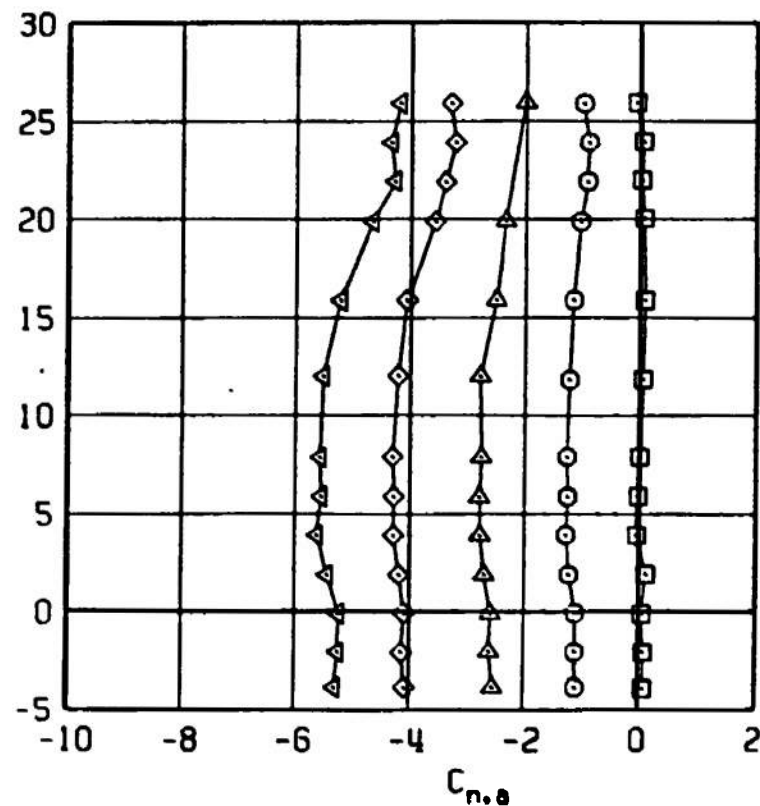
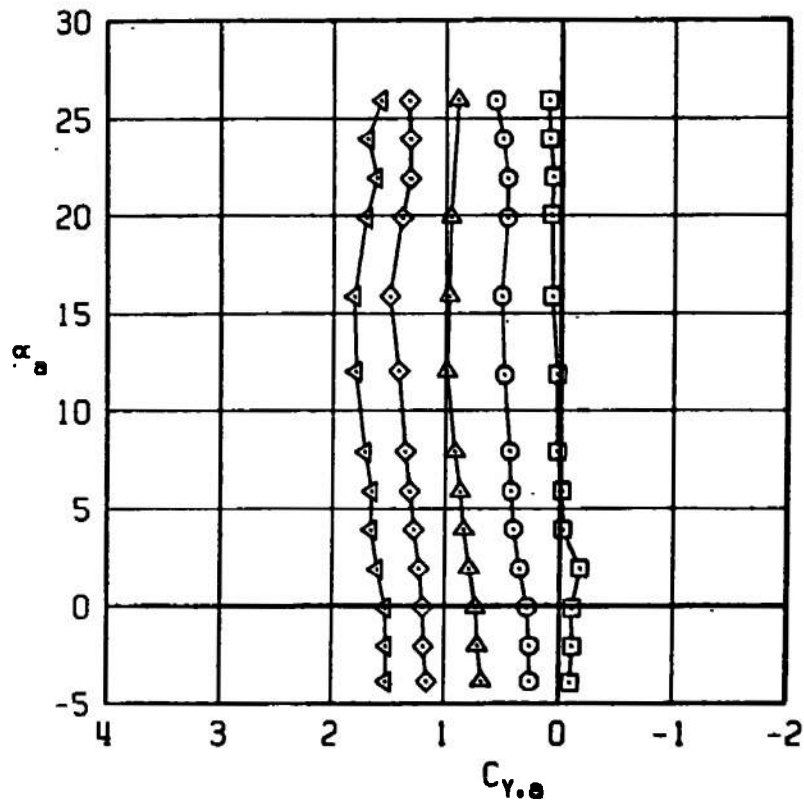


Figure 16. Continued.

SYM	CONFIGURATION	MACH NO	δp	δq	δr
□	B2S13W4T3F7	1.60	0	0	0
○	B2S13W4T3F7	1.60	0	0	5
△	B2S13W4T3F7	1.60	0	0	10
◇	B2S13W4T3F7	1.60	0	0	15
◄	B2S13W4T3F7	1.60	0	0	20

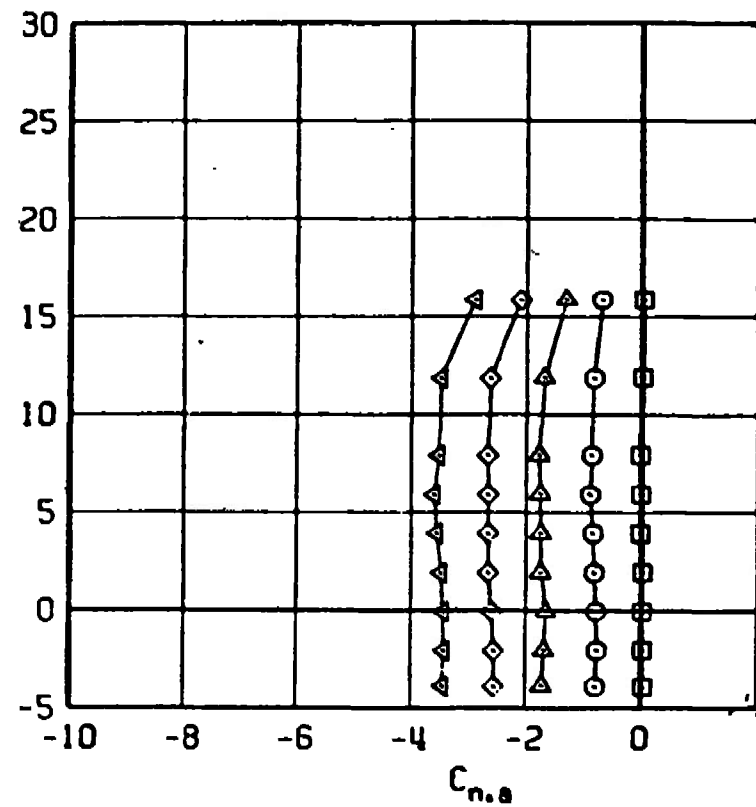
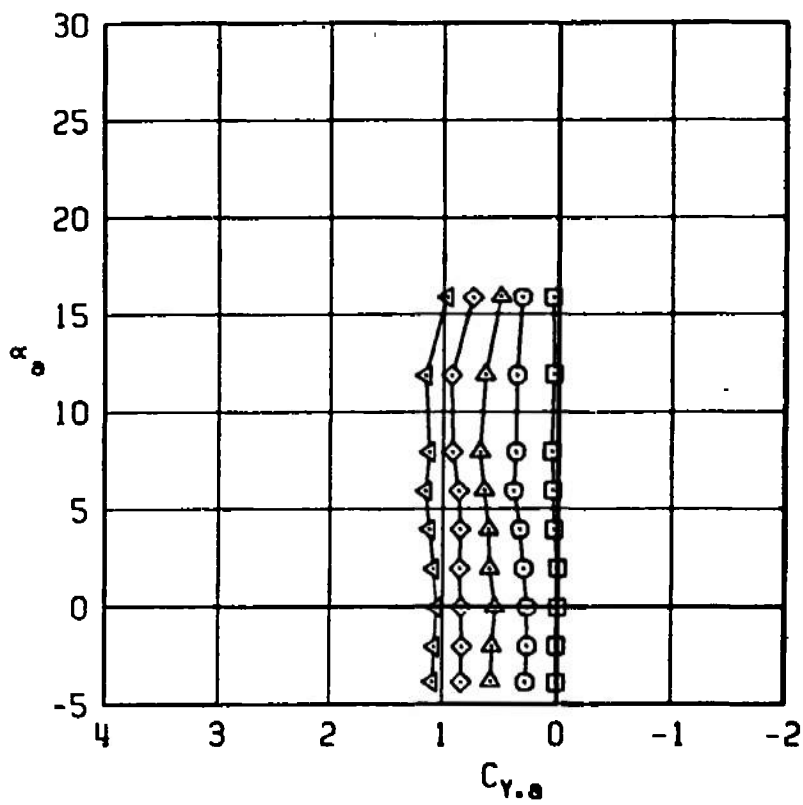


Figure 16. Concluded.

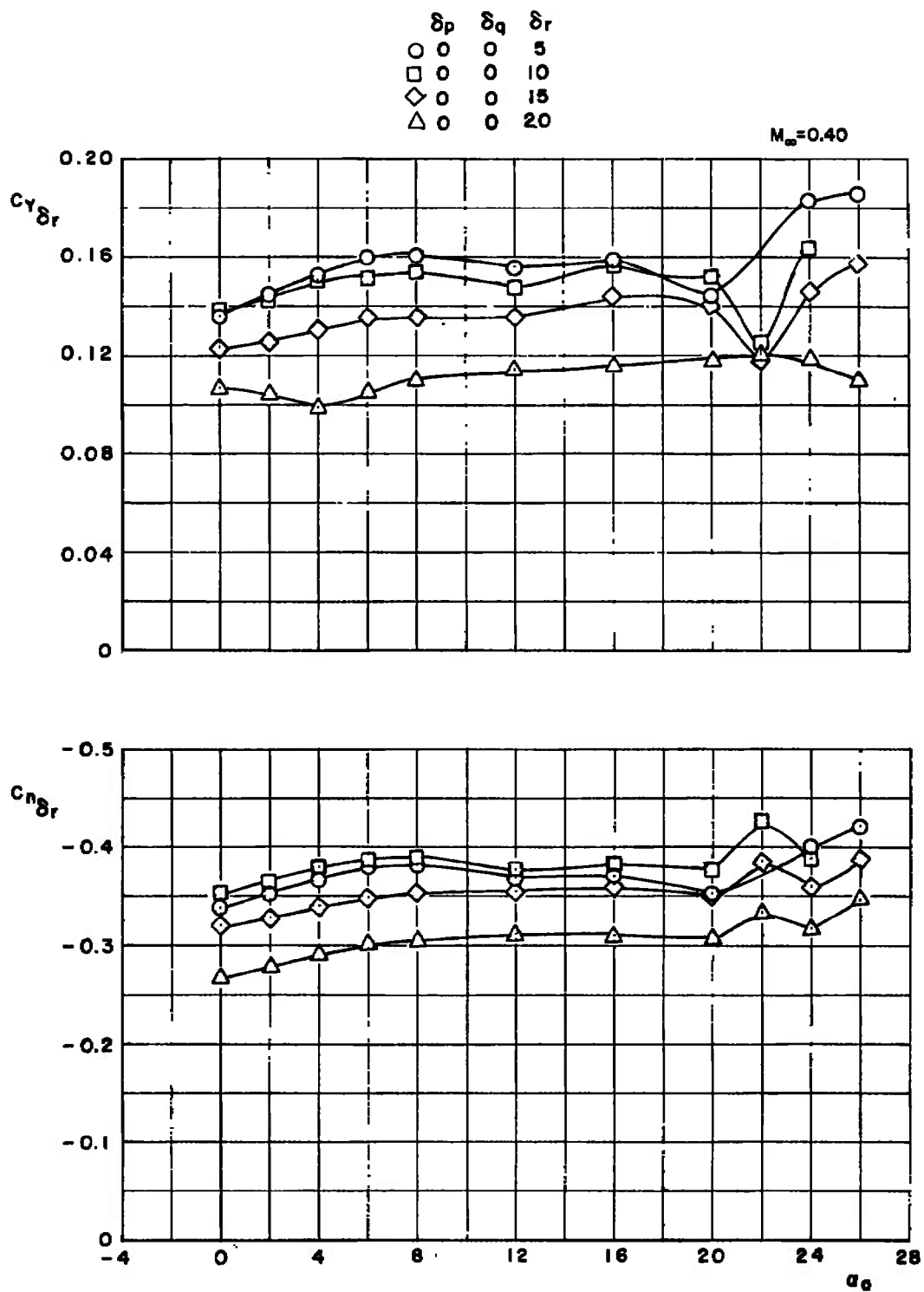


Figure 17. Side-force increment and yaw control effectiveness for several yaw control deflections.

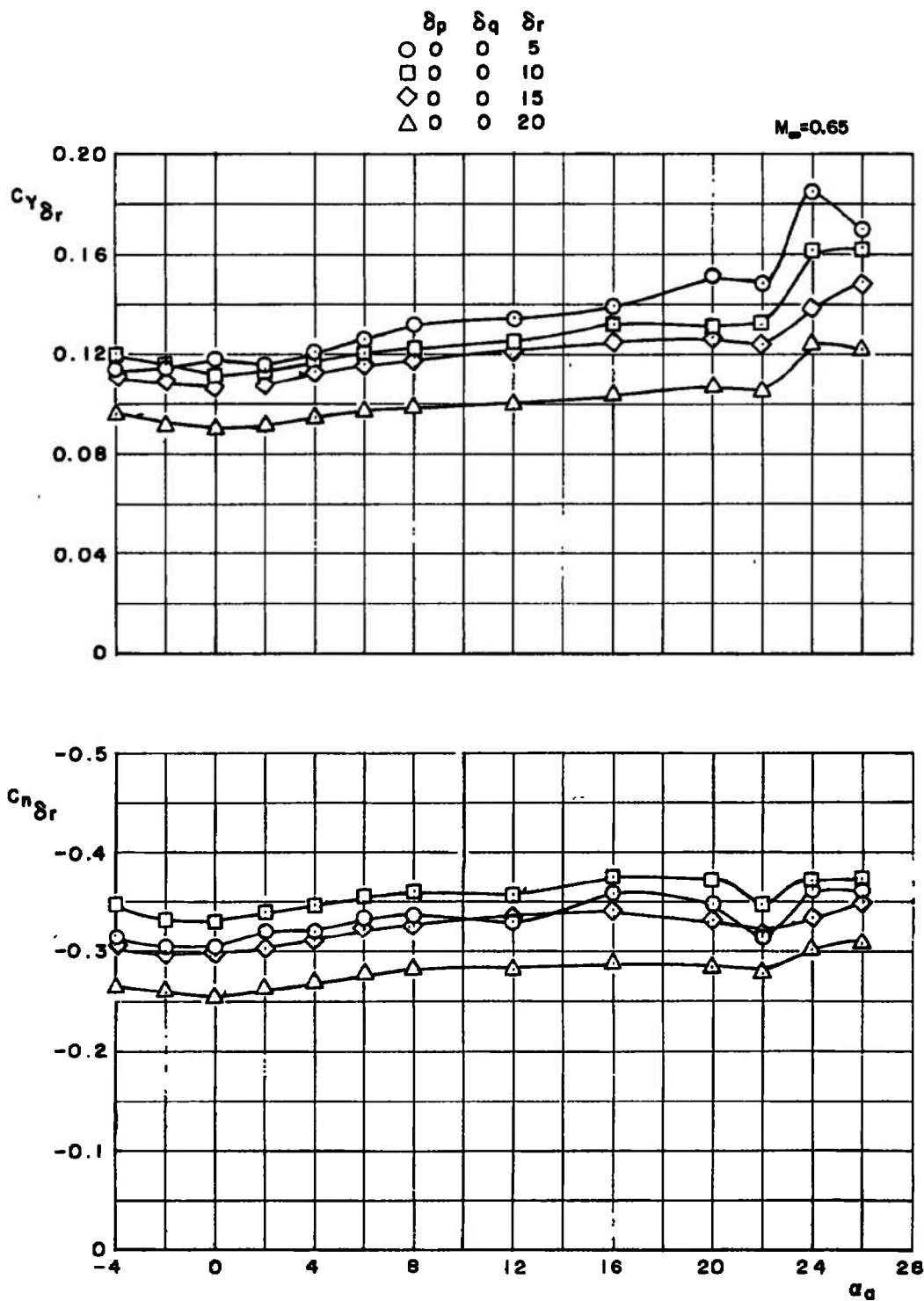


Figure 17. Continued.

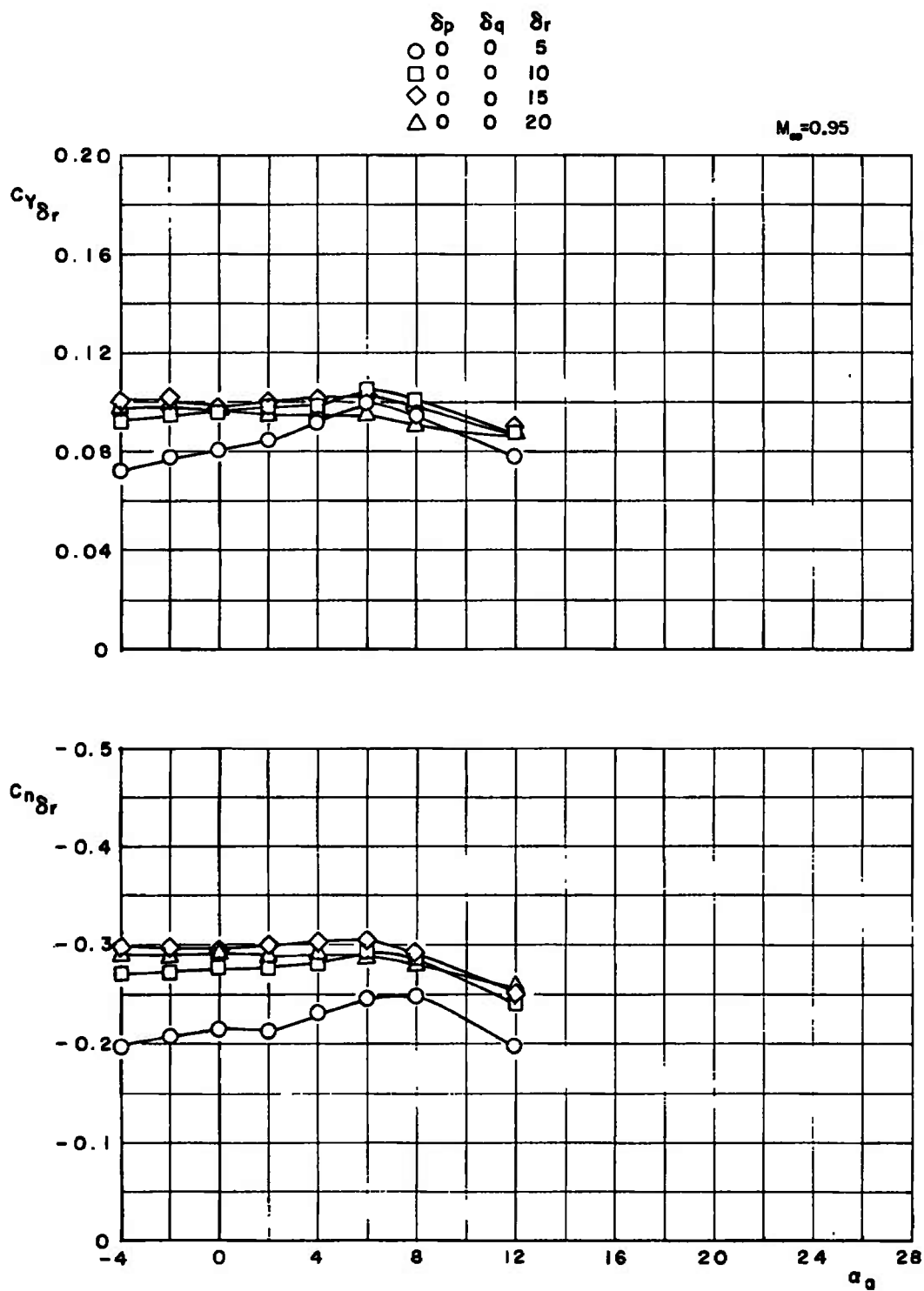


Figure 17. Continued.

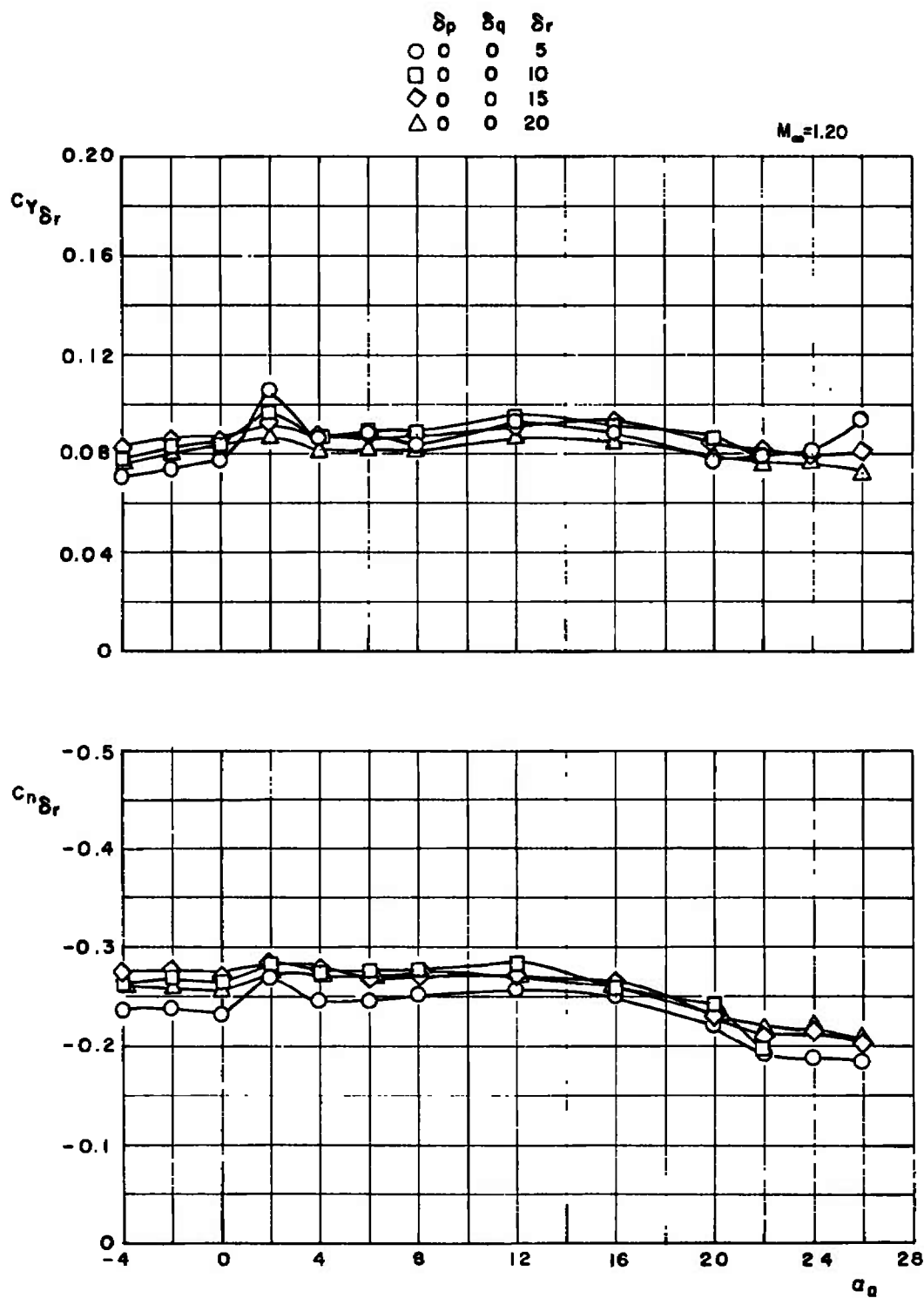


Figure 17. Continued.

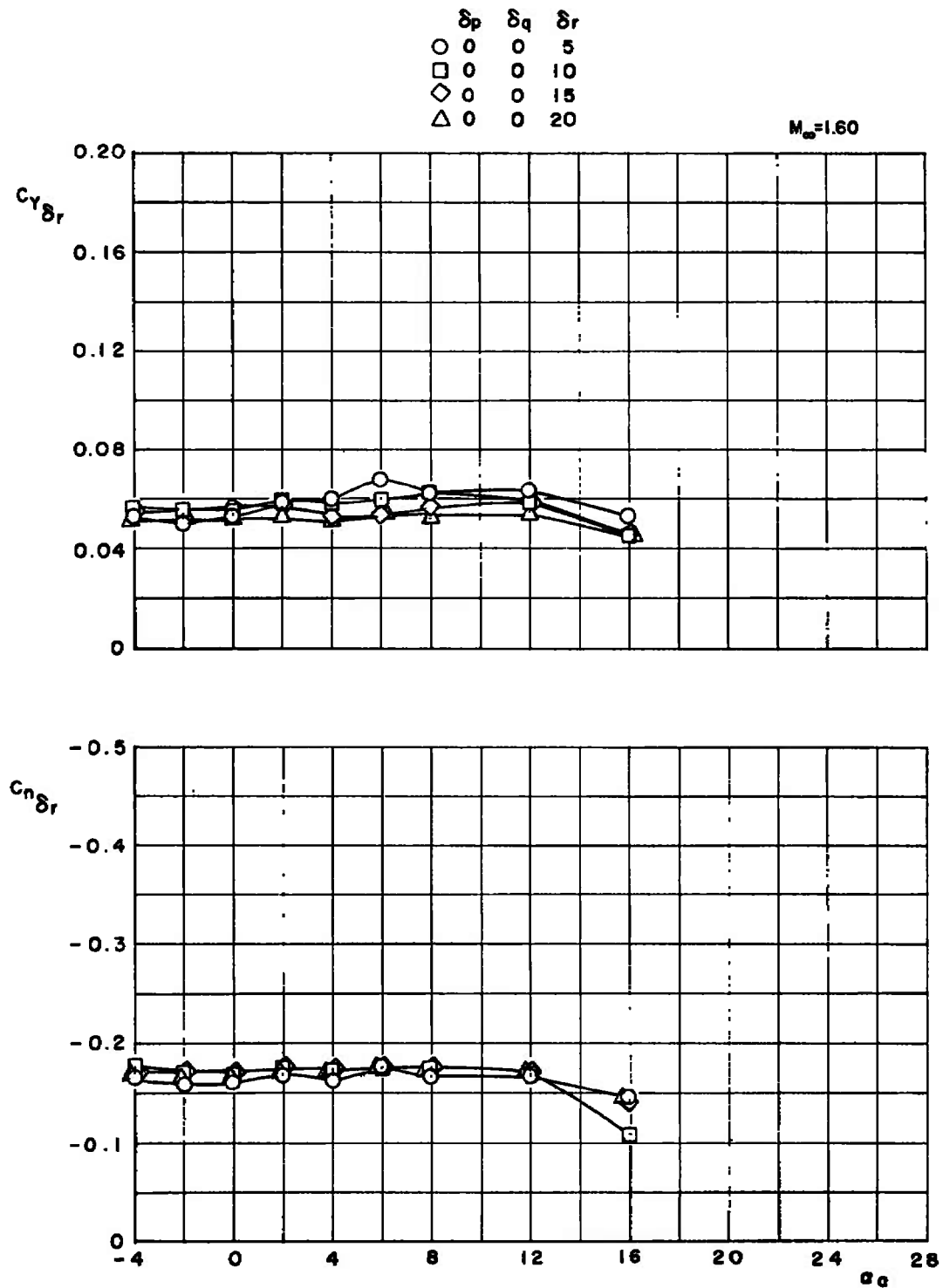


Figure 17. Concluded.

SYM	CONFIGURATION	MACH NO	δp	δq	δr
□	B2S13W4T3F7	0.40	0	0	0
○	B2S13W4T3F7	0.40	-5	0	0
△	B2S13W4T3F7	0.40	0	-10	0
◇	B2S13W4T3F7	0.40	-5	-10	0

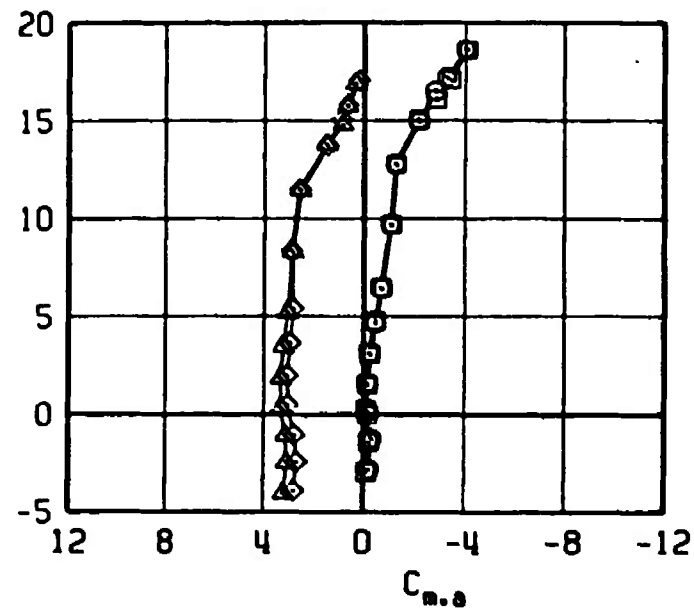
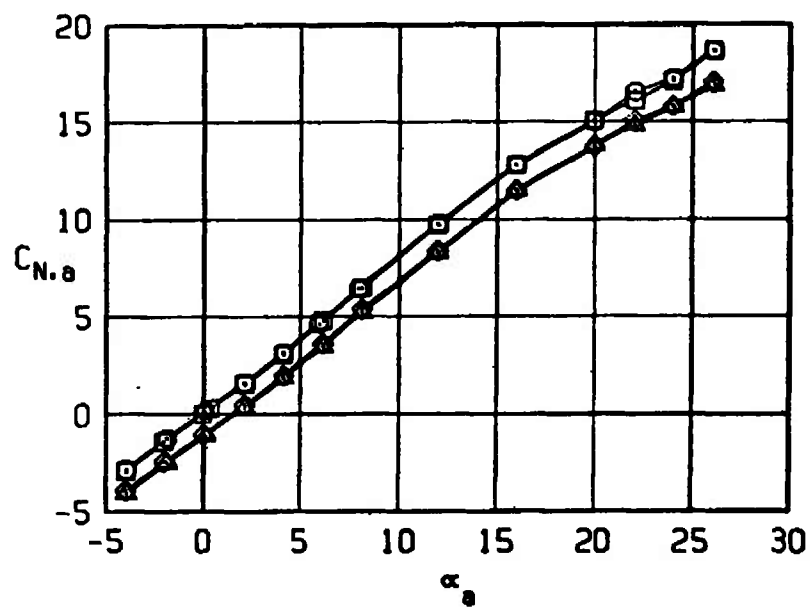


Figure 18. Effect of roll control, $\delta p = -5$ deg, and pitch control, $\delta q = -10$ deg, deflections on the normal-force and pitching-moment coefficients of the Super HOBOS/MK-84.

SYM	CONFIGURATION	MACH NO	δp	δq	δr
□	B2S13W4T3F7	0.65	0	0	0
○	B2S13W4T3F7	0.65	-5	0	0
△	B2S13W4T3F7	0.65	0	-10	0
◇	B2S13W4T3F7	0.65	-5	-10	0

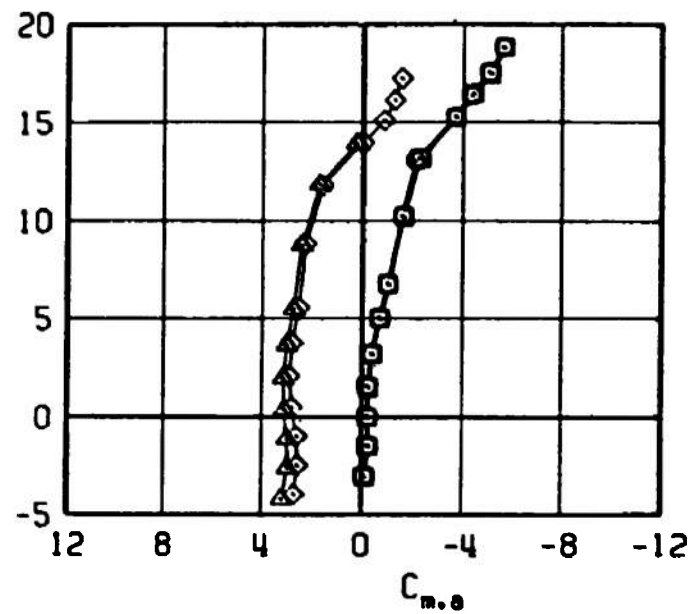
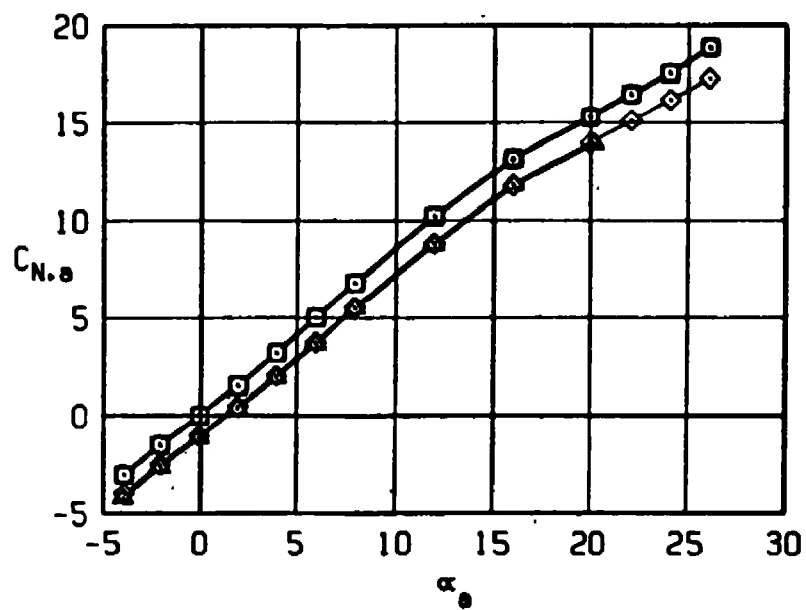


Figure 18. Continued.

SYM	CONFIGURATION	MACH NO	δp	δq	δr
□	B2S13W4T3F7	0.95	0	0	0
○	B2S13W4T3F7	0.95	-5	0	0
△	B2S13W4T3F7	0.95	0	-10	0
◇	B2S13W4T3F7	0.95	-5	-10	0

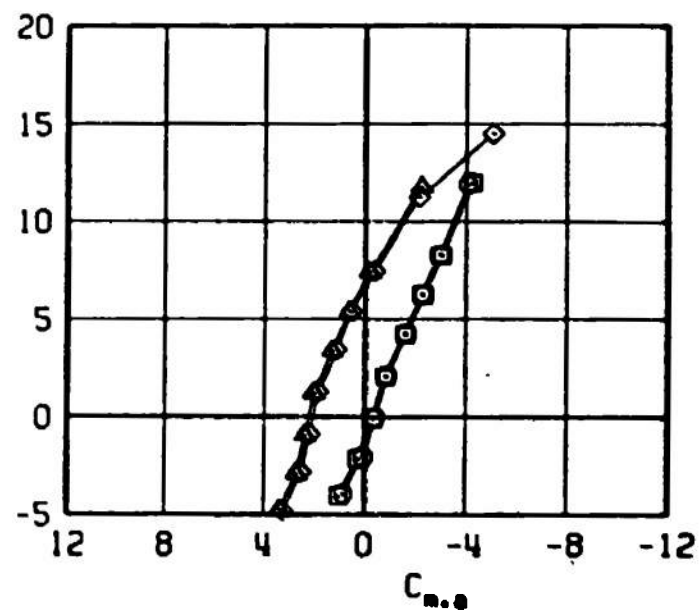
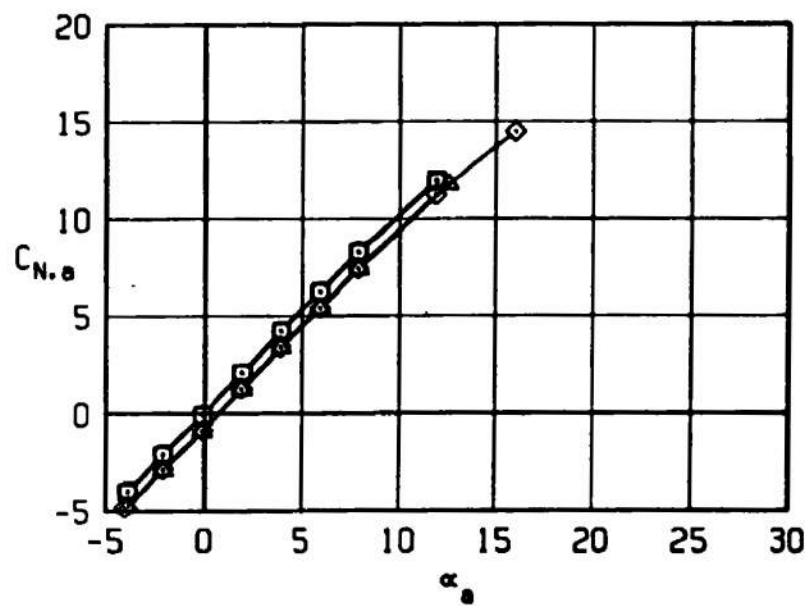


Figure 18. Continued.

SYM	CONFIGURATION	MACH NO	δp	δq	δr
□	B2S13W4T3F7	1.20	0	0	0
○	B2S13W4T3F7	1.20	-5	0	0
△	B2S13W4T3F7	1.20	0	-10	0
◇	B2S13W4T3F7	1.20	-5	-10	0

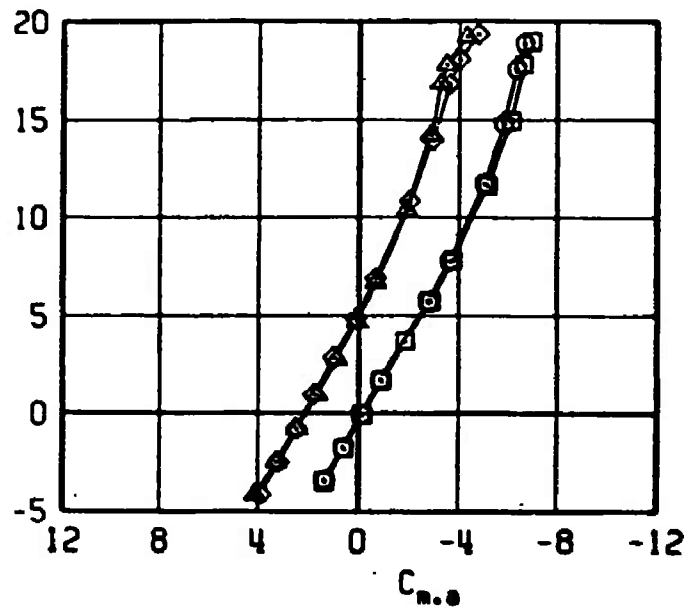
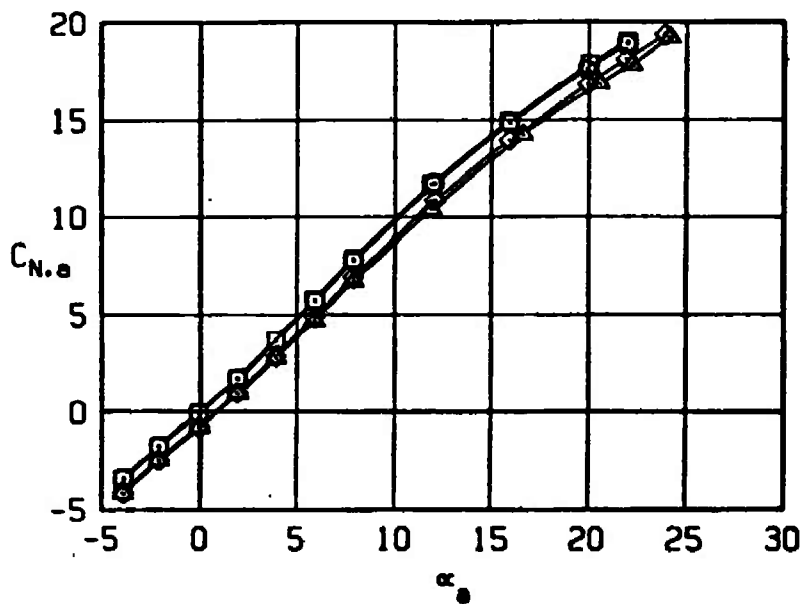


Figure 18. Continued.

SYM	CONFIGURATION	MACH NO	δp	δq	δr
□	B2S13W4T3F7	1.60	0	0	0
○	B2S13W4T3F7	1.60	-5	0	0
△	B2S13W4T3F7	1.60	0	-10	0
◇	B2S13W4T3F7	1.60	-5	-10	0

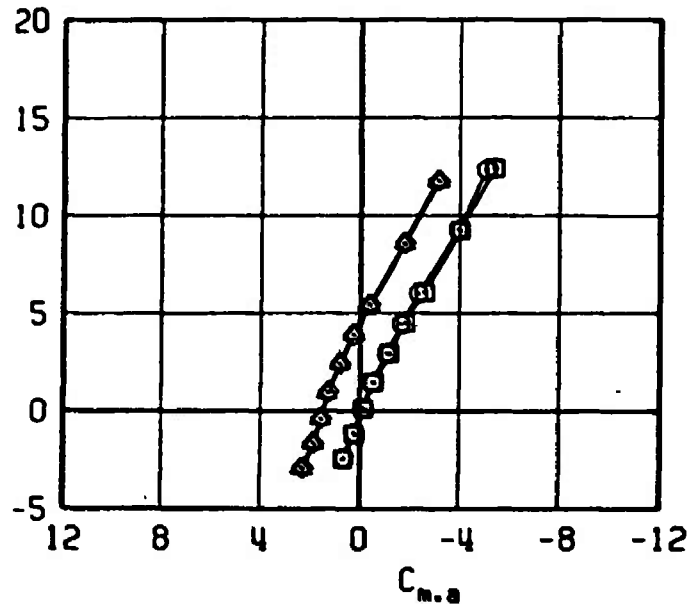
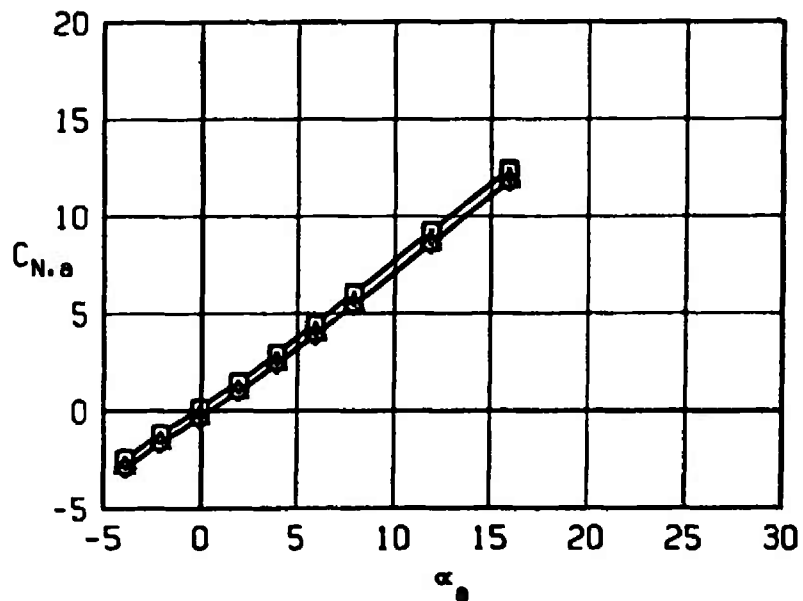


Figure 18. Concluded.

SYM	CONFIGURATION	MACH NO	δp	δq	δr
□	B2S13WIT3F7	0.40	0	0	0
○	B2S13WIT3F7	0.40	-5	0	0
△	B2S13WIT3F7	0.40	0	-10	0
◇	B2S13WIT3F7	0.40	-5	-10	0

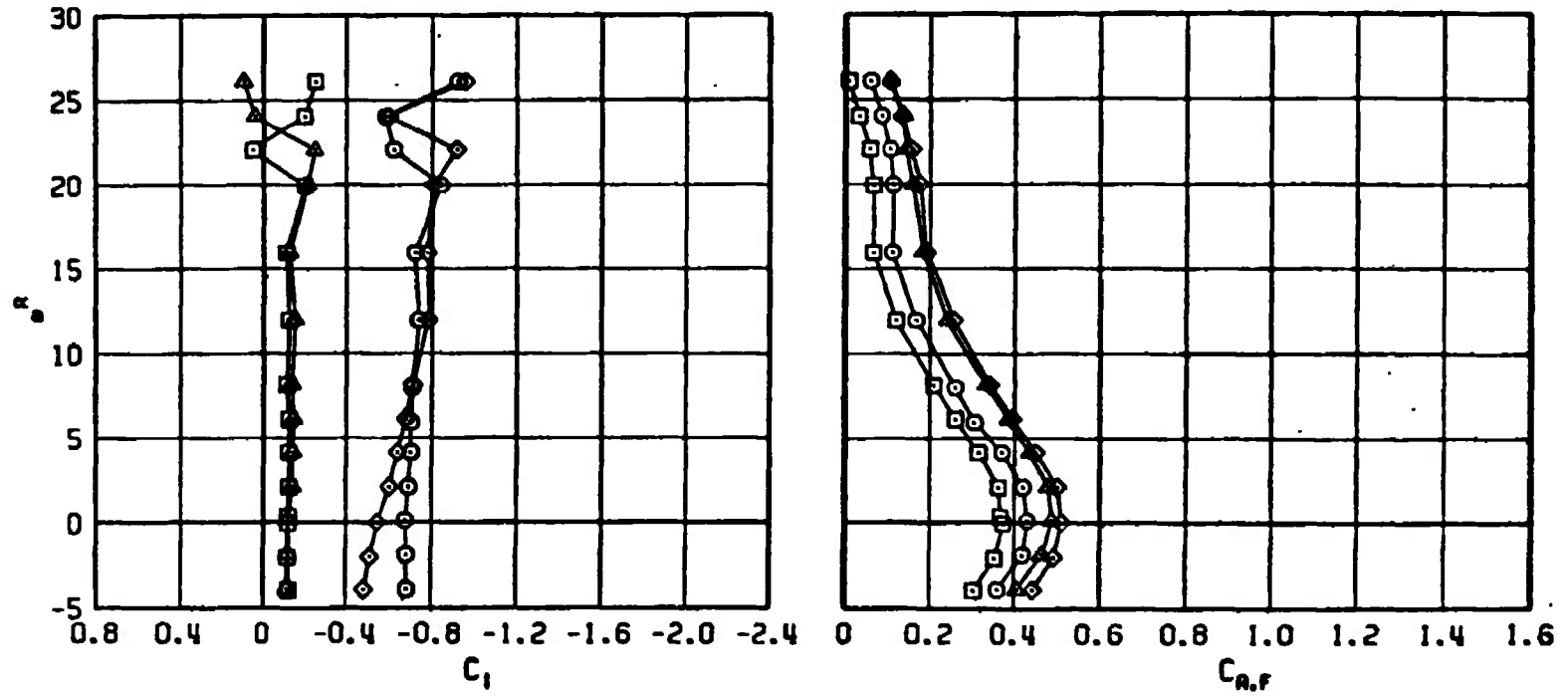


Figure 19. Effect of roll control, $\delta p = -5$ deg, and pitch control, $\delta q = -10$ deg, deflections on the rolling-moment and axial-force coefficients of the Super HOBOS/MK-84.

SYM	CONFIGURATION	MACH NO	δp	δq	δr
□	B2S13W4T3F7	0.65	0	0	0
○	B2S13W4T3F7	0.65	-5	0	0
△	B2S13W4T3F7	0.65	0	-10	0
◇	B2S13W4T3F7	0.65	-5	-10	0

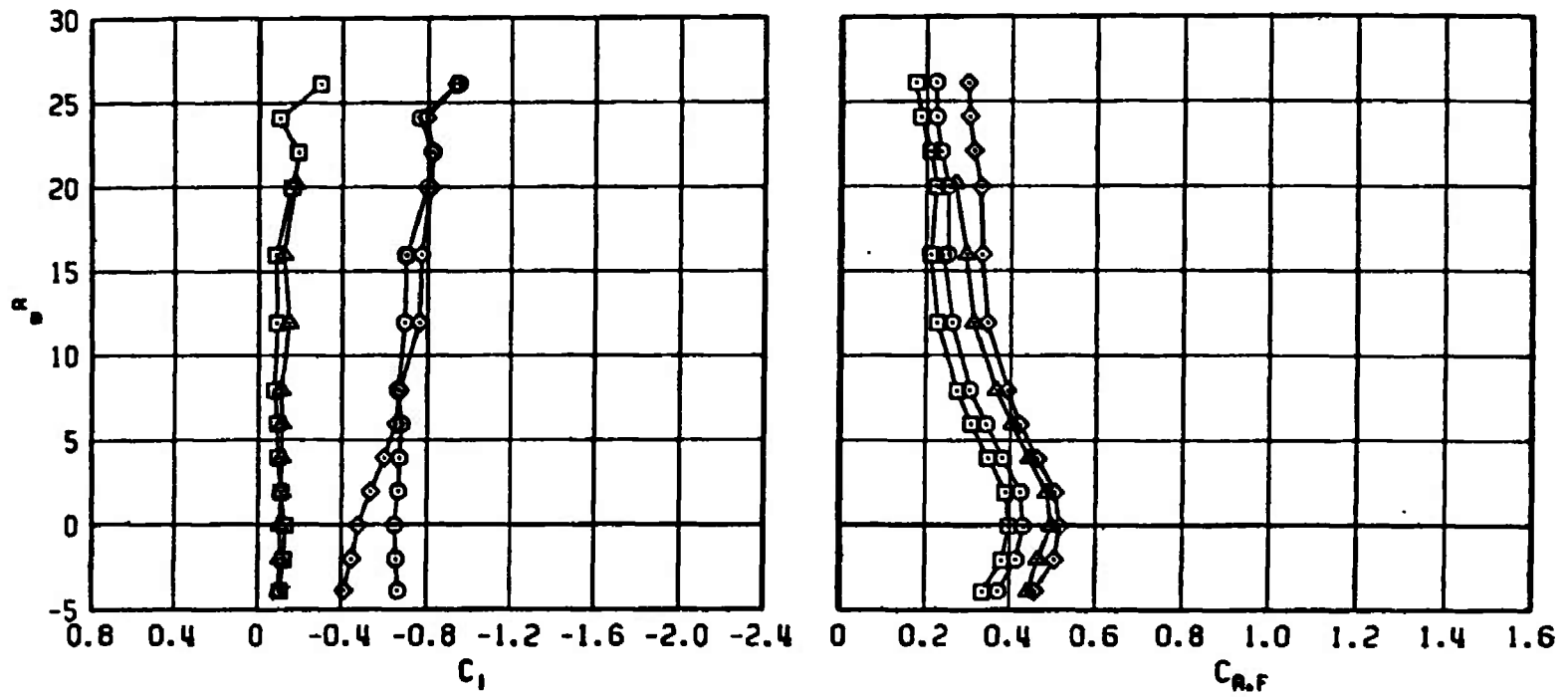


Figure 19. Continued.

SYM	CONFIGURATION	MACH NO	δp	δq	δr
□	B2S13W4T3F7	0.95	0	0	0
○	B2S13W4T3F7	0.95	-5	0	0
△	B2S13W4T3F7	0.95	0	-10	0
◇	B2S13W4T3F7	0.95	-5	-10	0

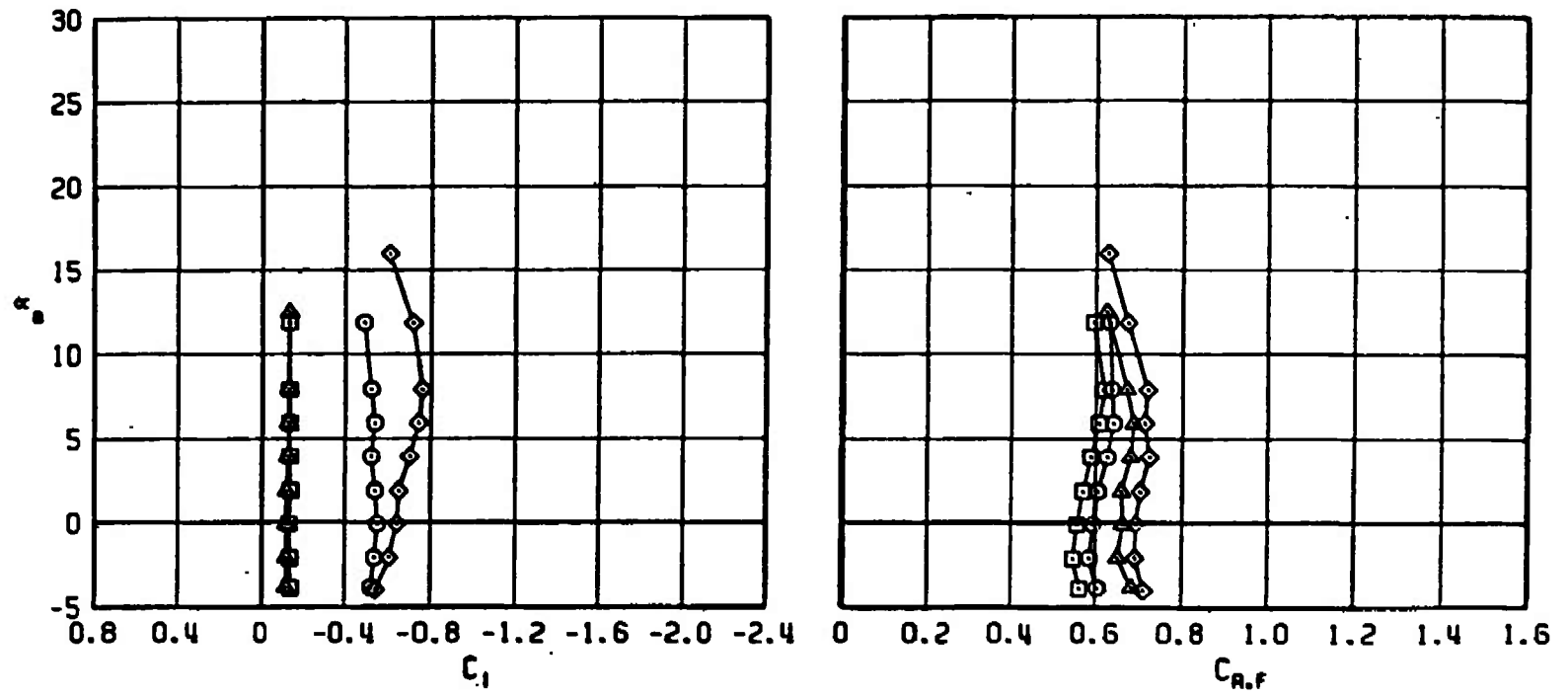


Figure 19. Continued.

SYM	CONFIGURATION	MACH NO	δp	δq	δr
□	B2S13W4T3F7	1.20	0	0	0
○	B2S13W4T3F7	1.20	-5	0	0
△	B2S13W4T3F7	1.20	0	-10	0
◇	B2S13W4T3F7	1.20	-5	-10	0

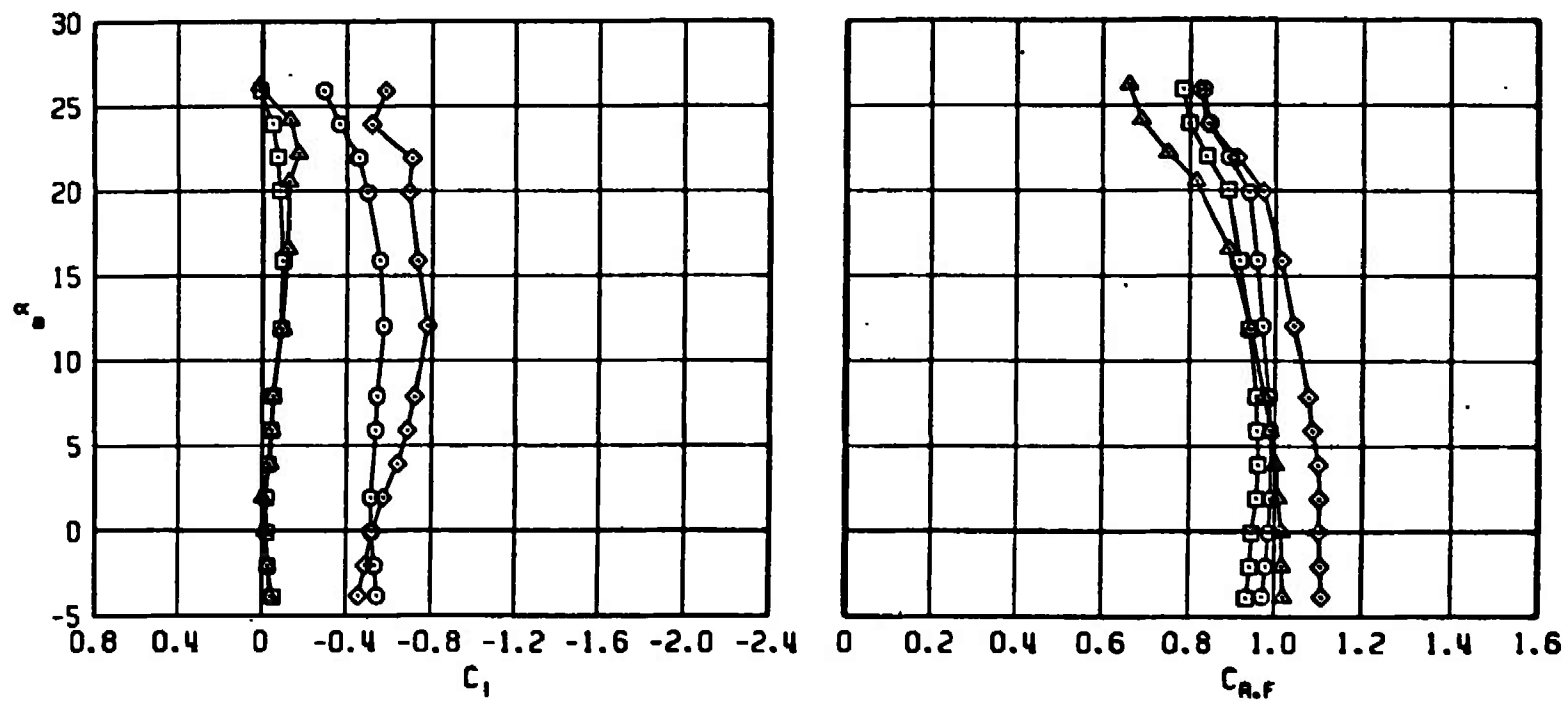


Figure 19. Continued.

SYM	CONFIGURATION	MACH NO	δp	δq	δr
□	B2S13W4T3F7	1.60	0	0	0
○	B2S13W4T3F7	1.60	-5	0	0
▲	B2S13W4T3F7	1.60	0	-10	0
◇	B2S13W4T3F7	1.60	-5	-10	0

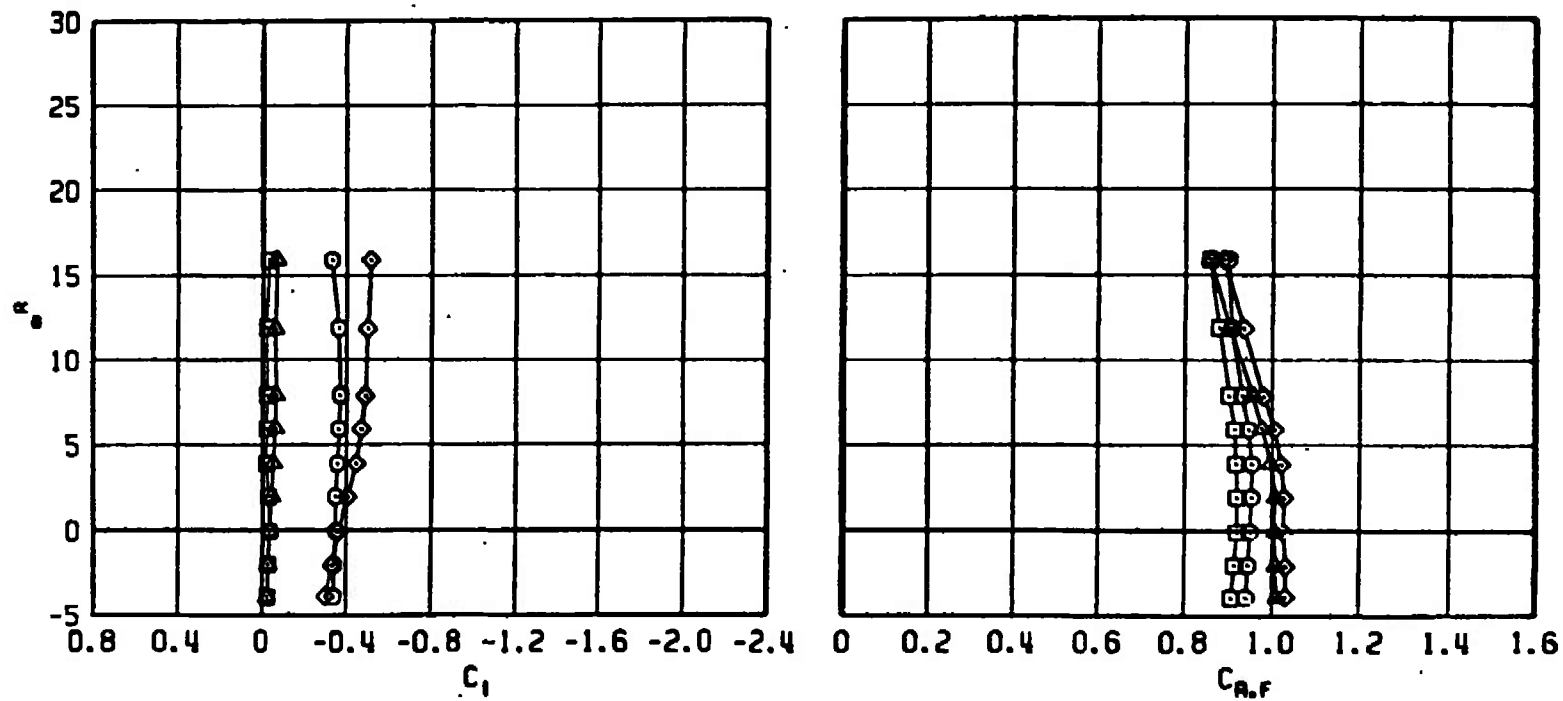


Figure 19. Concluded.

SYM	CONFIGURATION	MACH NO	δp	δq	δr
□	B2S13W4T3F7	0.40	0	0	0
○	B2S13W4T3F7	0.40	-5	0	0
△	B2S13W4T3F7	0.40	0	-15	0
◇	B2S13W4T3F7	0.40	-5	-15	0

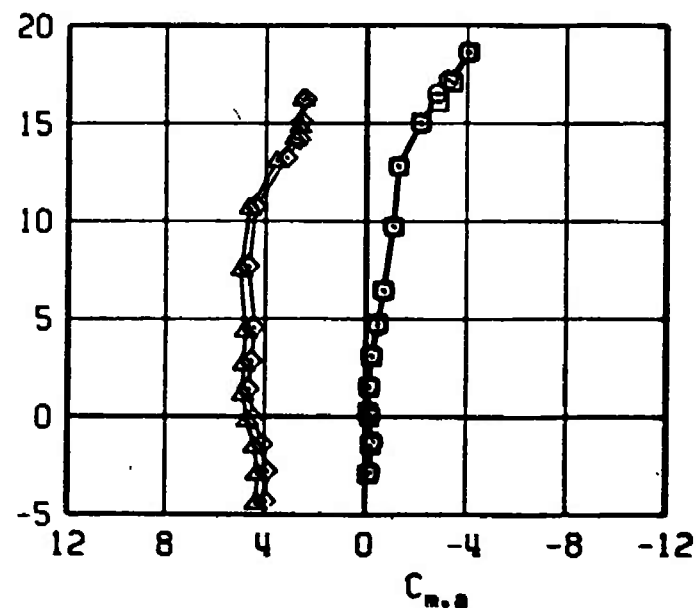
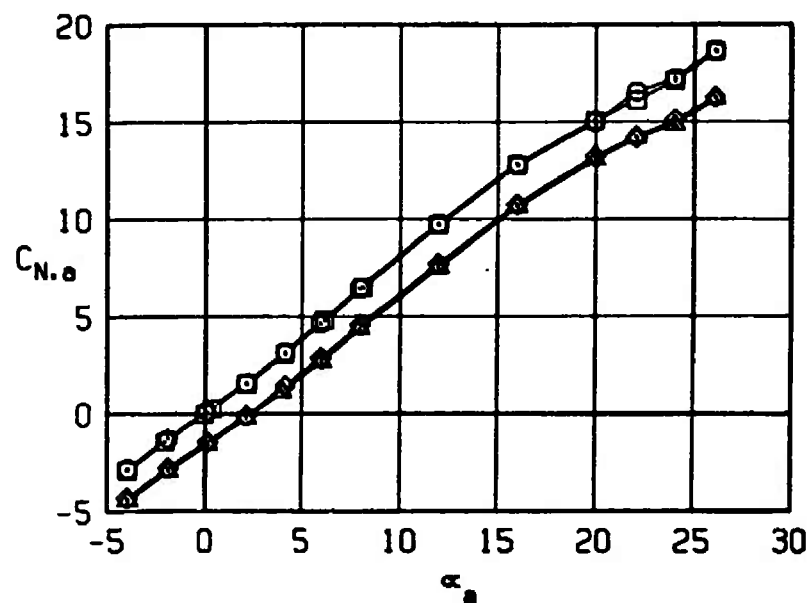


Figure 20. Effect of roll control, $\delta p = -5$ deg, and pitch control, $\delta q = -15$ deg, deflections on the normal-force and pitching-moment coefficients of the Super HOBOS/MK-84.

SYM	CONFIGURATION	MACH NO	δp	δq	δr
□	B2S13W4T3F7	0.65	0	0	0
○	B2S13W4T3F7	0.65	-5	0	0
△	B2S13W4T3F7	0.65	0	-15	0
◇	B2S13W4T3F7	0.65	-5	-15	0

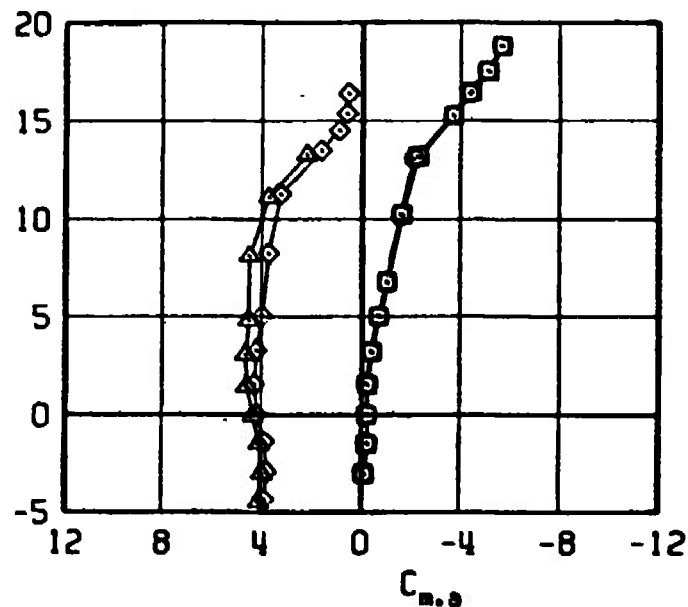
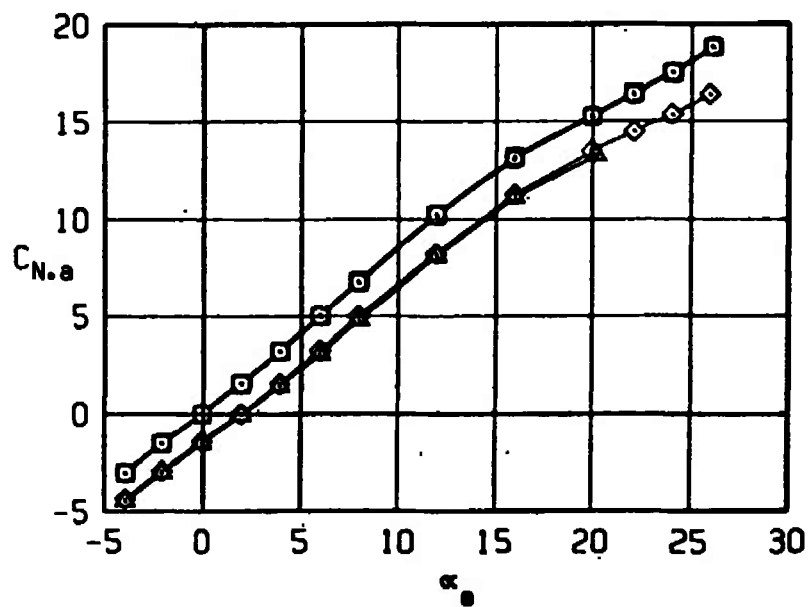


Figure 20. Continued.

SYM	CONFIGURATION	MACH NO	δp	δq	δr
□	B2S13W4T3F7	0.95	0	0	0
○	B2S13W4T3F7	0.95	-5	0	0
△	B2S13W4T3F7	0.95	0	-15	0
◇	B2S13W4T3F7	0.95	-5	-15	0

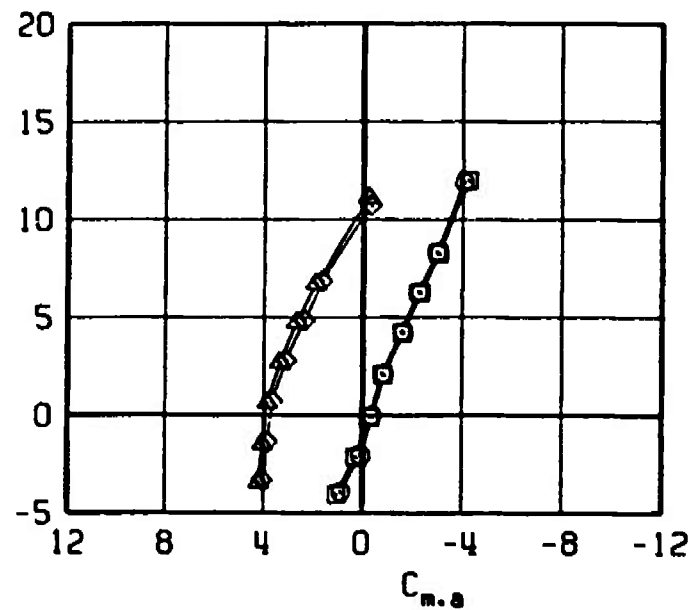
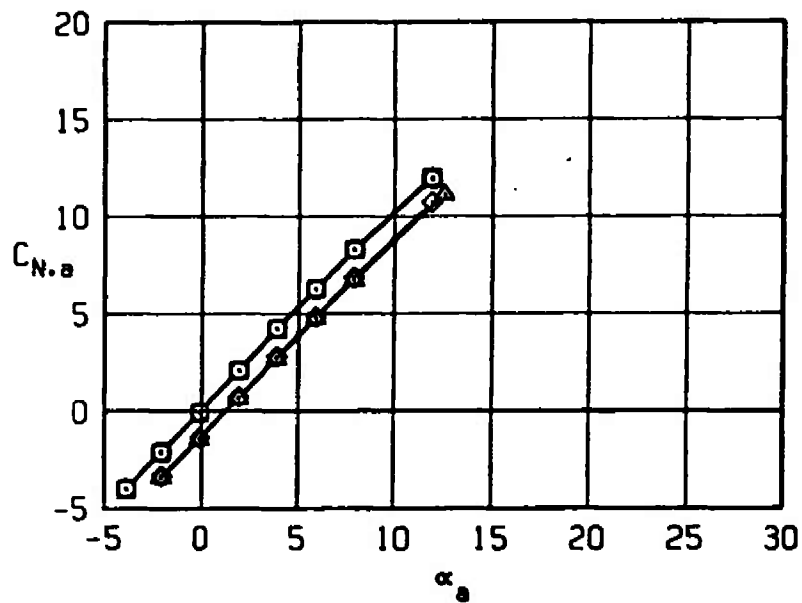


Figure 20. Continued.

SYM	CONFIGURATION	MACH NO	δp	δq	δr
□	B2S13W4T3F7	1.20	0	0	0
○	B2S13W4T3F7	1.20	-5	0	0
△	B2S13W4T3F7	1.20	0	-15	0
◇	B2S13W4T3F7	1.20	-5	-15	0

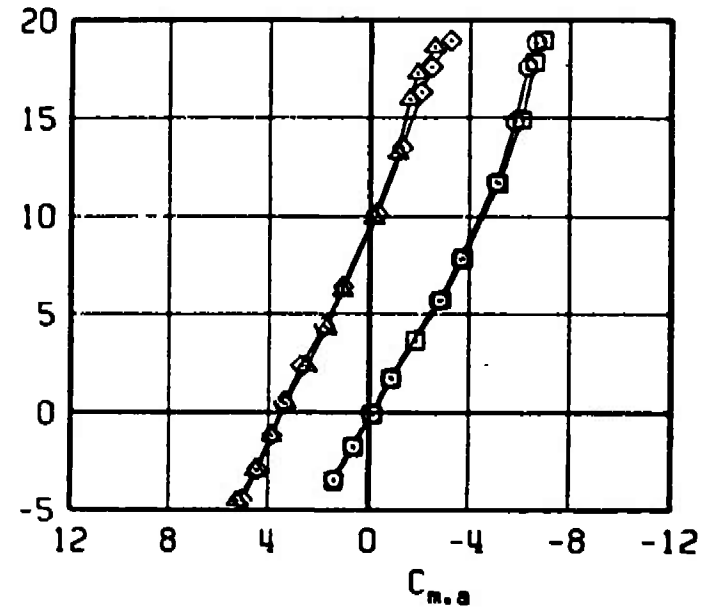
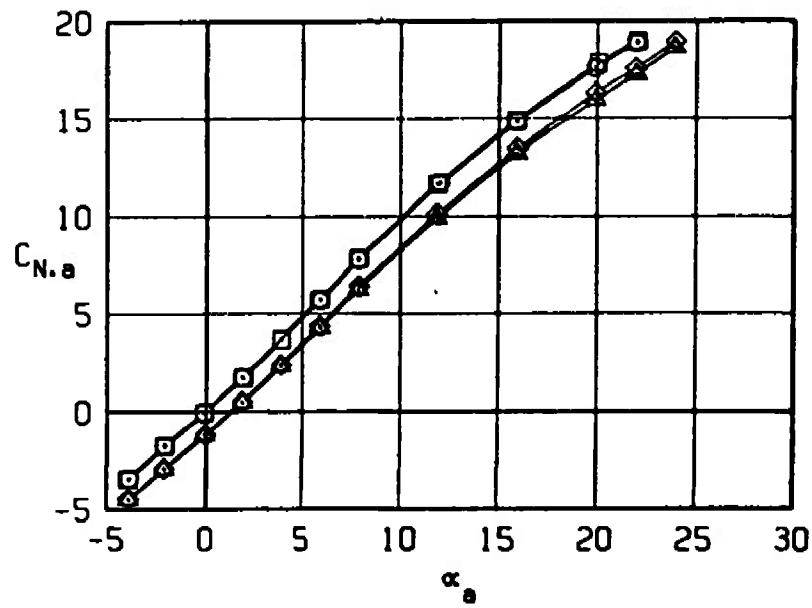


Figure 20. Continued.

SYM	CONFIGURATION	MACH NO	δp	δq	δr
□	B2S13W4T3F7	1.60	0	0	0
○	B2S13W4T3F7	1.60	-5	0	0
△	B2S13W4T3F7	1.60	0	-15	0
◇	B2S13W4T3F7	1.60	-5	-15	0

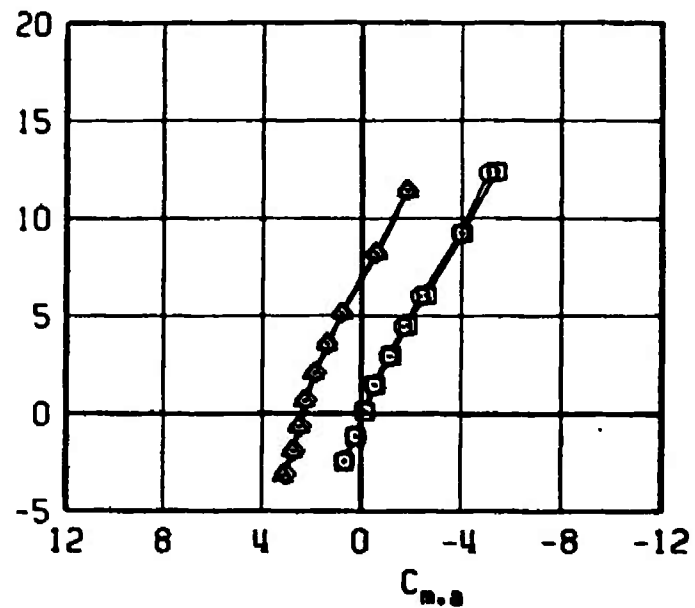
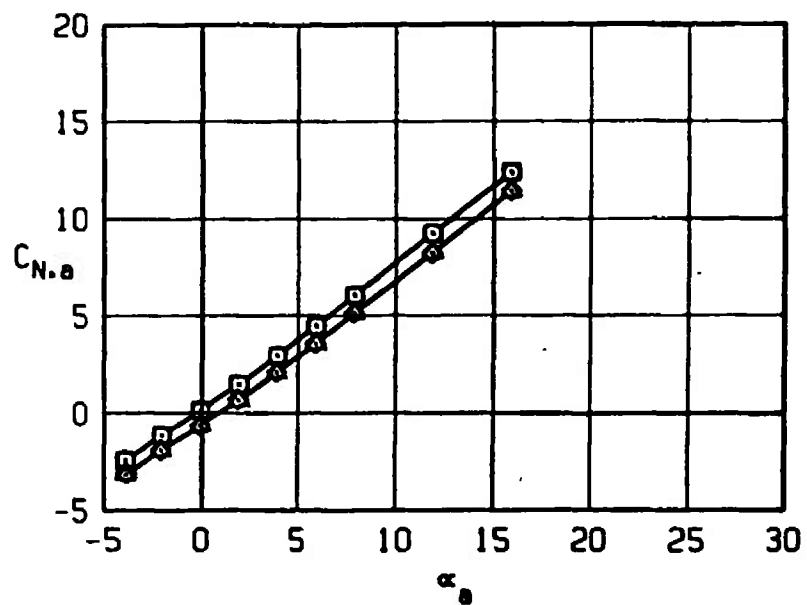


Figure 20. Concluded.

SYM	CONFIGURATION	MACH NO	δp	δq	δr
□	B2S13W4T3F7	0.40	0	0	0
○	B2S13W4T3F7	0.40	-5	0	0
△	B2S13W4T3F7	0.40	0	-15	0
◇	B2S13W4T3F7	0.40	-5	-15	0

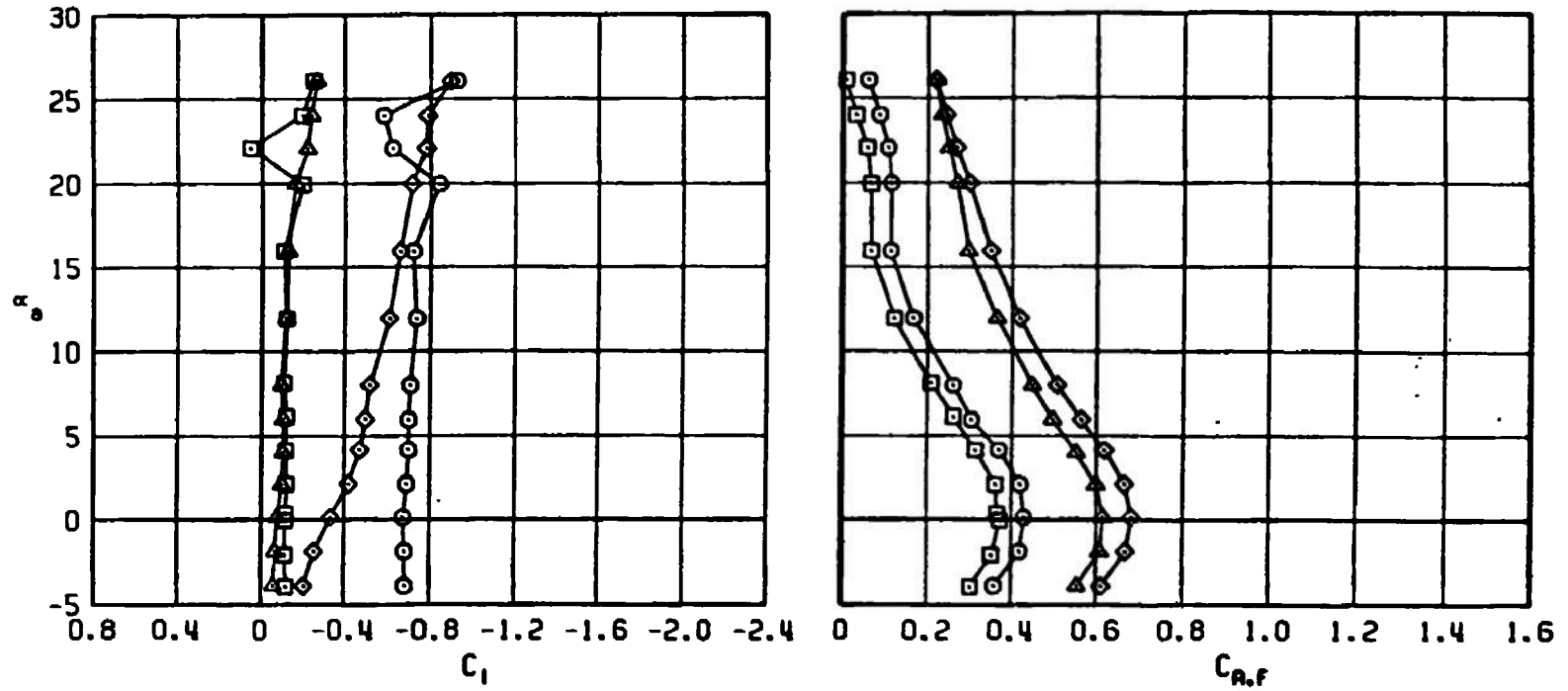


Figure 21. Effect of roll control, $\delta p = -5$ deg, and pitch control, $\delta q = -15$ deg, deflections on the normal-force and pitching-moment coefficients of the Super HOBOS/MK-84.

SYM	CONFIGURATION	MACH NO	δp	δq	δr
□	B2S13W4T3F7	0.65	0	0	0
○	B2S13W4T3F7	0.65	-5	0	0
△	B2S13W4T3F7	0.65	0	-15	0
◇	B2S13W4T3F7	0.65	-5	-15	0

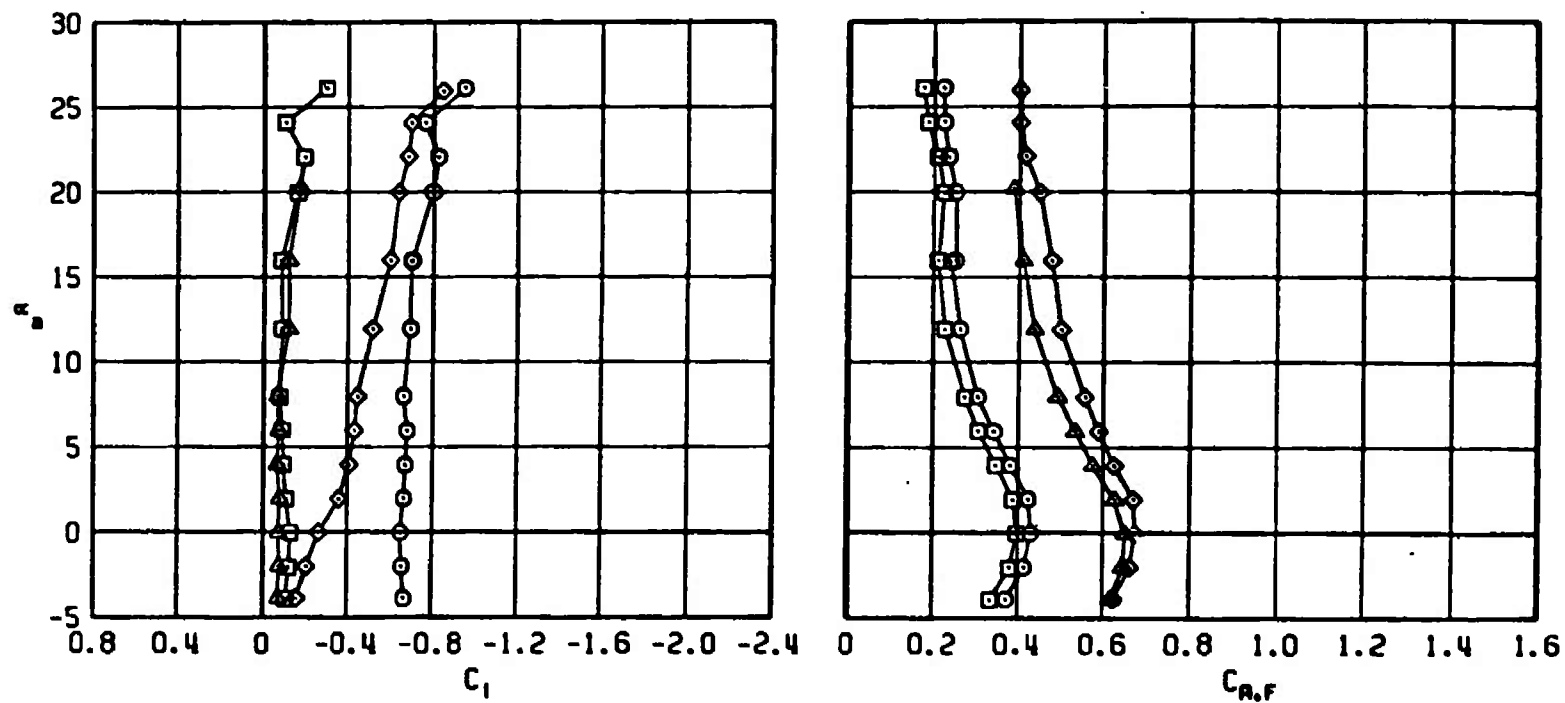


Figure 21. Continued.

SYM	CONFIGURATION	MACH NO	δp	δq	δr
□	B2S13W4T3F7	0.95	0	0	0
○	B2S13W4T3F7	0.95	-5	0	0
△	B2S13W4T3F7	0.95	0	-15	0
◇	B2S13W4T3F7	0.95	-5	-15	0

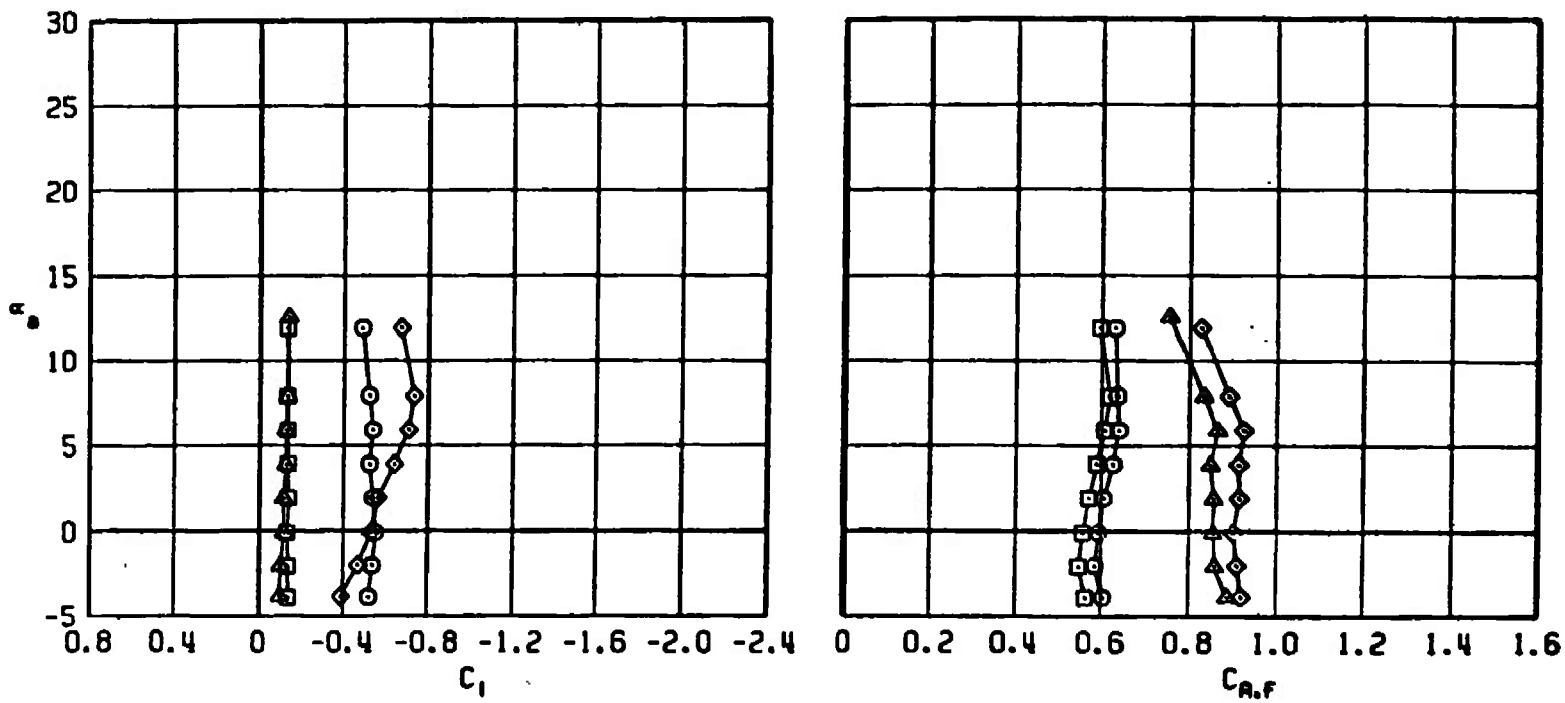


Figure 21. Continued.

SYM	CONFIGURATION	MACH NO	δp	δq	δr
□	B2S13W4T3F7	1.20	0	0	0
○	B2S13W4T3F7	1.20	-5	0	0
△	B2S13W4T3F7	1.20	0	-15	0
◇	B2S13W4T3F7	1.20	-5	-15	0

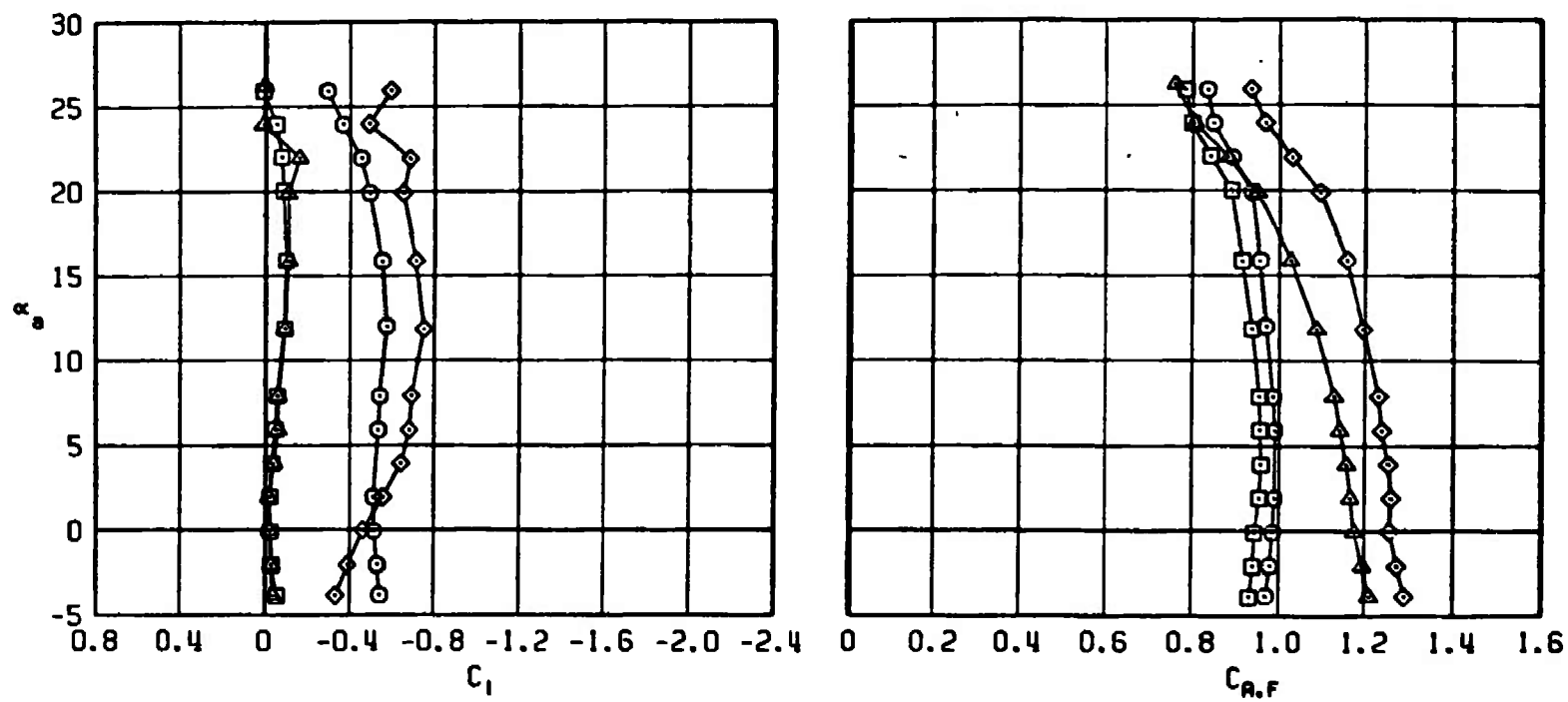


Figure 21. Continued.

SYM	CONFIGURATION	MACH NO	δp	δq	δr
□	B2S13W4T3F7	1.60	0	0	0
○	B2S13W4T3F7	1.60	-5	0	0
△	B2S13W4T3F7	1.60	0	-15	0
◇	B2S13W4T3F7	1.60	-5	-15	0

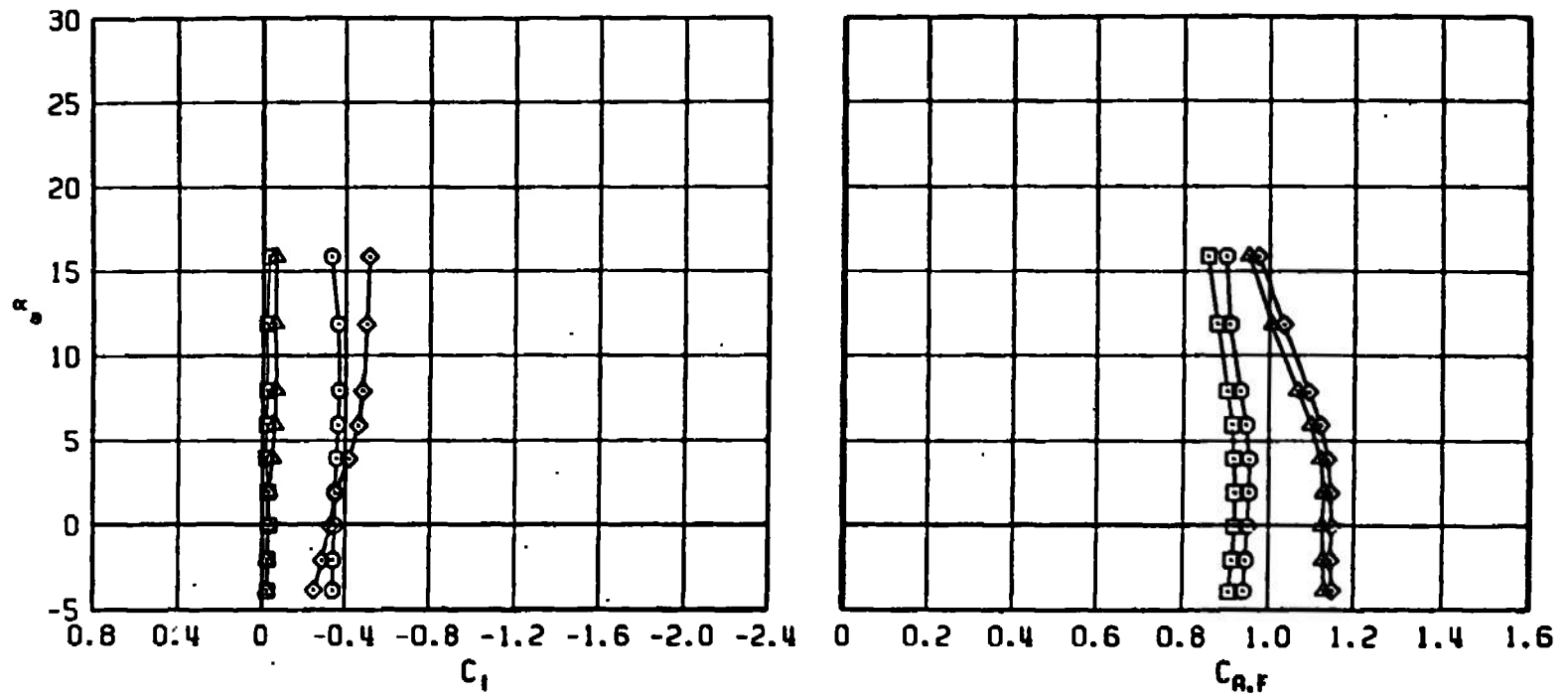


Figure 21. Concluded.

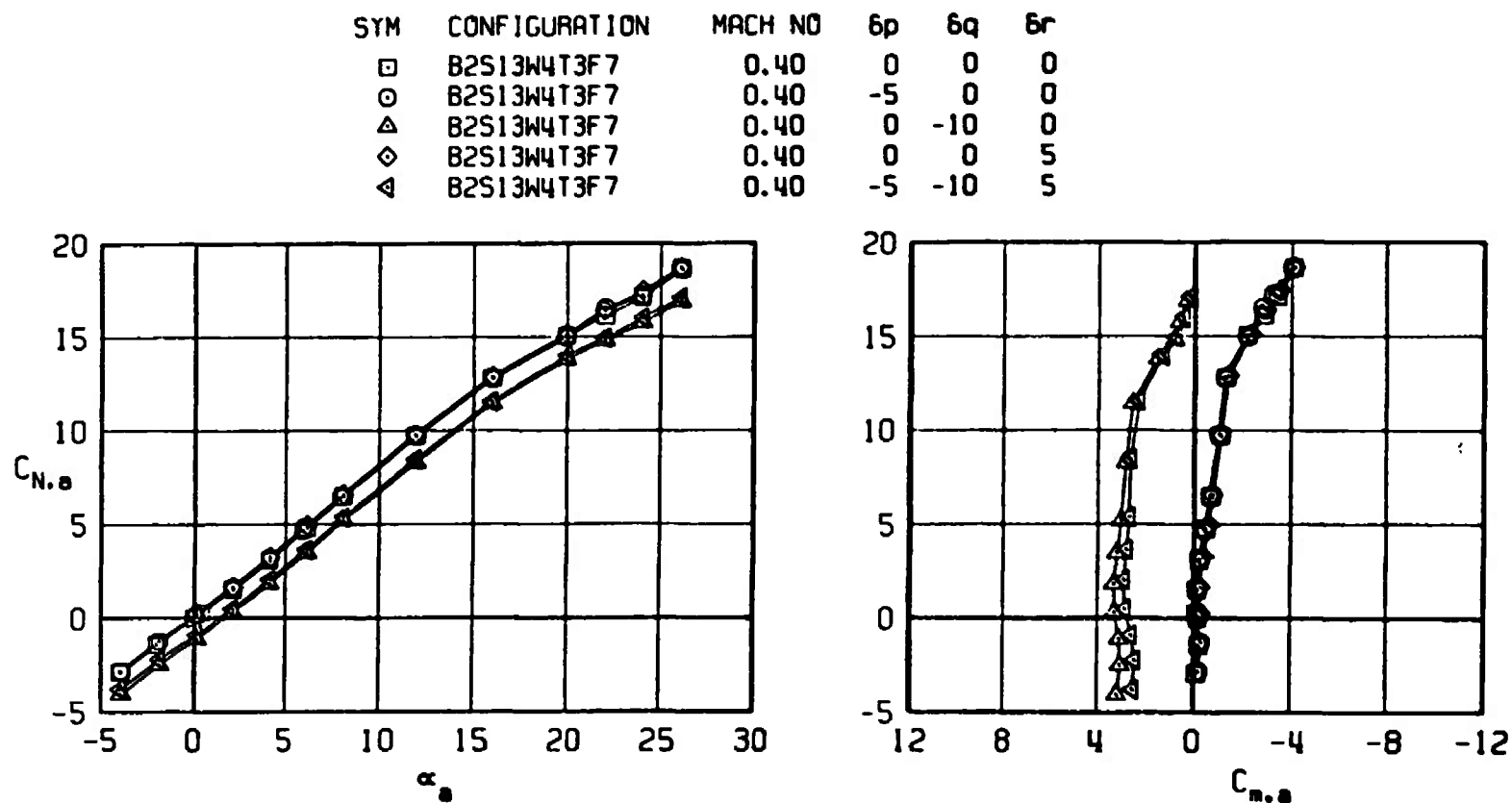


Figure 22. Effect of roll control, $\delta p = -5$ deg, and pitch control, $\delta q = -10$ deg, and yaw control, $\delta r = 5$ deg, deflections on the normal-force and pitching-moment coefficients of the super HOBOS/MK-84.

SYM	CONFIGURATION	MACH NO	δp	δq	δr
□	B2S13W4T3F7	0.65	0	0	0
○	B2S13W4T3F7	0.65	-5	0	0
△	B2S13W4T3F7	0.65	0	-10	0
◇	B2S13W4T3F7	0.65	0	0	5
◁	B2S13W4T3F7	0.65	-5	-10	5

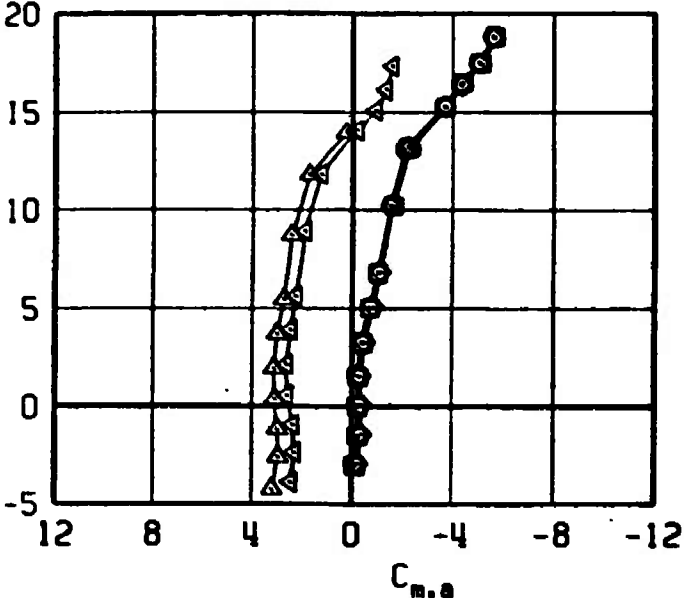
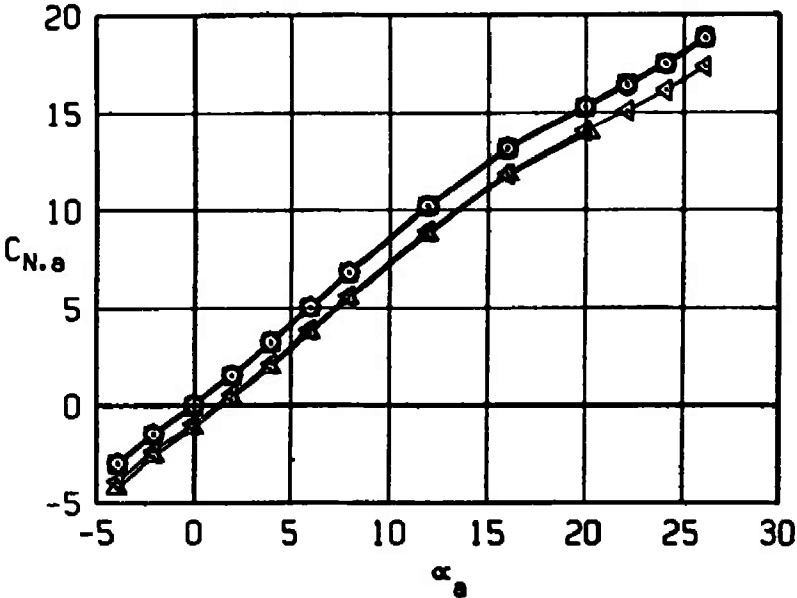


Figure 22. Continued.

SYM	CONFIGURATION	MACH NO	δp	δq	δr
□	B2S13W4T3F7	0.95	0	0	0
○	B2S13W4T3F7	0.95	-5	0	0
△	B2S13W4T3F7	0.95	0	-10	0
◇	B2S13W4T3F7	0.95	0	0	5
◁	B2S13W4T3F7	0.95	-5	-10	5

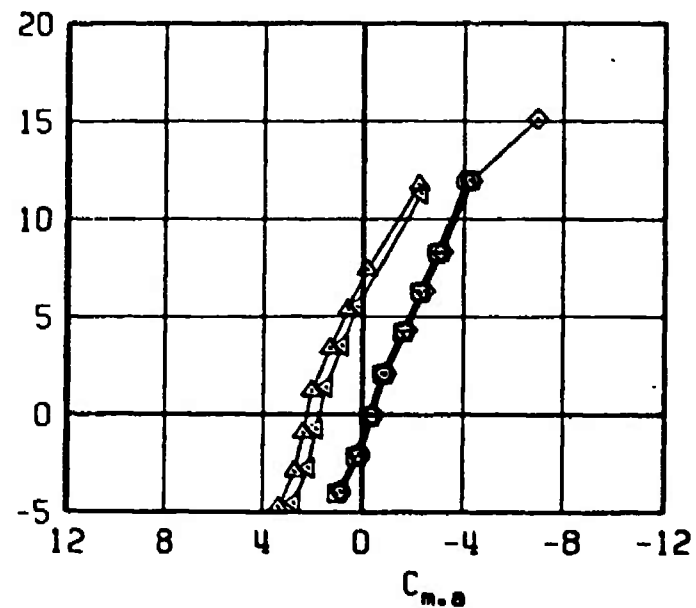
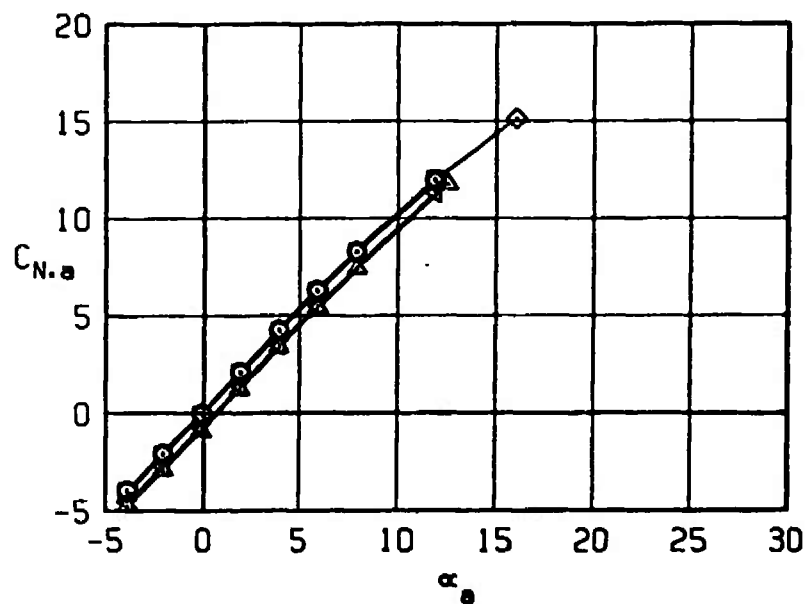


Figure 22. Continued.

SYM	CONFIGURATION	MACH NO	δp	δq	δr
□	B2S13W4T3F7	1.20	0	0	0
○	B2S13W4T3F7	1.20	-5	0	0
△	B2S13W4T3F7	1.20	0	-10	0
◇	B2S13W4T3F7	1.20	0	0	5
◁	B2S13W4T3F7	1.20	-5	-10	5

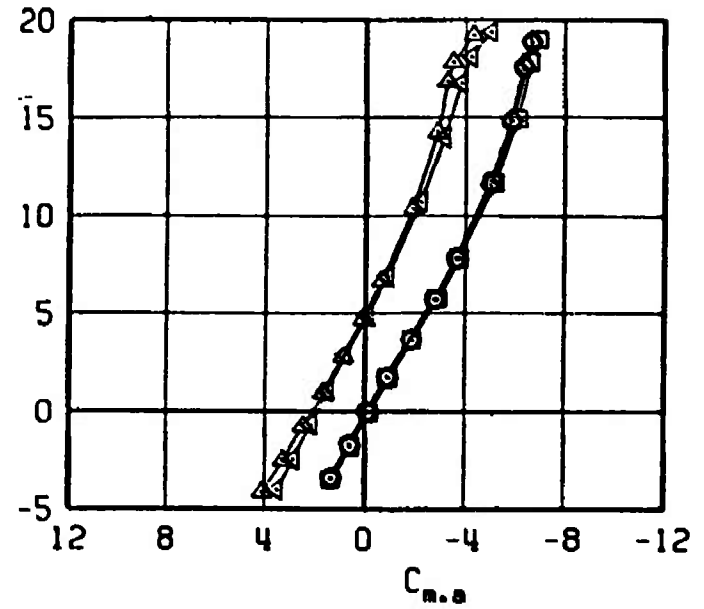
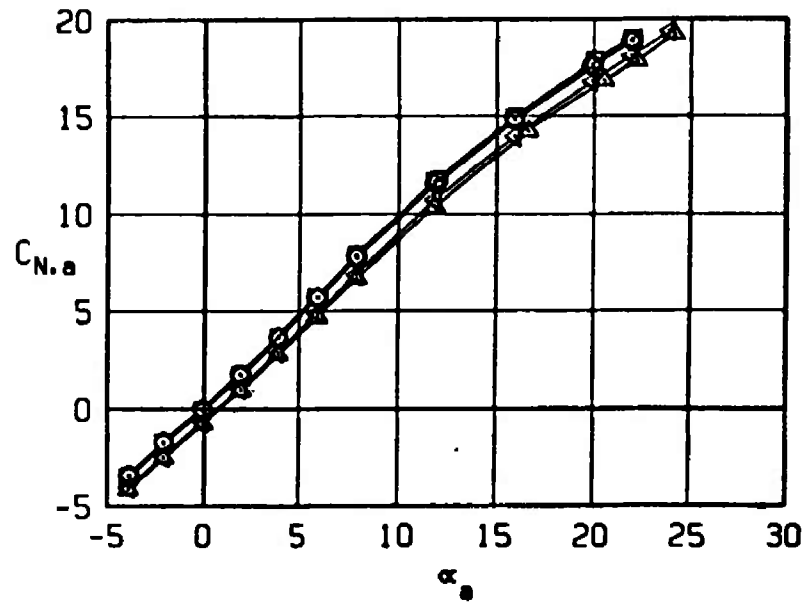


Figure 22. Continued.

SYM	CONFIGURATION	MACH NO	δp	δq	δr
□	B2S13W4T3F7	1.60	0	0	0
○	B2S13W4T3F7	1.60	-5	0	0
△	B2S13W4T3F7	1.60	0	-10	0
◇	B2S13W4T3F7	1.60	0	0	5
◁	B2S13W4T3F7	1.60	0	-10	5

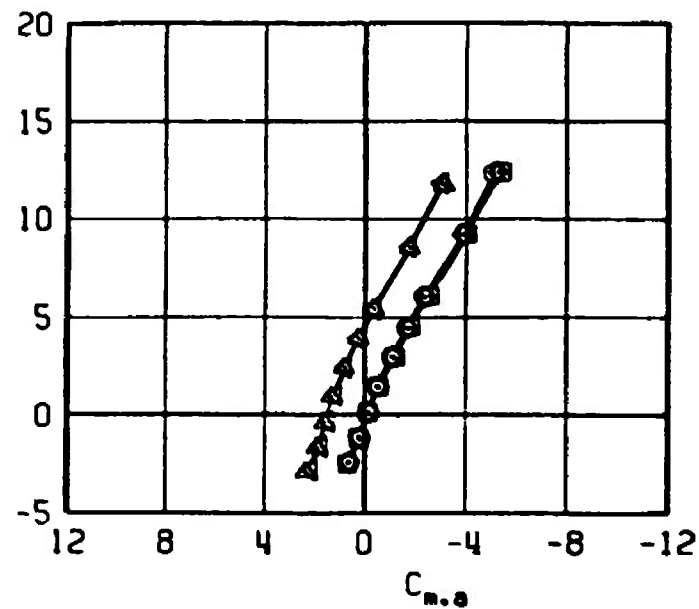
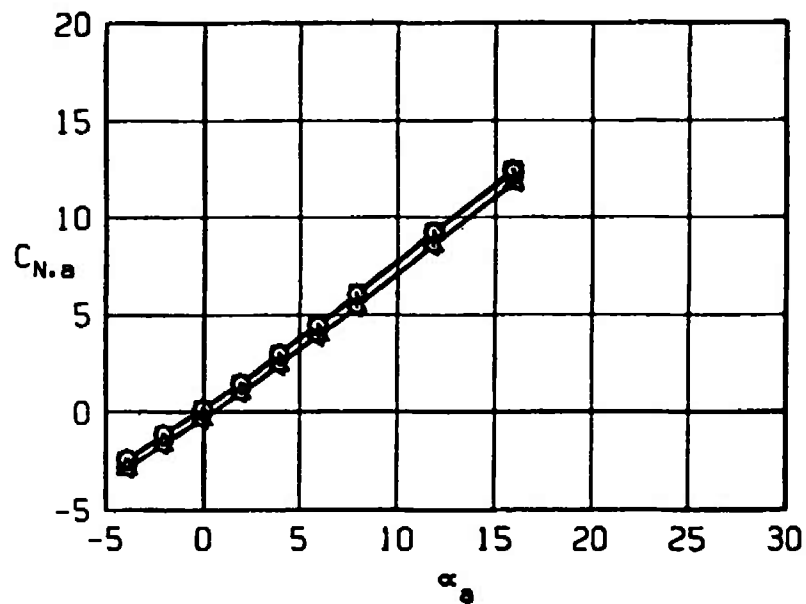


Figure 22. Concluded.

SYM	CONFIGURATION	MACH NO	δp	δq	δr
□	B2S13W4T3F7	0.40	0	0	0
○	B2S13W4T3F7	0.40	-5	0	0
△	B2S13W4T3F7	0.40	0	-10	0
◇	B2S13W4T3F7	0.40	0	0	5
◁	B2S13W4T3F7	0.40	-5	-10	5

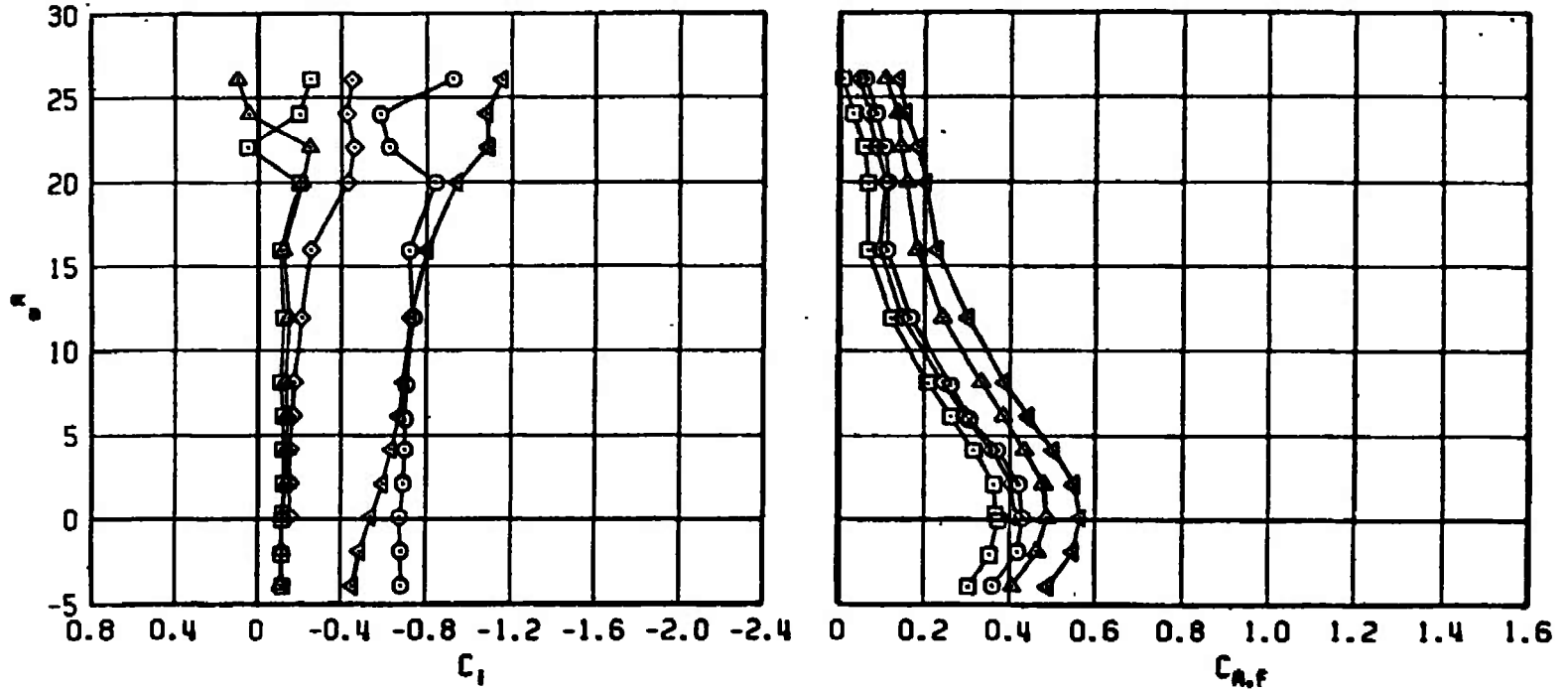


Figure 23. Effect of roll control, $\delta p = -5$ deg, pitch control, $\delta q = -10$ deg, and yaw control, $\delta r = 5$ deg, deflections on the rolling-moment and axial-force coefficients of the Super HOBOS/MK-84.

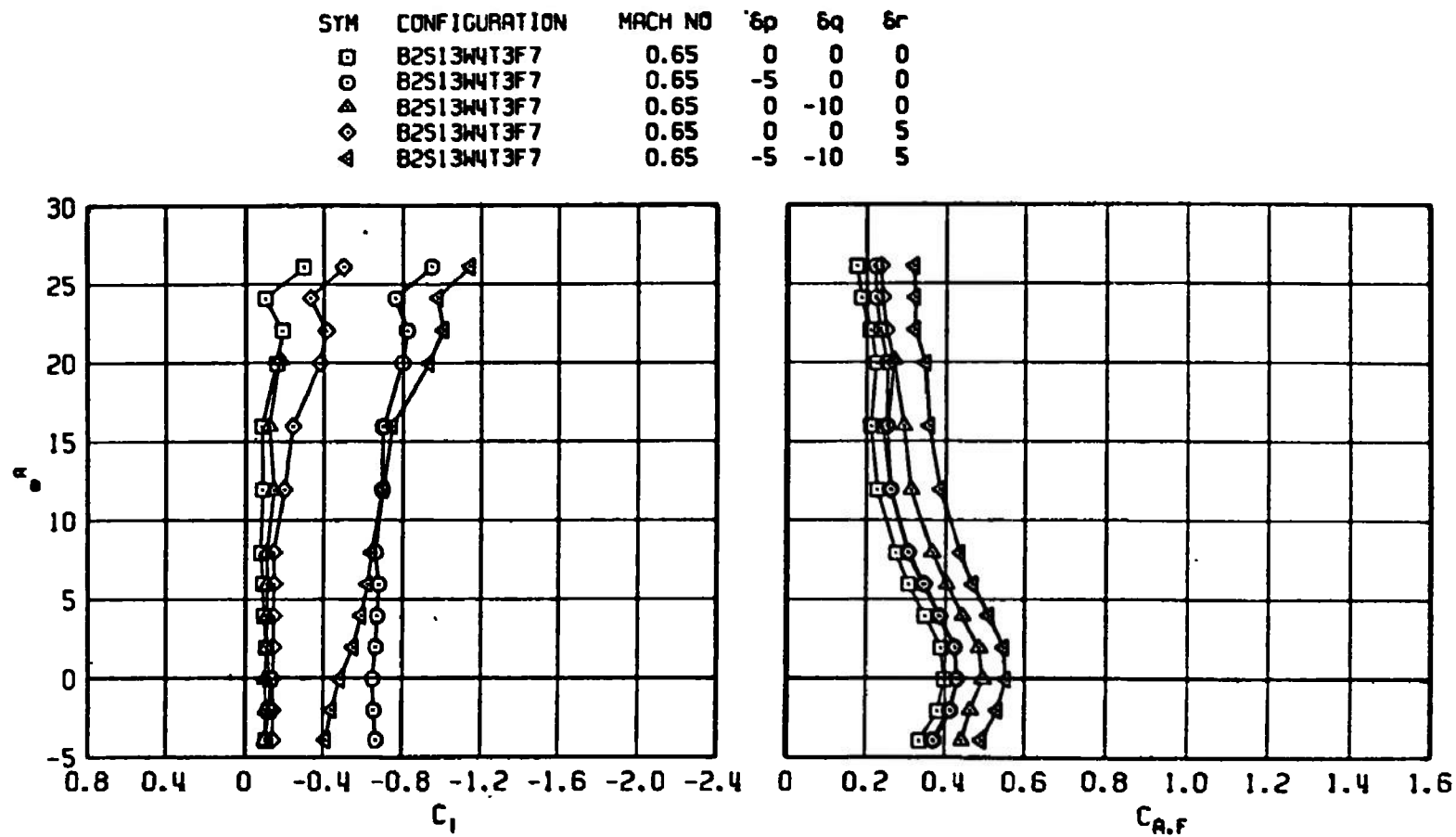


Figure 23. Continued.

SYM	CONFIGURATION	MACH NO	δp	δq	δr
□	B2S13W4T3F7	0.95	0	0	0
○	B2S13W4T3F7	0.95	-5	0	0
△	B2S13W4T3F7	0.95	0	-10	0
◇	B2S13W4T3F7	0.95	0	0	5
◀	B2S13W4T3F7	0.95	-5	-10	5

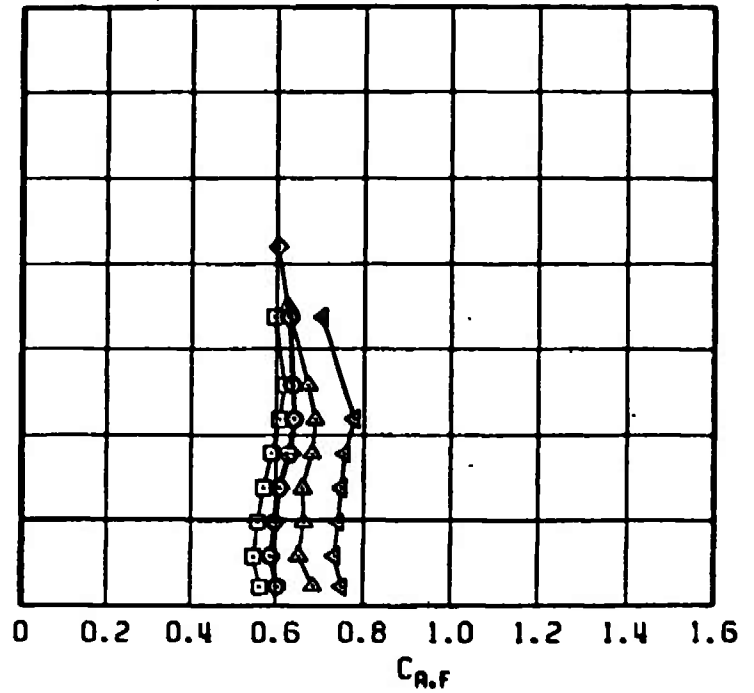
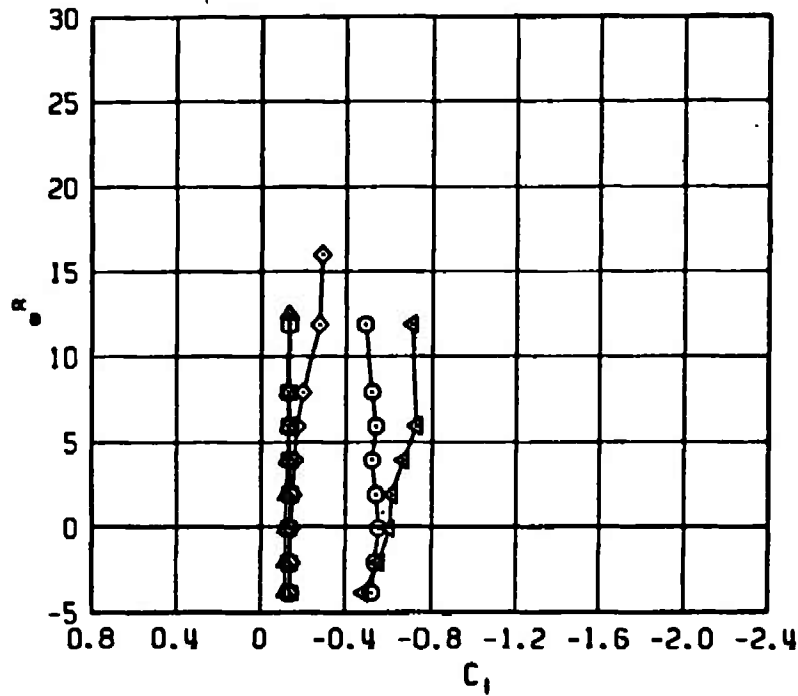


Figure 23. Continued.

SYM	CONFIGURATION	MACH NO	δp	δq	δr
□	B2S13W4T3F7	1.20	0	0	0
○	B2S13W4T3F7	1.20	-5	0	0
△	B2S13W4T3F7	1.20	0	-10	0
◇	B2S13W4T3F7	1.20	0	0	5
◄	B2S13W4T3F7	1.20	-5	-10	5

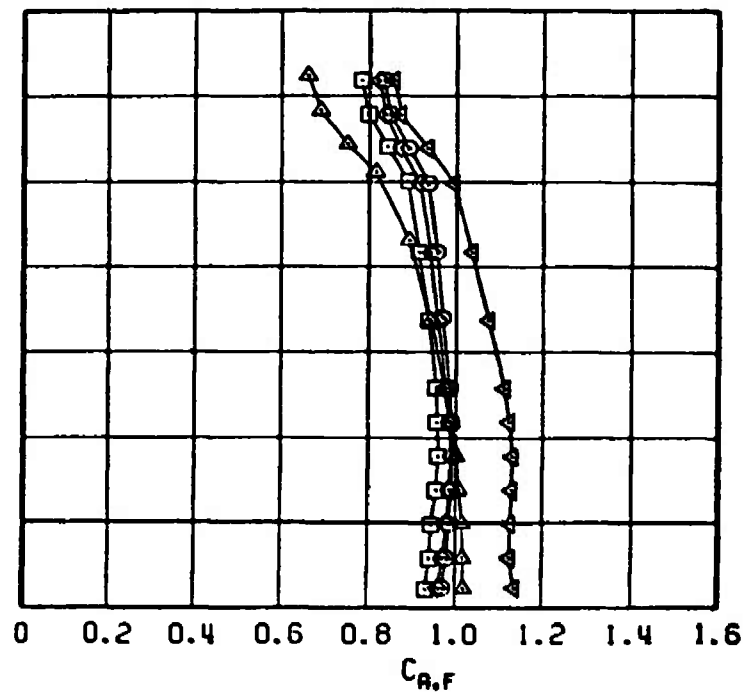
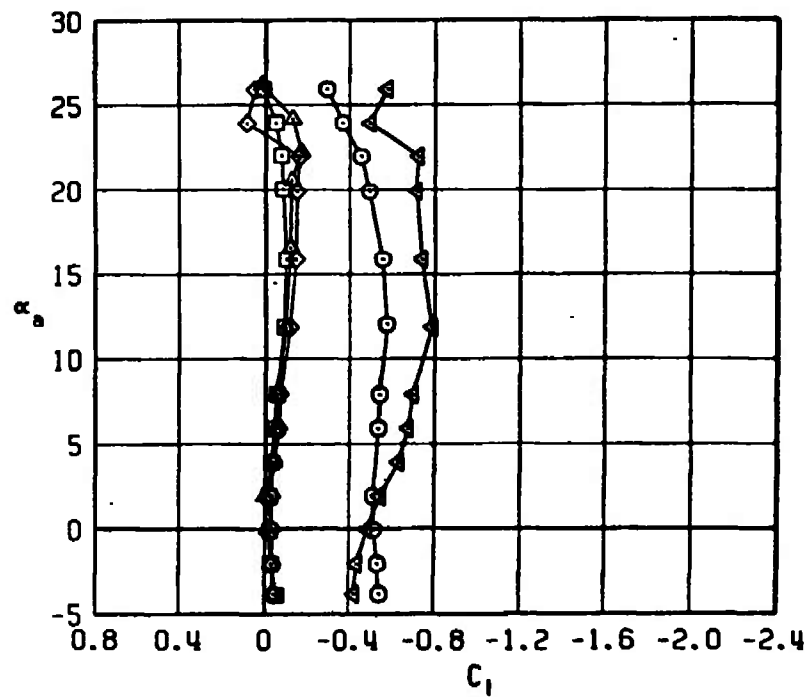


Figure 23. Continued.

SYM	CONFIGURATION	MACH NO	δp	δq	δr
□	B2S13W4T3F7	1.60	0	0	0
○	B2S13W4T3F7	1.60	-5	0	0
△	B2S13W4T3F7	1.60	0	-10	0
◇	B2S13W4T3F7	1.60	0	0	5
◀	B2S13W4T3F7	1.60	0	-10	5

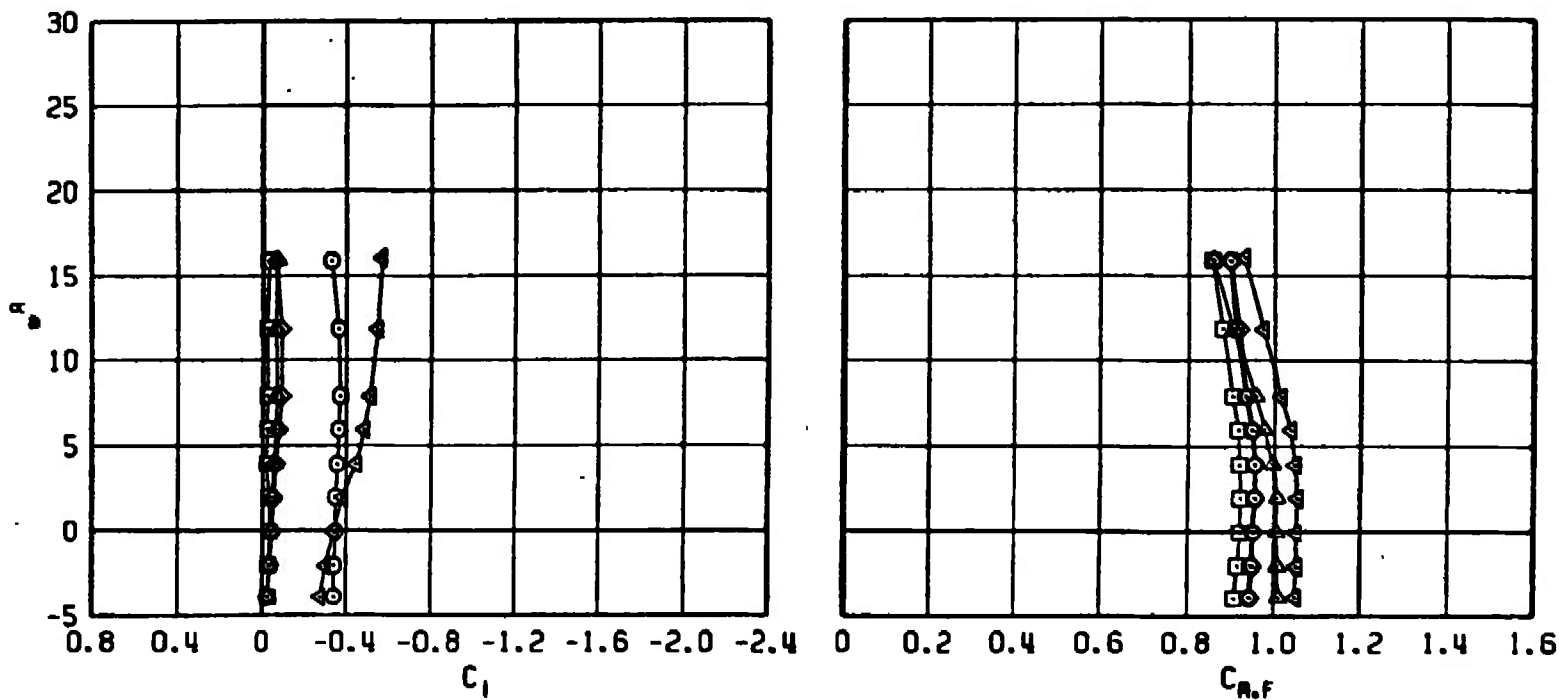


Figure 23. Concluded.

SYM	CONFIGURATION	MACH NO	δp	δq	δr
□	B2S13W4T3F7	0.40	0	0	0
○	B2S13W4T3F7	0.40	-5	0	0
△	B2S13W4T3F7	0.40	0	-10	0
◇	B2S13W4T3F7	0.40	0	0	5
◁	B2S13W4T3F7	0.40	-5	-10	5

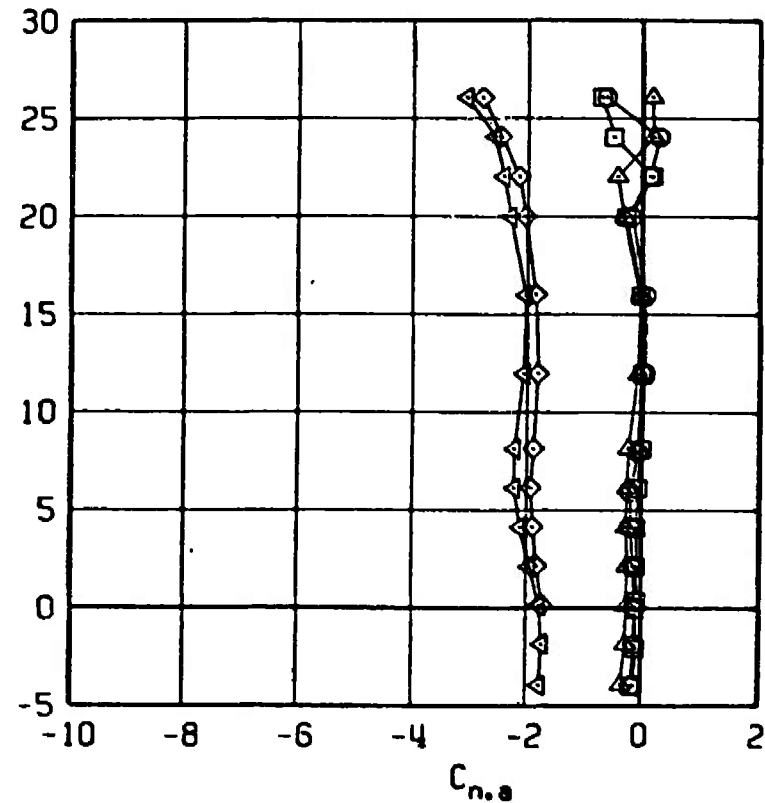
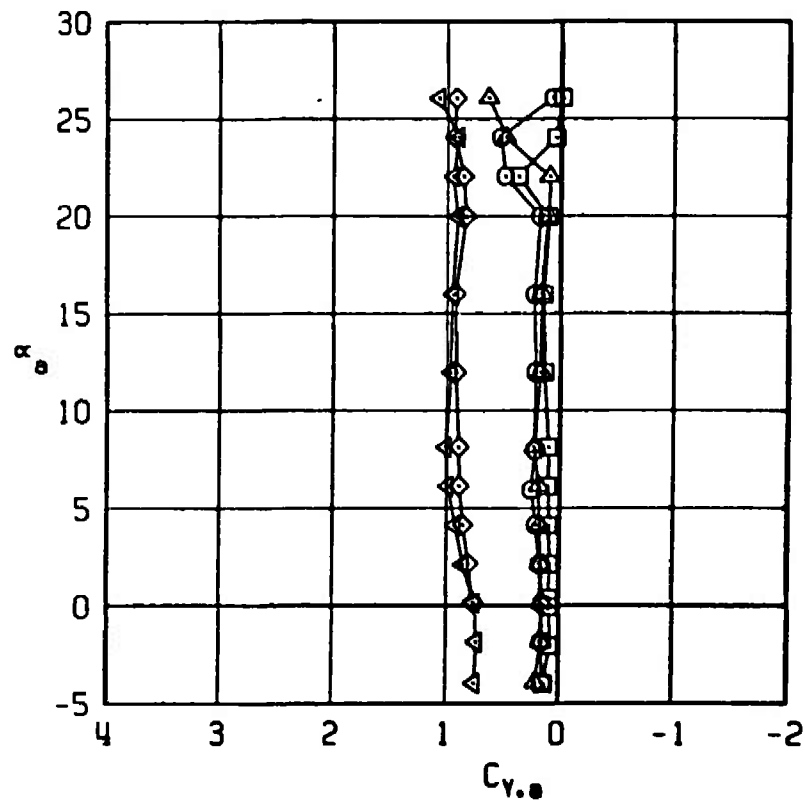


Figure 24. Effect of roll control, $\delta p = -5$ deg, pitch control, $\delta q = -10$ deg, and yaw control, $\delta r = 5$ deg, deflections on the side-force and yawing-moment coefficients of the Super HOBOS/MK-84.

SYM	CONFIGURATION	MACH NO	δp	δq	δr
□	B2S13W4T3F7	0.65	0	0	0
○	B2S13W4T3F7	0.65	-5	0	0
△	B2S13W4T3F7	0.65	0	-10	0
◇	B2S13W4T3F7	0.65	0	0	5
◁	B2S13W4T3F7	0.65	-5	-10	5

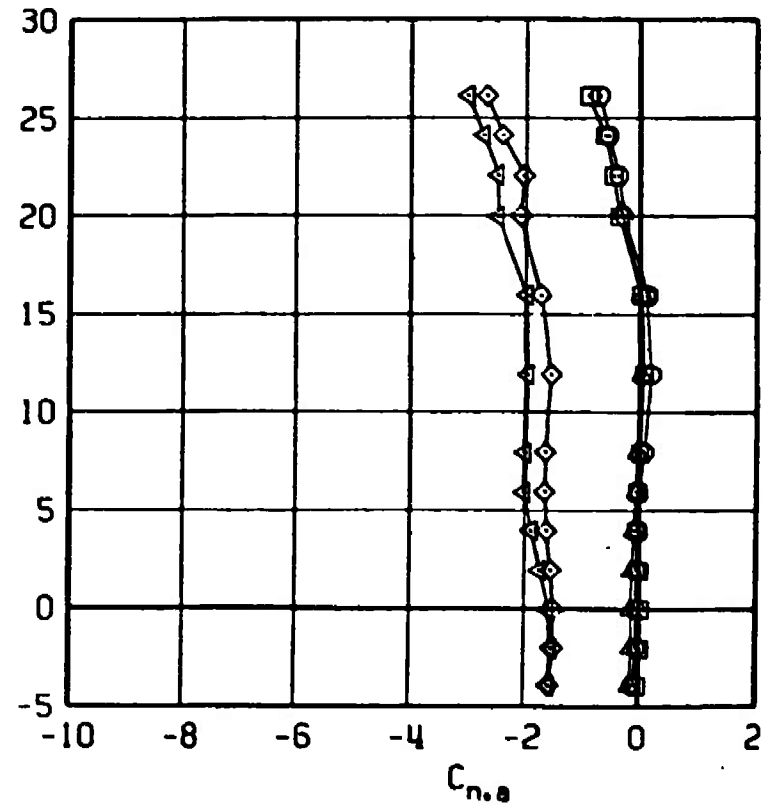
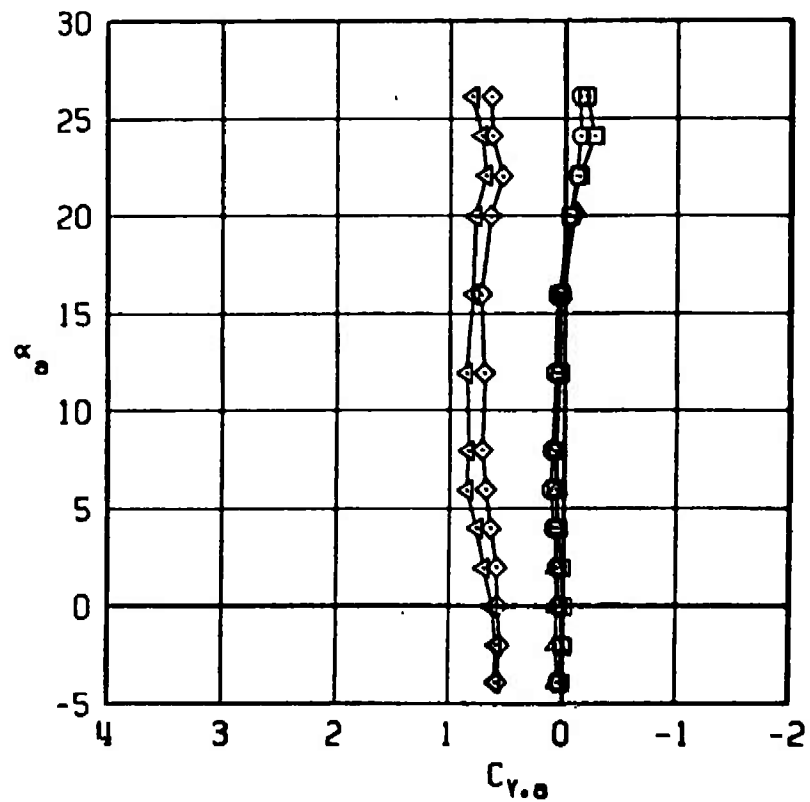


Figure 24. Continued.

SYM	CONFIGURATION	MACH NO	δp	δq	δr
□	B2S13W4T3F7	0.95	0	0	0
○	B2S13W4T3F7	0.95	-5	0	0
△	B2S13W4T3F7	0.95	0	-10	0
◇	B2S13W4T3F7	0.95	0	0	5
◁	B2S13W4T3F7	0.95	-5	-10	5

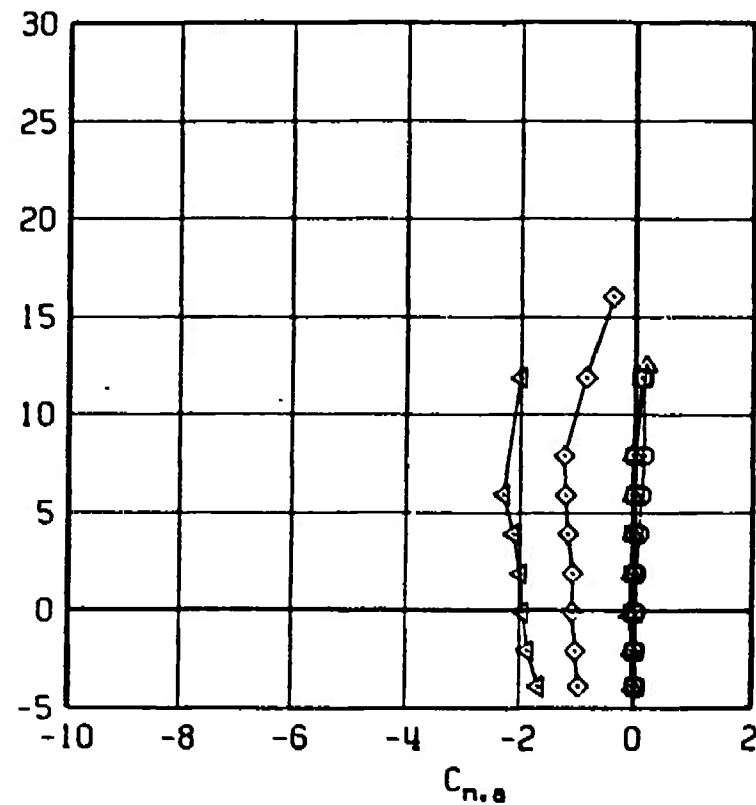
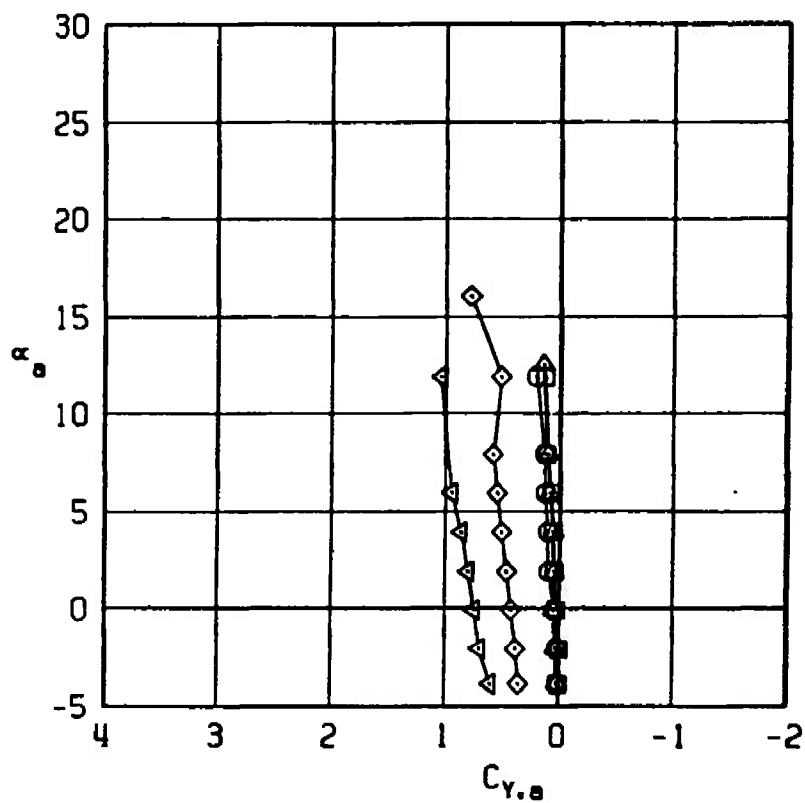


Figure 24. Continued.

SYM	CONFIGURATION	MACH NO	δp	δq	δr
□	B2S13W4T3F7	1.20	0	0	0
○	B2S13W4T3F7	1.20	-5	0	0
△	B2S13W4T3F7	1.20	0	-10	0
◇	B2S13W4T3F7	1.20	0	0	5
◀	B2S13W4T3F7	1.20	-5	-10	5

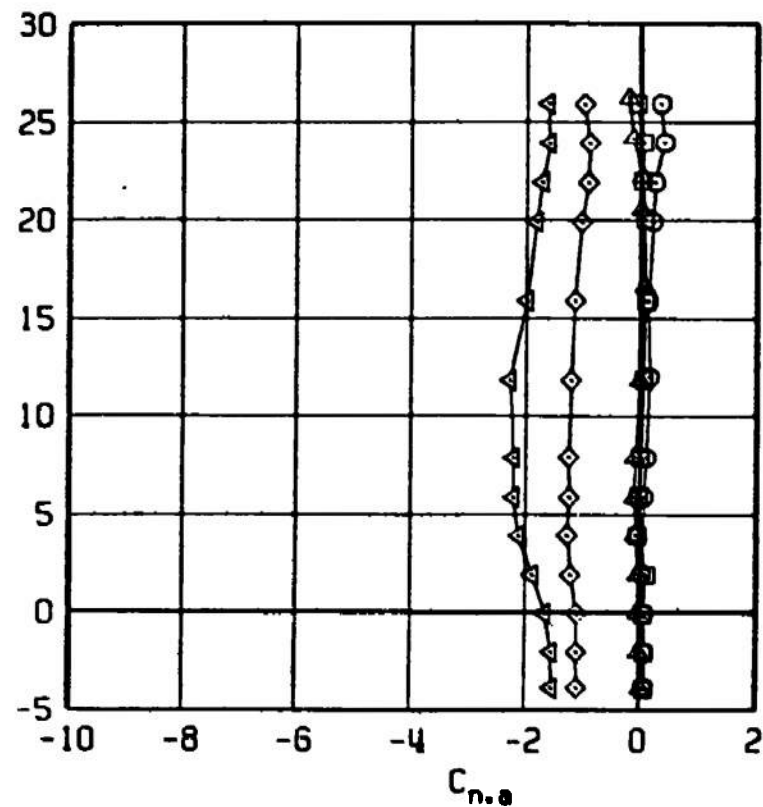
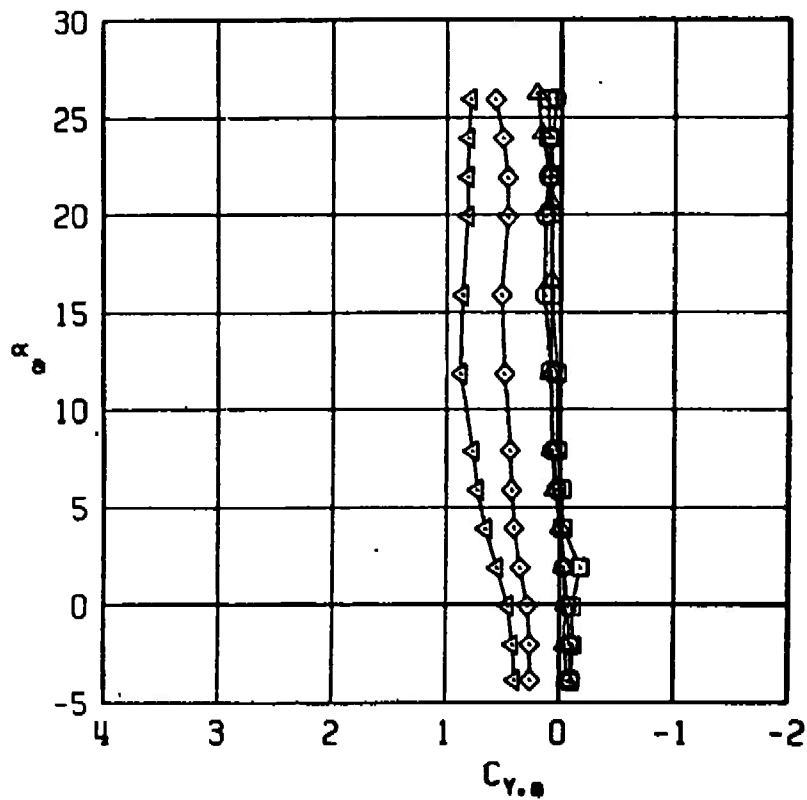


Figure 24. Continued.

SYM	CONFIGURATION	MACH NO	δp	δq	δr
□	B2S13W4T3F7	1.60	0	0	0
○	B2S13W4T3F7	1.60	-5	0	0
△	B2S13W4T3F7	1.60	0	-10	0
◇	B2S13W4T3F7	1.60	0	0	5
◄	B2S13W4T3F7	1.60	0	-10	5

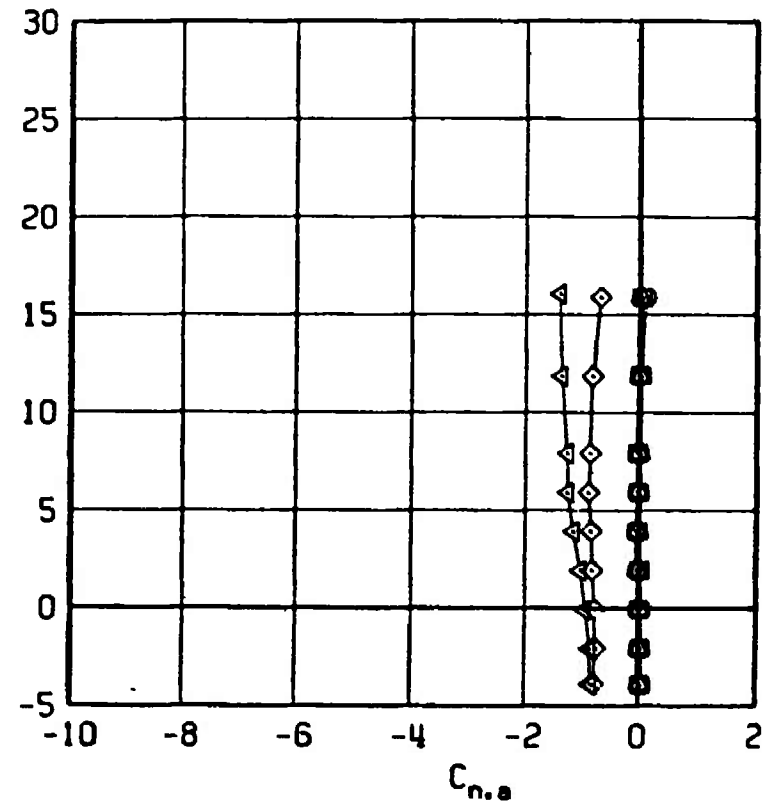
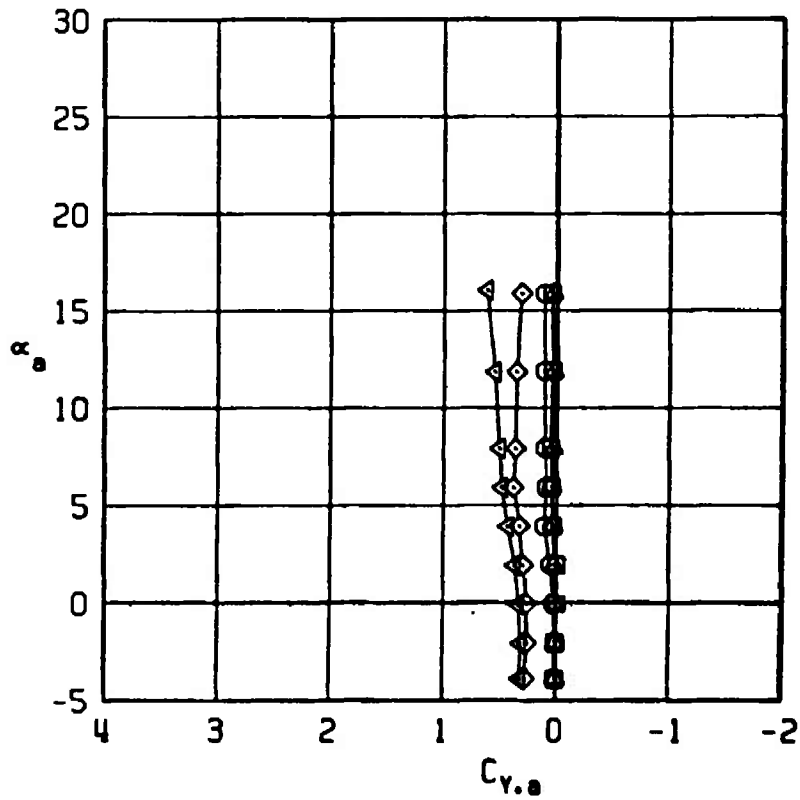


Figure 24. Concluded.

SYM	CONFIGURATION	MACH NO	δp	δq	δr
□	B2S13W4T3F7	0.40	0	0	0
○	B2S13W4T3F7	0.40	0	-10	0
△	B2S13W4T3F7	0.40	0	0	5
◇	B2S13W4T3F7	0.40	0	-10	5

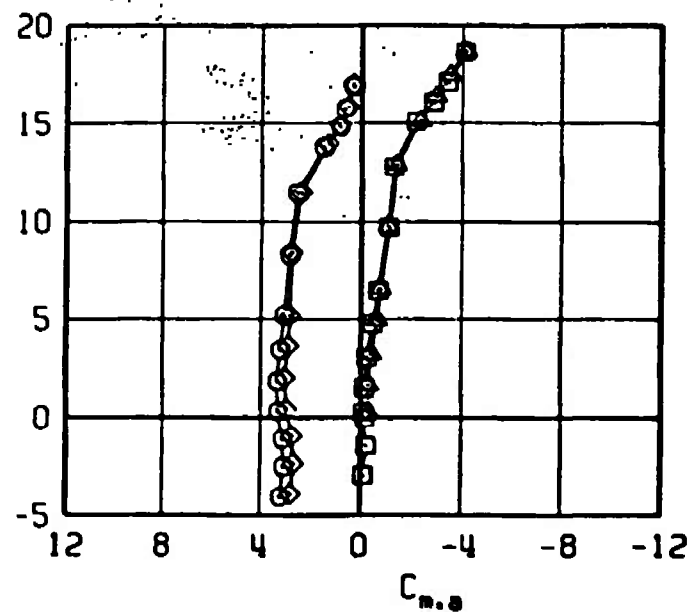
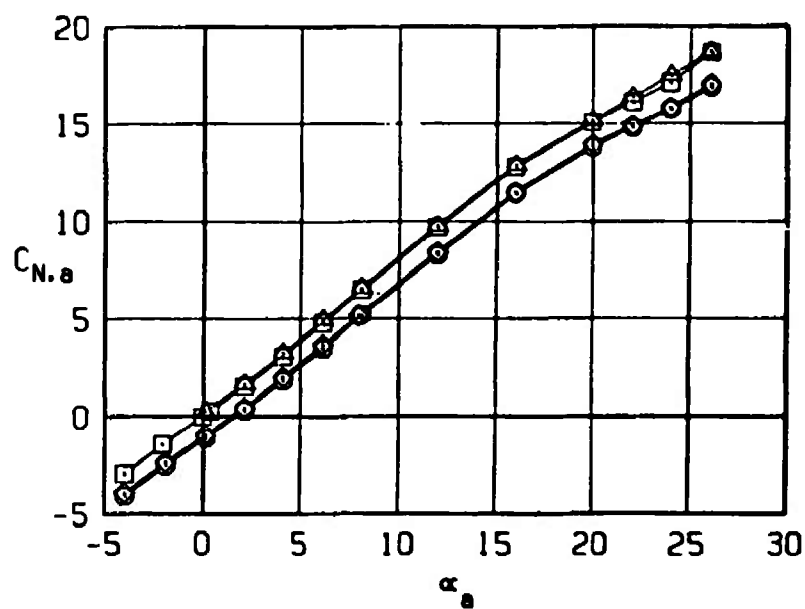


Figure 25. Effect of pitch control, $\delta q = -10$ deg, and yaw control, $\delta r = 5$ deg, deflections on the normal-force and pitching-moment coefficients of the Super HOBOS/MK-84.

SYM	CONFIGURATION	MACH NO	δp	δq	δr
□	B2S13W4T3F7	0.65	0	0	0
○	B2S13W4T3F7	0.65	0	-10	0
△	B2S13W4T3F7	0.65	0	0	5
◇	B2S13W4T3F7	0.65	0	-10	5

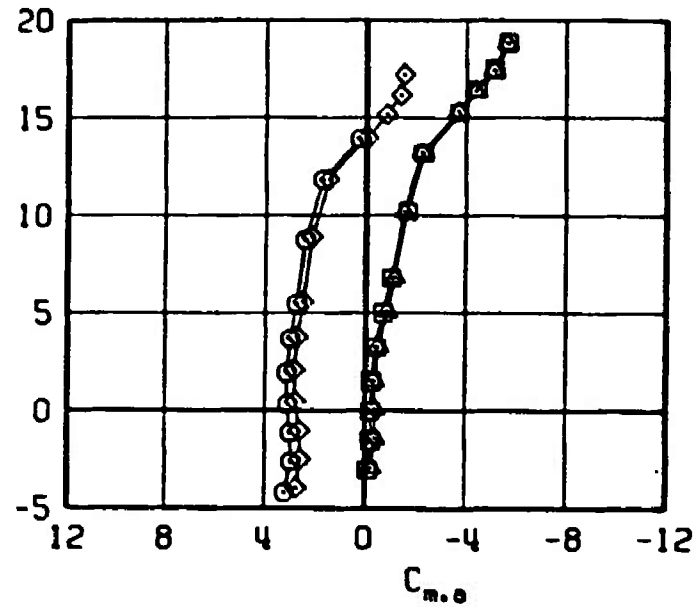
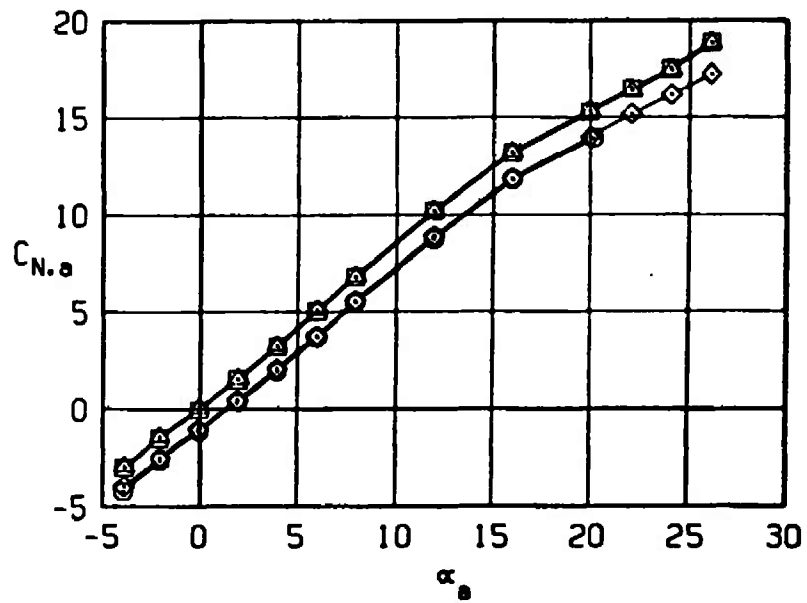


Figure 25. Continued.

SYM	CONFIGURATION	MACH NO	δp	δq	δr
□	B2S13W4T3F7	0.95	0	0	0
○	B2S13W4T3F7	0.95	0	-10	0
△	B2S13W4T3F7	0.95	0	0	5
◇	B2S13W4T3F7	0.95	0	-10	5

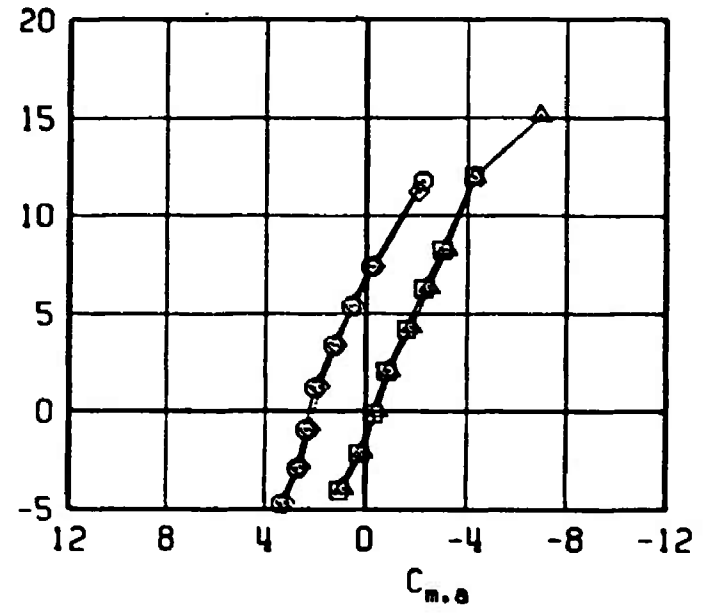
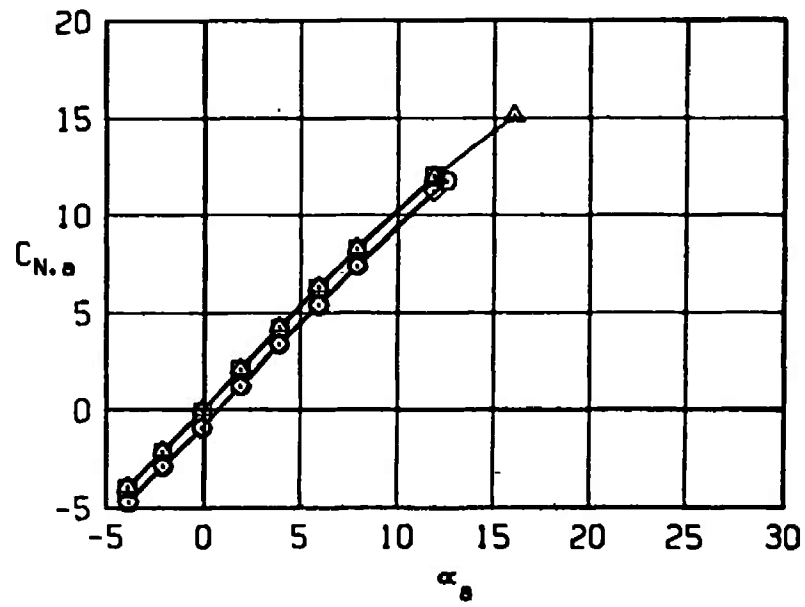


Figure 25. Continued.

SYM	CONFIGURATION	MACH NO	δp	δq	δr
□	B2S13W4T3F7	1.20	0	0	0
○	B2S13W4T3F7	1.20	0	-10	0
△	B2S13W4T3F7	1.20	0	0	5
◇	B2S13W4T3F7	1.20	0	-10	5

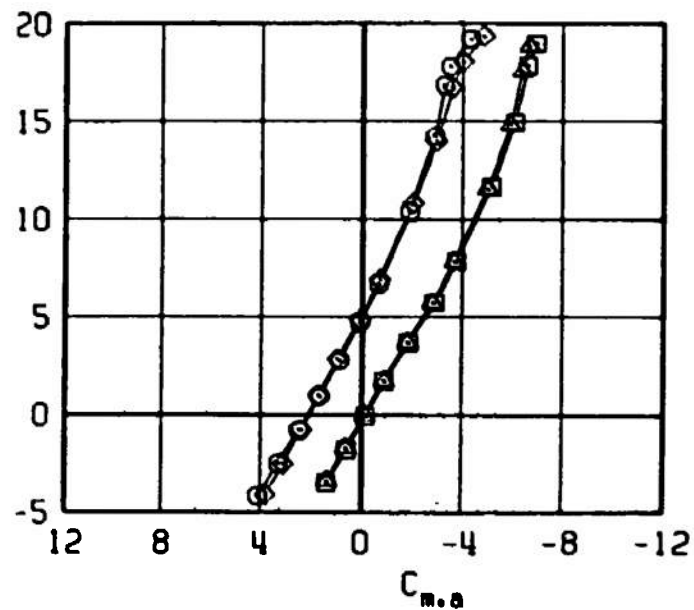
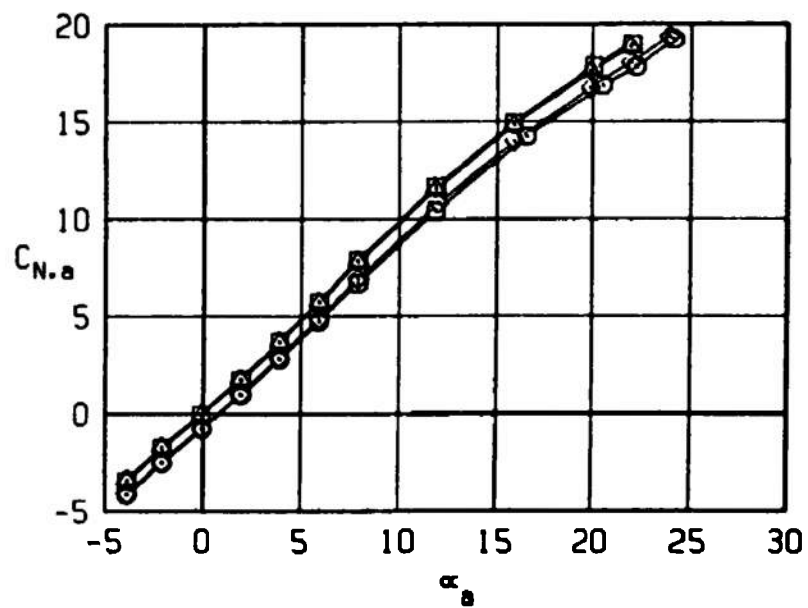


Figure 25. Continued.

SYM	CONFIGURATION	MACH NO	δp	δq	δr
□	B2S13W4T3F7	1.60	0	0	0
○	B2S13W4T3F7	1.60	0	-10	0
△	B2S13W4T3F7	1.60	0	0	5
◇	B2S13W4T3F7	1.60	0	-10	5

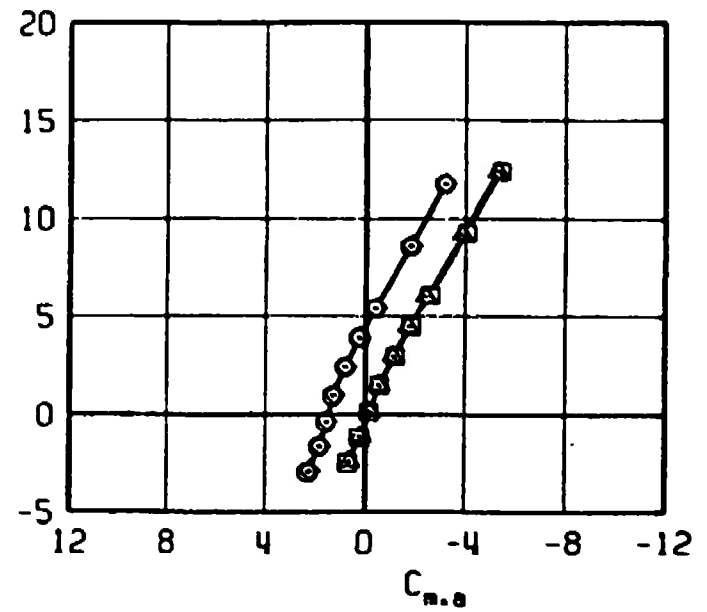
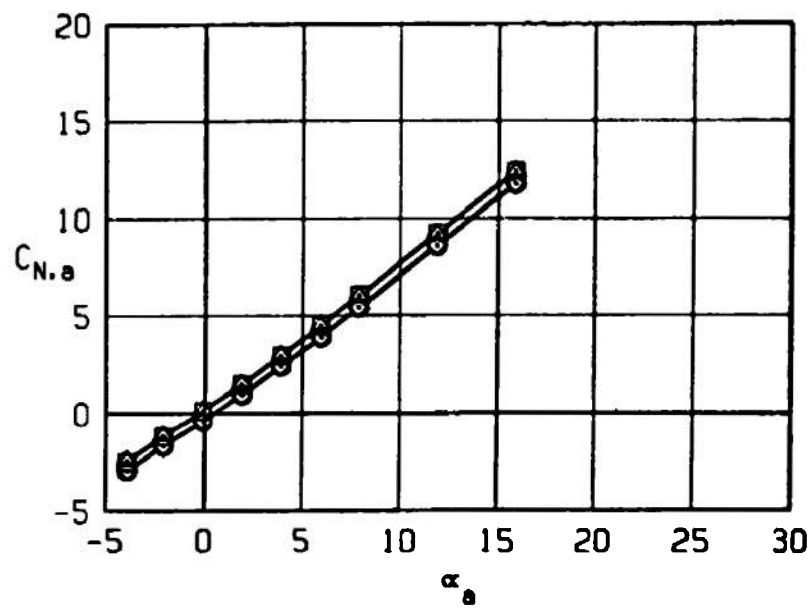


Figure 25. Concluded.

SYM	CONFIGURATION	MACH NO	δp	δq	δr
□	B2S13W4T3F7	0.40	0	0	0
○	B2S13W4T3F7	0.40	0	-10	0
△	B2S13W4T3F7	0.40	0	0	5
◇	B2S13W4T3F7	0.40	0	-10	5

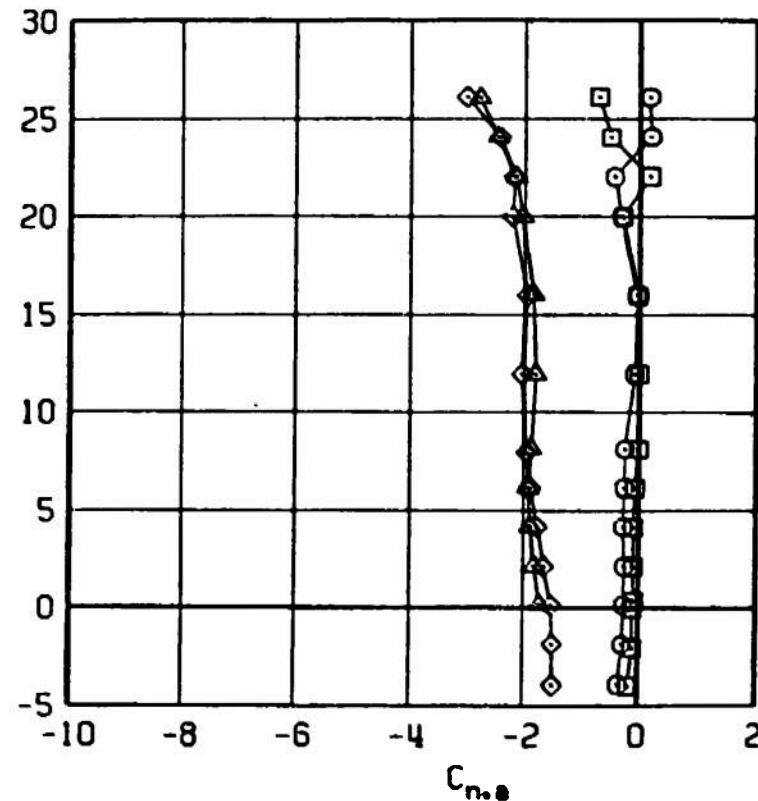
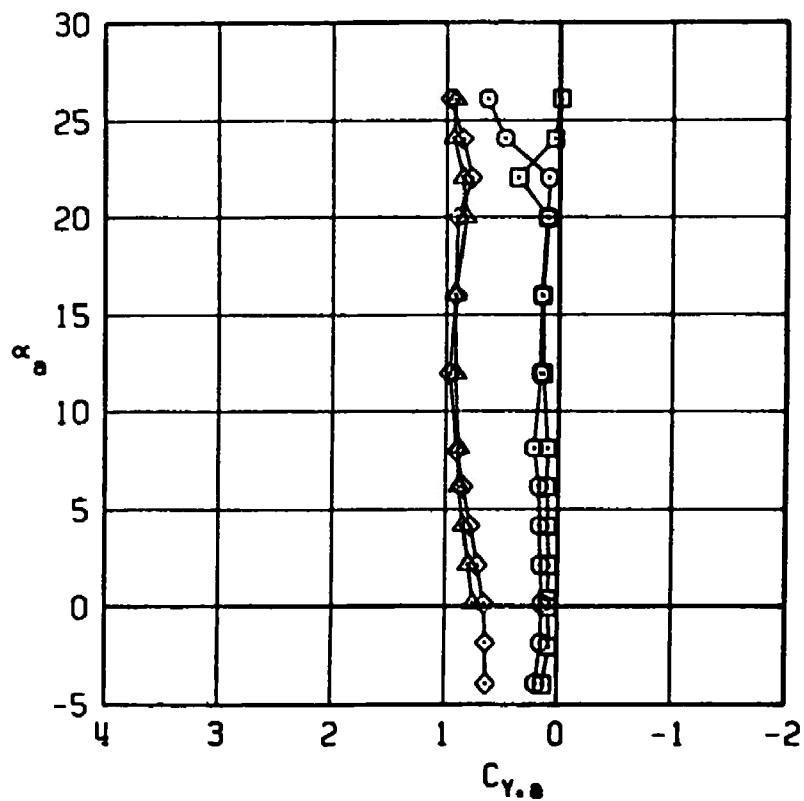


Figure 26. Effect of combined pitch control, $\delta q = -10$ deg, and yaw control, $\delta r = 5$ deg, deflections on the side-force and yawing-moment coefficients of the Super HOBOS/MK-84.

SYM	CONFIGURATION	MACH NO	δp	δq	δr
□	B2S13W4T3F7	0.65	0	0	0
○	B2S13W4T3F7	0.65	0	-10	0
△	B2S13W4T3F7	0.65	0	0	5
◇	B2S13W4T3F7	0.65	0	-10	5

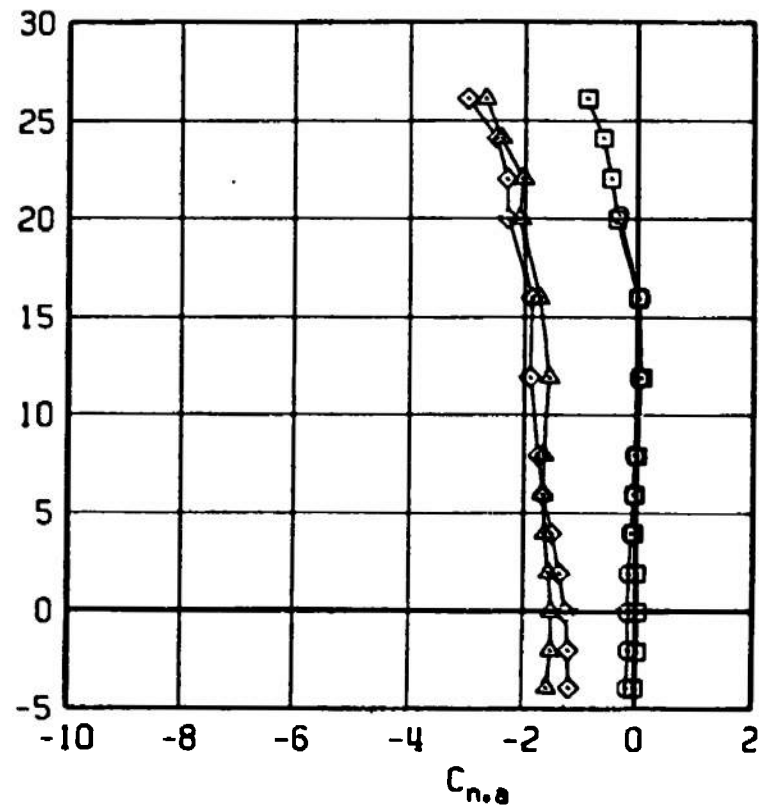
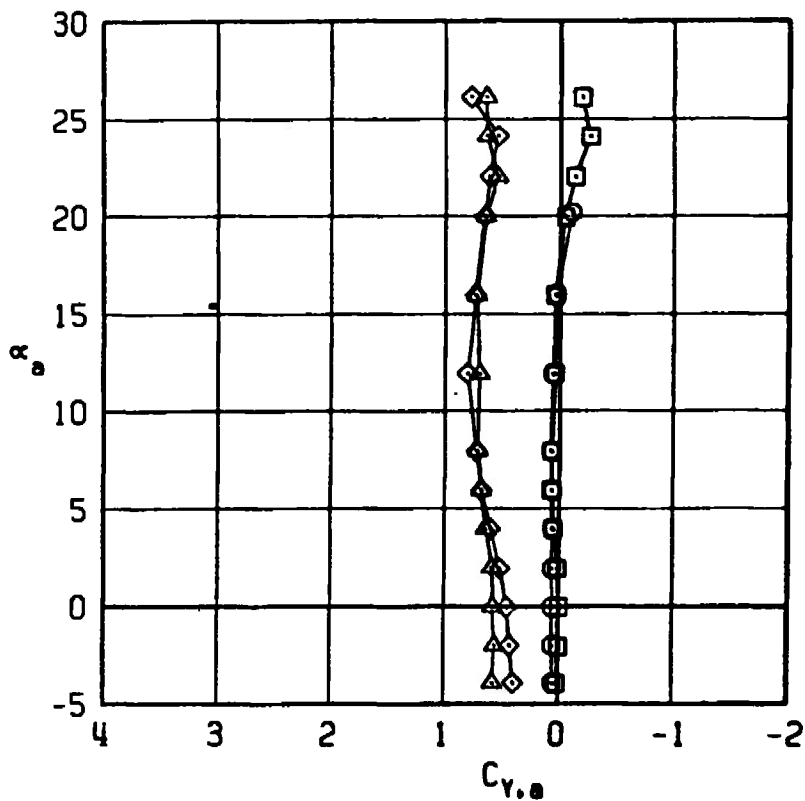


Figure 26. Continued.

SYM	CONFIGURATION	MACH NO	δp	δq	δr
□	B2S13W4T3F7	0.95	0	0	0
○	B2S13W4T3F7	0.95	0	-10	0
△	B2S13W4T3F7	0.95	0	0	5
◇	B2S13W4T3F7	0.95	0	-10	5

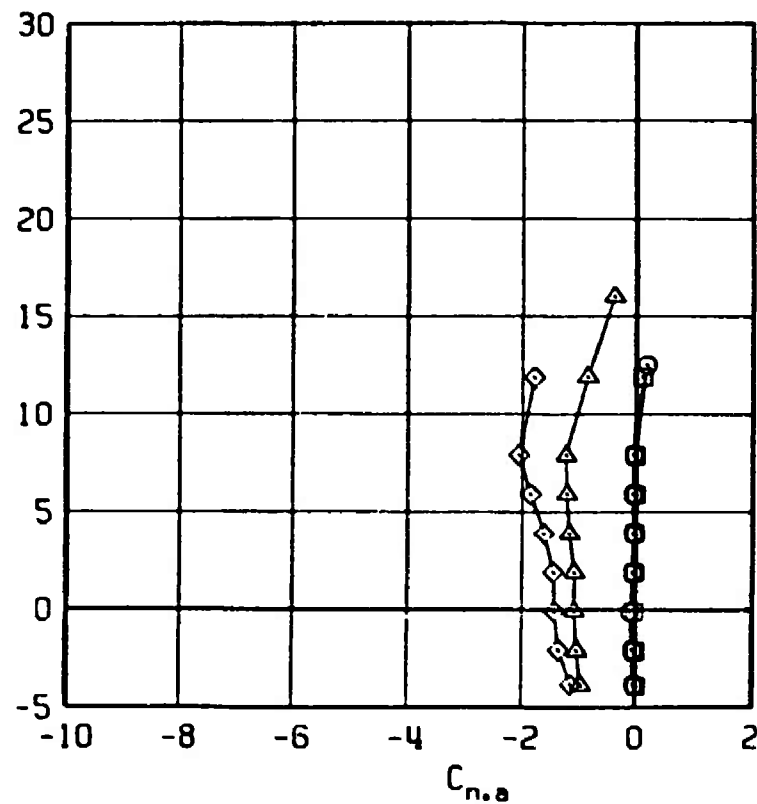
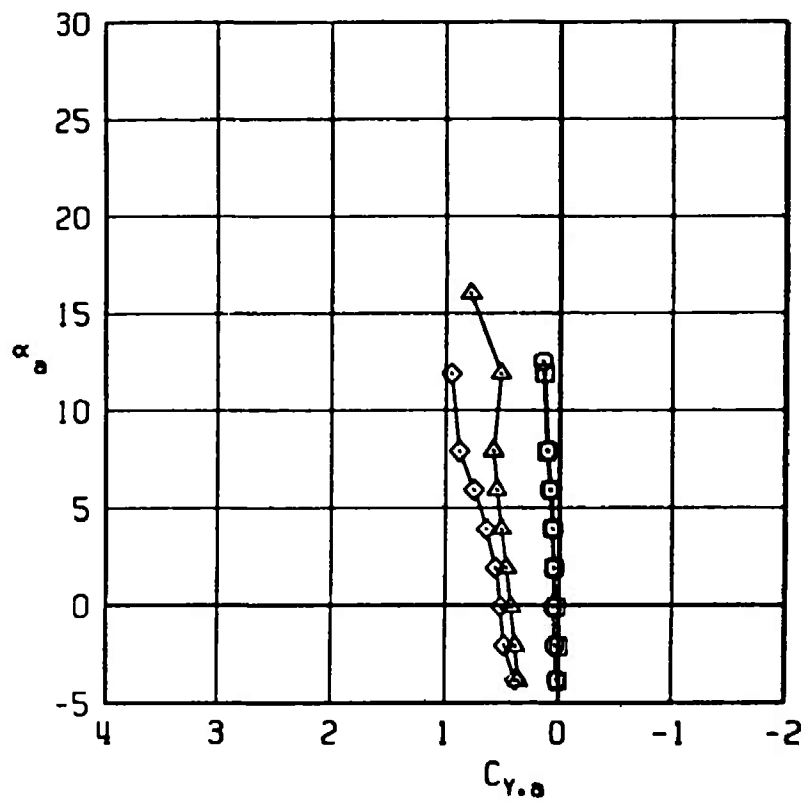


Figure 26. Continued.

SYM	CONFIGURATION	MACH NO	6p	6q	6r
□	B2S13W4T3F7	1.20	0	0	0
○	B2S13W4T3F7	1.20	0	-10	0
△	B2S13W4T3F7	1.20	0	0	5
◇	B2S13W4T3F7	1.20	0	-10	5

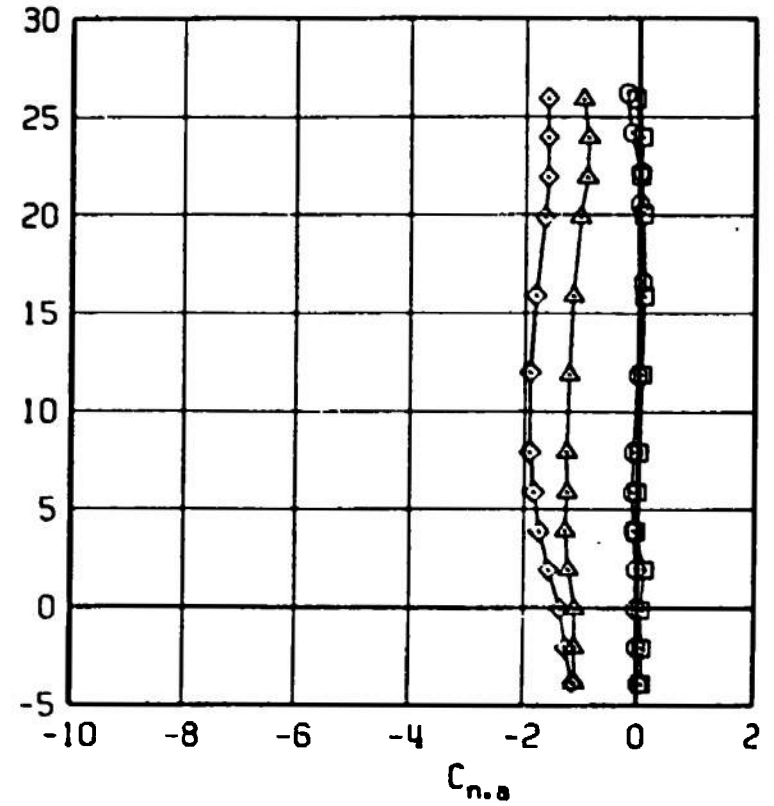
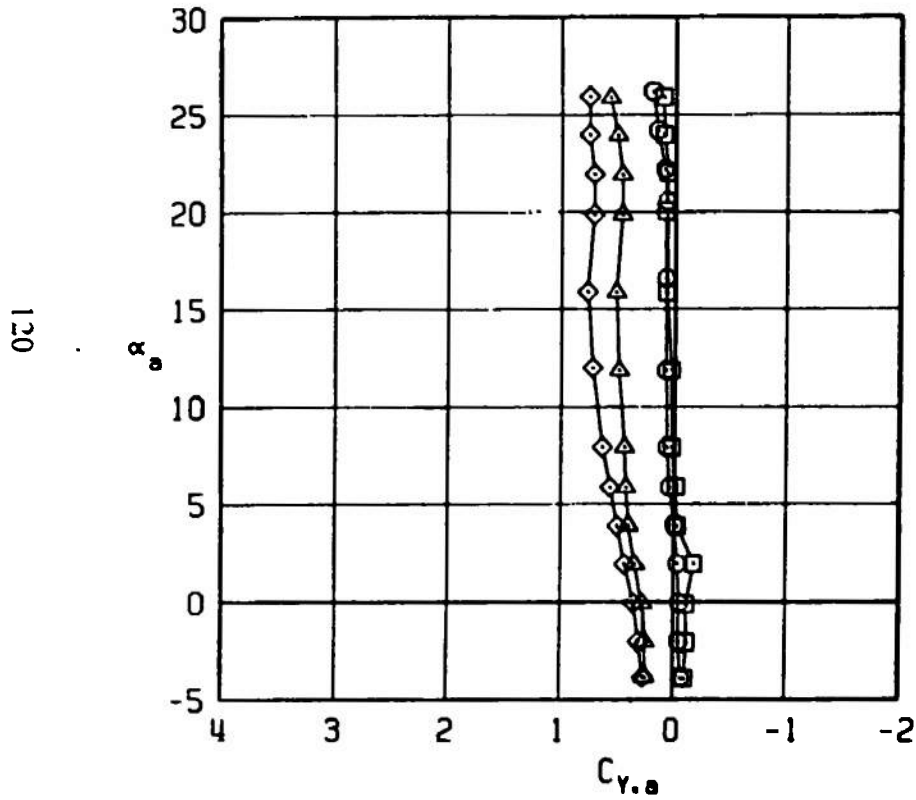


Figure 26. Continued.

SYM	CONFIGURATION	MACH NO	δp	δq	δr
□	B2S13W4T3F7	1.60	0	0	0
⊙	B2S13W4T3F7	1.60	0	-10	0
△	B2S13W4T3F7	1.60	0	0	5
◇	B2S13W4T3F7	1.60	0	-10	5

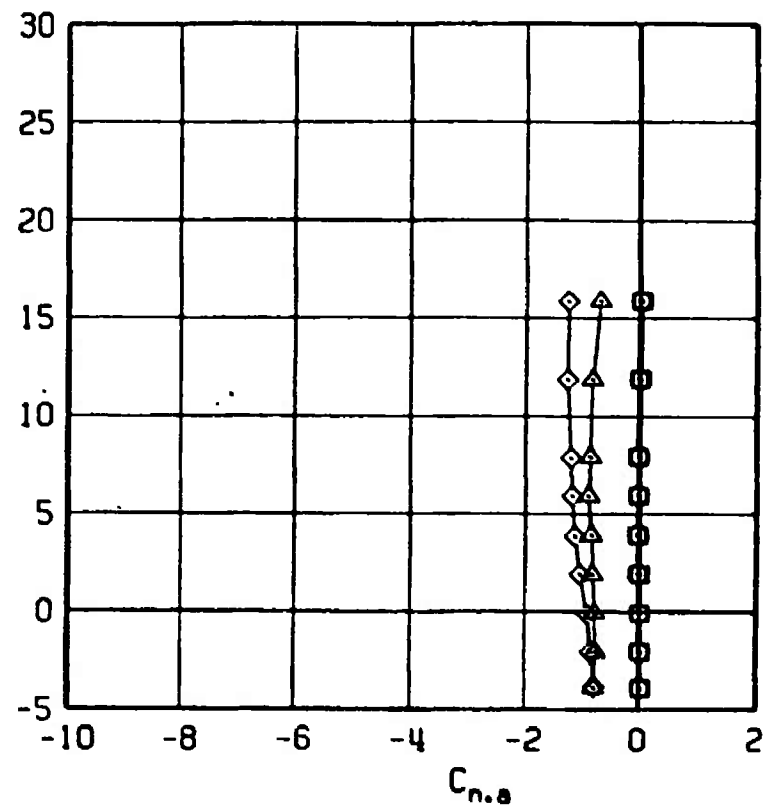
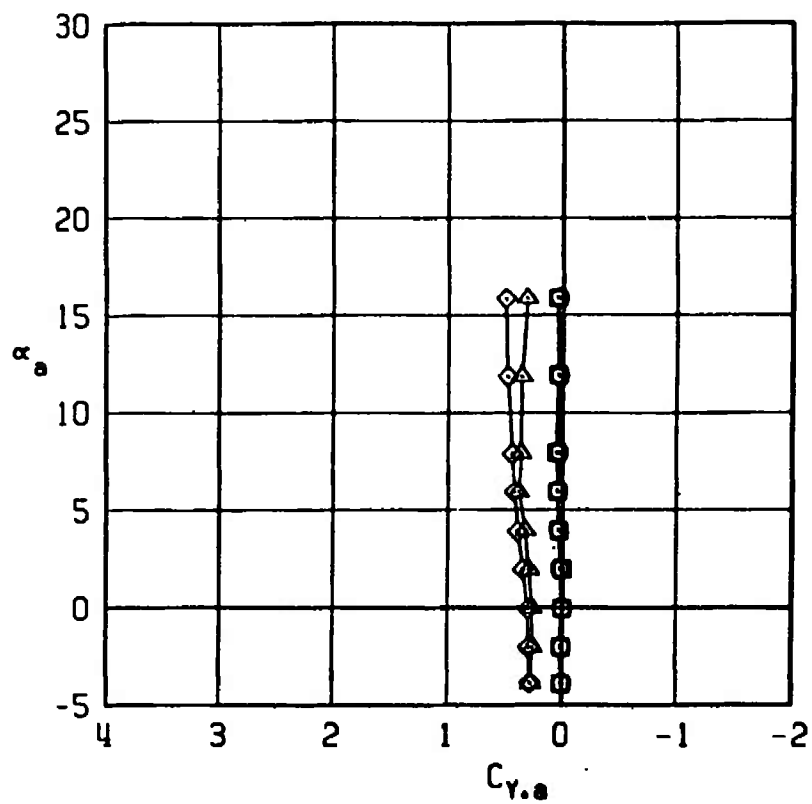


Figure 26. Concluded.

SYM	CONFIGURATION	MACH NO	δp	δq	δr
□	B2S13W4T3F7	0.40	0	0	0
○	B2S13W4T3F7	0.40	0	-15	0
△	B2S13W4T3F7	0.40	0	0	5
◇	B2S13W4T3F7	0.40	0	-15	5

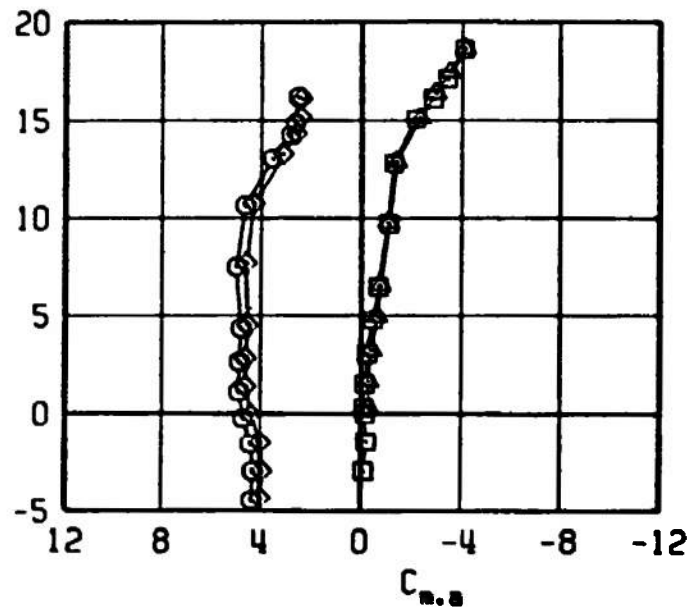
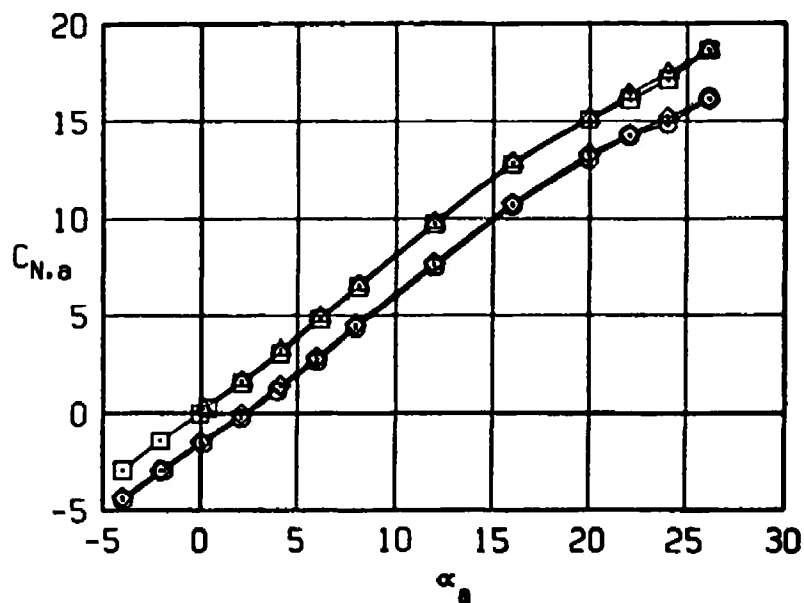


Figure 27. Effect of pitch control, $\delta q = -15$ deg, and yaw control, $\delta r = 5$ deg, deflections on the normal-force and pitching-moment coefficients of the Super HOBOS/MK-84.

SYM	CONFIGURATION	MACH NO	δp	δq	δr
□	B2S13W4T3F7	0.65	0	0	0
○	B2S13W4T3F7	0.65	0	-15	0
△	B2S13W4T3F7	0.65	0	0	5
◇	B2S13W4T3F7	0.65	0	-15	5

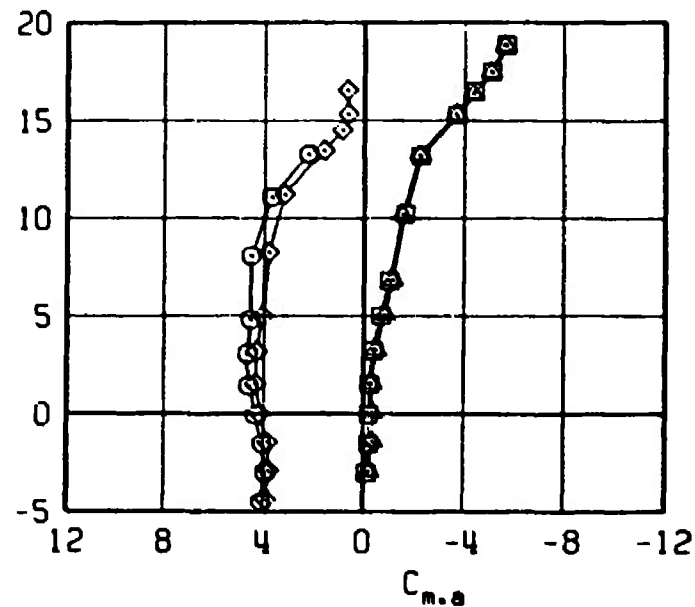
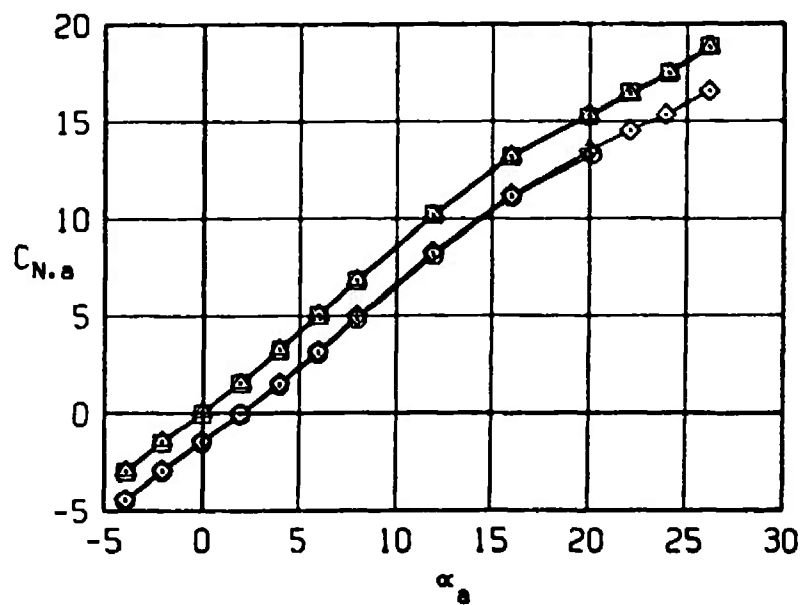


Figure 27. Continued.

SYM	CONFIGURATION	MACH NO	δp	δq	δr
□	B2S13W4T3F7	0.95	0	0	0
○	B2S13W4T3F7	0.95	0	-15	0
△	B2S13W4T3F7	0.95	0	0	5
◇	B2S13W4T3F7	0.95	0	-15	5

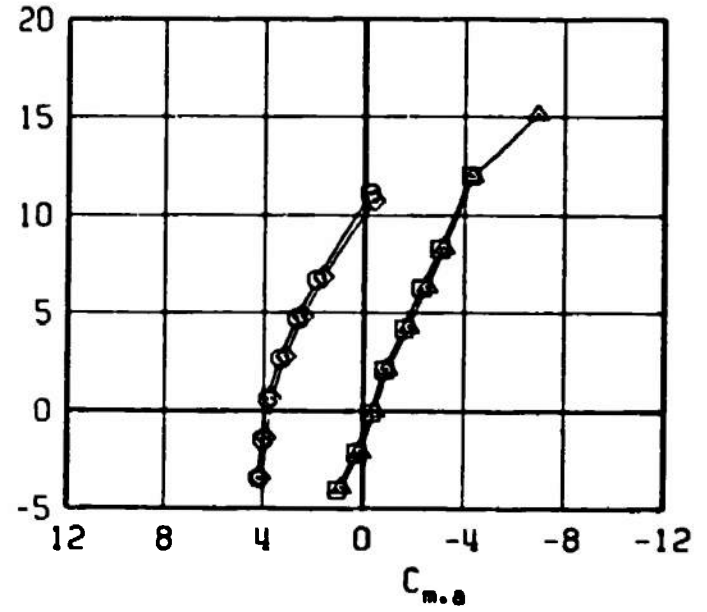
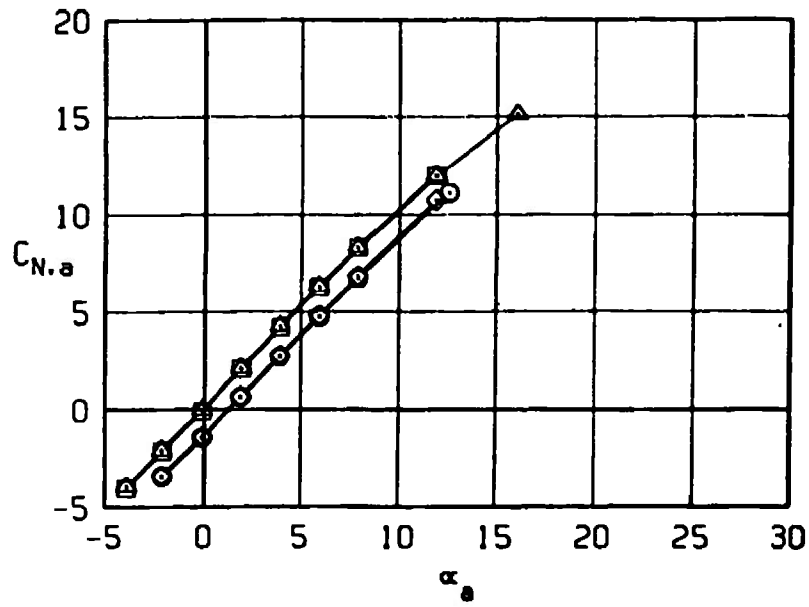


Figure 27. Continued.

SYM	CONFIGURATION	MACH NO	δp	δq	δr
□	B2S13W4T3F7	1.20	0	0	0
○	B2S13W4T3F7	1.20	0	-15	0
△	B2S13W4T3F7	1.20	0	0	5
◇	B2S13W4T3F7	1.20	0	-15	5

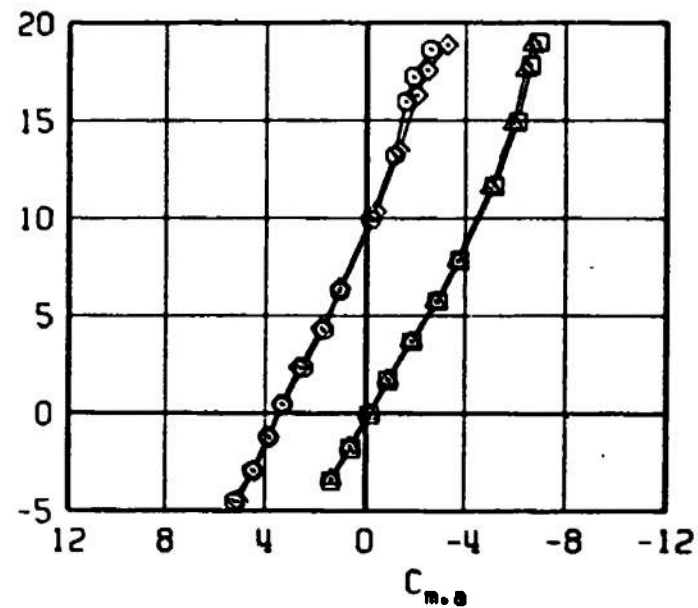
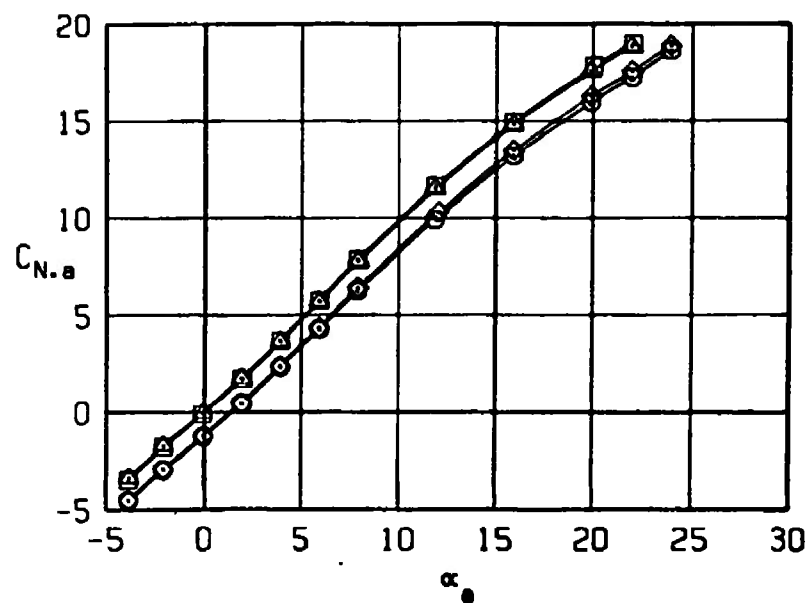


Figure 27. Continued.

SYM	CONFIGURATION	MACH NO	δp	δq	δr
□	B2S13W4T3F7	1.60	0	0	0
○	B2S13W4T3F7	1.60	0	-15	0
△	B2S13W4T3F7	1.60	0	0	5
◇	B2S13W4T3F7	1.60	0	-15	5

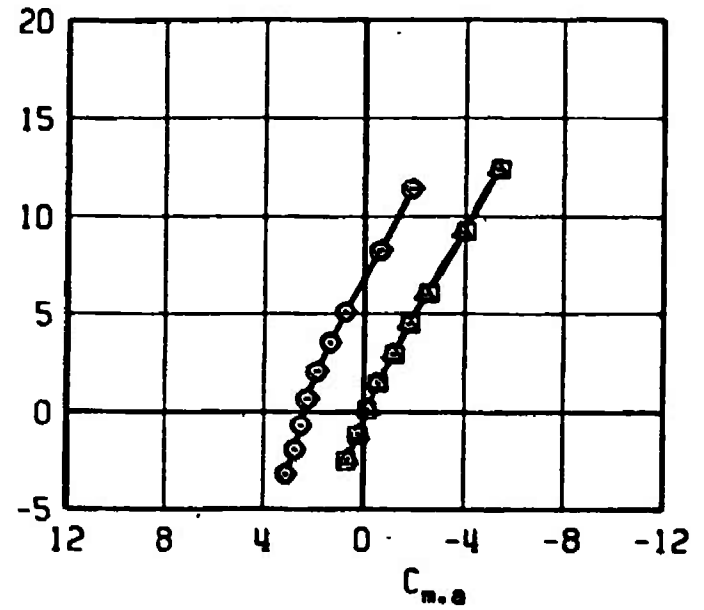
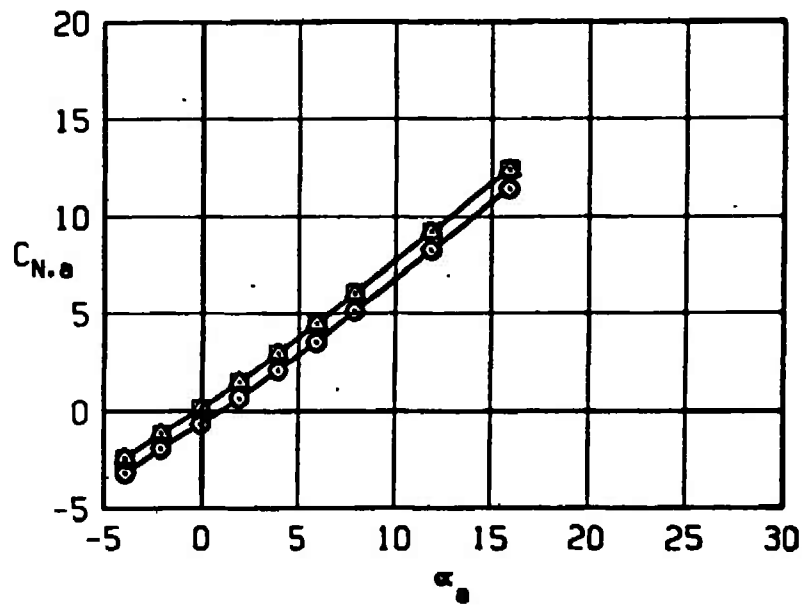


Figure 27. Concluded.

SYM	CONFIGURATION	MACH NO	δp	δq	δr
□	B2S13W4T3F7	0.40	0	0	0
○	B2S13W4T3F7	0.40	0	-15	0
△	B2S13W4T3F7	0.40	0	0	5
◇	B2S13W4T3F7	0.40	0	-15	5

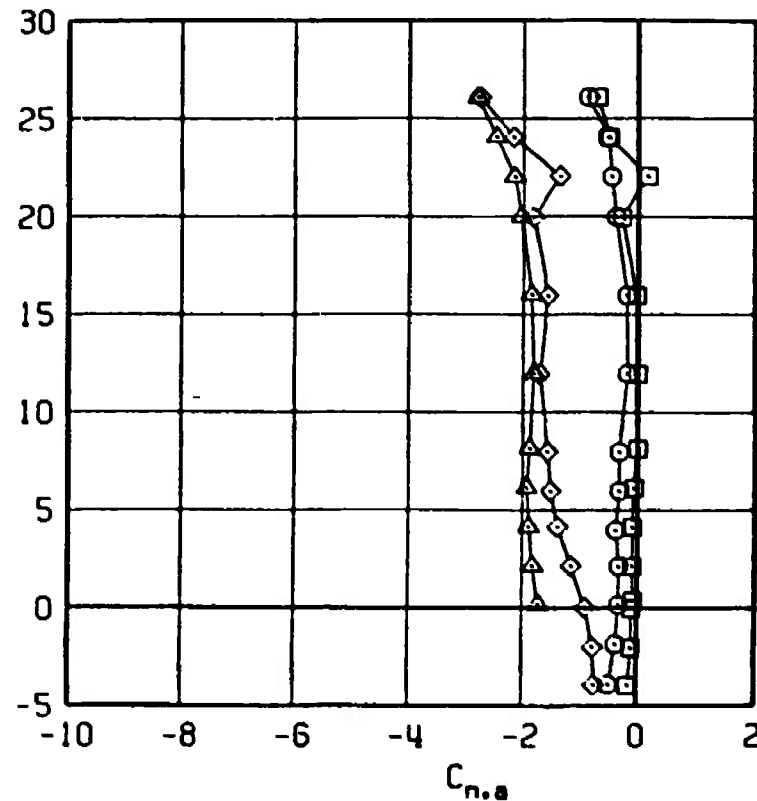
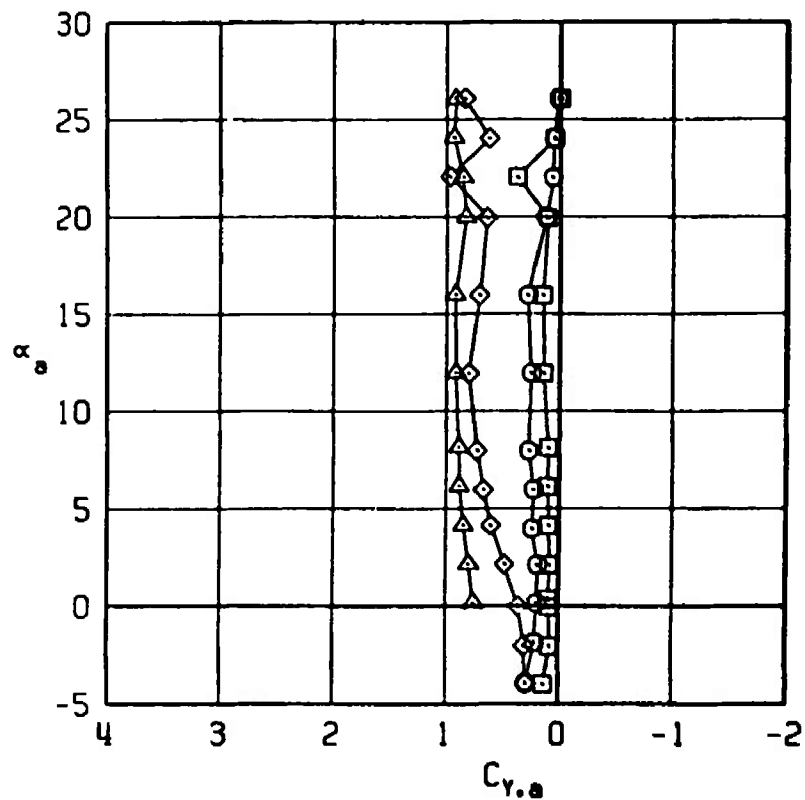


Figure 28. Effect of pitch control, $\delta q = -15$ deg, and yaw control, $\delta r = 5$ deg, deflections on the side-force and yawing-moment coefficients of the Super HOBOS/MK-84.

SYM	CONFIGURATION	MACH NO	δp	δq	δr
□	B2S13W4T3F7	0.65	0	0	0
○	B2S13W4T3F7	0.65	0	-15	0
△	B2S13W4T3F7	0.65	0	0	5
◇	B2S13W4T3F7	0.65	0	-15	5

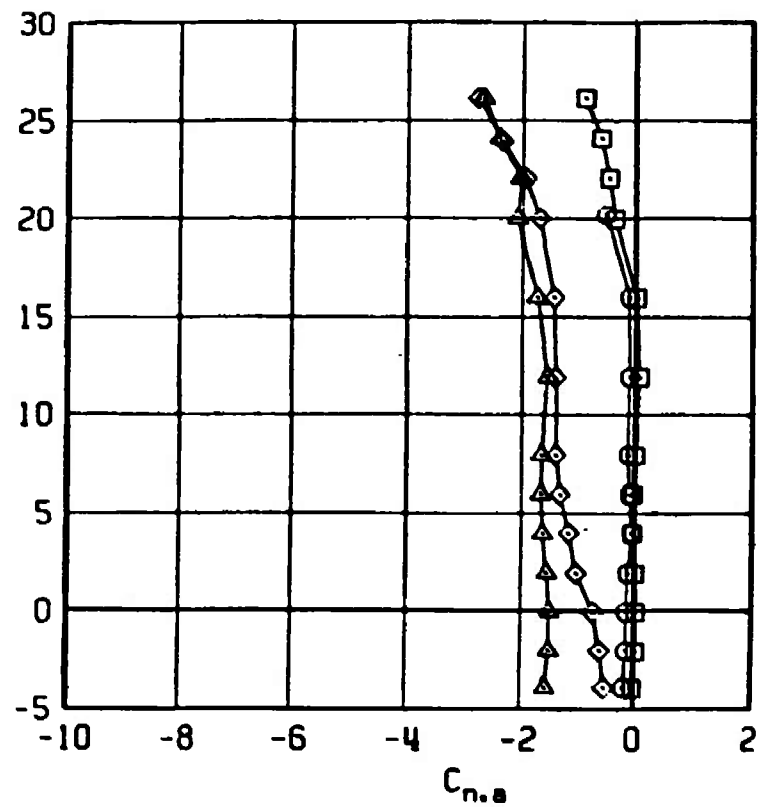
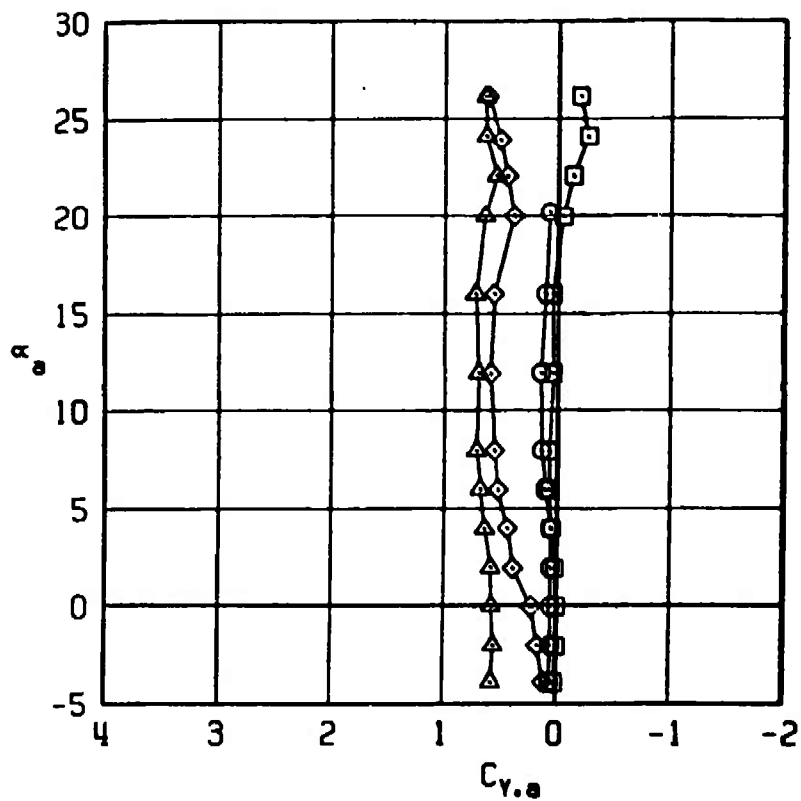


Figure 28. Continued.

SYM	CONFIGURATION	MACH NO	δp	δq	δr
□	B2S13W4T3F7	0.95	0	0	0
○	B2S13W4T3F7	0.95	0	-15	0
△	B2S13W4T3F7	0.95	0	0	5
◇	B2S13W4T3F7	0.95	0	-15	5

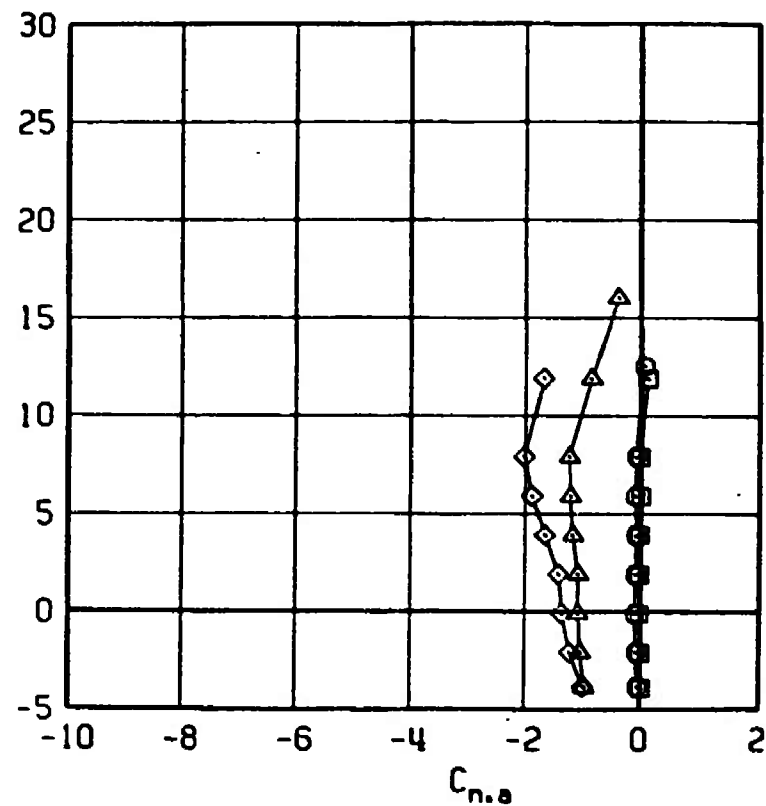
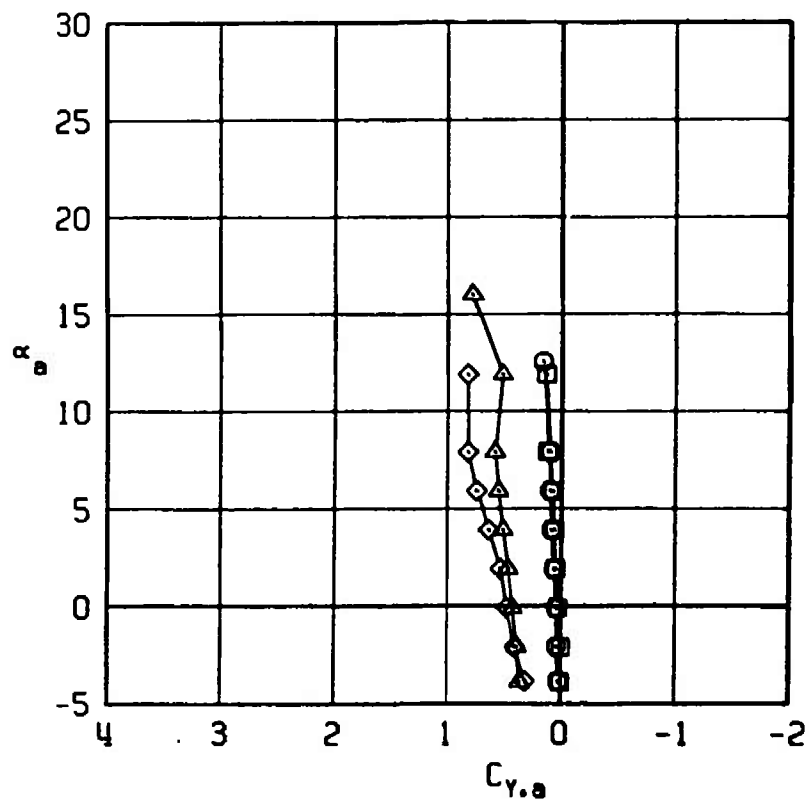


Figure 28. Continued.

SYM	CONFIGURATION	MACH NO	δp	δq	δr
□	B2S13W4T3F7	1.20	0	0	0
○	B2S13W4T3F7	1.20	0	-15	0
△	B2S13W4T3F7	1.20	0	0	5
◇	B2S13W4T3F7	1.20	0	-15	5

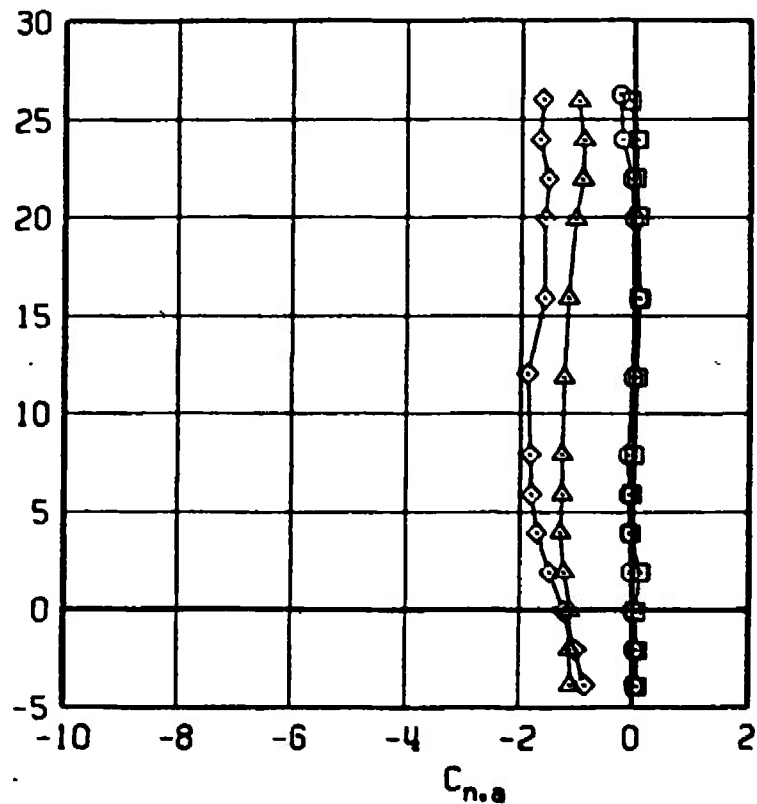
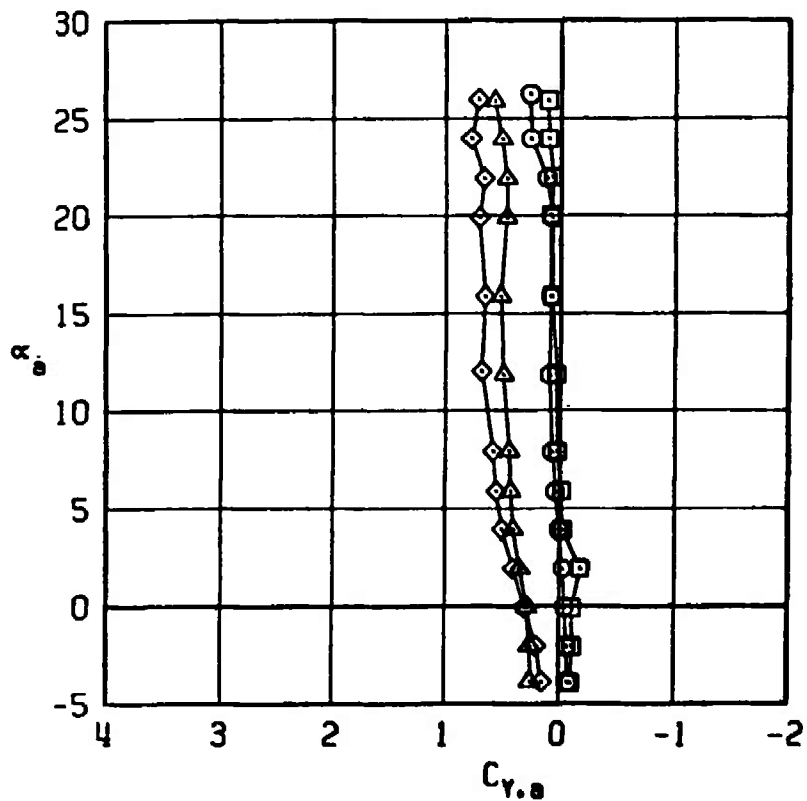


Figure 28. Continued.

SYM	CONFIGURATION	MACH NO	δp	δq	δr
□	B2S13W4T3F7	1.60	0	0	0
○	B2S13W4T3F7	1.60	0	-15	0
△	B2S13W4T3F7	1.60	0	0	5
◇	B2S13W4T3F7	1.60	0	-15	5

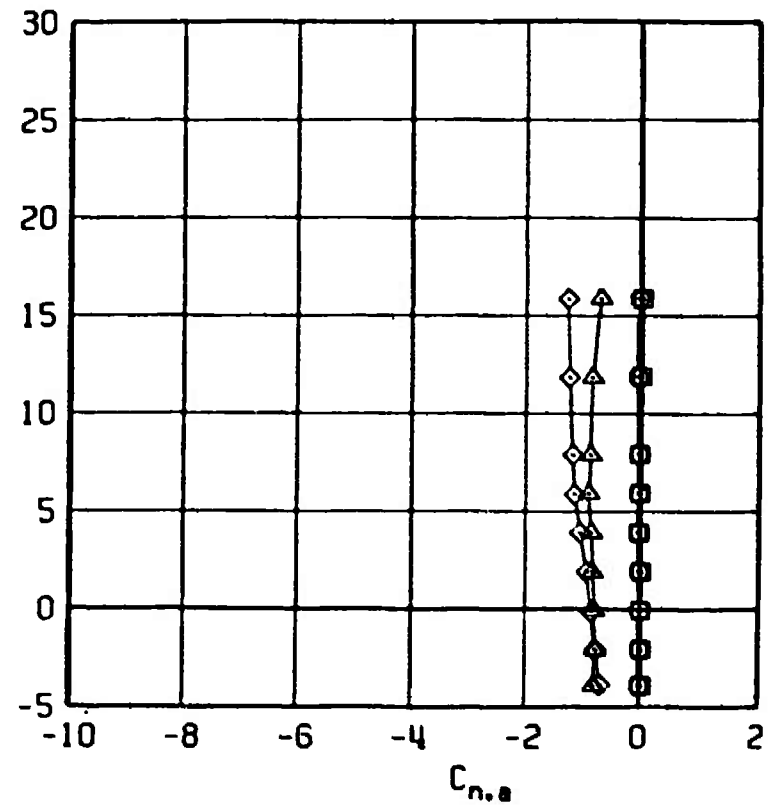
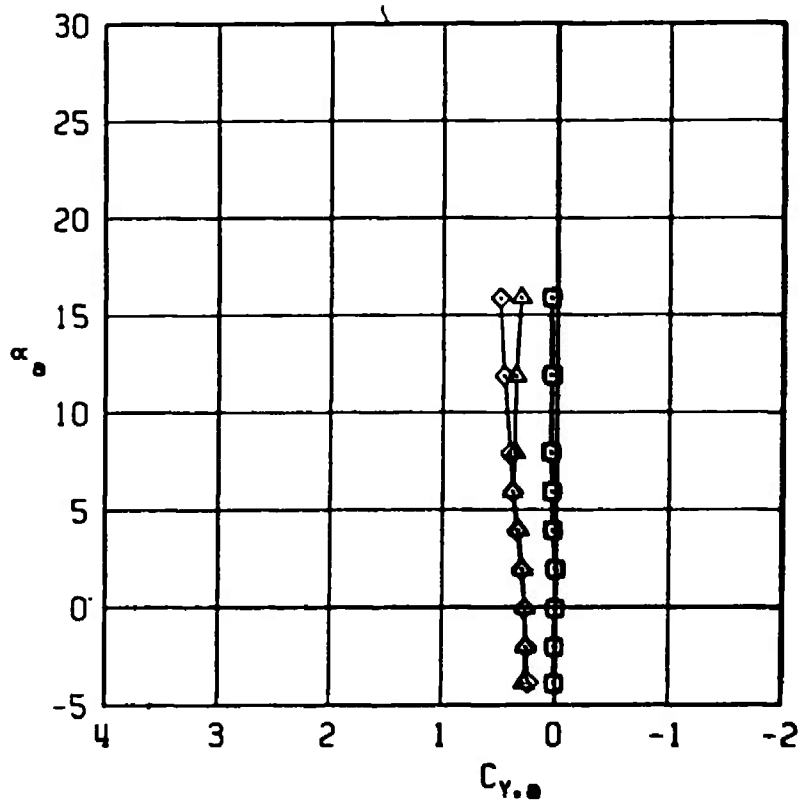


Figure 28. Concluded.

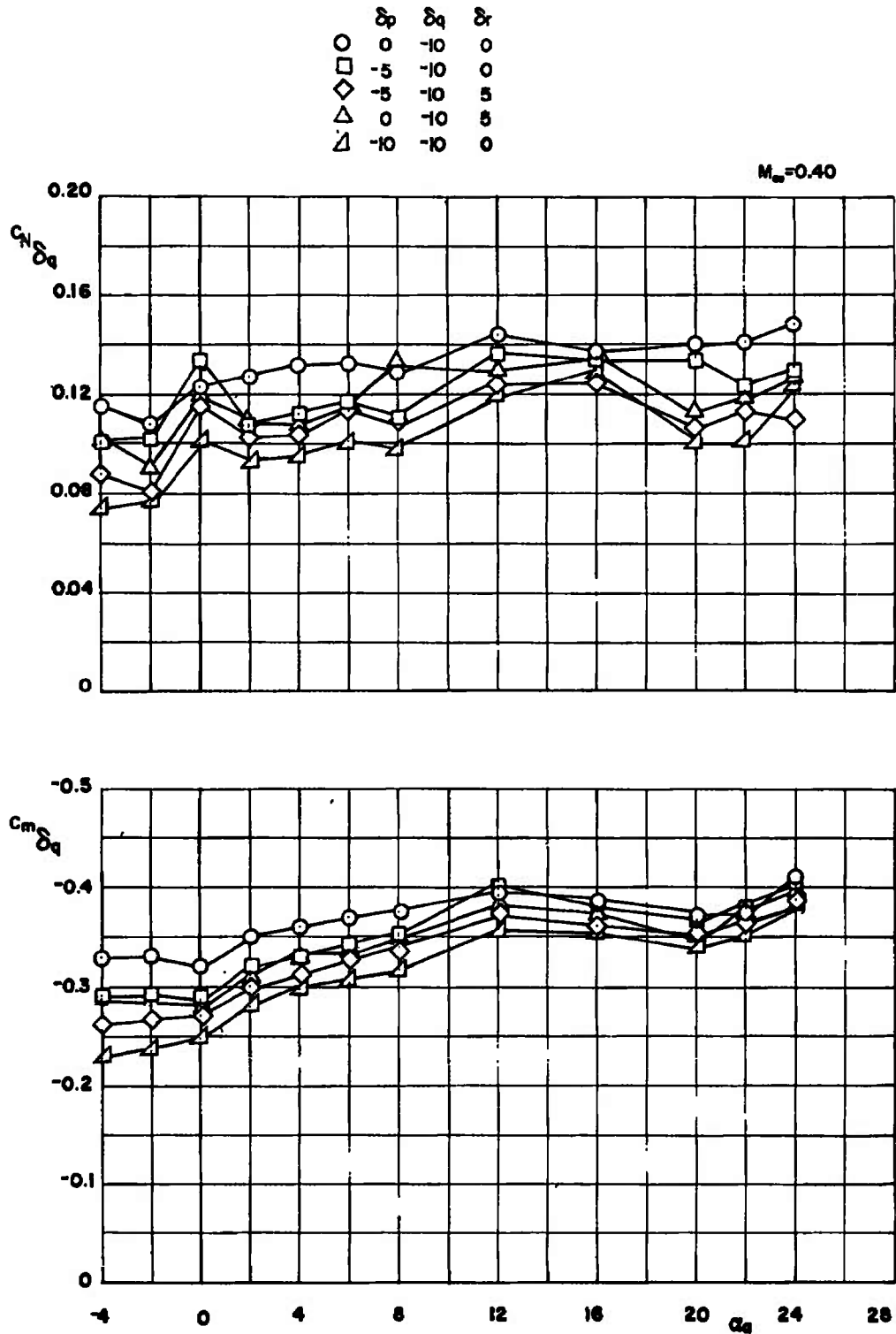


Figure 29. Normal-force increment and pitch control effectiveness for a pitch control deflection of $\delta q = -10$ deg, combined with roll and yaw control deflections.

	δp	δq	δr
○	0	-10	0
□	-5	-10	0
◇	-5	-10	5
△	0	-10	5
▽	-10	-10	0

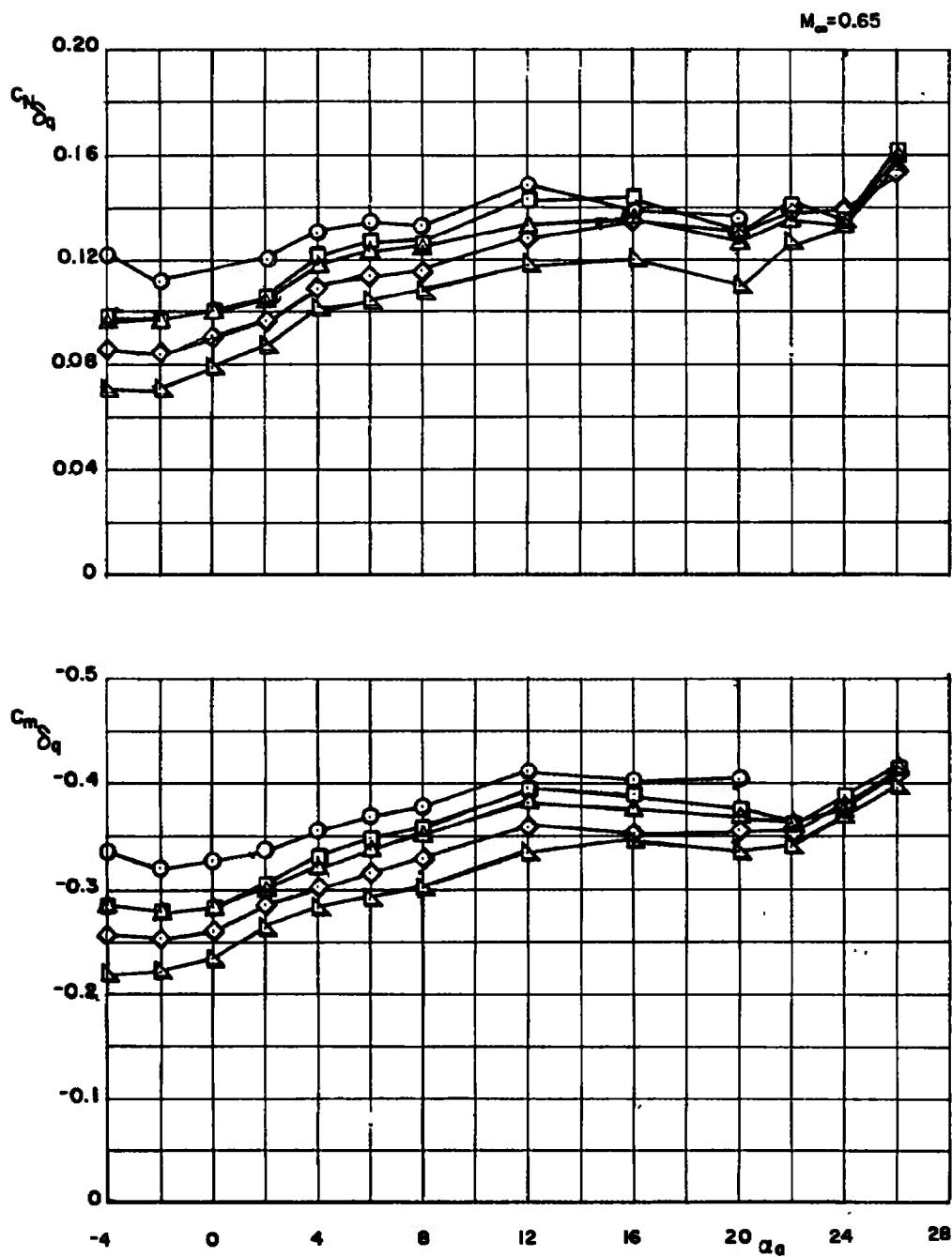


Figure 29. Continued.

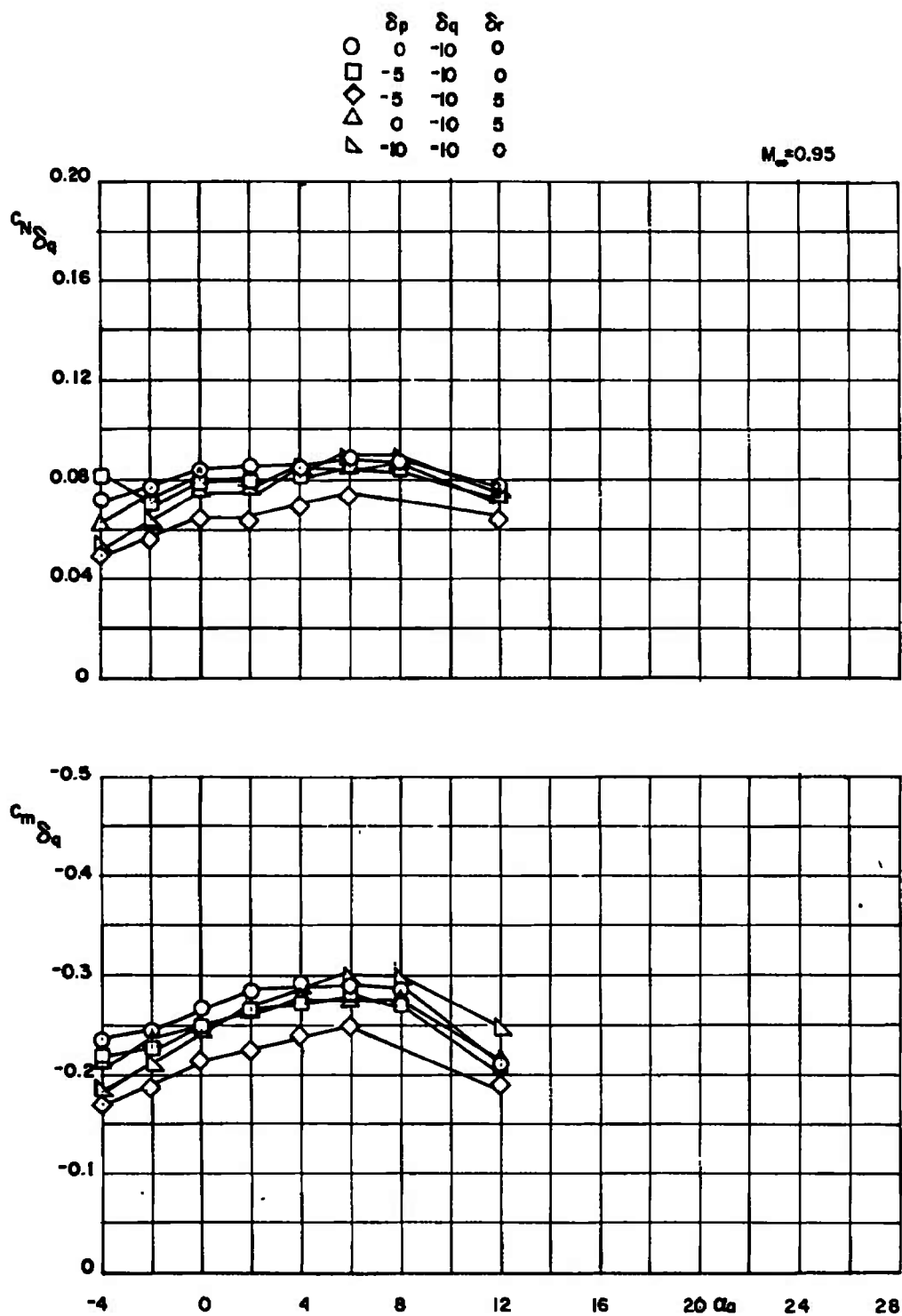


Figure 29. Continued.

	δp	δq	δr
○	0	-10	0
□	-5	-10	0
◇	-5	-10	5
△	0	-10	5

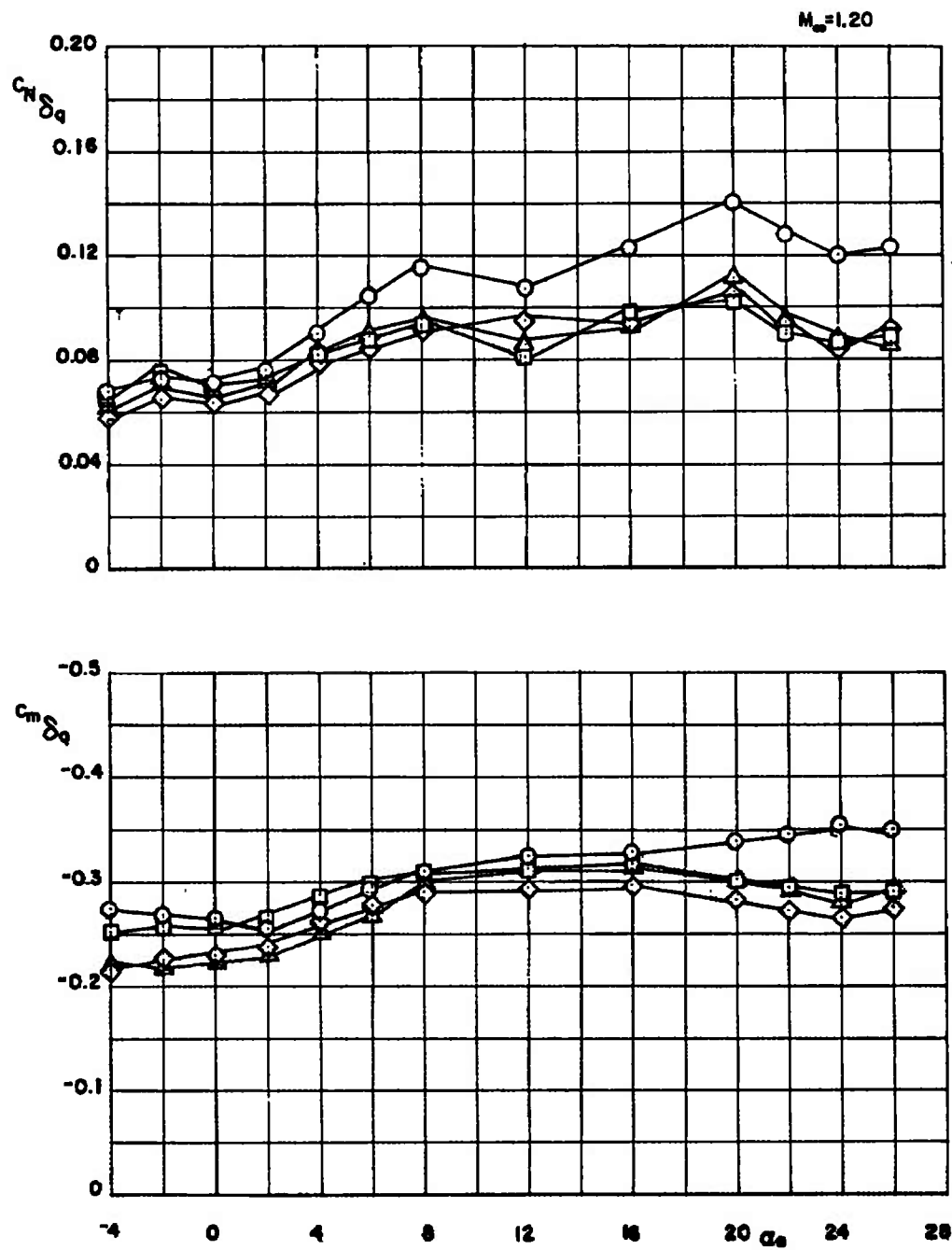


Figure 29. Continued.

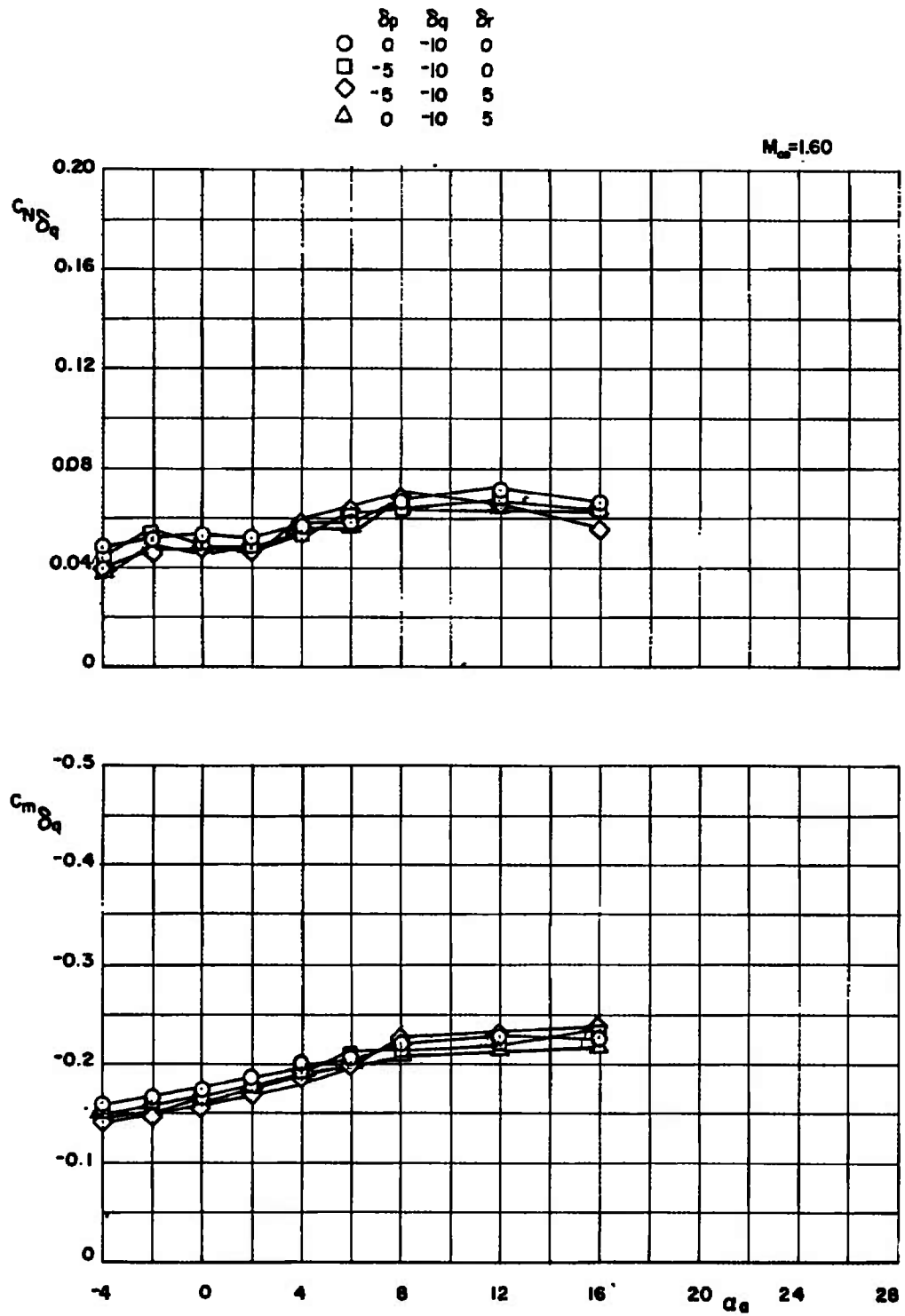


Figure 29. Concluded.

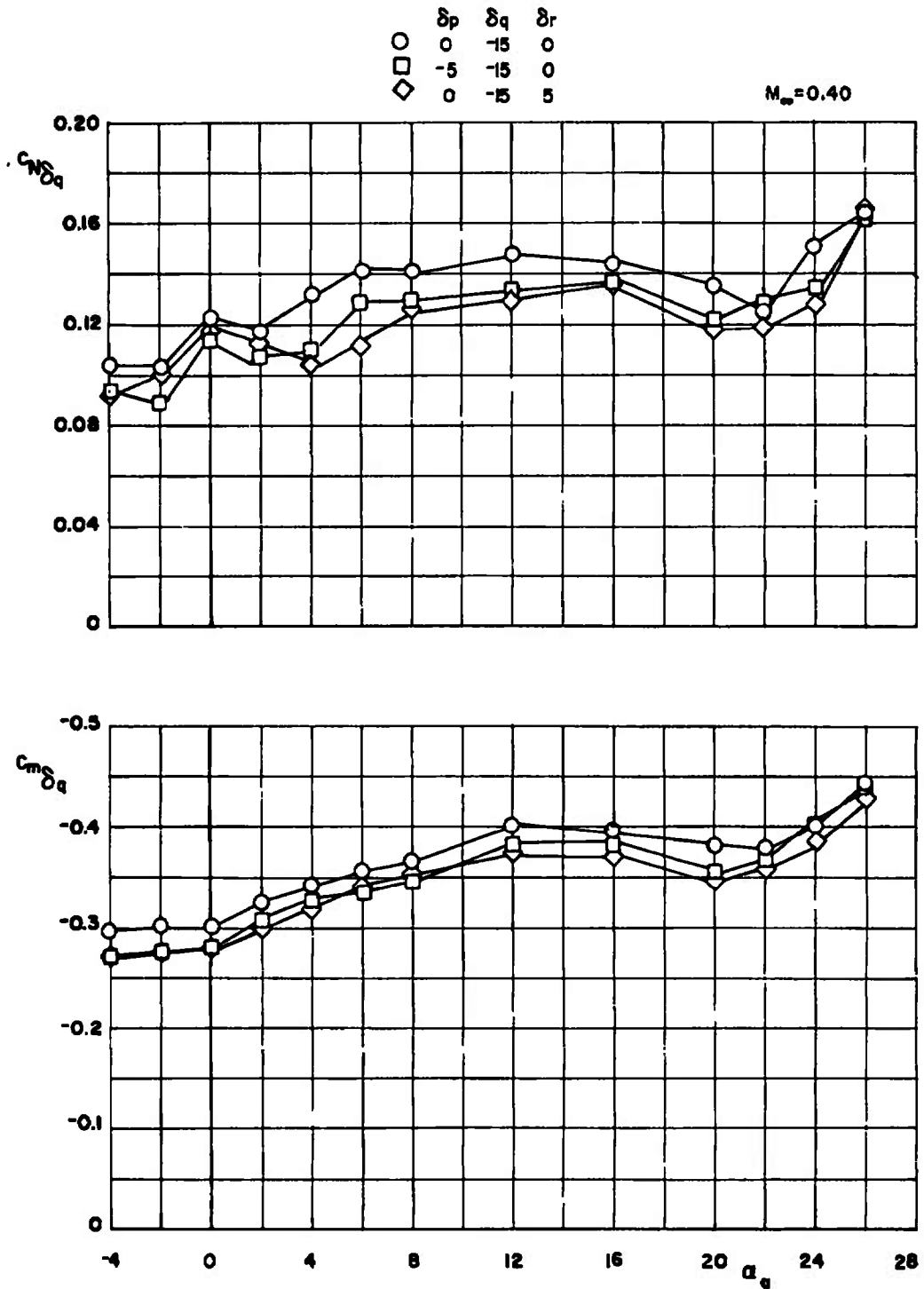


Figure 30. Normal-force increment and pitch control effectiveness for a pitch control deflection of $\delta q = -15$ deg, combined with roll and yaw control deflections.

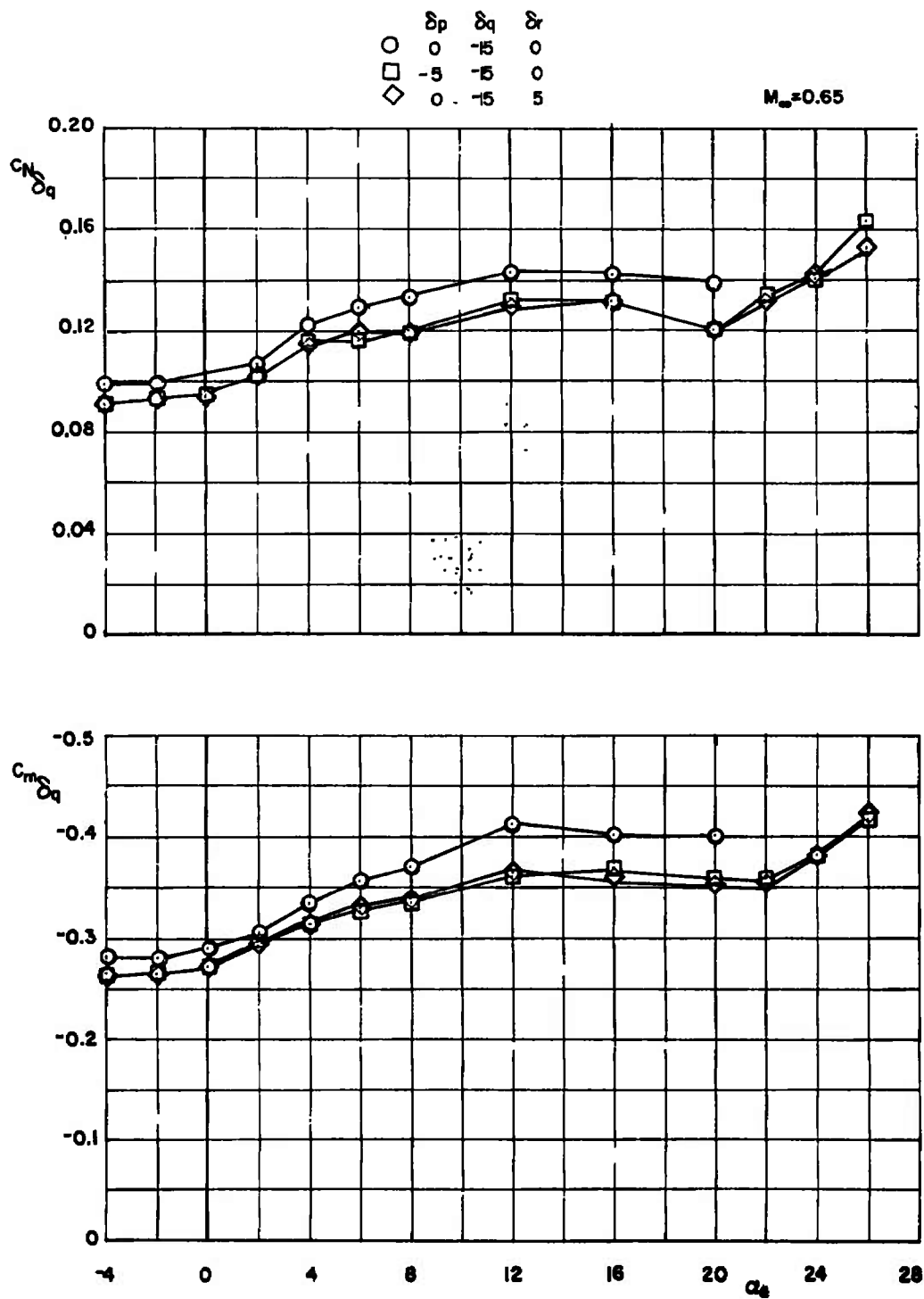


Figure 30. Continued.

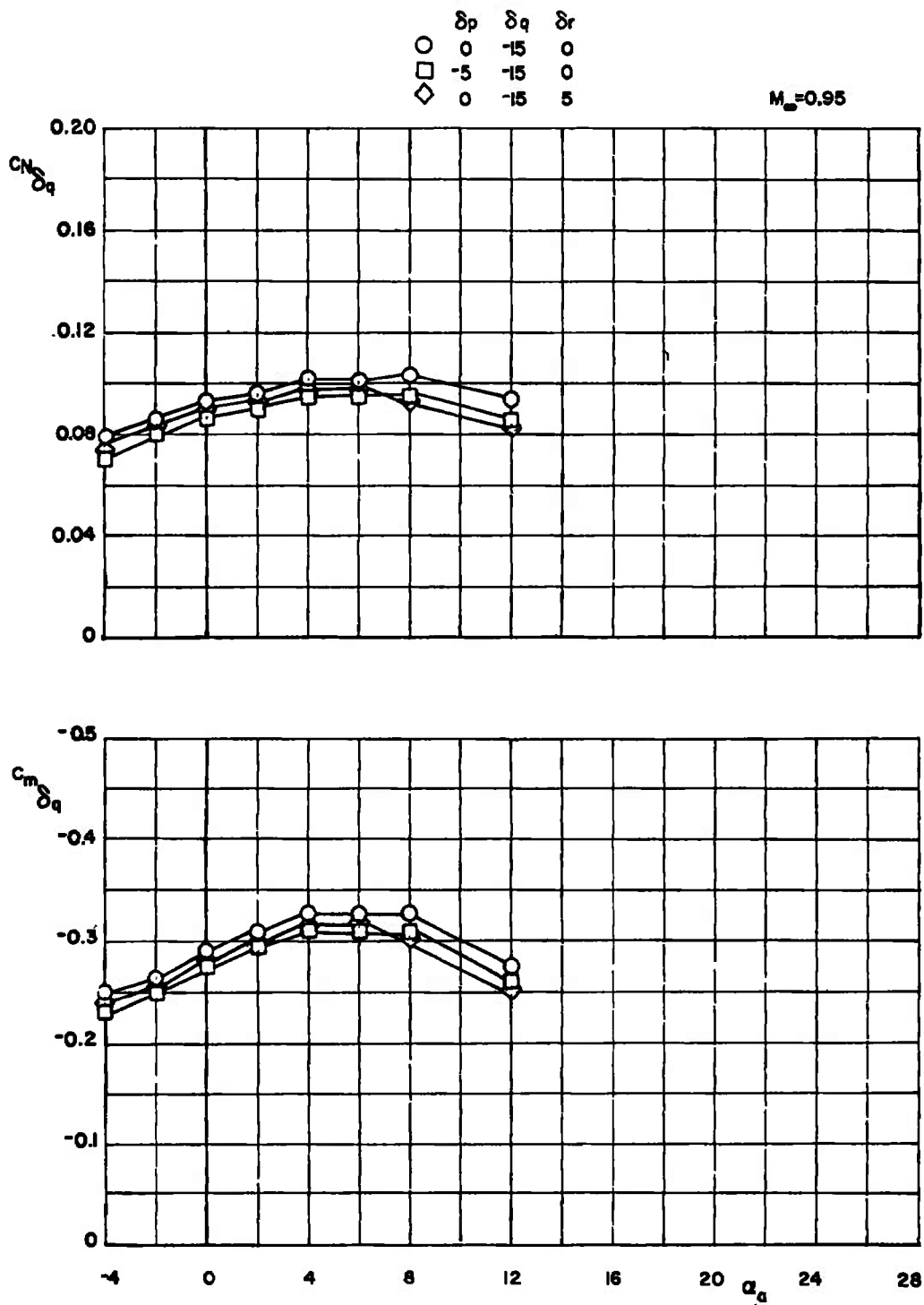


Figure 30. Continued.

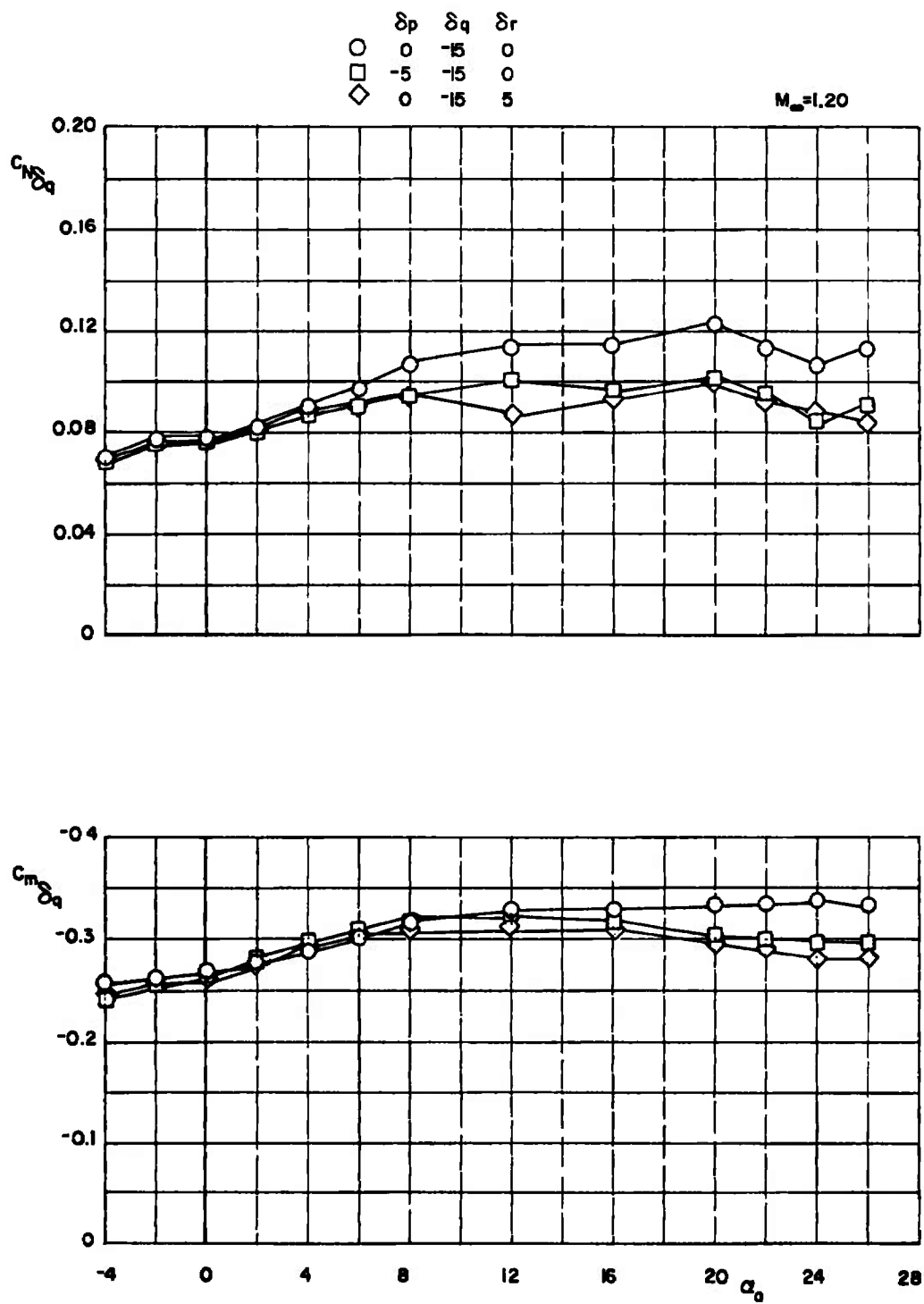


Figure 30. Continued.

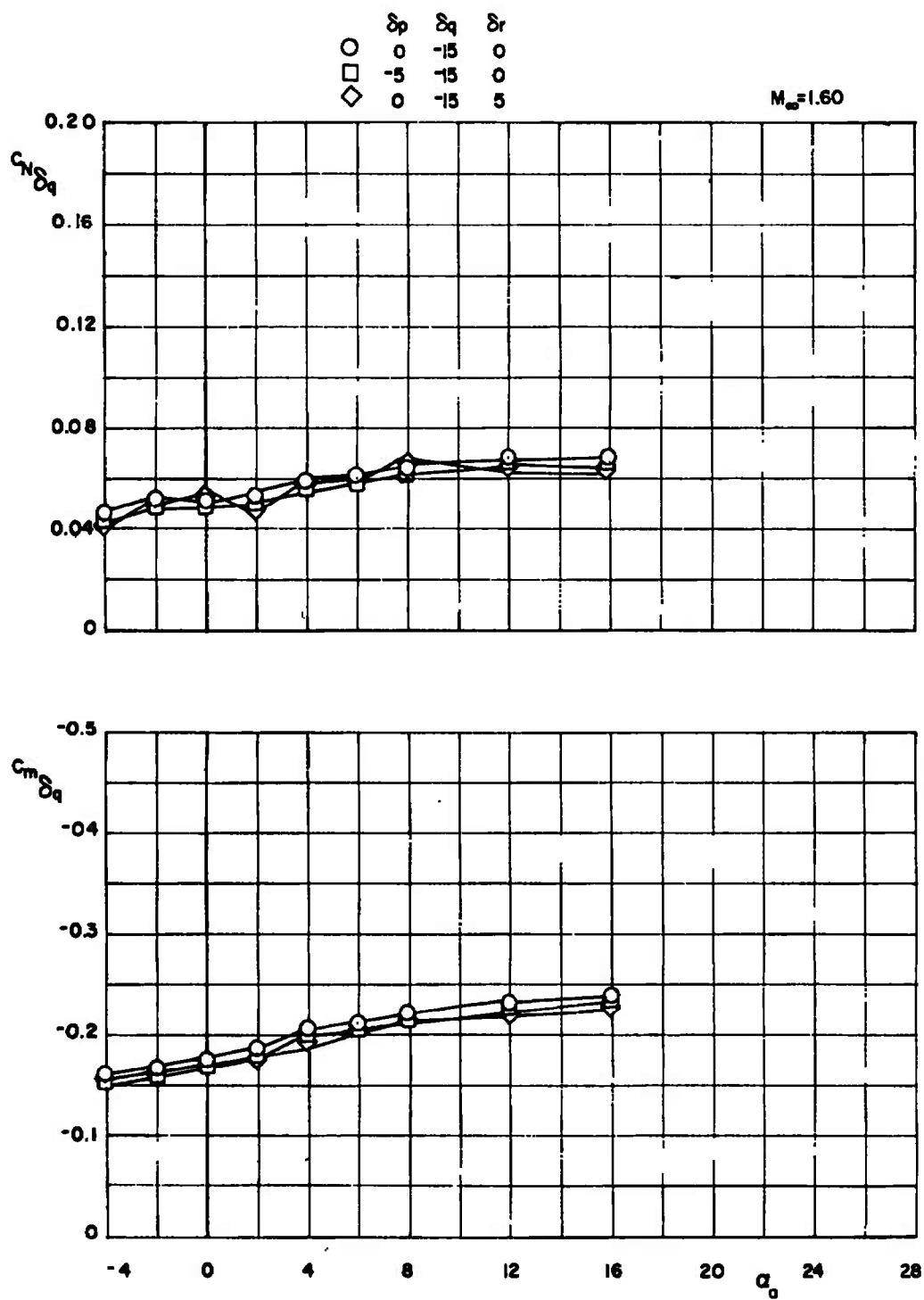


Figure 30. Concluded.

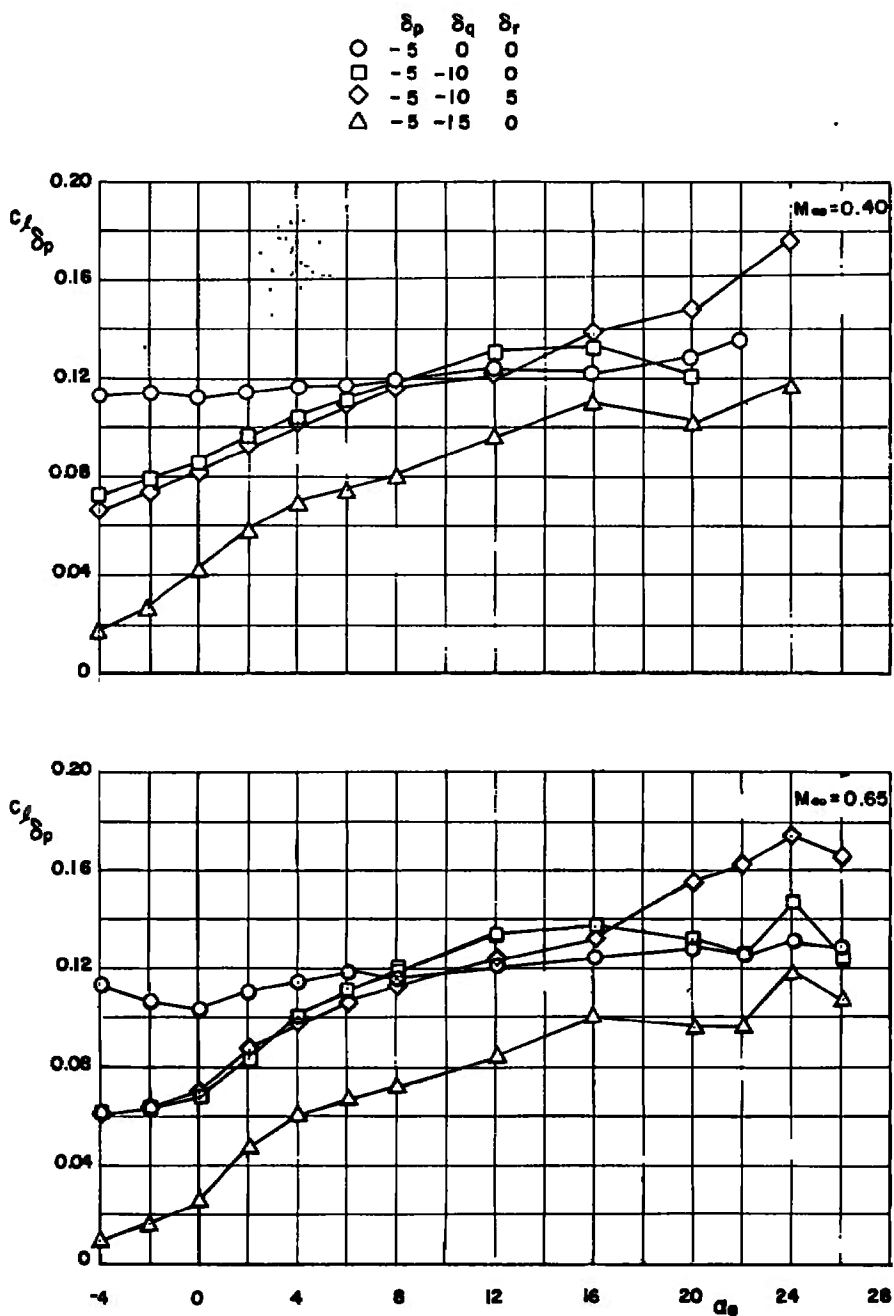


Figure 31. Roll control effectiveness for a roll control deflection of $\delta_p = -5$ deg, combined with pitch and yaw control deflections.

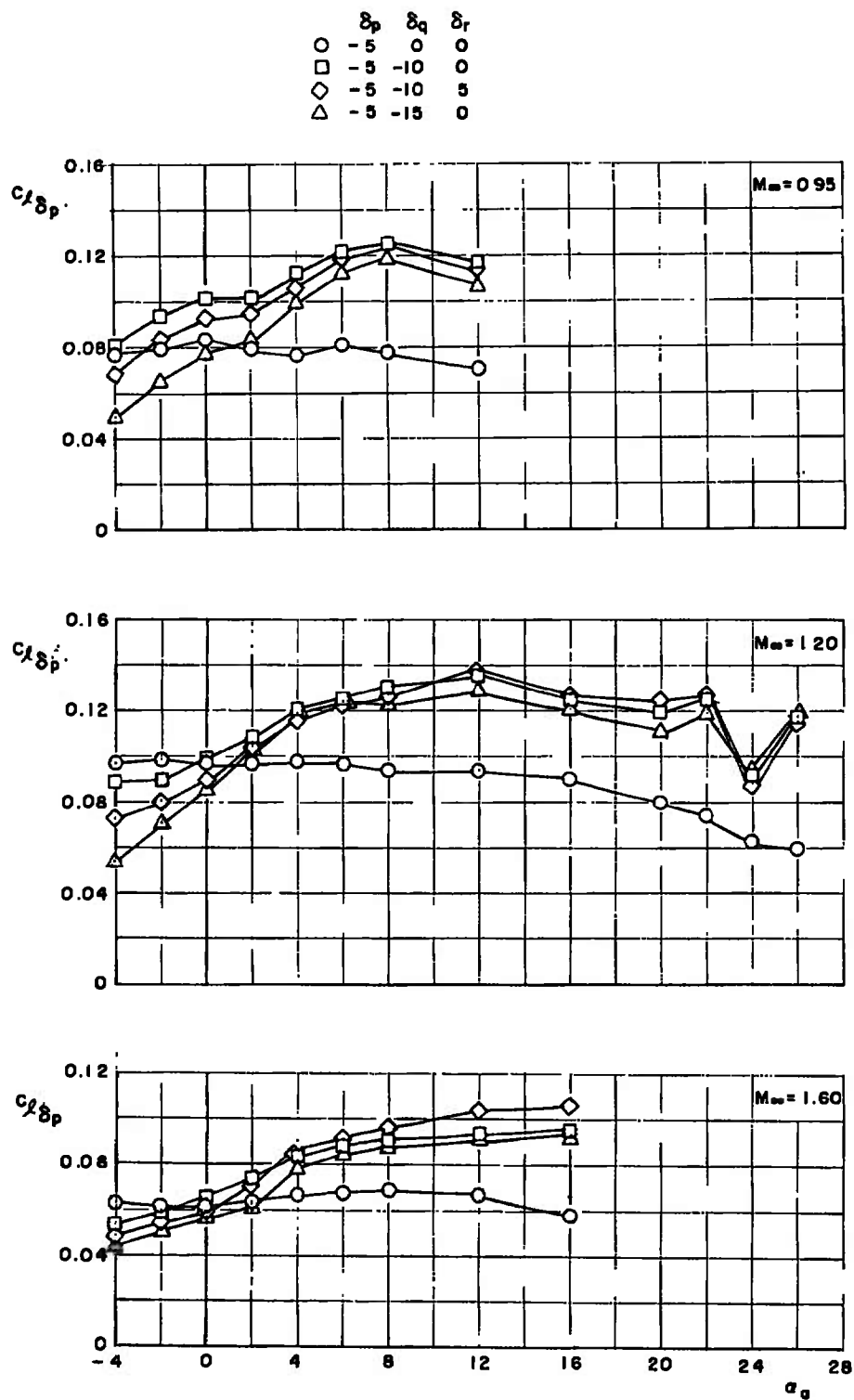


Figure 31. Concluded.

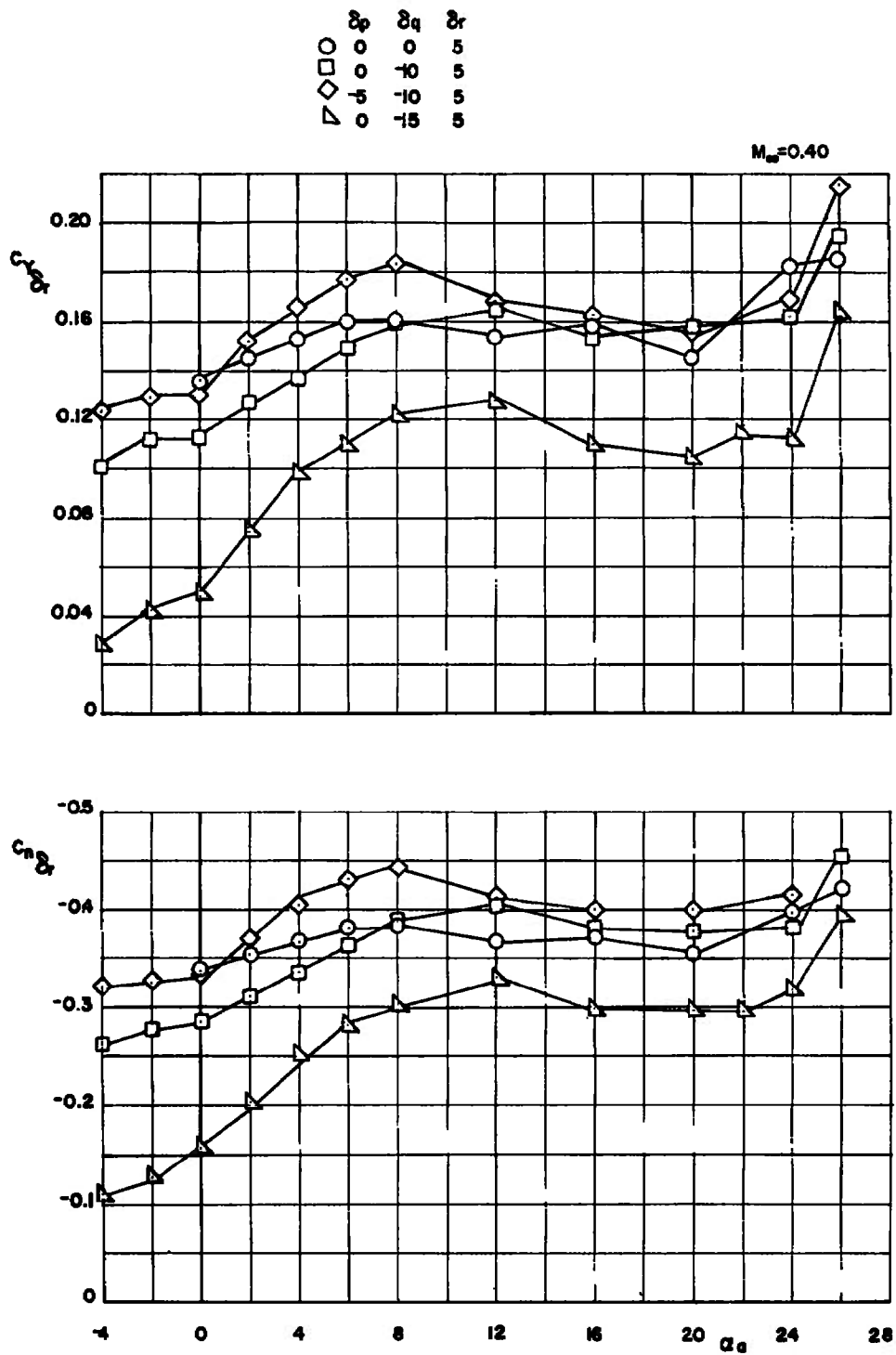


Figure 32. Side-force increment and yaw control effectiveness for a yaw control deflection of $\delta r = 5$ deg, combined with roll and pitch control deflections.

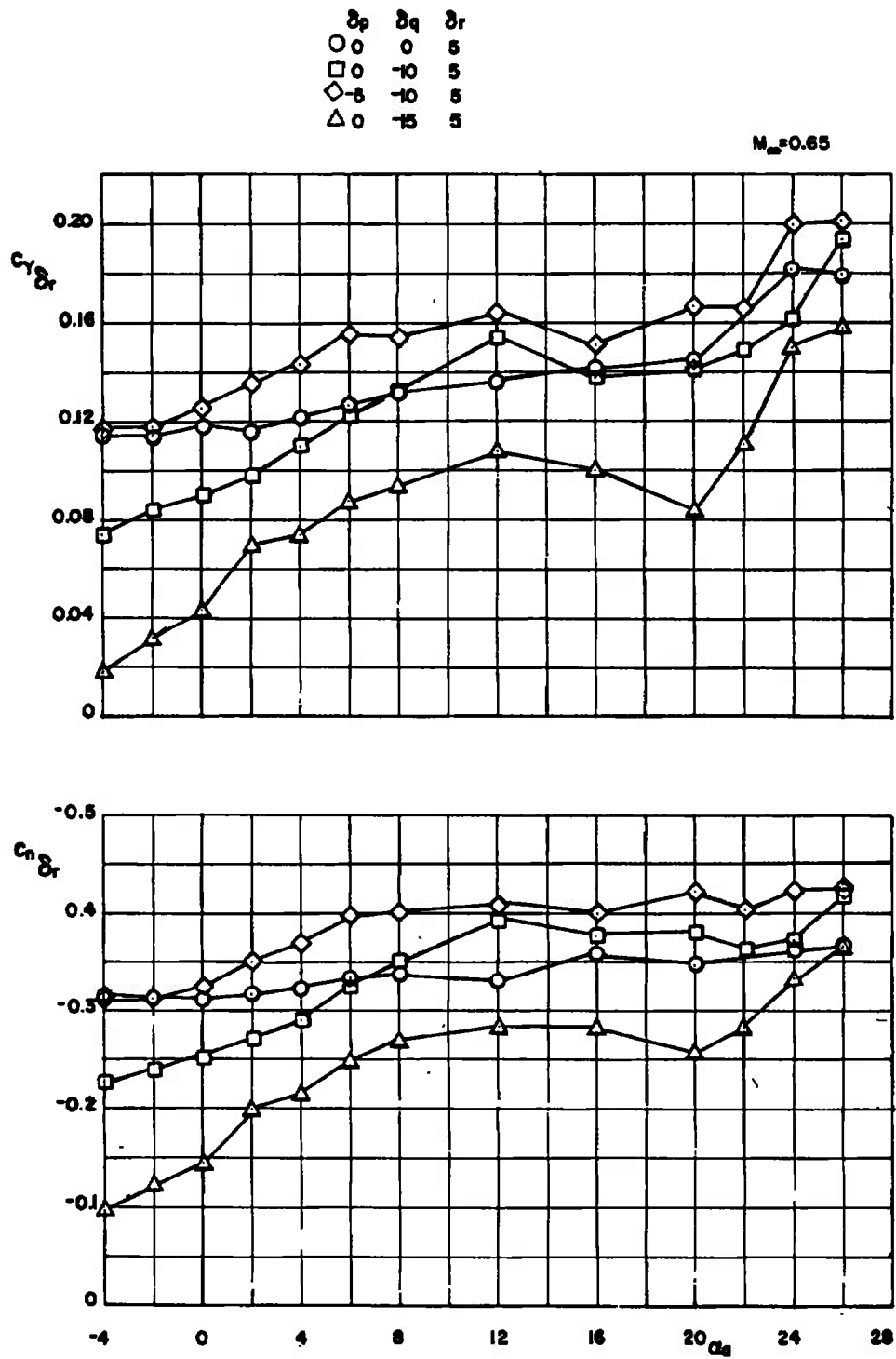


Figure 32. Continued.

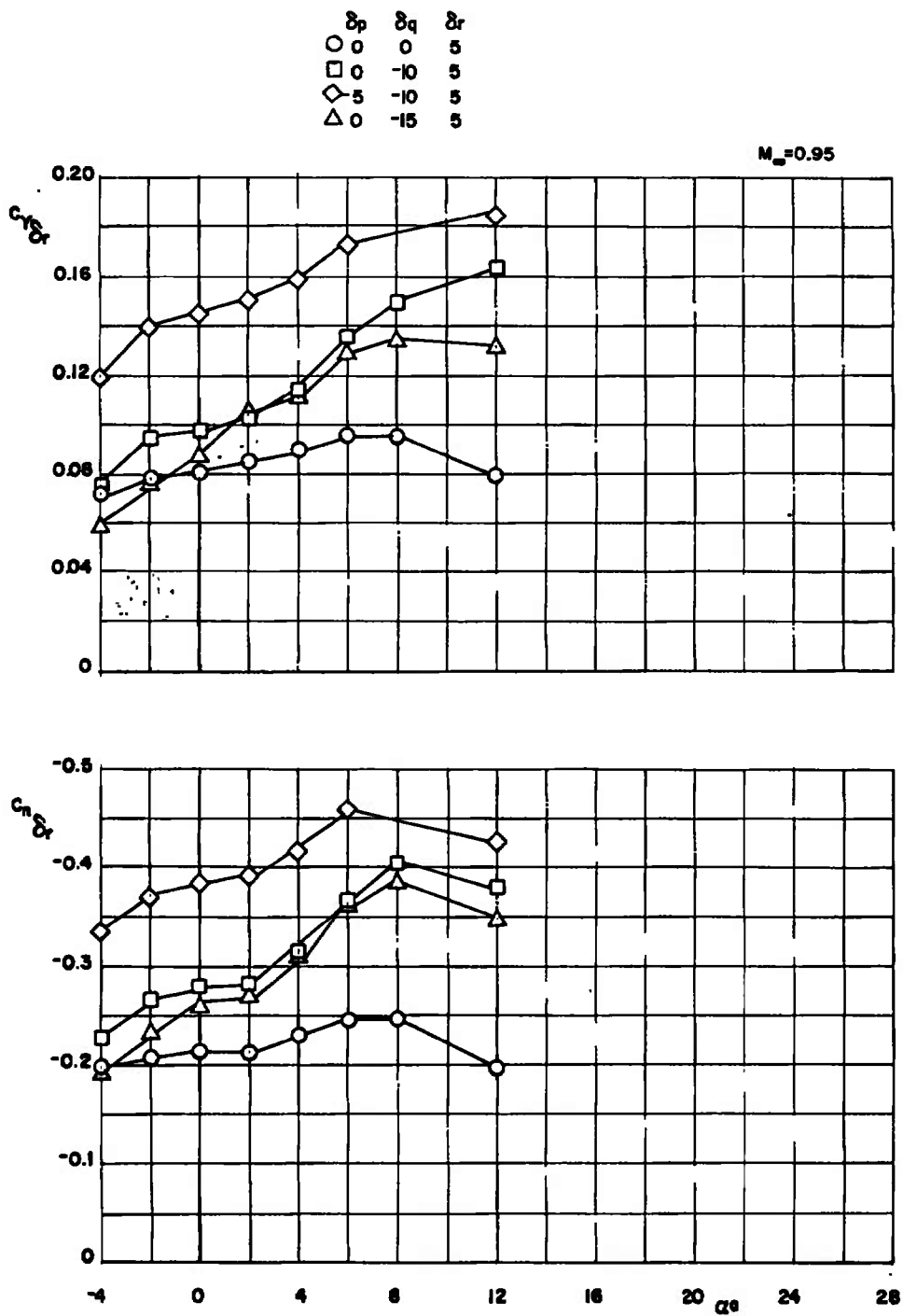


Figure 32. Continued.

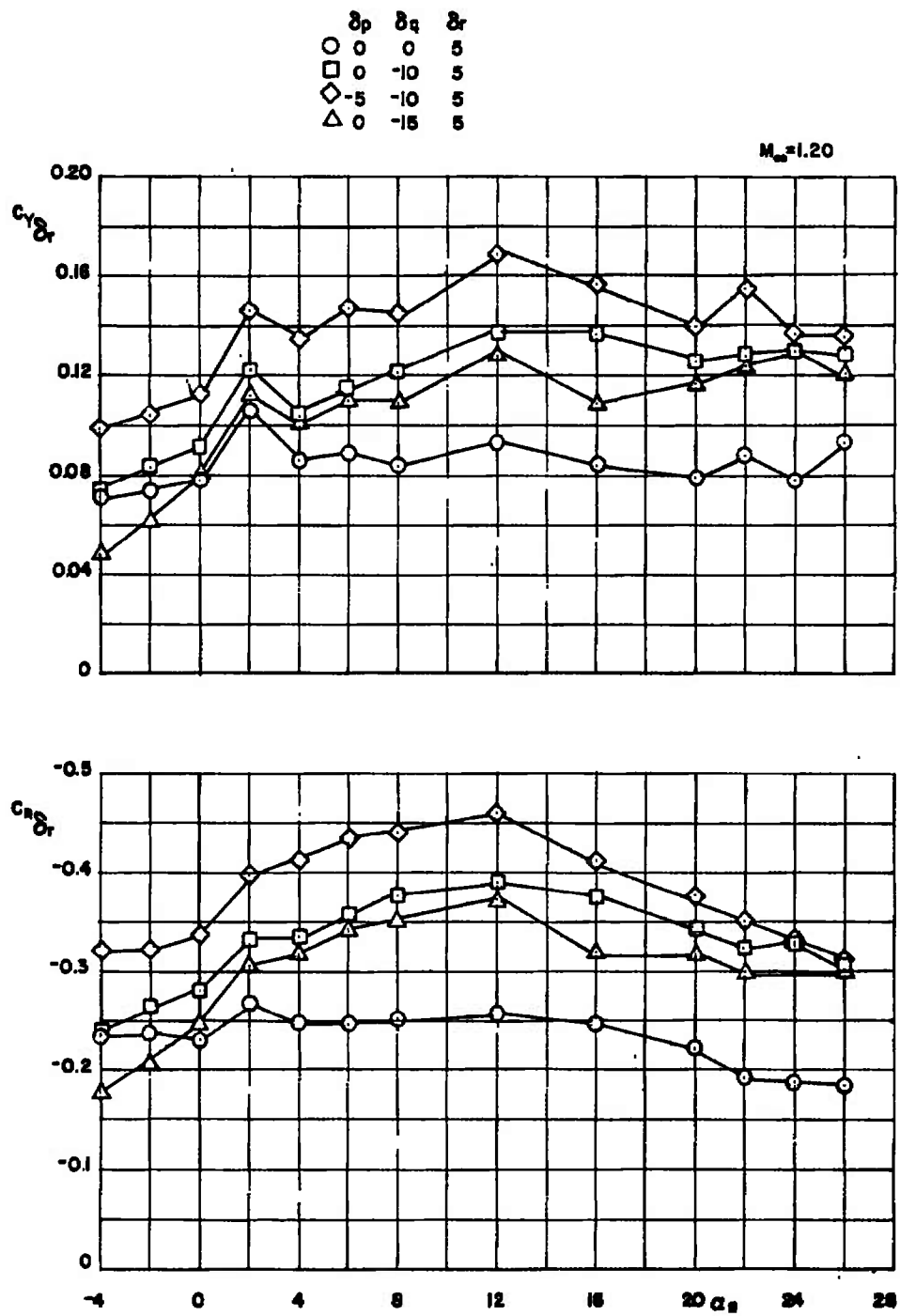


Figure 32. Continued.

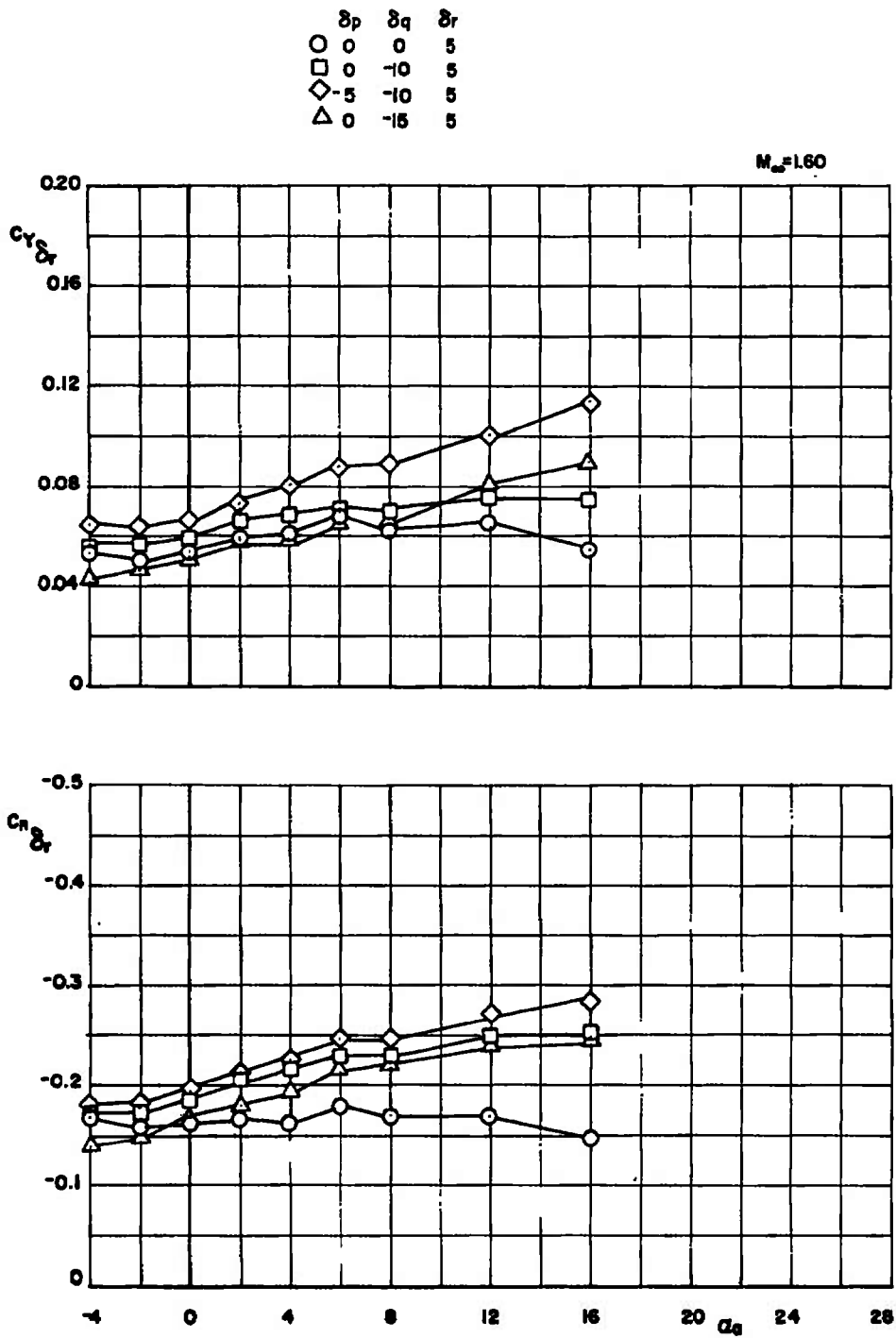


Figure 32. Concluded.

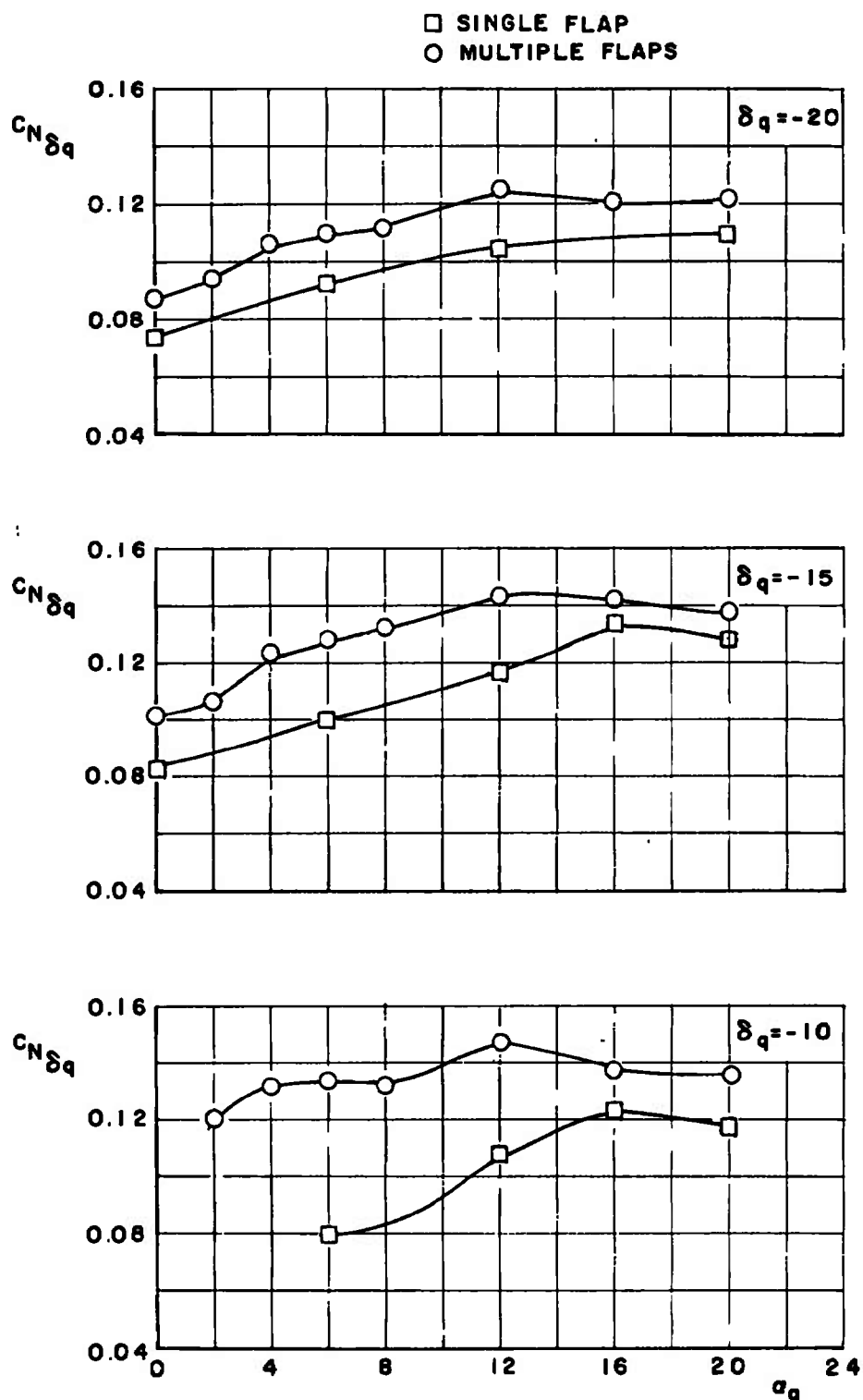


Figure 33. Comparison of normal-force increment calculated from single flap and multiple flap techniques.

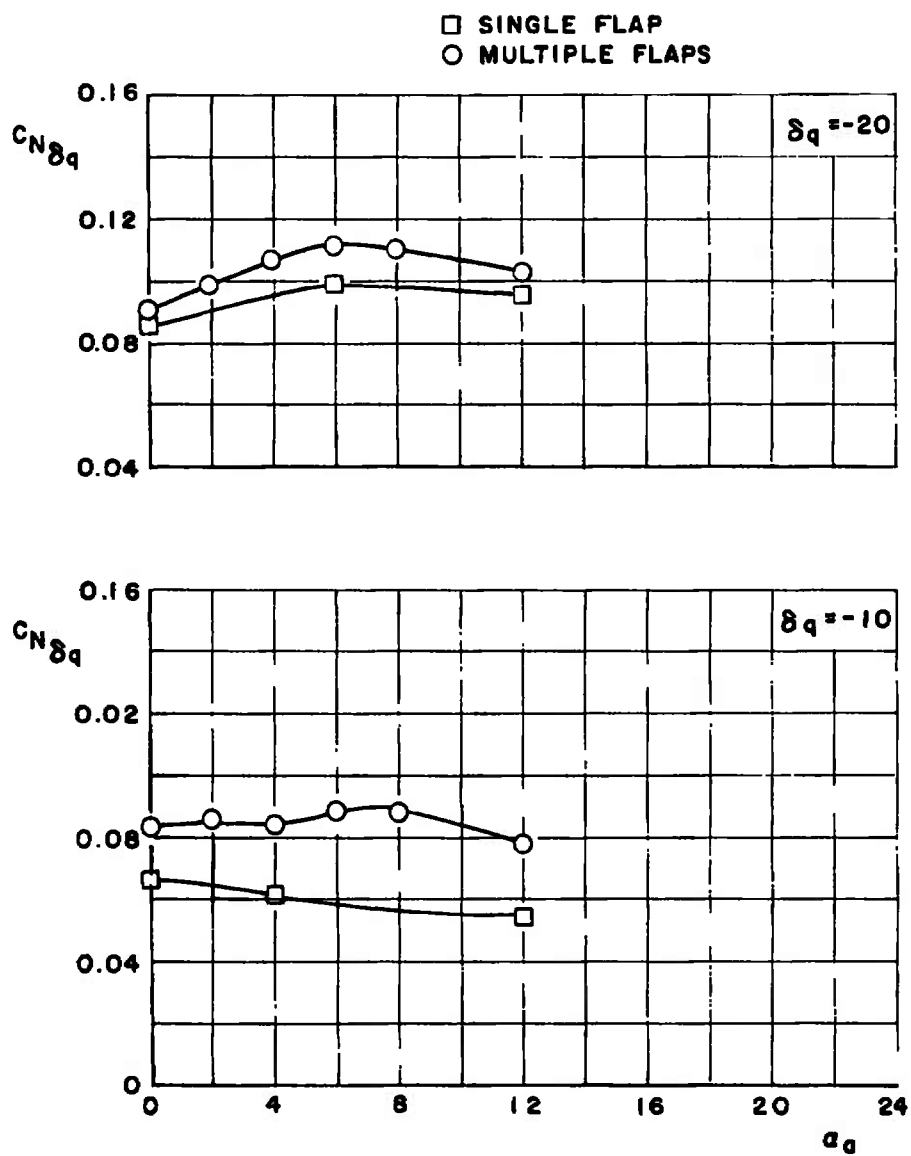


Figure 33. Concluded.

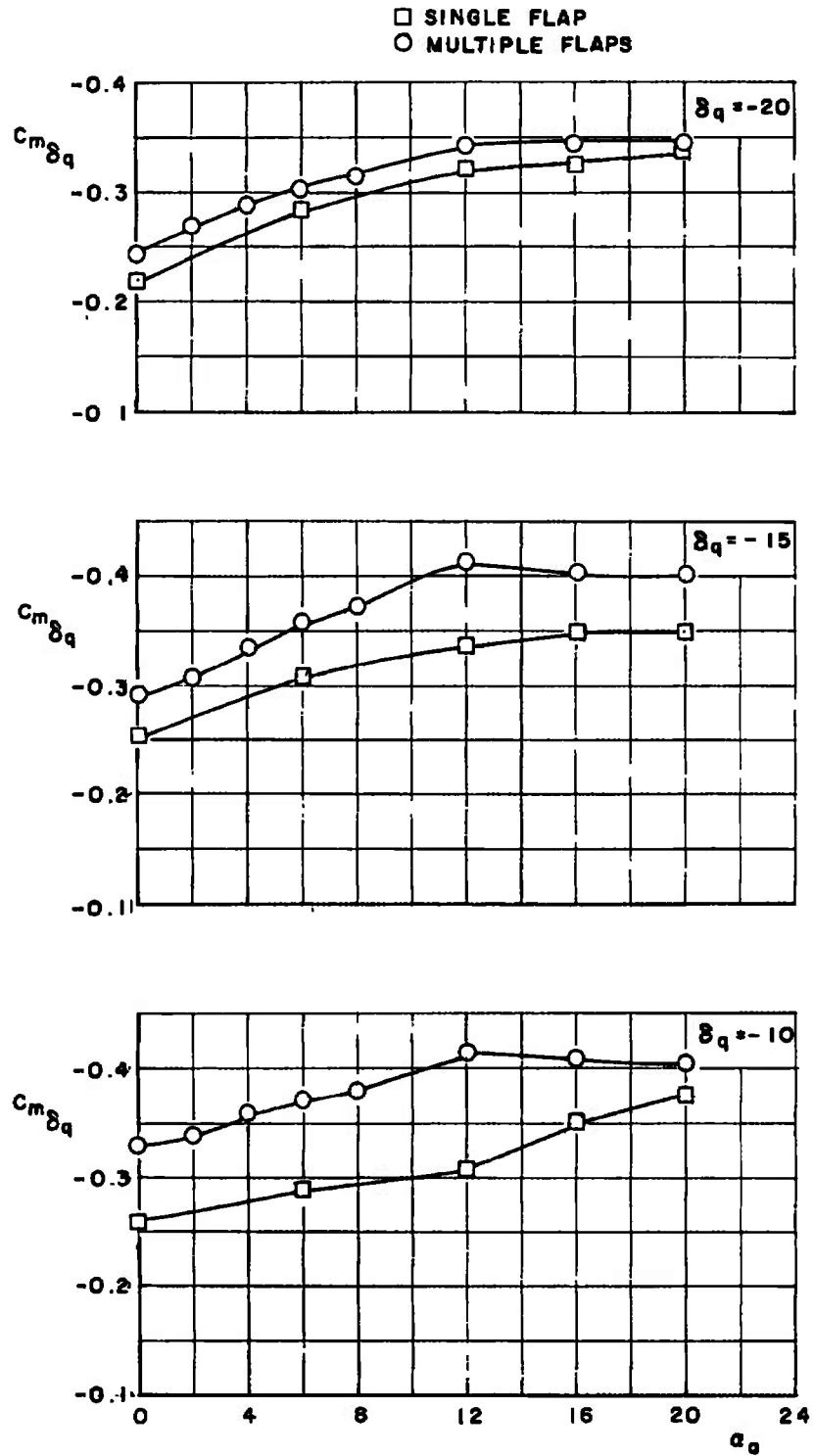


Figure 34. Comparison of pitch control effectiveness calculated from single flap and multiple flap techniques.

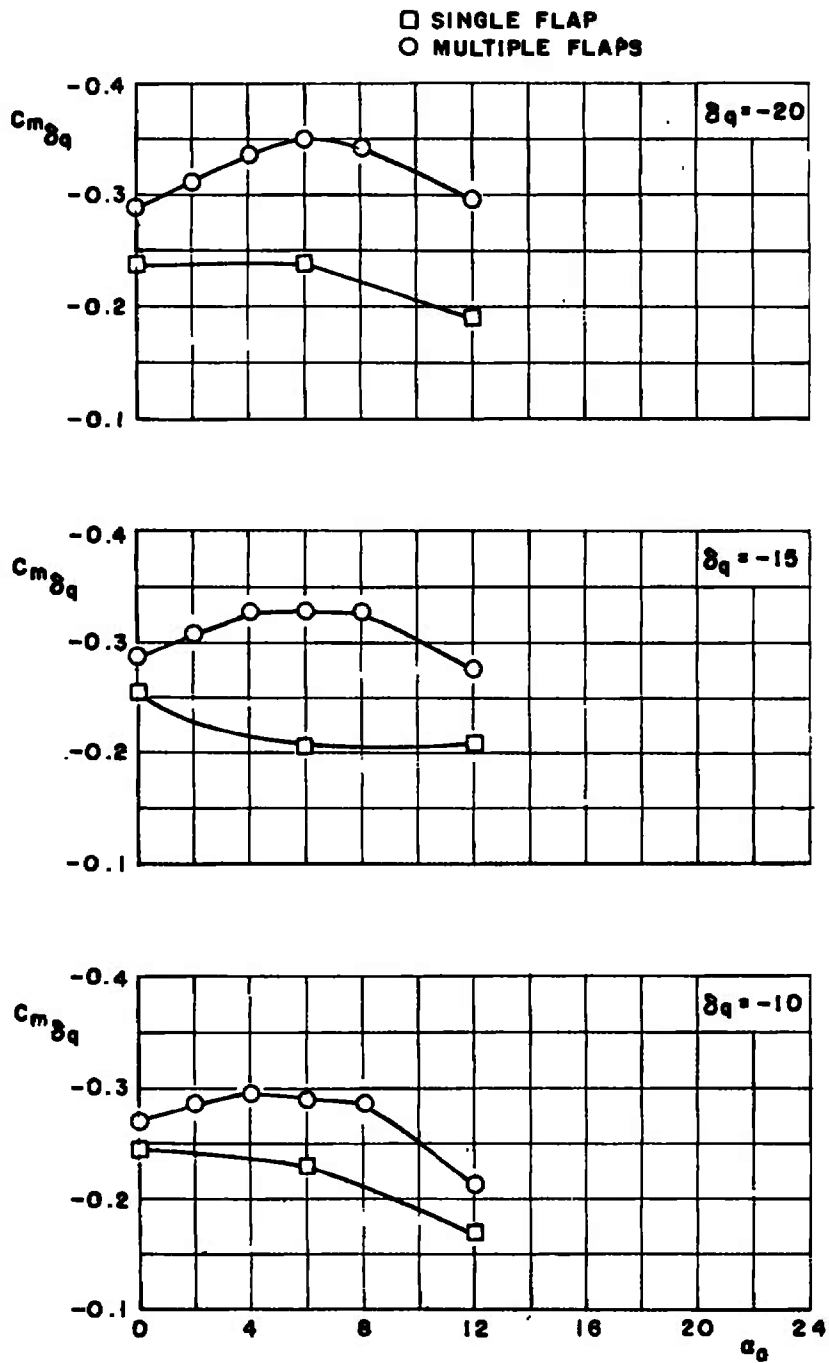


Figure 34. Concluded.

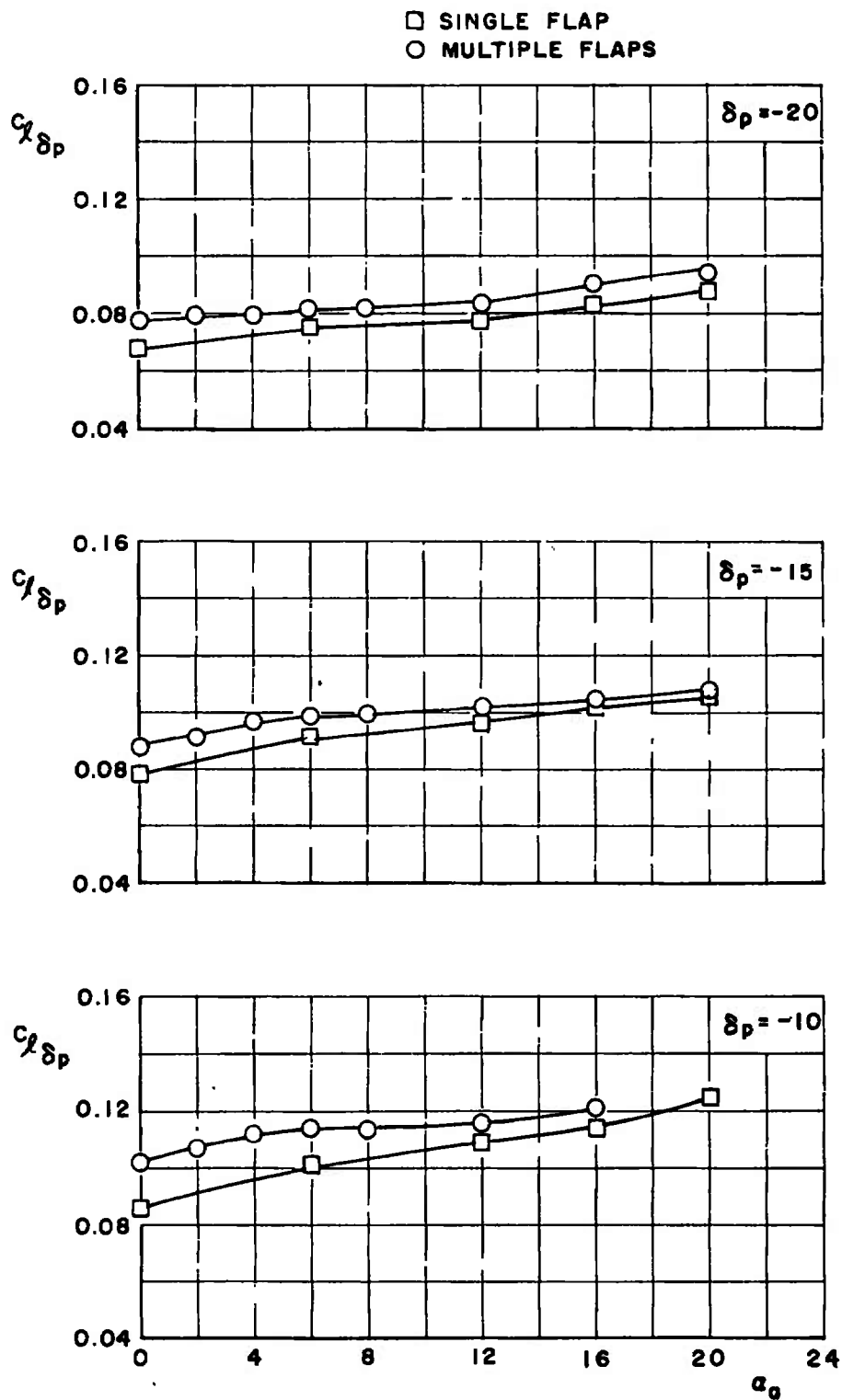


Figure 35. Comparison of roll control effectiveness calculated from single flap and multiple flap techniques.

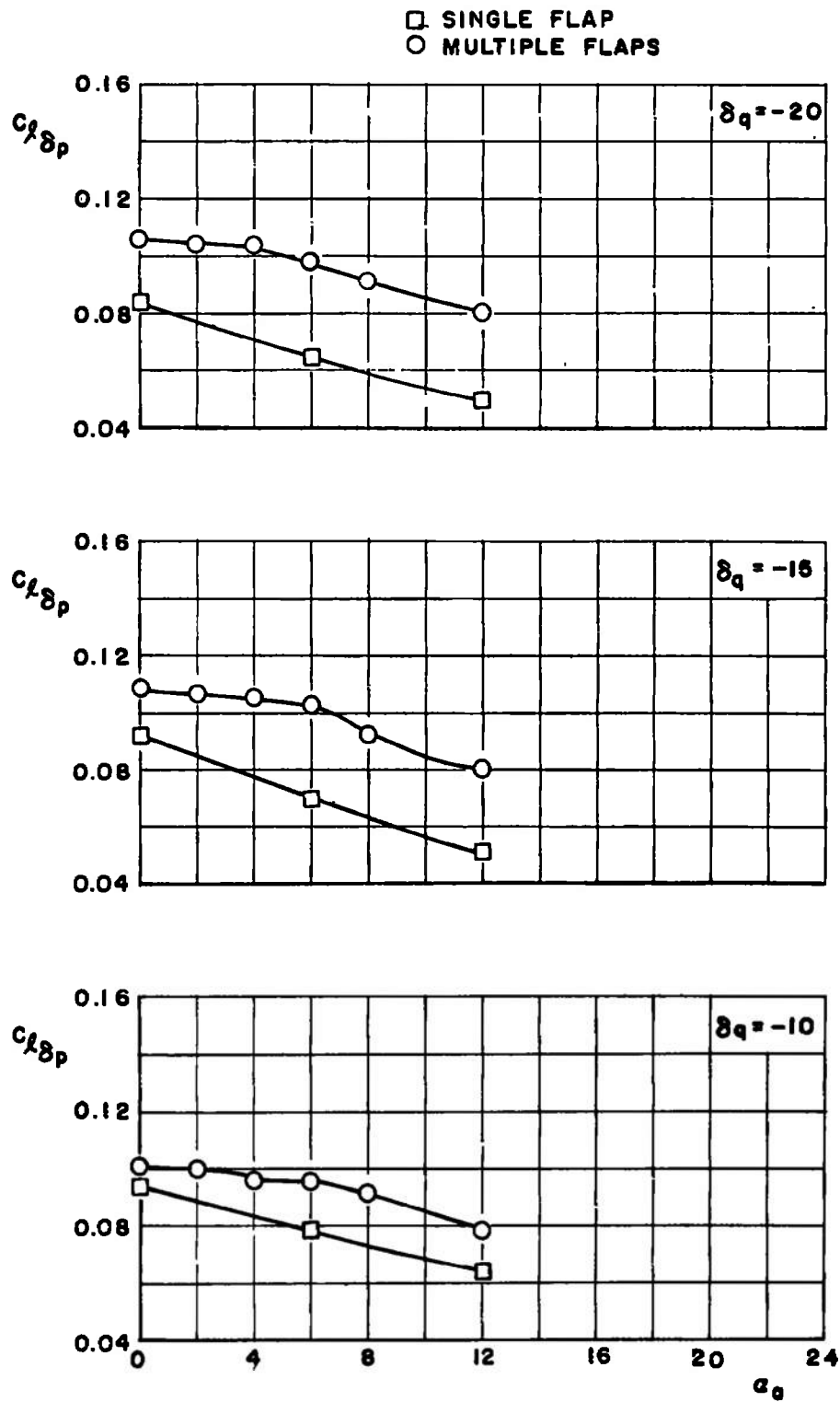


Figure 35. Concluded.

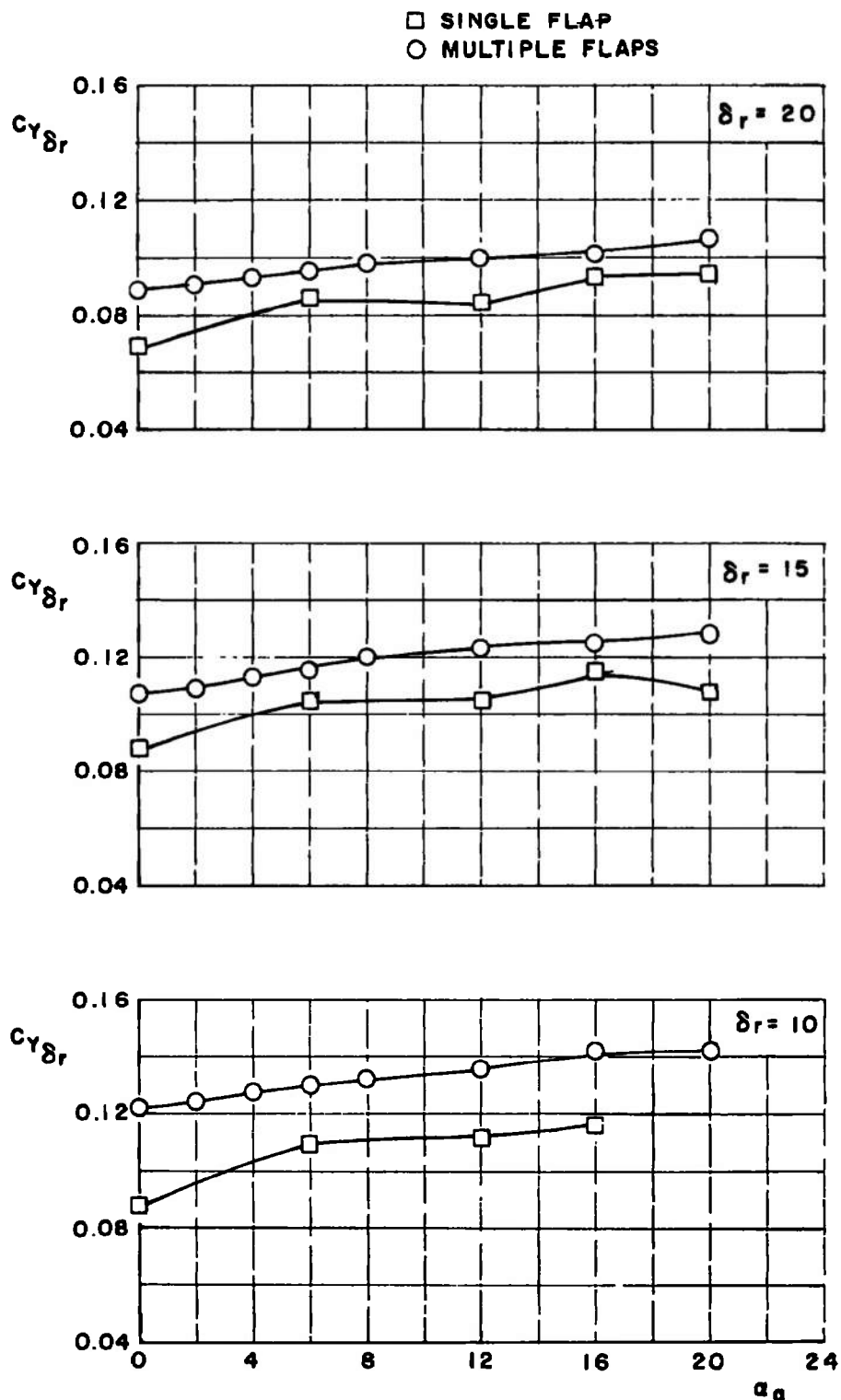


Figure 36. Comparison of side-force increment calculated from single flap and multiple flap techniques.

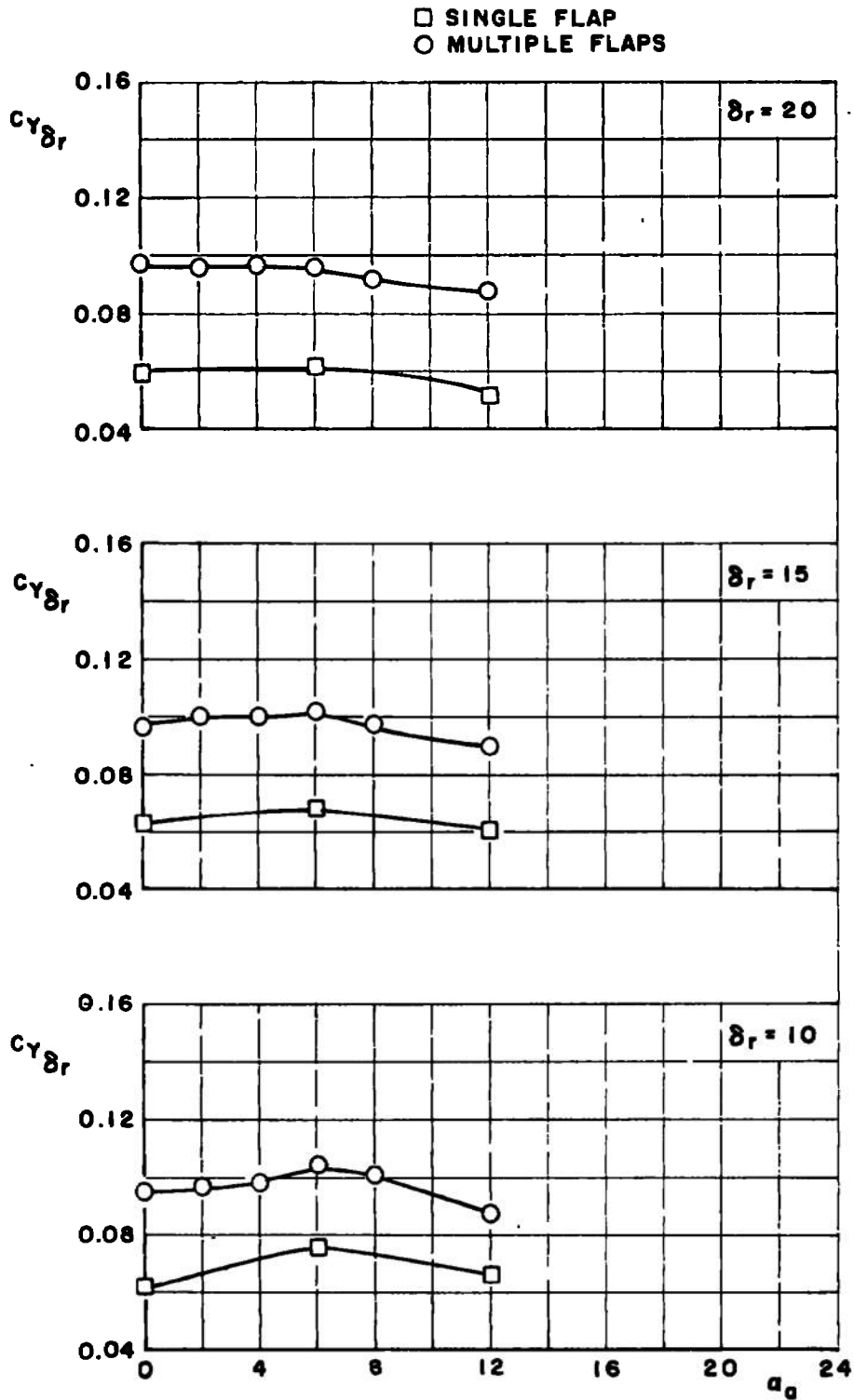


Figure 36. Concluded.

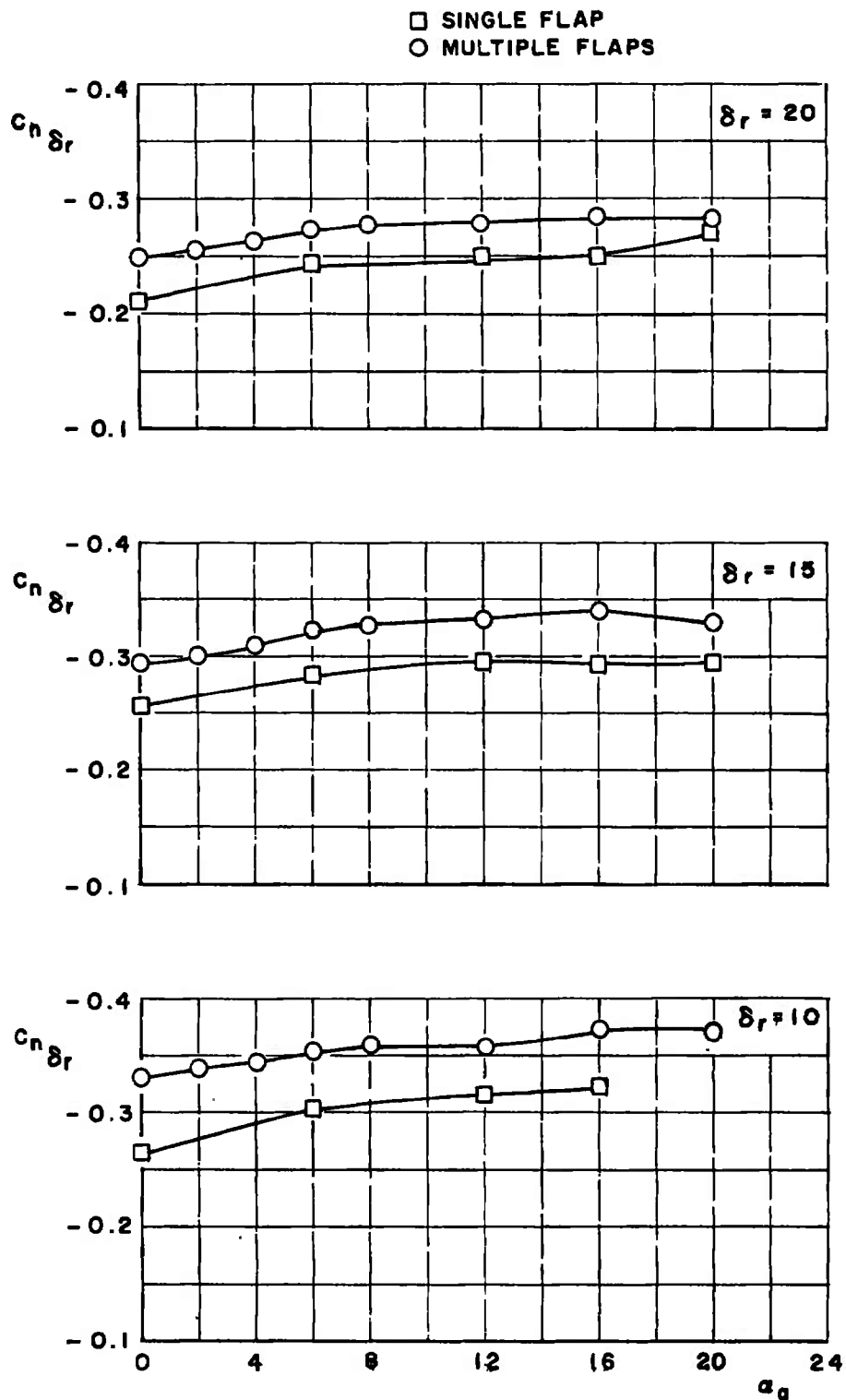


Figure 37. Comparison of yaw control effectiveness calculated from single flap and multiple flap technique.

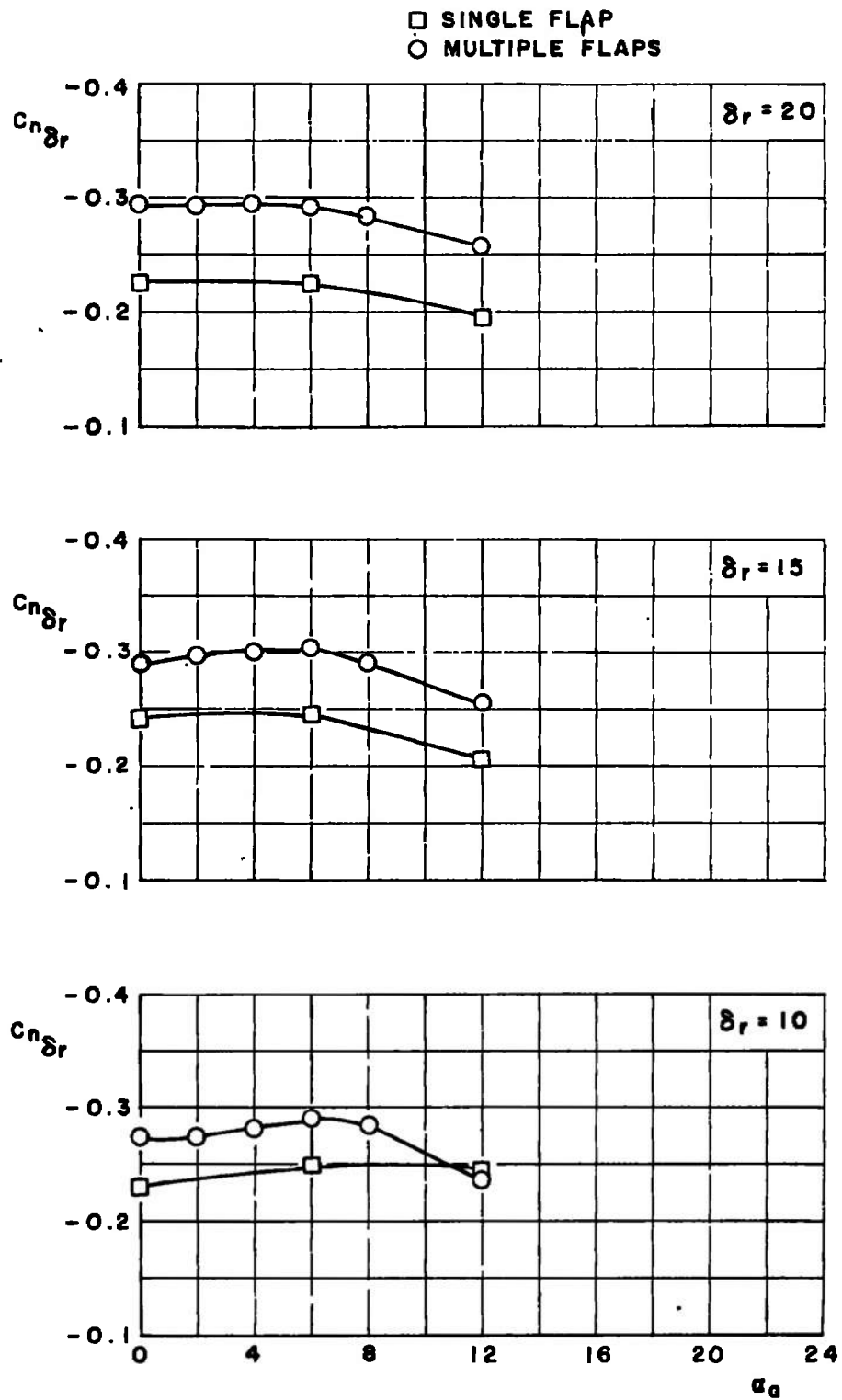


Figure 37. Concluded.

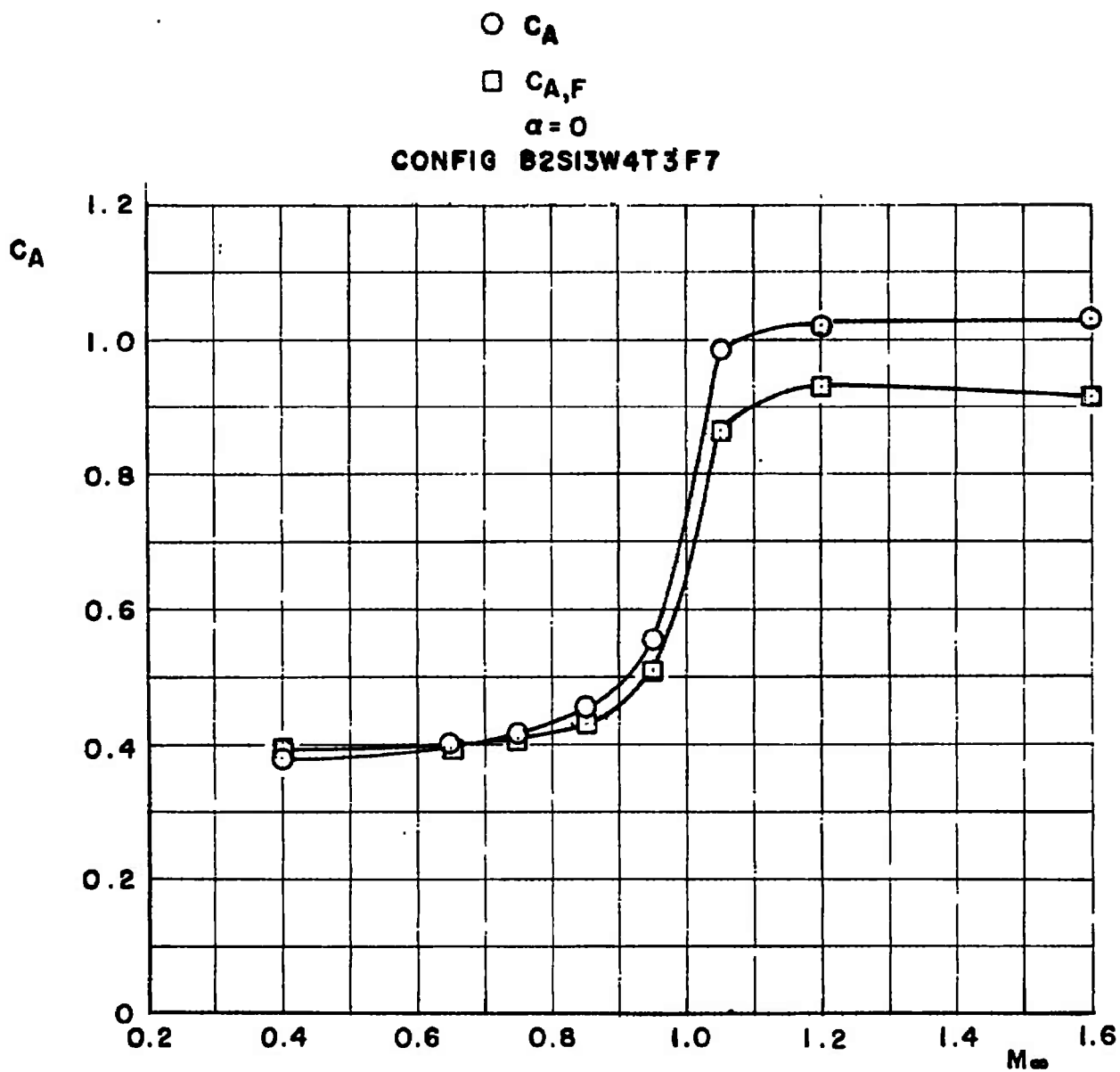


Figure 38. Axial-force coefficients versus Mach number.

SYM	CONFIGURATION	MACH NO	δp	δq	δr
□	B2S13W4T3F7	0.40	0	0	0
○	B2S13W4T3F7	0.40	0	-5	0
△	B2S13W4T3F7	0.40	0	-10	0
◇	B2S13W4T3F7	0.40	0	-15	0
◁	B2S13W4T3F7	0.40	0	-20	0

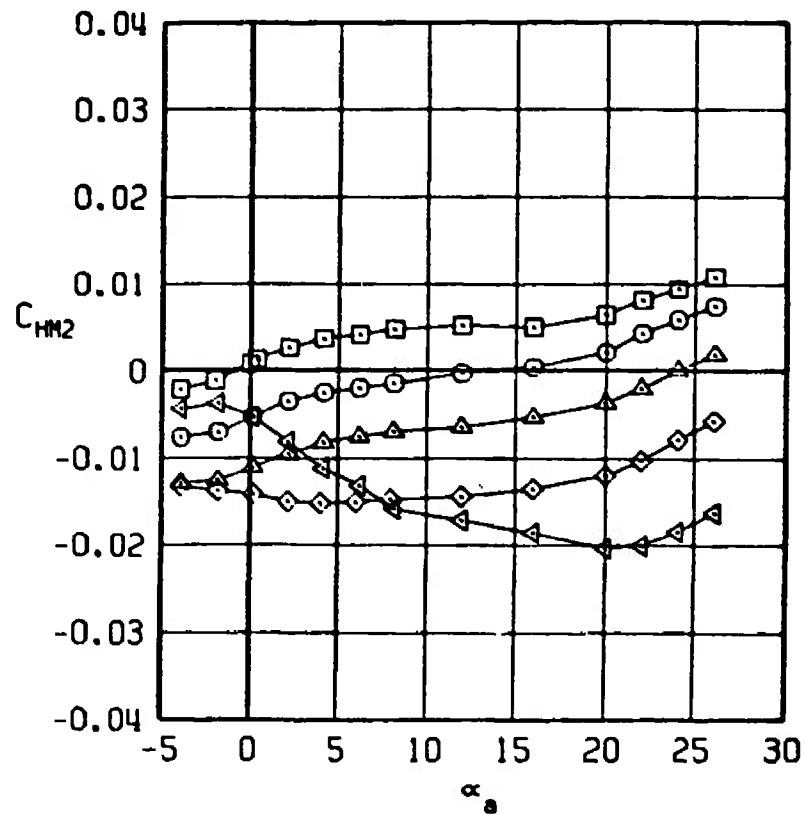
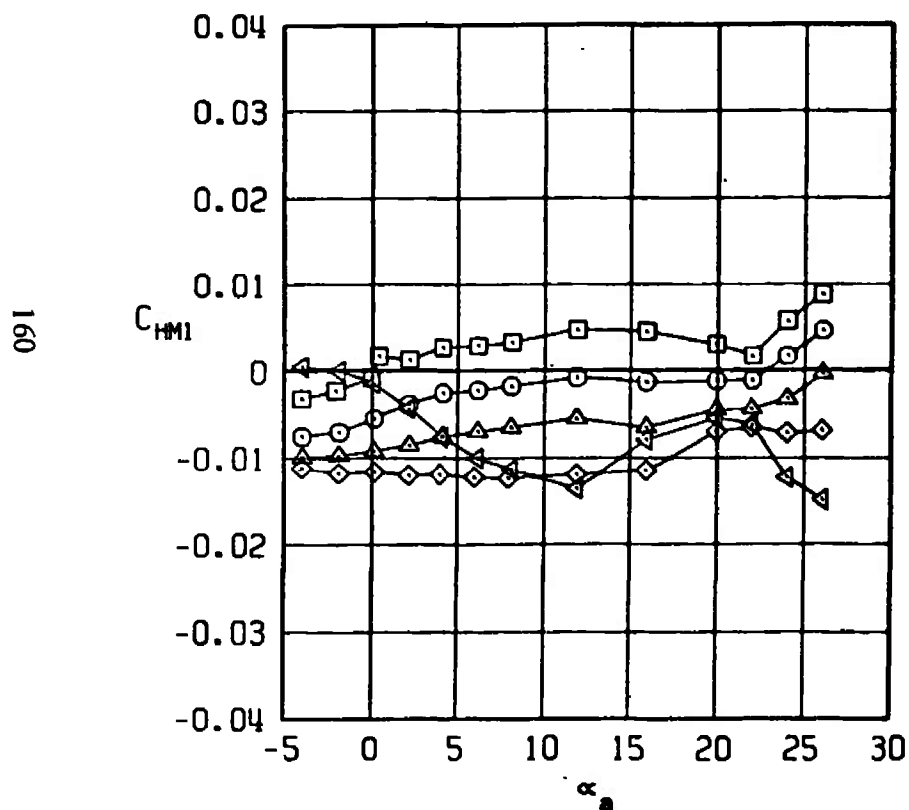


Figure 39. Control surface hinge-moment coefficients for several pitch control deflections.

SYM	CONFIGURATION	MACH NO	δp	δq	δr
□	B2S13W4T3F7	0.65	0	0	0
○	B2S13W4T3F7	0.65	0	-5	0
△	B2S13W4T3F7	0.65	0	-10	0
◇	B2S13W4T3F7	0.65	0	-15	0
◁	B2S13W4T3F7	0.65	0	-20	0

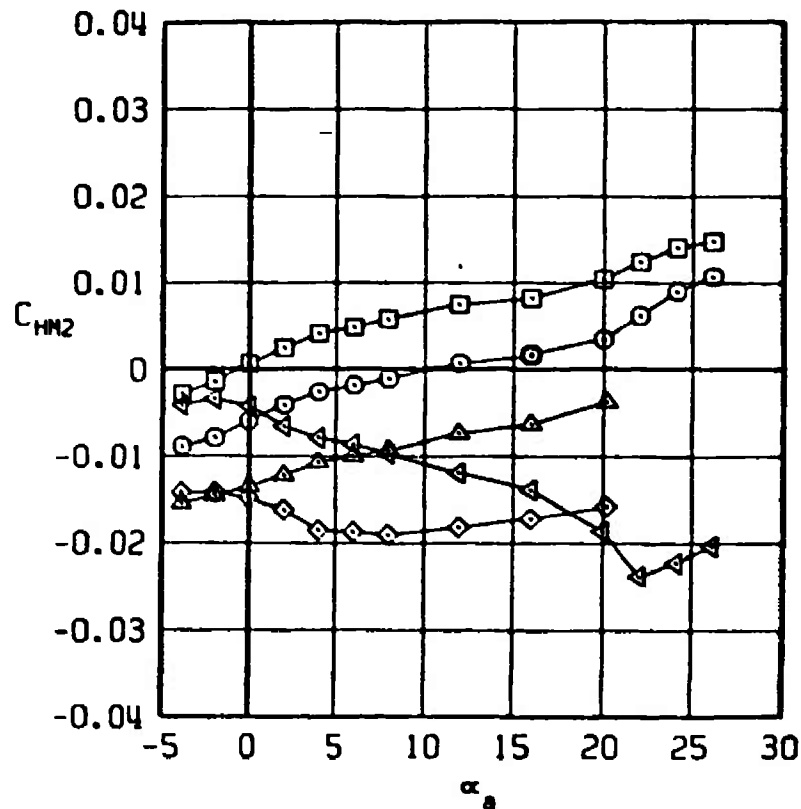
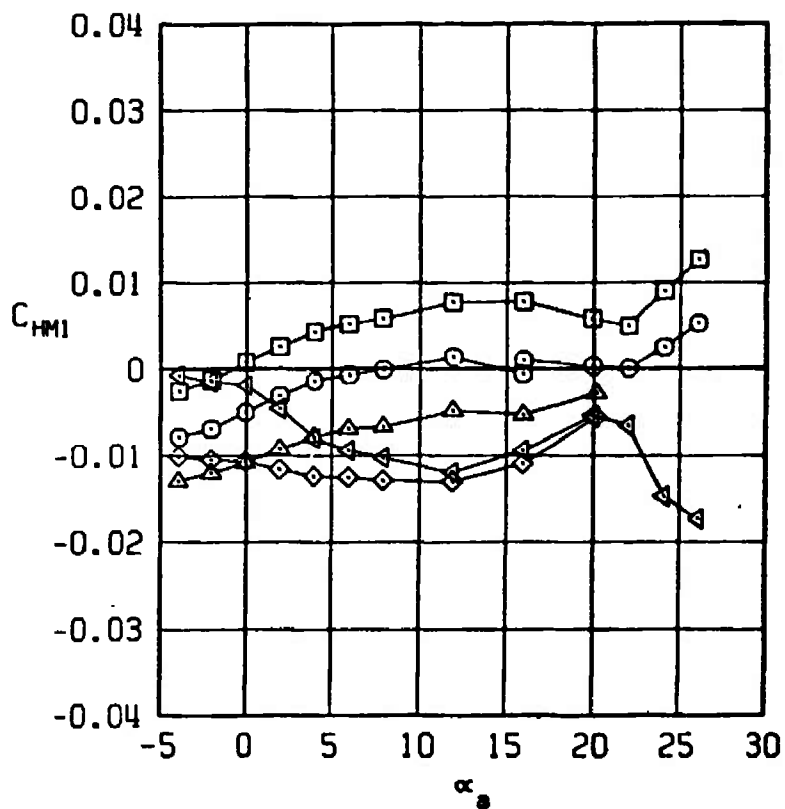


Figure 39. Continued.

SYM	CONFIGURATION	MACH NO	δp	δq	δr
□	B2S13W4T3F7	0.95	0	0	0
○	B2S13W4T3F7	0.95	0	-5	0
△	B2S13W4T3F7	0.95	0	-10	0
◇	B2S13W4T3F7	0.95	0	-15	0
◁	B2S13W4T3F7	0.95	0	-20	0

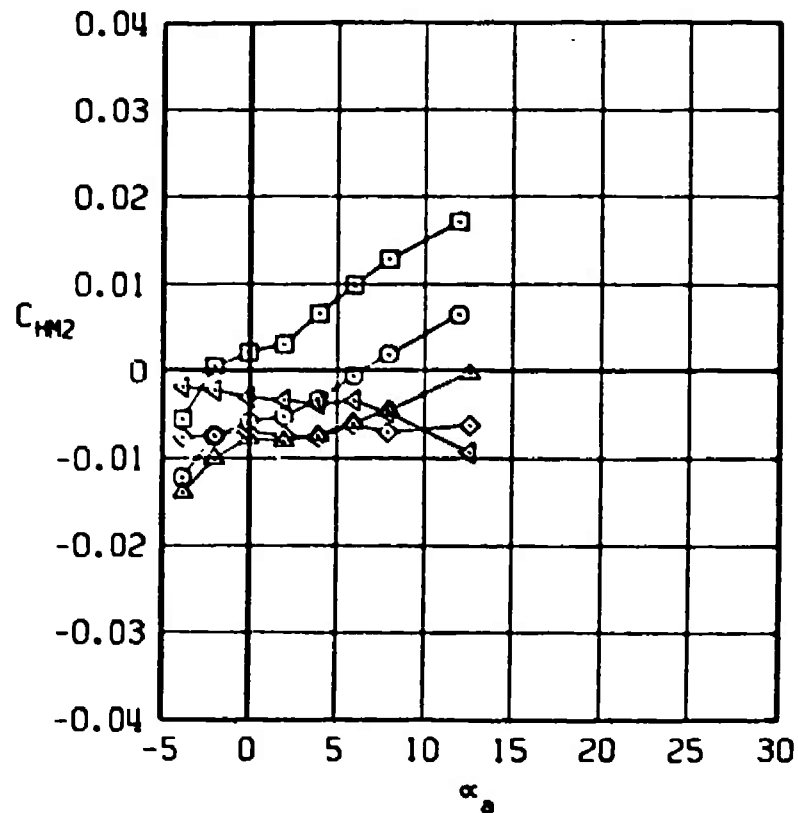
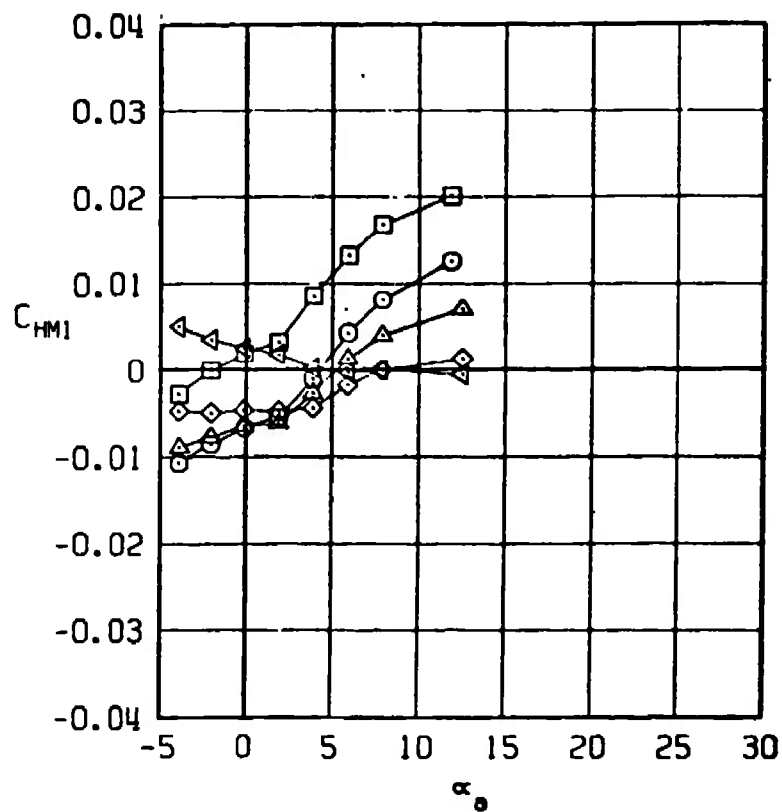


Figure 39. Continued.

SYM	CONFIGURATION	MACH NO	δp	δq	δr
□	B2S13W4T3F7	1.20	0	0	0
○	B2S13W4T3F7	1.20	0	-5	0
△	B2S13W4T3F7	1.20	0	-10	0
◇	B2S13W4T3F7	1.20	0	-15	0
◁	B2S13W4T3F7	1.20	0	-20	0

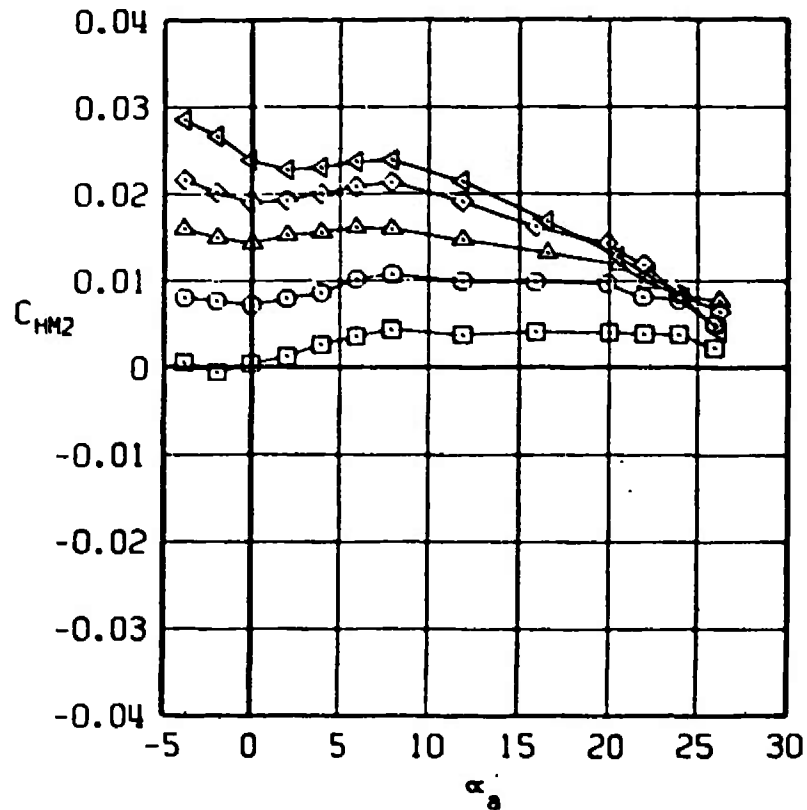
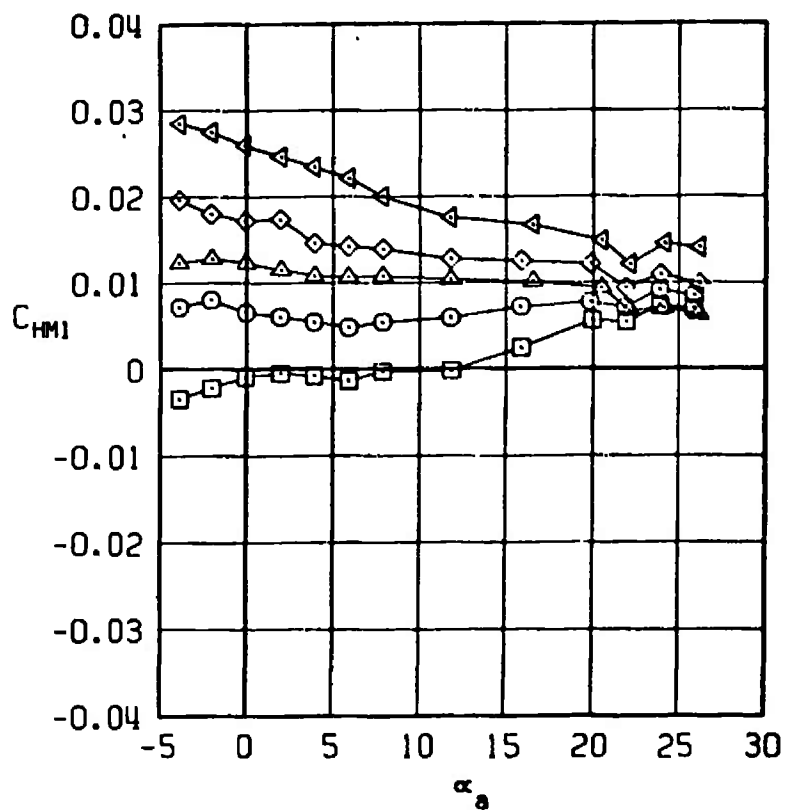


Figure 39. Continued.

SYM	CONFIGURATION	MACH NO	δp	δq	δr
□	B2S13W4T3F7	1.60	0	0	0
○	B2S13W4T3F7	1.60	0	-5	0
△	B2S13W4T3F7	1.60	0	-10	0
◇	B2S13W4T3F7	1.60	0	-15	0
◁	B2S13W4T3F7	1.60	0	-20	0

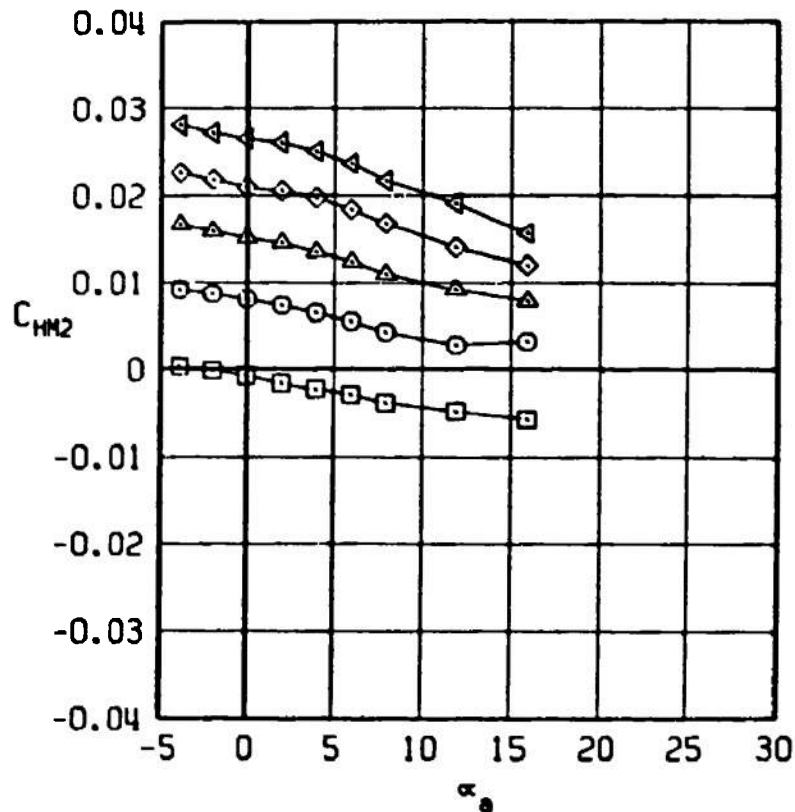
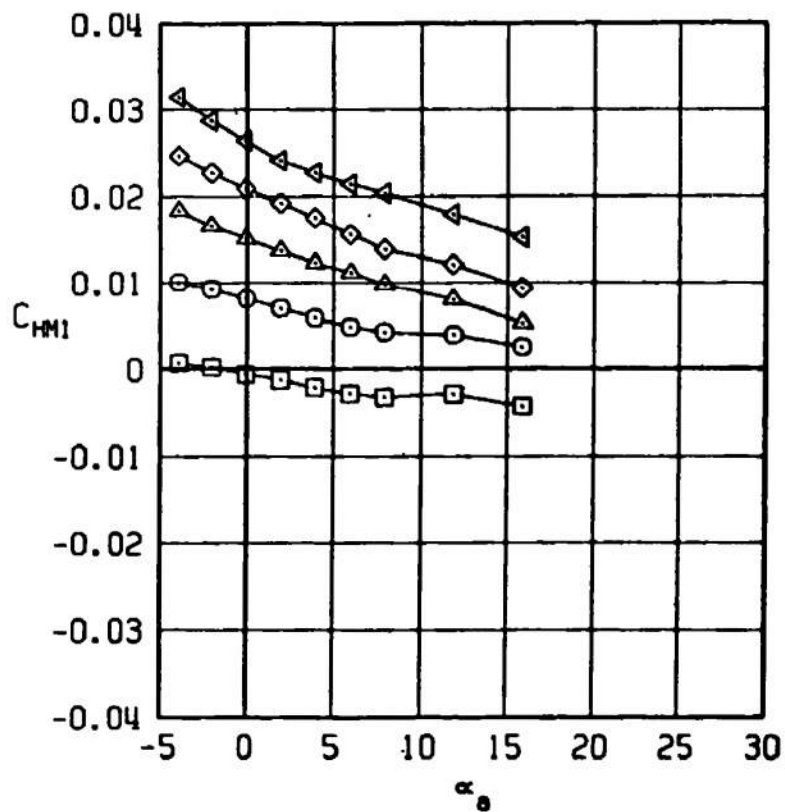


Figure 39. Concluded.

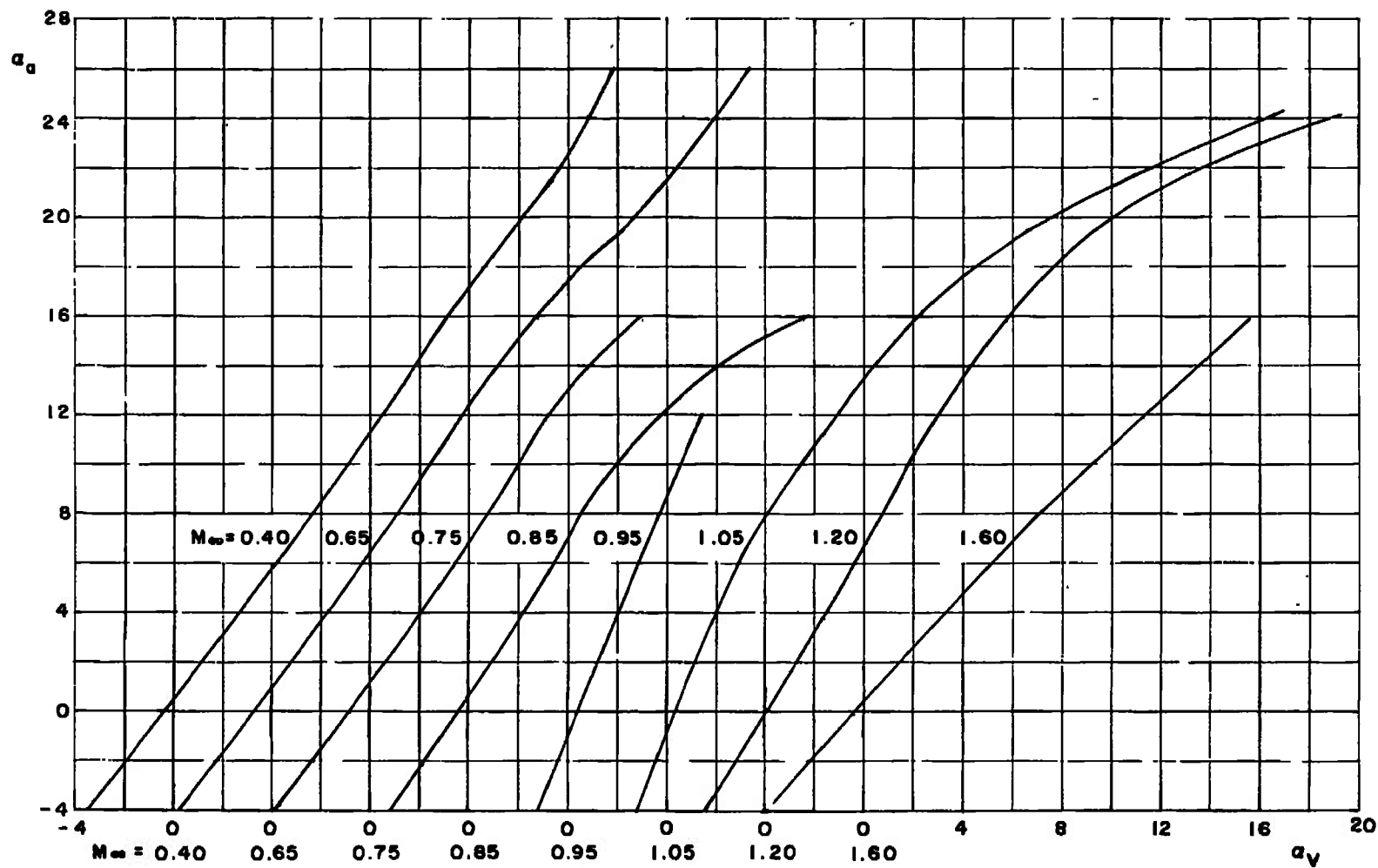


Figure 40. Vane calibration data, a_a versus a_v .

Table 1. Summary of Model Configurations and Flap Deflections Tested
a. Multiple Flap Deflections

Configuration	δp	δq	δr	M_{∞}^*							
				0.40	0.65	0.75	0.85	0.95	1.05	1.20	1.60
B2S13W4T3F7	0 -5 -10 -15 -20 0 0 0 0 -5 -5 -5 0 0	0 0 0 0 -5 -10 -15 -20 0 0 -10 -10 -10 -15	0 0 0 0 0 5 10 15 20 0 0 5 5 5	x x x x x x x x x x x x x x	x x x x x x x x x x x x x x	x x x x x x x x x x x x x x	x x x x x x x x x x x x x x	x x x x x x x x x x x x x x	x x x x x x x x x x x x x x	x x x x x x x x x x x x x x	
B2W4T3F7	0	0	0	---	x	---	---	x	---	x	---
B2S13W4F7	0	0	0	---	x	---	---	x	---	x	x
B2S13	---	---	---	---	x	---	---	x	---	x	x
B2	---	---	---	---	x	---	---	x	---	x	x

b. Single Flap Deflections ($\delta_2 = \delta_3 = \delta_4 = 0$)

Configuration	$\delta 1$	α , deg	M_{∞}^*			
			0.65	0.85	0.95	1.05
B2S13W4T3F7	0	0	x	x	x	x
		6		x	x	x
		12		x	x	x
		16		x	---	---
	↓	20		---	---	---
	-10	0		x	x	x
		6		x	x	x
		12		x	x	x
		16		x	---	---
	↓	20			---	---
	-15	0		x	x	x
		6		x	x	x
		12		x	x	x
		16		x	---	---
	↓	20		---	---	---
	-20	0		x	x	x
		6		x	x	x
		12		x	x	x
		16		x	---	---
	↓	20		---	---	---

* x - indicates Mach numbers tested.

Table 2. Summary of Nominal Test Conditions

M_∞	p_T , psfa	p_∞ , psfa	q_∞ , psf	$Re \times 10^{-6}/ft$
0.40	3000	2700	300	3.4
0.65	2000	1500	440	3.3
0.75	2000	1400	530	3.6
0.85	1500	930	470	2.9
0.95	↓	840	530	3.0
1.05		750	580	3.1
1.20		620	620	3.1
1.60		350	650	3.0

Table 3. Summary of Model Roll Angles Required for Single Flap Imaging*

Flap and Deflection Angle, deg	Model Roll Angle, ϕ , deg
+ δ_1	-90 [†]
- δ_1	0
+ δ_2	180 [†]
- δ_2	90
+ δ_3	180
- δ_3	90 [†]
+ δ_4	-90
- δ_4	0 [†]

*Data Obtained with Negative Deflections of Flap No. 1.

[†]Change Signs of Incremental Side-Force, Yawing-Moment, and Rolling-Moment Coefficients.

Table 4. Summary of Data Precision

M_∞	$\Delta C_{N,a}$	$\Delta C_{m,a}$	$\Delta C_{Y,a}$	$\Delta C_{n,a}$	$\Delta C_{l,a}$	$\Delta C_{A,a,F}$	ΔC_{HMX}	Δq
0.40	±0.39	±0.43	±0.39	±0.24	±0.026	±0.077	±0.0027	±6.7
0.65	±0.25	±0.29	±0.27	±0.16	±0.017	±0.052	±0.0018	±4.9
0.95	±0.20	±0.24	±0.22	±0.14	±0.014	±0.043	±0.0015	±2.6
1.20	±0.17	±0.21	±0.19	±0.12	±0.012	±0.037	±0.0013	±2.3
1.60	±0.16	±0.20	±0.18	±0.11	±0.011	±0.035	±0.0012	±1.6

NOMENCLATURE*

C_A	Axial-force coefficient, axial force/ $q_\infty S$
$C_{A,F}$	Forebody axial-force coefficient, $C_A - C_{A,b}$
$C_{A,b}$	Base axial-force coefficient $(p_\infty - p_b) A_b / q_\infty S$
$C_{A,\delta q}$	Axial-force increment attributable to a pitch control deflection, $\frac{[(C_A)_{\delta q=x} - (C_A)_{\delta q=0}]}{\delta q = x}, \text{ deg}^{-1}$
C_l	Rolling-moment coefficient, rolling moment/ $q_\infty Sd$
$C_{l,\delta p}$	Roll control effectiveness attributable to a roll deflection, $\frac{[(C_l)_{\delta p=x} - (C_l)_{\delta p=0}]}{\delta p = x}, \text{ deg}^{-1}$
$C_{m,a}$	Pitching-moment coefficient, pitching moment/ $q_\infty Sd$, moment reference point at MS 16.00
$C_{m,\delta q}$	Pitch control effectiveness attributable to a pitch control deflection, $\frac{[(C_{m,a})_{\delta q=x} - (C_{m,a})_{\delta q=0}]}{\delta q = x}, \text{ deg}^{-1}$
$C_{N,a}$	Normal-force coefficient, normal force/ $q_\infty S$
$C_{N,\delta q}$	Normal-force increment attributable to a pitch control deflection, $\frac{[(C_{N,a})_{\delta q=x} - (C_{N,a})_{\delta q=0}]}{\delta q = x}, \text{ deg}^{-1}$
$C_{n,a}$	Yawing-moment coefficient, yawing moment/ $q_\infty Sd$, moment reference point at MS 16.00
$C_{n,\delta r}$	Yaw control effectiveness attributable to a yaw control deflection, $\frac{[(C_{n,a})_{\delta r=x} - (C_{n,a})_{\delta r=0}]}{\delta r = x}, \text{ deg}^{-1}$
$C_{Y,a}$	Side-force coefficient, side force/ $q_\infty S$

$C_{Y\delta r}$	Side-force increment attributable to a yaw control deflection, $\frac{[(C_{Y,a})_{\delta r=x} - (C_{Y,a})_{\delta r=0}]}{\delta r = 0}, \text{ deg}^{-1}$
C_{HM1}	Hinge-moment coefficient for control flap number, 1, hinge moment/ $q_\infty Sd$, positive trailing edge down
C_{HM2}	Hinge-moment coefficient for control flap number 2, moment/ $q_\infty Sd$, positive trailing edge down
DEL $C_{m,a}$	Incremental pitching-moment coefficient attributable to a single flap deflection, $[(C_{m,a})_{\delta 1=-x} - (C_{m,a})_{\delta 1=0}]_{\delta 2=\delta 3=\delta 4=0}$
d	Reference model diameter, 0.375 ft
MS	Model station
M_∞	Free-stream Mach number
p_b	Model base pressure, psfa
p_T	Free-stream total pressure, psfa
p_∞	Free-stream static pressure, psfa
q_∞	Free-stream dynamic pressure, psf
Re	Free-stream unit Reynolds number, ft^{-1}
S	Reference area, $(\pi d^2)/2$, 0.110 ft^2
α_a	Total or complex angle of attack, deg
α_v	Angle of attack as indicated by a vane-type angle-of-attack indicator, deg
$\delta 1-4$	Control deflection angles for the respective control surfaces 1 through 4 (see Fig. 4), positive when trailing edge is down, deg
δp	Control deflection angle for roll control, $\delta p = (-\delta 1 - \delta 2 + \delta 3 + \delta 4)/4, \text{ deg}$
δq	Control deflection angle for pitch control, $\delta q = (\delta 1 + \delta 2 + \delta 3 + \delta 4)/4, \text{ deg}$

δ_r Control deflection angle for yaw control,
 $\delta_r = (-\delta_1 + \delta_2 - \delta_3 + \delta_4)/4$, deg

ϕ Model roll angle, deg

ϕ_a Aerodynamic roll angle, deg

MODEL NOMENCLATURE

B2 Basic fuselage with boattail and the following protuberances: (1) side conduit, (2) umbilical fitting, (3) harness fairing, (4) launch lugs, and (5) angle-of-attack vane

F7 Flap or control surface

S13 Strake

T3 Wing tip

W4 Wing with wing fence

*Force and moments are oriented to an aeroballistic-axis system as shown in Fig. 4.